

Balancing Pathways in DNA Double Strand Break Repair

Inger Brandsma

ISBN: 9789462954564

Cover design: Inger Brandsma
Lay-out: Kishan Naipal and Inger Brandsma
Printed by: Proefschriftmaken.nl, Uitgeverij BOXpress
Published by: Uitgeverij BOXpress, 's Hertogenbosch

The studies presented in this thesis were mainly performed at the department of Genetics of the Erasmus University Medical Center, Rotterdam, The Netherlands.

Copyright © Inger Brandsma 2016, Rotterdam, The Netherlands

All rights reserved. No part of this thesis may be reproduced, stored in a retrieval system, or transmitted in any form or by any means, without prior written permission of the author.

Balancing Pathways in DNA Double Strand Break Repair

De balans tussen verschillende reparatiemechanismen
voor DNA-dubbelstrengsbreuken

Thesis

to obtain the degree of Doctor from the
Erasmus University Rotterdam
by command of the
rector magnificus

Prof.dr. H.A.P. Pols

and in accordance with the decision of the Doctorate Board.

The public defence shall be held on

6 April 2016 at 9:30 hrs

by

Inger Brandsma
born in Nieuwegein

Promotiecommissie

Promotor:

Prof.dr. J.H.J. Hoeijmakers

Overige leden:

Dr. H. van Attikum

Dr. W.M. Baarends

Prof.dr. R. Kanaar

Copromotor:

Dr. D.C. van Gent

Without passion, we would not take on new challenges.
Without planning and focus, we would not stay on track.
Without tenacity, we would not finish.

Lothar Hennighausen

Table of Contents

Chapter		Page
Chapter 1	DNA repair – A general introduction	9
	Scope of this thesis	24
Chapter 2	Pathway choice in DNA double strand break repair: observations of a balancing act	29
Chapter 3	REV7 counteracts DNA double strand break resection and affects PARP inhibition	45
Chapter 4	Mechanistic insight into PARP inhibitor resistance due to REV7 loss in BRCA1-deficient cells	71
Chapter 5	Overexpression of HSF2BP, a new BRCA2 interactor, results in a Fanconi Anemia-like phenotype	97
Chapter 6	New findings and the future of cancer treatment - General discussion	141
Appendix	Summary	156
	Samenvatting	158
	Curriculum Vitae	160
	List of publications	161
	PhD Portfolio	162
	Acknowledgements	164

Chapter 1

DNA repair

A general introduction

Introduction

All information a cell needs to live and survive is stored in the DNA and therefore nothing is more important than the maintenance of an intact and uncompromised genome. Unfortunately, endogenous as well as exogenous damaging agents such as reactive oxygen species, UV light and ionizing radiation constantly attack the genome. These agents cause DNA lesions, which can block transcription and replication and thereby impair protein production and cell division. If the DNA lesions are not repaired properly they can lead to mutations and even large-scale genomic rearrangements. These changes in the genome can result in for example oncogene activation or tumor suppressor inactivation and thereby increase cancer risk. To counteract these constant threats to genome stability, several specialized DNA damage recognition and repair pathways have evolved. These pathways are commonly known as the DNA damage response (DDR).

Types of DNA damage and their repair pathways

Nucleotide excision repair

UV light from the sun damages the DNA, causing mainly cyclobutane–pyrimidine dimers (CPDs) and 6–4 pyrimidine–pyrimidone photoproducts (6–4PPs). These lesions, as well as interstrand crosslinks and other bulky lesions caused by numerous chemicals or reactive oxygen species (ROS), are repaired via the nucleotide excision repair pathway (NER). NER consist of two sub-pathways: transcription-coupled and global genome nucleotide excision repair (TC-NER and GG-NER). Both pathways culminate in the same repair steps, but differ in the proteins involved in damage recognition.

Global genome NER is a surveillance mechanism detecting helix-distorting lesions throughout the genome. Lesions such as 6-4 photoproducts are detected by XPC in complex with RAD23 and Centrin 2 (CETN2)^{2,3}. CPDs, on the other hand, only mildly distort the helix and are a poor XPC

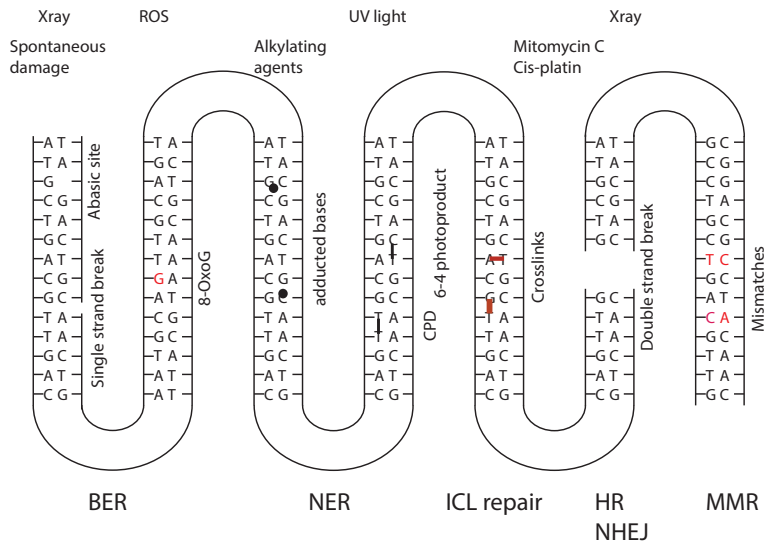


Figure 1 Types of DNA damage

Common DNA-damaging agents cause many different types of damage. Each type of damage requires one or more of the indicated pathways for repair. BER, base excision repair; CPD, cyclobutane–pyrimidine dimers; HR, homologous recombination; ICL, interstrand crosslink; MMR, mismatch repair; NER, nucleotide excision repair; NHEJ, non-homologous end joining; ROS, Reactive oxygen species; 8-oxoG, 8-hydroxyguanine. Based on¹

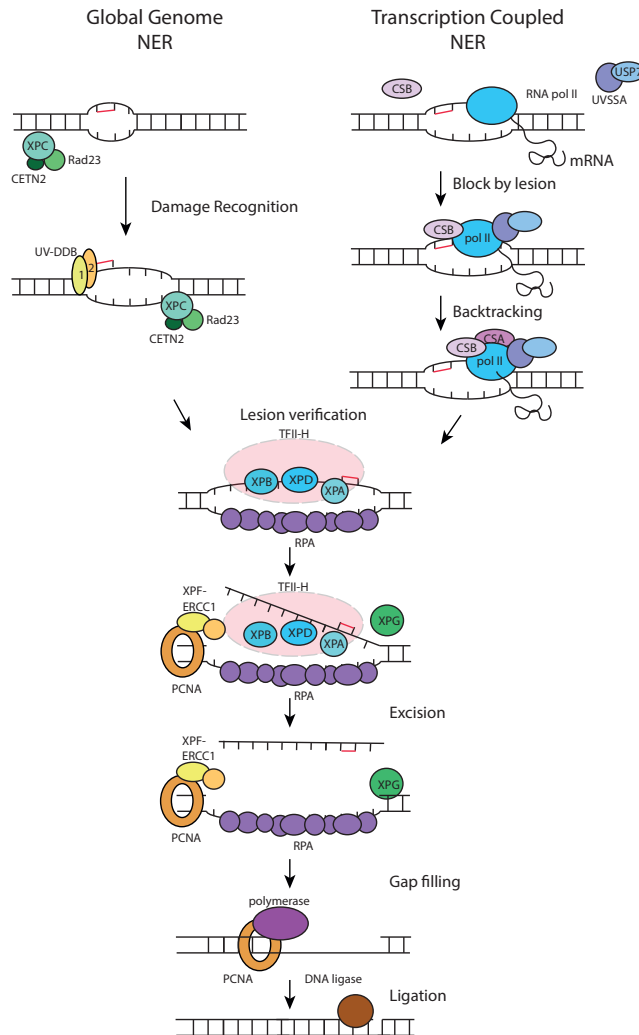


Figure 2 Nucleotide excision repair

The global genome (GG-NER) repair pathway is initiated by XPC, in complex with RAD23 and Centrin 2, detects a lesion, either on its own, or with the help of UV-DDB complex. In transcription-coupled repair (TC-NER) RNA polymerase II stalls at a lesion and CSB, UVSSA and USP7 bind. It is postulated that with the help of CSA the polymerase backtracks, exposing the lesion. After damage recognition, the multi-subunit complex TFII-H binds to the lesion and unwinds the surrounding DNA with the help of XPB and XPD. RPA coats the exposed intact single-strand DNA. XPA helps to verify the presence of a lesion and recruits the nuclease XPF-ERCC1, which incises the DNA on the 5' end of the lesion. XPG cleaves on the 3' side and a stretch of approximately 30 base pair is removed. The gap is filled by a polymerase and the nick ligated by DNA ligase. Figure based on⁹

substrate. To facilitate CPD detection, the UV-DDB1-DDB2 complex helps XPC to repair those lesions^{4,5}. After binding of XPC, the transcription initiation and repair complex TFII-H is recruited. The subsequent steps are identical for TC-NER and GG-NER (explained below).

GG-NER is not fast and efficient enough to repair all lesions and transcription stops when RNA polymerase II (RNA pol II) encounters a lesion. This stalling activates the transcription-coupled repair pathway. Cockayne syndrome protein A and B (CSA and CSB) together with UV-stimulated scaffold protein A (UVSSA)

and ubiquitin-specific-processing protease 7 (USP7) transiently bind to RNA pol II⁶⁻⁸. The CSA-CSB complex helps to remove the stalled polymerase to make the lesion accessible for repair and the TFII-H complex is recruited⁹.

The TFII-H complex contains two helicases, XPB and XPD, which open the DNA around the lesion^{10,11} and, with the help of XPA, verify the presence of damaged DNA¹². The ssDNA that becomes exposed in this step is bound by RPA. The damaged bases and approximately 30 base pairs of surrounding DNA are excised by XPG and XPF-ERCC1¹³. The

gap filling is performed via PCNA, replication factor C (RFC), DNA Pol δ , DNA Pol ϵ or DNA Pol κ , and DNA ligase I or XRCC1–DNA ligase III ligate the nick⁹.

Base excision repair

The bases in DNA can be damaged by oxidation, alkylation, deamination, and depurination/depyrimidination. Damaged bases no longer form the canonical base pairs, leading to mis-incorporation of nucleotides during replication and thereby mutations. To prevent mutations, the damaged bases are

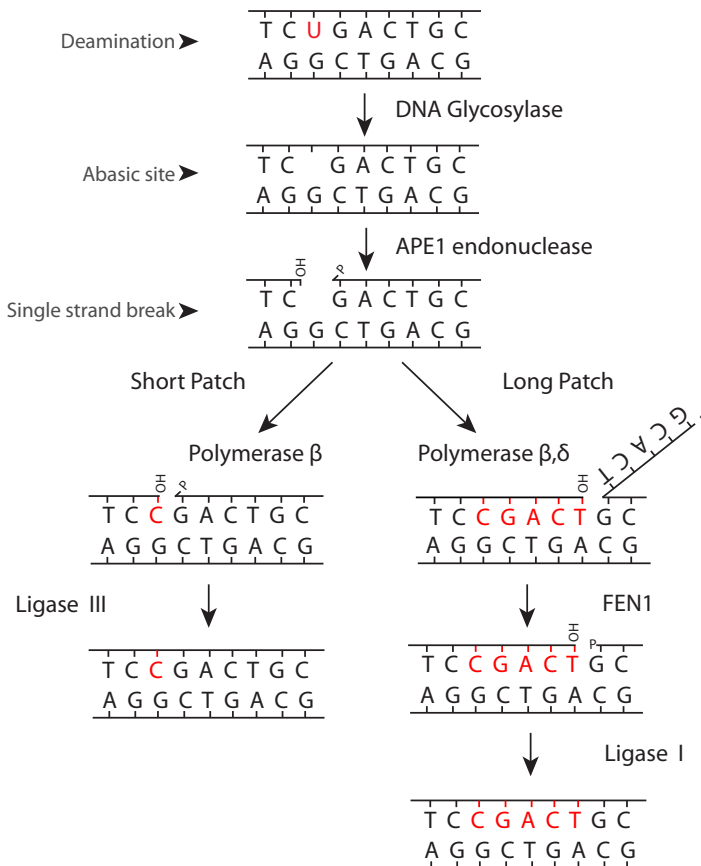


Figure 3 Base excision repair

Base damage, such as a deaminated cytosine (uracil) can be repaired either by short or long patch repair. In both cases a DNA glycosylase cleaves off the damaged base and an AP-endonuclease or AP-lyase removes the DNA backbone. In short patch repair, polymerase β inserts a new base and removes the overhang and the nick is ligated by DNA ligase III. In long patch repair, polymerase β or δ inserts a stretch of nucleotides, displacing the intact DNA. The protruding DNA flap is removed by FEN1 and the nick ligated by DNA ligase I. Figure based on¹⁴

removed by the base excision repair pathway (BER). BER can be divided into two sub pathways: long patch and short patch repair. In short patch repair only a single nucleotide is repaired, while in long patch repair a stretch of DNA containing the damaged base is removed¹⁴.

DNA glycosylases recognize damaged bases and cleave off the damaged base, leaving an apurinic or apyrimidinic site (AP site). The part of the DNA backbone without a base is then removed by an AP-endonuclease or an AP-lyase. A DNA polymerase, specifically DNA polymerase β , can fill the gap and a DNA ligase seals the nicks. In long patch repair the polymerase filling of the gap replaces more than one base, resulting in displacement of the DNA strand. This flap is then removed by FEN1 to create a ligatable nick¹⁴.

Mismatch repair

Mismatches arise due to the incorporation of the wrong nucleotide during replication and are corrected via the mismatch repair pathway (MMR). Although replicative polymerases have proofreading activities, some mismatches still occur. Inactivation of mismatch repair leads to increased numbers of mutations in the genome and predisposes for example to colon cancer^{15,16}. Apart from correcting mismatches and insertion/deletion loops, mismatch repair also plays a role in the repair of oxidative damage and meiotic and mitotic recombination¹⁷.

In mammalian cells mismatches are recognized by MSH2/MSH6 (MutS α) or MSH2/MSH3 (MutS β) during replication. Subsequently, MutL α is recruited and this complex then slides along the DNA until it encounters a strand discontinuity and binds PCNA¹⁷. At the gap EXO1 is recruited and initiates degradation of the nicked strand past the mismatch. The newly formed single-strand DNA is stabilized by RPA and filled in by polymerase δ . DNA ligase I seals the nick¹⁸.

Single strand break repair

Single-strand breaks can be caused by ionizing radiation as well as reactive oxygen

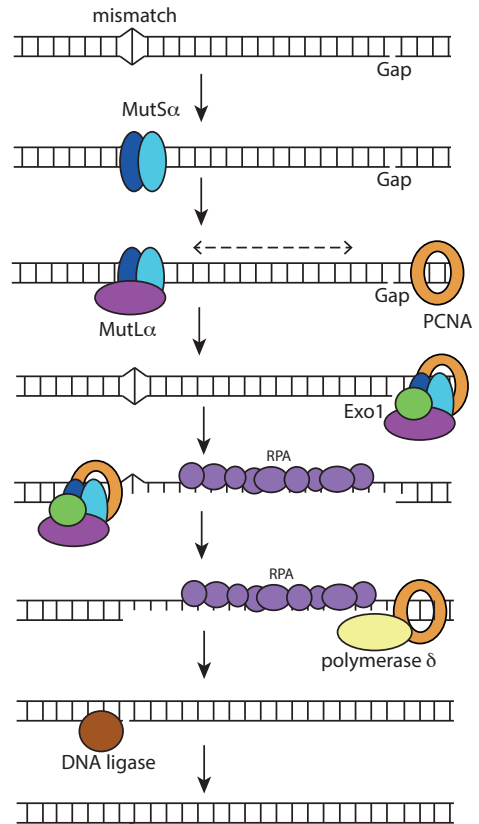


Figure 4 Mismatch repair

MutS α recognizes single DNA mismatches, while MutS β recognizes loops. Upon binding to a mismatch, MutS α undergoes a conformational change and recruits MutL α . This complex scans the DNA for a gap and once it has found one, binds PCNA and a nuclease such as EXO1. At the gap, degradation of the nicked strand is initiated and the DNA is degraded past the mismatch. The exposed single-strand DNA is bound by RPA, the gap is filled in by polymerase δ and a ligase ligates the nick. Figure based on¹⁷

species (ROS) generated by the cellular metabolism. Single-strand breaks are rapidly recognized by poly (ADP-ribose) polymerase protein (PARP), which sequesters the scaffold protein XRCC1. Most single-strand breaks have damaged termini and end processing by polynucleotide kinases, polymerases and other enzymes can be required. Gap filling is usually performed by polymerase β and DNA ligase I or III ligates the nicks.¹⁹

Intermezzo: Role of PARPs in DNA repair

Poly(ADP-ribose) polymerase (PARP) enzymes add negatively charged poly(ADP-ribose) (PAR) chains to itself and/or other proteins as a posttranslational modification. The ADP-ribose monomers are derived from NAD⁺ and are attached to glutamine, asparagine, and lysine residues. In total there are 17 PARP enzymes, but only PARP1, PARP2 and PARP3 have been linked to DNA damage and repair so far. PARP1 is responsible for about 85% of all PARYlation in the cells, while the remaining 15% is catalyzed by PARP2. The activity of PARP3 seems to be very limited²⁰.

PARP1 and PARP2 seem to have overlapping roles, since the enzymes are partially redundant. *Parp1*^{-/-} mice and *Parp2*^{-/-} mice are viable, but the double knockout is lethal²¹. *Parp1*^{-/-} and *Parp2*^{-/-} mice are hypersensitive to ionizing radiation and display signs of chromosomal instability such as increased sister chromatid exchange and micronuclei^{21,22}.

PARP1 is abundant in chromatin²³ and has a high affinity for DNA single and double strand breaks²⁴. At single-strand breaks, PARP1 (and PARP2 to a much lesser extent) rapidly synthesize PAR-chains, which are soon after removed by the (poly(ADP-ribose) glycohydrolase (PARG). In the absence of PARP1, the repair rate of single-strand breaks is decreased. However, for PARP2-depletion there is no effect, even in the absence of PARP1²⁵. It is important to note that in the absence of PARP1 the repair is only slower, but still functioning²⁵.

PARP1 also plays a role during the detection and repair of other types of damage. At stalled replication forks, PARP1 stimulates HR by suppressing NHEJ. PARP1^{-/-} chicken DT40 cells show decreased HR, but this phenotype is rescued by the deletion of Ku or DNA ligase IV, indicating that NHEJ needs to be prevented at stalled forks²⁶. Additionally, PARYlation might promote recruitment of HR factors such as MRE11 at stalled forks²⁷. PARP1 is also recruited to UV

damage by DDB2. Recruitment of PARP1 and subsequent PARYlation of DDB2 result in decreased DDB2 auto-ubiquitination and this auto-ubiquitination increases the retention time of DDB2 at sites of damage²⁰.

PARP3 has been linked to NHEJ via the PAR binding protein Aprataxin-and-PNK-like Factor (APLF). In the absence of PARP3, γ H2AX foci disappear more slowly, indicating a decrease in NHEJ efficiency. This phenotype can be rescued by overexpression of APLF, which binds to PARP3-ribosylated substrates²⁸. In the absence of APLF, the retention of XRCC4 at laser damage is decreased, so PARYlation by PARP3 at sites of damage probably increases NHEJ by retention of XRCC4-DNA ligase IV via APLF²⁸. PARP3 has also been linked to the stabilization of the mitotic spindle and in telomere integrity²⁹.

As described above, the enzyme PARG rapidly removes PAR chains from substrates. Deletion of PARG is embryonically lethal, but MEFs could be isolated by Min et al.³⁰ These cells show micronuclei, chromosomal aberrations and increased sister chromatid exchange, demonstrating that the removal of PAR-chains is also important for genomic stability and efficient DNA repair.

DNA double strand break repair

One of the most detrimental types of DNA damage is the double strand break (DSB). Improper repair can lead to mutations and gross chromosomal rearrangements. DSBs are caused by ionizing radiation or can result from collapsed replication forks. Furthermore, DSBs are generated as an intermediate in the repair of interstrand crosslinks, during meiotic recombination and in antigen receptor gene rearrangements in T- and B-cells. There are two main pathways to repair a double strand break: HR and NHEJ.

The most accurate and reliable way to repair a DSB is via HR. This pathway relies on an intact sister chromatid, present during S and G2 phase of the cell cycle, as a template for accurate repair^{31,32}. First, the DNA is resected by the MRE11, RAD50, NBS1 (MRN)-complex^{33,34} together with CtIP^{35,36} and other

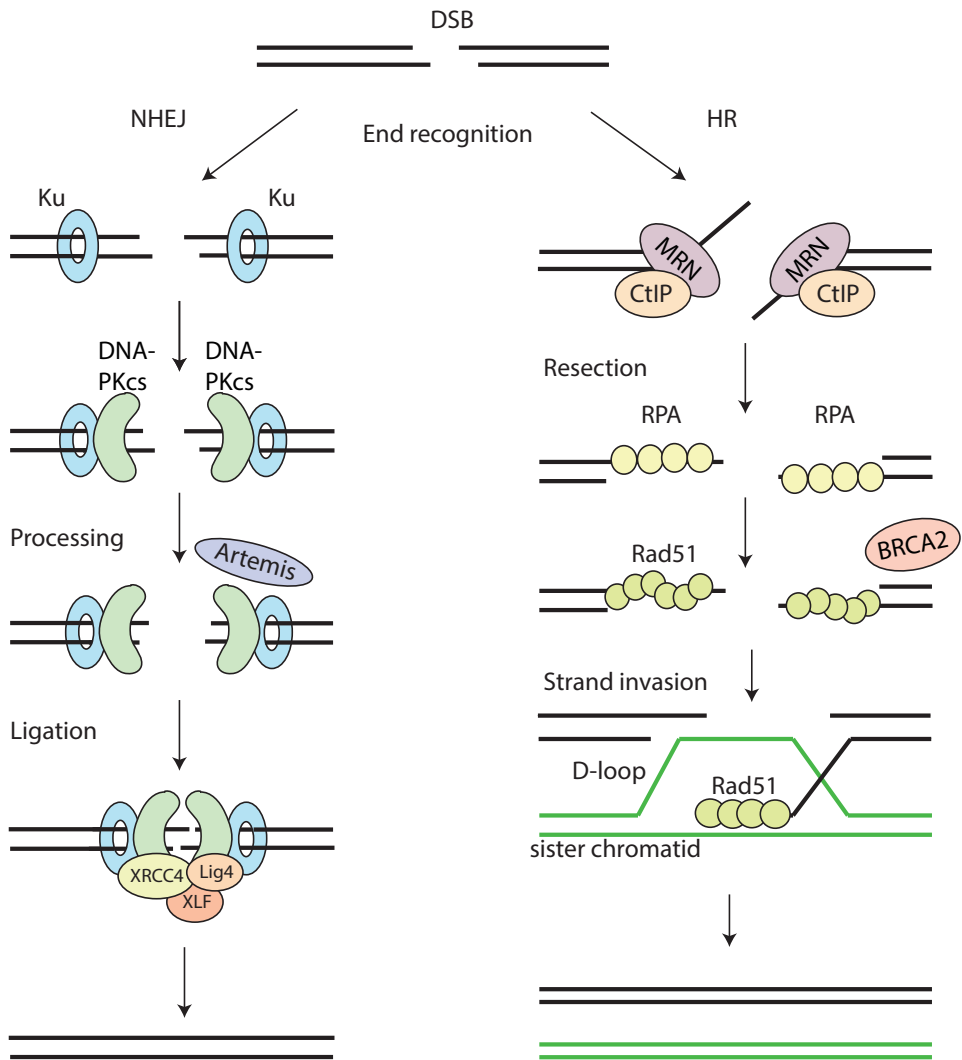


Figure 5 Homologous recombination and non-homologous end joining

NHEJ starts with recognition of the DNA ends by the Ku70/80 heterodimer, which recruits DNA-PKcs. If the ends are incompatible, nucleases such as Artemis can trim the ends. The XRCC4-DNA Ligase IV-XLF and PAXX ligation complex seals the break. For HR, the MRN-CtIP-complex starts resection on the breaks to generate single-stranded DNA (ssDNA). After resection the break can no longer be repaired by NHEJ. The ssDNA is first coated by RPA, which is subsequently replaced by RAD51 with the help of BRCA2. These RAD51 nucleoprotein filaments mediate strand invasion on the homologous template (the sister chromatid). Extension of the D-loop, capture of the second end and resolution of the Holliday junctions leads to repair. Figure from³¹ (Chapter 2).

nucleases, generating a 3'-ssDNA overhang. This overhang is coated by replication protein A (RPA). RAD51 then replaces RPA with the help of BRCA2, forming nucleoprotein filaments. During strand invasion, these filaments invade the homologous

sequence on the sister chromatid and the DNA is extended using the intact DNA of the sister chromatid as a template. The second end of the broken DNA is captured and the junctions are resolved, resulting in two intact DNA strands.

NHEJ can take place throughout the cell cycle and does not require a template³¹. In this pathway, the Ku70/80 heterodimer binds the end of the broken DNA and the catalytic subunit of the DNA dependent protein kinase (DNA-PKcs) is recruited. Compatible ends can be created with the help of polymerases or nucleases such as Artemis³⁷. The ligation complex, consisting of DNA ligase IV, X-ray cross-complementation group 4 (XRCC4) and XRCC4 like factor (XLF)/Cernunnos ligates the ends^{38,39}. Recently a new component of the NHEJ machinery, PARalog of XRCC4 and XLF (PAXX), was identified^{40,41}. PAXX interacts with Ku and is required for the formation of a

stable NHEJ complex. Defects in NHEJ result in hypersensitivity to IR, immunodeficiency and genomic instability⁴²⁻⁴⁵.

Chapter 2 discusses the regulation of pathway choice and the importance of the balance between NHEJ and HR, as well as assays to measure these pathways.

Trans Lesion Synthesis

Trans lesion synthesis (TLS) is a DNA damage tolerance mechanism. Many DNA lesions can block replication fork progression, eventually resulting in collapsed forks and DSBs. The TLS polymerases prevent prolonged fork stalling by bypassing

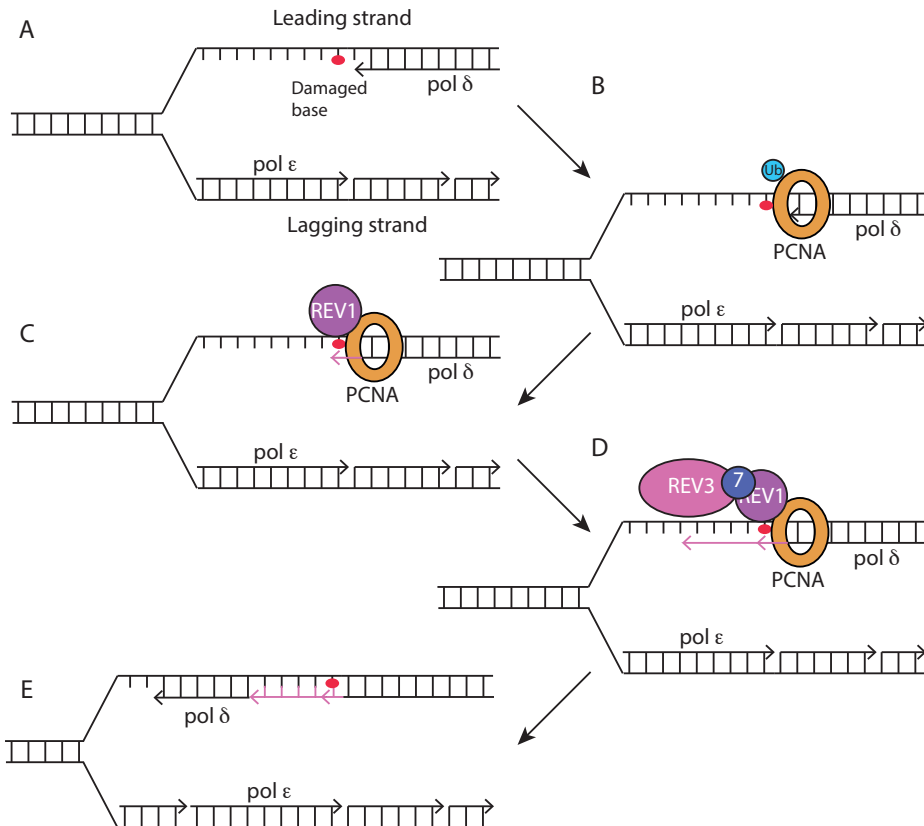


Figure 6 Trans Lesion Synthesis

When a replicative polymerase such as polymerase δ or ϵ encounters a damaged or modified base, replication stalls (A) and PCNA is ubiquitinated (B) by the Rad6-Rad18 complex (not shown). A Y-family translesion polymerase such as Rev1 can place a base opposite a damaged base (C) and polymerase ζ or other TLS polymerases can take over to bypass the lesion (D). After several bases, the TLS polymerase probably falls off and a replicative polymerase takes over (E). Figure based on⁵⁵⁻⁵⁷

damaged or missing bases, ensuring timely completion of replication⁴⁶. To allow the incorporation of bases opposite damaged bases, TLS polymerases have a lower fidelity than normal replicative polymerases and their use increases the mutation frequency. However, TLS polymerases have a low processivity and detach from the DNA after synthesizing only a short stretch of DNA preventing excessive mutagenesis. In addition to bypassing replication blocks, TLS polymerases can repair ssDNA gaps left after completion of replication^{47,48}.

In mammals the main TLS polymerases can be subdivided into two groups: the Y family polymerases (REV1, Pol η , Pol ι and Pol κ) and the B-type polymerase ζ . Polymerase ζ consists of a polymerase subunit REV3 and three accessory subunits REV7, PolD2 and PolD3⁴⁹.

The recruitment of TLS polymerases is regulated by post-translational modifications on PCNA⁵⁰. RAD6-RAD18 associates with RPA and mono-ubiquitinates PCNA at Lys164, the marker for the recruitment of TLS polymerases^{51–53}. To bypass the lesion, it is generally thought that one of the Y-family polymerases inserts a nucleotide opposite a damaged base. These polymerases have an uncommonly large and flexible active site, which can accommodate such an altered template and lack proofreading activity^{48,54}. After insertion of a nucleotide opposite the damage polymerase ζ or possibly other TLS polymerases can extend the sequence after which a normal replicative polymerase can take over⁴⁷.

Interstrand crosslinks and the Fanconi Anemia pathway

Endogenous metabolites as well as chemotherapeutics such as cisplatin and Mitomycin C can form covalent bonds with proteins as well as DNA, causing crosslinks due to the presence of two reactive groups. Intrastrand crosslinks connect two adjacent bases on the same strand, while interstrand crosslinks are formed between two bases of complementary DNA strands, preventing

opening of the DNA to allow transcription and replication. To remove the crosslink, both strands of the DNA must be incised. Proteins involved in the Fanconi Anemia pathway are required for this process⁵⁸, as well as HR, TLS and NER.

When a replication fork encounters an interstrand crosslink, replication stalls and FANCM is recruited together with FAAP24 and MHF1/2. This complex remodels the replication fork⁵⁹, forming ssDNA. RPA localizes on the ssDNA, which activates ATR and thereby the DNA damage checkpoint⁶⁰. ATR also phosphorylates FANCD2 and FANCI^{61,62} and the MRN-complex, which is necessary for resection⁵⁸.

The FA-core complex consists of FANCA, B, C, E, F, G, L, M, FAAP20, FAAP24 and MHF1/2. Assembly of this complex is required for monoubiquitination of FANCD2 and FANCI by FANCL⁶², a critical and highly conserved step in ICL repair. The FANCM-FAAP24-MHF1/2-complex recruits the FA core complex to the stalled replication fork⁵⁹. Mono-ubiquitylation of FANCD2 precedes its translocation to chromatin^{63,64}, where it promotes chromatin remodeling together with FANCI⁶⁵. Ubiquitinated FANCD2 acts as a recruitment platform for nucleases involved in the excision of the ICL⁵⁹. It is unclear exactly which nucleases perform the incision, but several nucleases such as XPF-ERCC1, MUS81-EME1, SLX4-SLX1, FAN1, SNM1A and SNM1B have been implicated in ICL repair⁵⁸.

Incision on both sides of the ICL results in unhooking of the lesion, which can then be bypassed by translesion synthesis forming an intact HR substrate. Numerous human TLS polymerases, including Pol η , Pol ι , Pol κ , Pol ν and REV1 have been shown to be able to bypass ICLs or to insert a base opposite and ICL⁵⁸. Also Pol ζ plays an important role in ICL repair, since deficiency in REV3 or REV7 strongly sensitizes cells to crosslinking agents⁵⁵. REV1 is thought to serve as a scaffold to coordinate the recruitment and activity of other TLS polymerases⁵⁹.

Once TLS is completed, the replication fork can be restarted using HR. Resection of

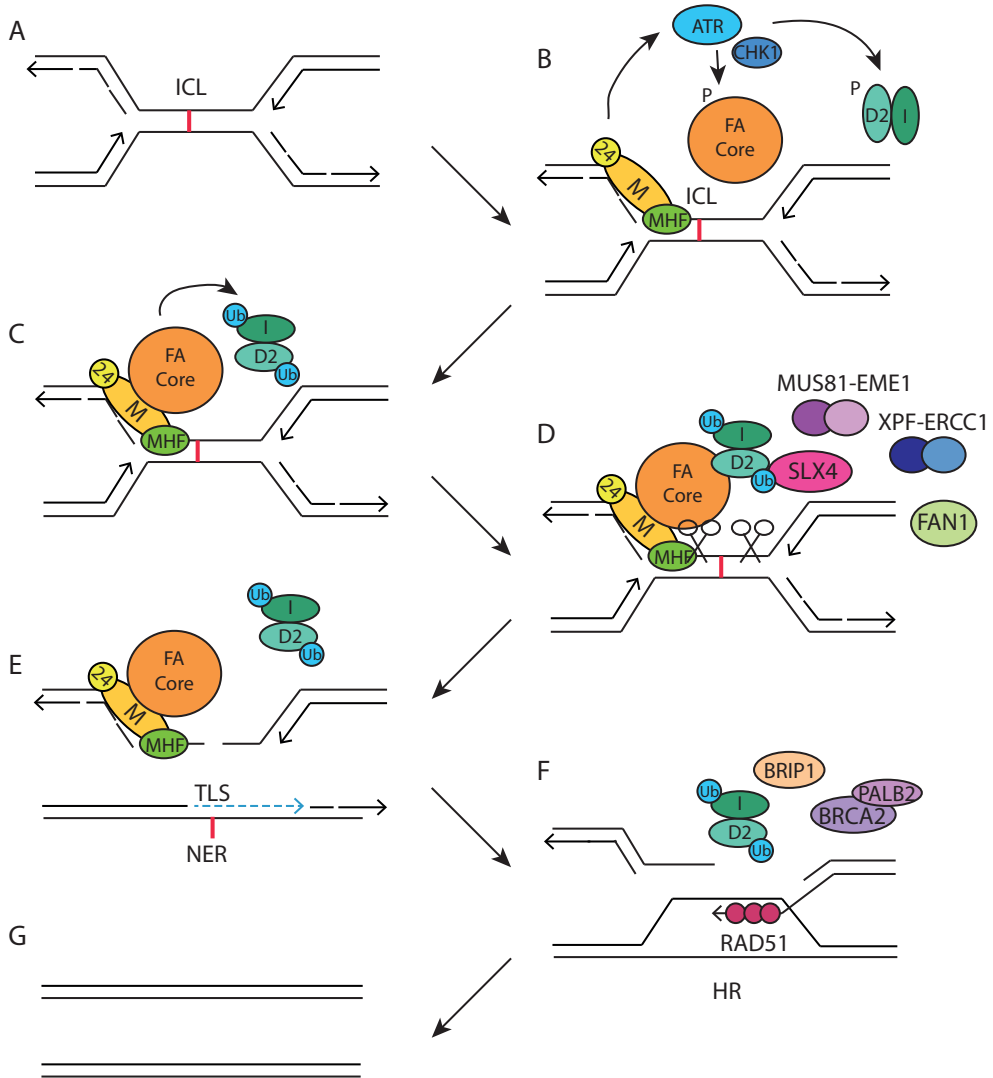


Figure 7 Interstrand crosslink repair

(A) Two forks converge at an interstrand crosslink. (B) The lesion is recognized by the FANCM-FAAP24-MHF1/2 complex, which recruits the multi subunit FA-core complex. FANCM also activates ATR, which phosphorylates FANCD2, FANCI and components of the FA core complex. (C) The FA core complex ubiquitinates FANCD2 and FANCI and this complex is recruited to the lesion. (D) The ubiquitinated FANCD2-FANCI acts as a recruitment platform for nucleases that make incisions next to the lesion. It is unclear which nuclease makes which incision, but SLX4, ERCC1-XPF, MUS81-EME1 and Fan1 are probably involved. (E) After incision, the lesion is unhooked and can be bypassed by a translesion polymerase. The lesion with the crosslink attached is probably repaired via nucleotide excision repair. (F, G) Replication is restarted via homologous recombination. Figure based on ⁵⁹

the break and RAD51 nucleoprotein filament formation appears to be independent of the FA core complex^{66,67}. The remaining unhooked ICL is no longer an obstacle and is a likely substrate for NER. Finally, the FANCD2, FANCI complex is deubiquitinated by the DUB complex USP1-UAF1^{68,69}.

BRCA1

BRCA1 function

In 1994 Miki et al. identified the tumour suppressor protein BRCA1 (Breast cancer type 1 susceptibility protein)⁷⁰. Four years earlier, the location had already been linked to early-onset familial breast cancer⁷¹. BRCA1 is an E3 ubiquitin-ligase that plays multiple roles in the repair of DNA damage, cell cycle regulation and transcription.

BRCA1 contains an N-terminal RING domain and two C-terminal BRCT repeats. The RING domain, found in many E3 ubiquitin ligases, is likely to be required for BRCA1's function as a tumour suppressor, since many pathogenic mutations are found in this domain. The RING domain of BRCA1 interacts with the RING domain of BARD1⁷² and this interaction stimulates the ubiquitin ligase activity of the complex. The pathogenic C61G mutation in BRCA1 disrupts the interaction between BRCA1 and BARD1 and abolishes the ubiquitin ligase activity⁷³. The BRCA1/BARD1 complex forms K6-linked ubiquitin chains and auto-ubiquitylates BRCA1⁷⁴.

Upon DNA damage, BRCA1 is hyperphosphorylated and relocates to sites of damage^{75,76}, where it colocalizes with RAD51⁷⁷. BRCA1-deficient cells are unable to form RAD51 foci⁷⁸, indicating that BRCA1 is essential for homologous recombination. Unlike BRCA2, BRCA1 does not play a role in one specific step of HR, but seems to be required for multiple processes such as checkpoint activation, damage signalling, and DNA repair, each linked to specific interaction partners.

BRCA1 interacts with BRCA2 via PALB2 (partner and localizer of BRCA2). PALB2 was first identified as an essential component

for BRCA2 and RAD51 loading at sites of damage⁷⁹. BRCA1 localization at sites of damage does not require PALB2⁸⁰, but localization of PALB2 does require BRCA1⁸¹. The interaction between BRCA1 and PALB2 is important for homologous recombination, because expression of proteins with mutations that abrogate this interaction results in a reduction in homologous recombination⁸⁰.

BRCA1 also plays a role in resection, the generation of ssDNA at sites of damage, via its interaction with CtIP⁸². CtIP is activated by a CDK-mediated phosphorylation on T847 and this activation is essential for viability and maintenance of genomic stability⁸³. However, the interaction between BRCA1 and CtIP might not be essential for resection⁸⁴, as BRCA1 only seems to affect the speed of the process⁸⁵. CtIP also interacts with the MRN complex³⁶ and plays an important role in DSB repair pathway choice⁸⁶.

BRCA1 deficiency and rescue of the phenotype

To date, many BRCA1-deficient mouse models have been generated. 87. Homozygous deletion of *Brca1* is lethal in mice and nullizygous embryos die early in development. This phenotype is partially ameliorated by homozygous deletion of *p53* and death of the embryo shifts to a later stage⁸⁸. *Brca1*^{Δ11/Δ11} mice also die before birth and this can be rescued by haploid loss of *p53* as well⁸⁹. However, these mice develop tumours later in life and display premature ageing⁹⁰. *Chk2* loss can also rescue the embryonic lethality of *Brca1* loss and these mice live longer than *Brca1*^{Δ11/Δ11}*p53*^{+/-} mice⁹⁰. Later in life the mice still develop tumours. This indicates that the ATM-CHK2-p53 pathway is important for inducing senescence, apoptosis and cell cycle arrest in BRCA1-deficient cells, preventing growth of these cells.

Brca1^{Δ11/Δ11} fibroblasts rapidly undergo senescence in culture. This phenotype can be rescued by the loss of *53bp1*⁹¹. *53BP1* loss also rescued the lethality of *Brca1*^{Δ11/Δ11} mice and while *Brca1*^{Δ11/Δ11}*p53*^{+/-} mice showed

signs of accelerated ageing at the age of seven months, *Brca1*^{Δ11/Δ11}*53bp1*^{-/-} mice did not⁹¹. Furthermore, the cancer incidence was also much lower in *Brca1*^{Δ11/Δ11}*53bp1*^{-/-} mice compared to *Brca1*^{Δ11/Δ11}*p53*^{+/-} mice.

In BRCA1-deficient cells, in the absence of functional homologous recombination, breaks are aberrantly joined via non-homologous end joining. This is dependent on 53BP1 and DNA ligase IV^{92,93}. In the absence of 53BP1, ATM-dependent processing of DNA breaks is stimulated, resulting in restoration of homologous recombination⁹². Additionally, 53BP1 loss abrogates the ATM-dependent G2 checkpoint that is activated upon DNA double strand break damage⁹³. Deletion of DNA ligase IV does not rescue HR in BRCA1-deficient cells⁹² and although 53BP1 loss rescues HR in BRCA1-deficient cells, this seems to be a specific effect. 53BP1 loss does not rescue BRCA2-deficiency⁹³, XRCC2-deficiency⁹² or CtIP-deficiency⁸³.

BRCA1 and PARP inhibitors

Women carrying heterozygous germ line mutations in the tumour-suppressor genes BRCA1 and BRCA2 have a strongly increased lifetime risk of developing breast and ovarian cancer⁹⁴. In the absence of functional HR the use of other error-prone DNA repair mechanisms can lead to chromosomal aberrations and can enhance tumorigenesis⁹⁵.

Women with breast cancer are commonly treated with chemotherapy. These chemotherapeutics have severe side effects because they target all dividing cells in the patient's body. Recently a new treatment strategy has been developed, targeting specifically the tumour cells with a defect in homologous recombination^{96,97} and thereby reducing side effects⁹⁵. Cells deficient in homologous recombination are extremely sensitive to inhibition of the enzyme PARP1.

The extreme sensitivity of HR-deficient cells to PARP inhibition is an excellent example of synthetic lethality. Synthetic lethality describes a situation where a defect or mutation in only one of two separate genes is compatible with life, but the combination

of the defects results in lethality. This defect can be genetic, but it can also be induced by drugs, as is the case for PARP inhibitors.

Several mechanisms probably contribute to the synthetic lethality of PARP inhibitors in BRCA1- and BRCA2-deficient cells. Firstly, the inhibition of PARP1 leads to decreased repair of single-strand breaks. At these single-strand breaks replication forks collapse and their repair requires functional homologous recombination. In the absence of HR, damage is thought to accumulate or to be repaired via error-prone repair mechanism, resulting in cell death. However, Patel et al. showed that the synthetic lethal interaction between PARP inhibitors and HR does not depend on the essential BER protein XRCC1⁹⁸. Therefore, plain inhibition of BER is not sufficient to kill HR-deficient cells and other mechanisms are probably at play as well.

Secondly, it has been postulated that PARP inhibitors trap the PARP enzyme on DNA, blocking access of other DNA repair enzymes. PARP inhibitors such as Olaparib, Niraparib, Veliparib and BMN673 are generally small molecule inhibitors that mimic the PARP1 cofactor β-NAD⁺ and bind to the catalytic site in PARP1⁹⁵. PARP1 catalyses the PARylation of various substrates, including itself (auto-PARylation). This auto-PARylation increases the negative charge on the enzyme, eventually resulting in its release from DNA⁹⁹. Upon inhibition of its enzymatic activity, PARP would no longer be able to release itself from DNA. This process could contribute to the cytotoxicity of PARP inhibitors in both HR-proficient and deficient cells.

NHEJ is probably also involved in PARP inhibitor mediated cell killing in HR-deficient cells. Collapsed replication forks result in one-ended DNA double strand breaks that should not be repaired via NHEJ, since this leads to chromosomal rearrangements and is toxic. The combination of a DNA-PK inhibitor and a PARP inhibitor reduces the hypersensitivity of BRCA1- and BRCA2-deficient cells to PARP inhibitors and decreased the number of PARP inhibitor induced chromosomal aberrations⁹⁸.

Resistance to PARP inhibitors

The treatment of BRCA1- and BRCA2-deficient tumours with PARP inhibitors is very promising, but unfortunately most tumours eventually become resistant^{95,100}. Identification of these mechanisms of resistance is important for patient selection and the identification of biomarkers. Additionally, knowledge of the mechanisms will help to select treatment strategies for resistant tumours.

A pharmacological cause of resistance is overexpression of the P-glycoprotein efflux pump¹⁰¹. The PgP-efflux pump is a multi-drug transporter that simply pumps small molecules such as olaparib out of the cells, resulting in a lower toxicity. This mechanism of resistance was observed in a genetically engineered mouse model (GEMM) for BRCA1-associated breast cancer. Tumours initially responded to treatment with the PARP inhibitor Olaparib (AZD2281), but eventually became resistant. The resistance could be overcome by using the P-glycoprotein inhibitor Tariquidar¹⁰¹ or using a PARP inhibitor that is a poor PgP substrate, such as

AZD2461¹⁰². When the P-glycoprotein efflux pump is genetically inactivated, tumours respond to PARP inhibitors for a longer period, but still become resistant eventually¹⁰². This indicates that there are other mechanisms of resistance at play as well.

Most pathogenic mutations in BRCA1 and BRCA2 result in a frame shift or a premature stop and expression of a truncated or non-functional protein. One of the main genetic mechanisms of resistance is reversion of the BRCA mutation or an internal deletion. These new mutations result in restoration of the reading frame and expression of a functional protein. Since there is no longer a defect in HR, these tumours are resistant to PARP inhibitors. This mechanism of resistance has been shown to occur in BRCA2-deficient CAPAN-1 cells and can also occur in response to cisplatin in BRCA- mutated ovarian cancers in patients whose tumours have become resistant to cisplatin treatment^{103,104}. Norquist et al. showed that these secondary mutations arise in hereditary ovarian carcinomas after cisplatin treatment and that they also confer resistance to PARP inhibitors¹⁰⁵. In that study

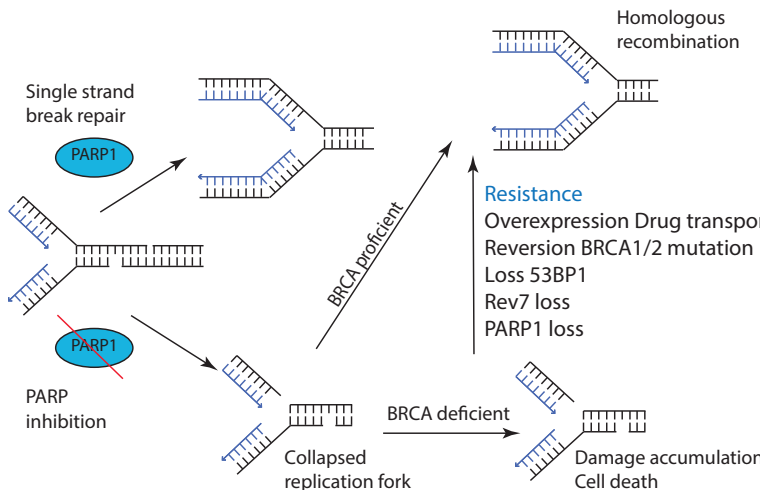


Figure 8 PARP inhibitors

Single-strand breaks occur spontaneously and are repaired efficiently by single-strand break repair. If PARP enzymes are blocked by a PARP inhibitor, single-strand breaks are repaired less efficiently and may remain open when the DNA is replicated in S-phase. When a replication forks runs into a single-strand break, the fork collapses. Homologous recombination is required to restart the replication fork. In BRCA1-deficient tumours, homologous recombination is impaired, resulting in accumulation of damage and eventually cell death. BRCA1-deficient cell and tumours can become resistant to PARP inhibitors via several mechanisms.

six patients were first treated with cisplatin and then with PARP inhibitors. So far, this is the only mechanism of resistance that has been demonstrated to occur in patients.

Another genetic mechanism of resistance that does not depend on restoration of BRCA1 or BRCA2 protein expression but still leads to restoration of HR is the loss of 53BP1. *Brca1^{Δ11/Δ11}53bp1^{-/-}* cells are not hypersensitive to PARP inhibition while *Brca1^{Δ11/Δ11}* MEFs are hypersensitive to the drug⁹². Loss of 53BP1 in BRCA1-deficient cells results in an almost complete restoration of homologous recombination. BRCA1-deficient cells are unable to form RAD51 foci after damage (described above), but after deletion of 53BP1, cells can form RAD51 foci to a similar extent as wild-type cells^{92,93}. Also genotargeting⁹³, sister chromatid exchange and HR as measured via the DR-GFP assay⁹² were increased in BRCA1 and 53BP1-deficient cells compared to BRCA1-deficient cells. Addition of an ATM inhibitor resensitized *Brca1^{Δ11/Δ11}53bp1^{-/-}* cells to PARP inhibition, because 53BP1 loss restores ATM-dependent RPA phosphorylation levels back to wild-type levels⁹². Jaspers et al. showed that in a fraction of cases (3 out of 11), 53BP1 loss occurs as a mechanism of resistance in mice bearing mammary tumours from *K14cre;Brca1^{F/F};p53^{F/F};Mdr1a/b^{-/-}* mice, a model for breast cancer in which the P-glycoprotein efflux pump is genetically inactivated (*Mdr1a/b^{-/-}*)¹⁰².

It thus seems that restoration or increase of resection is an important mechanism of resistance. This hypothesis is further supported by the finding that expression of a phospho-mimicking mutant of CtIP that is constitutively active (CtIP-T847E) is able to rescue the sensitivity to PARP inhibitors in BRCA1-deficient cells⁸³.

In vitro loss of PARP1 has also been observed as a mechanism of resistance in haploid cells that were not HR-deficient¹⁰⁶. This mechanism is less likely to occur in HR-deficient cells, because PARP1 loss decreases survival⁹⁷. However, after restoration of HR by another resistance mechanism, PARP1 loss may be beneficial.

BRCA2

Wooster et al. identified the locus of the second breast cancer susceptibility gene in 1994⁹⁴ and few years later it was discovered that BRCA2 is required for HR and thereby maintenance of chromosomal stability^{107,108}. BRCA2 also plays a role in the loading of RAD51¹⁰⁹ during meiotic recombination and via the meiosis specific recombinase DMC1¹¹⁰.

BRCA2 consist of a largely unexplored N-terminal domain, a middle domain which contains BRC repeats that interact with RAD51¹¹¹ and a large C-terminal domain. PALB2 interacts with BRCA2 at the N-terminal part, but the structure of this domain is still unknown. The C-terminal domain contains the DNA-binding domain (DBD), which consists of three OB-folds and a helical domain¹¹². FANCD2 and HSF2BP interact with BRCA2 in the C-terminal region.

The main function of BRCA2 in homologous recombination is to load RAD51 on the single-stranded DNA, replacing RPA. BRCA2 interacts with RAD51¹¹³ via its BRC repeats¹¹⁴. Loss of BRCA2 results in mislocalization of RAD51 in the cytoplasm, indicating that BRCA2 is required to keep RAD51 in the nucleus¹¹⁴. Upon DNA damage such as ionizing radiation, RAD51 and BRCA2 colocalize in nuclear foci¹¹⁵.

PALB2 interacts with BRCA1 as well as BRCA2 and all three proteins colocalize in nuclear foci together with RAD51^{79,80}. PALB2 promotes stable nuclear localization and accumulation of BRCA2 and interacts with BRCA2 via its C-terminal WD40 domain¹¹⁶. In the absence of PALB2, BRCA2 foci formation is decreased⁷⁹. The interaction between PALB2 and BRCA2 is also important for tumour suppression, since several pathogenic mutations in BRCA2 disrupt the interaction with PALB2⁷⁹. Furthermore, mutations in PALB2 predispose to breast and pancreatic cancer¹¹⁷. Other functions of PALB2 in the DNA damage response are reviewed by Park et al.¹¹⁶.

BRCA2 also interacts with FANCD2, an

important player in the Fanconi Anemia pathway. BRCA2 and FANCD2 are in a complex that also contains FANCG and XRCC3¹¹⁸. In the BRCA2-mutated cell line CAPAN-1, FANCD2 still forms nuclear foci upon damage, indicating that the interaction between BRCA2 and FANCD2 is not required for the recruitment of FANCD2 to sites of damage¹¹⁹. Reciprocally, the absence of FANCD2 has little effect on HR and RAD51 foci formation¹²⁰.

Cell lines and phenotype

Cell lines expressing truncated BRCA2 proteins show decreased proliferation that worsens over time. This proliferation defect is associated with cell cycle arrest in G1 and G2/M and increased p21 and p53 expression¹²¹. The most studied BRCA2-deficient cell line is CAPAN-1. In this pancreatic cancer derived cell line one wild-type copy of BRCA2 is lost, while the other has a 6174delT mutation, which results in a truncation at amino acid 1982^{122,123}.

BRCA2-deficient cells are hypersensitive to DNA damaging agents such as UV, IR, MMS, MMC and PARP inhibitors^{96,97,113,121,124}. Since BRCA2 is essential for recombination, BRCA2-mutated cells lines such as CAPAN-1 display decreased homology directed repair as measured by the DR-GFP assay¹⁰⁷ and a homologous plasmid-targeting frequency assay¹²⁵. Furthermore, BRCA2-deficient cells are unable to form RAD51 foci¹⁰⁸.

Also for BRCA2, several different (conditional) mouse models have been created⁸⁷. BRCA2 deficiency is embryonically lethal and development of the embryo arrests after 6.5 days of gestation¹¹³. As for BRCA1, the phenotype of BRCA2 nullizygous mice is less severe in a p53 null background⁸⁸. However, even in a p53 null background no mice are born. Additionally, BRCA2 deficiency can not be rescued by deletion of 53BP1⁹³.

BRCA2 and the Fanconi Anemia pathway

Fanconi Anemia (FA) is a rare genetic disease characterized by congenital skeletal and renal anomalies, growth retardation, haematological abnormalities, bone marrow

failure and predisposition to a variety of cancers^{58,126}. The Fanconi Anemia pathway repairs interstrand crosslinks and cells from FA patients are hypersensitive to interstrand crosslinking agents such as MMC. Classically, FA was diagnosed by exposing patient cells to these agents, which results in increased levels of chromosomal aberrations compared to cells from a healthy control. Additionally, complementation studies were performed to distinguish between different FA subtypes. To date, 16 FA complementation groups have been described (FANCA, FANCB, FANCC, FANCD1, FANCD2, FANCE, FANCF, FANCG, FANCI, FANCI, FANCL, FANCM, FANCN, FANCO, FANCP and FANCO)^{126,127}. Different FA complementation groups differ in their causative mutations and severity of the disease. FANCA, FANCB, FANCC, FANCE, FANCF, FANCG, FANCL, and FANCM together form the FA core complex that ubiquitinates FANCD2 and FANCI and mutations in these genes account for approximately 90% of the patients¹²⁸.

To repair DNA interstrand crosslinks, both HR and the FA pathway are required and mutations in several HR proteins also give an FA-phenotype. For example FANCI is BRIP1/BACH1^{129,130} and FANCO is RAD51C^{131,132}.

Heterozygous mutations in *BRCA2* predispose to breast and ovarian cancer, but patients with certain homozygous mutations suffer from Fanconi Anemia (complementation group D1¹³³). *BRCA1*^{-/-} and *BRCA2*^{-/-} tumour cells are hypersensitive to MMC, similar to FA patient cells. Howlett et al. sequenced *BRCA1* and *BRCA2* in FA-B and FA-D1 patients cells and identified homozygous *BRCA2* mutations in two FA-D1 patient cell lines and two unclassified lines¹³³.

Mutations in BRCA2 partner PALB2 also cause Fanconi Anemia. Xia et al.¹³⁴ started from an unclassified FA line (EUFA1341) that showed normal FANCD2 ubiquitination and no mutations in the then known downstream proteins BRCA2 and FANCI. The individual was classified as a new FA complementation group FANCN. Western Blot analysis showed the absence of PALB2 and re-expression

of PALB2 in EUFA1341 rescued the MMC sensitivity¹³⁴. Reid et al identified PALB2 mutations in seven families affected with Fanconi Anemia¹³⁵.

Scope of this thesis

DNA repair pathways are essential for the maintenance of a healthy genome. Mutations in proteins involved in DNA repair can lead, on a cellular level, to increased numbers of mutations and chromosomal aberrations and eventually oncogenic transformation. On a the scale of a whole human, defective DNA repair proteins can cause syndromes such as Fanconi Anemia or predispose to certain types of cancer.

Excessive amounts of DNA damage can be used to treat cancer. Tumours can be treated with ionizing radiation, which causes single and double strand breaks or with interstrand crosslinking chemotherapeutics such as Mitomycin C. There are also targeted treatments available that are very effective against cancer cells with for example defective homologous recombination. These targeted treatments are very promising, since the side effects are less severe than for conventional chemotherapy. Unfortunately cancer cells can become resistant to these drugs by rerouting DNA repair pathways, genetic reversion of mutations or other mechanisms. Understanding how DNA repair mechanisms works on a molecular level can help to prevent and treat cancer. To increase our knowledge on the details of DNA repair mechanisms, we set out to identify mechanism of resistance to PARP inhibitors in the first part of this thesis and and to identify new interactors of BRCA2 in the second part.

Chapter 1 introduces the main DNA repair pathways and their function. This knowledge is important to understand the interplay between pathways. Damaged DNA can be a substrate for different pathways and then competition takes place, while in other cases several repair pathways are required to repair a lesion. For most pathways it is well known how they work, but the interaction between

pathways is still a largely unexplored area. Many proteins are also involved in multiple DNA repair pathways or have numerous functions in one pathway. The introduction focuses on BRCA1 and BRCA2 because these are main players in the subsequent chapters.

The balance between repair pathways is important for genomic stability. In **chapter 2** we review what is known about the balance between the DNA double strand break repair pathways homologous recombination and non-homologous end joining. Additionally, several assays are described that can be used to measure the activity of these pathways. Therapeutic strategies to exploit a disturbed balance are discussed as well.

Cells with mutations in the homologous recombination proteins BRCA1 are extremely sensitive to inhibition of the enzyme PARP1, which is required for the efficient repair of DNA single-strand breaks. In **chapter 3** we investigate how BRCA1-deficient cells can become resistant to treatment with PARP inhibitors. We show that loss of Rev7 leads to restoration of homologous recombination and thereby PARP inhibitor resistance. In **chapter 4** we continue this research to find out how this resistance mechanism works on a molecular level. REV7 plays a role in cell cycle progression, translesion synthesis and several other processes and we investigate which REV7 function is important in mediating PARP inhibitor resistance.

In **chapter 5** we identify a new interaction partner of BRCA2: HSF2BP. Overexpression of this protein gives a phenotype that is similar to that of cells from patients suffering from Fanconi Anemia. Upon overexpression of HSF2BP the cells become very sensitive to the chemotherapeutic Mitomycin C and show increased chromosomal aberrations after exposure to this drug. Finally we map the domain of BRCA2 that interacts with HSF2BP.

Chapter 6 discusses the findings described in this thesis as well as implications for the future of cancer research.

References

1. Hoeijmakers, J. H. Genome maintenance mechanisms for preventing cancer. *Nature* 411, 366–374 (2001).
2. Masutani, C. et al. Purification and cloning of a nucleotide excision repair complex involving the xeroderma pigmentosum group C protein and a human homologue of yeast RAD23. *EMBO J.* 13, 1831–43 (1994).
3. Nishi, R. et al. Centrin 2 stimulates nucleotide excision repair by interacting with xeroderma pigmentosum group C protein. *Mol. Cell. Biol.* 25, 5664–5674 (2005).
4. Wakasugi, M. et al. DDB accumulates at DNA damage sites immediately after UV irradiation and directly stimulates nucleotide excision repair. *J. Biol. Chem.* 277, 1637–1640 (2002).
5. Scrima, A. et al. Structural Basis of UV DNA-Damage Recognition by the DDB1-DDB2 Complex. *Cell* 135, 1213–1223 (2008).
6. Nakazawa, Y. et al. Mutations in UVSSA cause UV-sensitive syndrome and impair RNA polymerase II processing in transcription-coupled nucleotide-excision repair. *Nat Genet* 44, 586–592 (2012).
7. Schwertman, P. et al. UV-sensitive syndrome protein UVSSA recruits USP7 to regulate transcription-coupled repair. *Nature Genetics* 44, 598–602 (2012).
8. Zhang, X. et al. Mutations in UVSSA cause UV-sensitive syndrome and destabilize ERCC6 in transcription-coupled DNA repair. *Nature Genetics* 44, 593–597 (2012).
9. Marteijn, J. A., Lans, H., Vermeulen, W. & Hoeijmakers, J. H. J. Understanding nucleotide excision repair and its roles in cancer and ageing. *Nat Rev Mol Cell Biol* 15, 465–481 (2014).
10. Tapias, A. et al. Ordered Conformational Changes in Damaged DNA Induced by Nucleotide Excision Repair Factors. *J. Biol. Chem.* 279, 19074–19083 (2004).
11. Compe, E. & Egly, J.-M. TFIIH: when transcription met DNA repair. *Nature Reviews Molecular Cell Biology* 13, 476–476 (2012).
12. Camenisch, U., Dip, R., Schumacher, S. B., Schuler, B. & Naegeli, H. Recognition of helical kinks by xeroderma pigmentosum group A protein triggers DNA excision repair. *Nat. Struct. Mol. Biol.* 13, 278–284 (2006).
13. Fagbemi, A. F., Orelli, B. & Schärer, O. D. Regulation of endonuclease activity in human nucleotide excision repair. *DNA Repair* 10, 722–729 (2011).
14. Robertson, A. B., Klungland, A., Rognes, T. & Leiros, I. DNA repair in mammalian cells: Base excision repair: the long and short of it. *Cell. Mol. Life Sci.* 66, 981–993 (2009).
15. Fishel, R. et al. The human mutator gene homolog MSH2 and its association with hereditary nonpolyposis colon cancer. *Cell* 75, 1027–1038 (1993).
16. Leach, F. S. et al. Mutations of a mutS homolog in hereditary nonpolyposis colorectal cancer. *Cell* 75, 1215–1225 (1993).
17. Bak, S. T., Sakellariou, D. & Pena-diaz, J. Title : The dual nature of mismatch repair as antimutator and mutator : for better or for worse. 5, 1–12 (2014).
18. Hsieh, P. & Yamane, K. DNA mismatch repair: Molecular mechanism, cancer, and ageing. *Mech. Ageing Dev.* 129, 391–407 (2008).
19. McKinnon, P. J. & Caldecott, K. W. DNA strand break repair and human genetic disease. *Annu. Rev. Genomics Hum. Genet.* 8, 37–55 (2007).
20. Pines, A., Mullenders, L. H., van Attikum, H. & Luijsterburg, M. S. Touching base with PARPs: Moonlighting in the repair of UV lesions and double-strand breaks. *Trends in Biochemical Sciences* 38, 321–330 (2013).
21. Ménissier de Murcia, J. et al. Functional interaction between PARP-1 and PARP-2 in chromosome stability and embryonic development in mouse. *EMBO J.* 22, 2255–2263 (2003).
22. Shall, S. & De Murcia, G. Poly(ADP-ribose) polymerase-1: What have we learned from the deficient mouse model? *Mutation Research - DNA Repair* 460, 1–15 (2000).
23. Mullins, D. W., Giri, C. P. & Smulson, M. Poly(adenosine diphosphate-ribose) polymerase: the distribution of a chromosome-associated enzyme within the chromatin substructure. *Biochemistry* 16, 506–513 (1977).
24. Langelier, M.-F., Planck, J. L., Roy, S. & Pascal, J. M. Structural Basis for DNA Damage-Dependent Poly(ADP-ribosylation) by Human PARP-1. *Science* 336, 728–732 (2012).
25. Fisher, A. E. O., Hohegger, H., Takeda, S. & Caldecott, K. W. Poly(ADP-ribose) polymerase 1 accelerates single-strand break repair in concert with poly(ADP-ribose) glycohydrolase. *Mol. Cell. Biol.* 27, 5597–5605 (2007).
26. Hohegger, H. et al. Parp-1 protects homologous recombination from interference by Ku and Ligase IV in vertebrate cells. *EMBO J.* 25, 1305–1314 (2006).
27. Bryant, H. E. et al. PARP is activated at stalled forks to mediate Mre11-dependent replication restart and recombination. *EMBO J.* 28, 2601–2615 (2009).
28. Rulten, S. L. et al. PARP-3 and APLF function together to accelerate nonhomologous end-joining. *Mol. Cell* 41, 33–45 (2011).
29. Boehler, C. et al. Poly(ADP-ribose) polymerase 3 (PARP3), a newcomer in cellular response to DNA damage and mitotic progression. *Proc. Natl. Acad. Sci. U. S. A.* 108, 2783–2788 (2011).
30. Min, W. K., Cortes, U., Herceg, Z., Tong, W. M. & Wang, Z. Q. Deletion of the nuclear isoform of poly(ADP-ribose) glycohydrolase (PARG) reveals its function in DNA repair, genomic stability and tumorigenesis. *Carcinogenesis* 31, 2058–2065 (2010).
31. Brandsma, I. & van Gent, D. C. Pathway choice in DNA double strand break repair: observations of a balancing act. *Genome Integr.* 3, 9 (2012).
32. Wyman, C. & Kanaar, R. DNA double-strand break repair: all's well that ends well. *Annu. Rev. Genet.* 40, 363–383 (2006).
33. Heyer, W.-D., Ehmsen, K. T. & Liu, J. Regulation of homologous recombination in eukaryotes. *Annu. Rev. Genet.* 44, 113–139 (2010).
34. Stracker, T. H. & Petrini, J. H. J. The MRE11 complex:

starting from the ends. *Nat. Rev. Mol. Cell Biol.* 12, 90–103 (2011).

35. Limbo, O. et al. Ctp1 Is a Cell-Cycle-Regulated Protein that Functions with Mre11 Complex to Control Double-Strand Break Repair by Homologous Recombination. *Mol. Cell* 28, 134–146 (2007).
36. Sartori, A. A. et al. Human CtIP promotes DNA end resection. *Nature* 450, 509–514 (2007).
37. Lieber, M. R. The mechanism of double-strand DNA break repair by the nonhomologous DNA end-joining pathway. *Annu. Rev. Biochem.* 79, 181–211 (2010).
38. Ahnesorg, P., Smith, P. & Jackson, S. P. XLF interacts with the XRCC4-DNA Ligase IV complex to promote DNA nonhomologous end-joining. *Cell* 124, 301–313 (2006).
39. Buck, D. et al. Cernunnos, a novel nonhomologous end-joining factor, is mutated in human immunodeficiency with microcephaly. *Cell* 124, 287–299 (2006).
40. Ochi, T. et al. DNA repair. PAXX, a paralog of XRCC4 and XLF, interacts with Ku to promote DNA double-strand break repair. *Science* 347, 185–188 (2015).
41. Xing, M. et al. Interactome analysis identifies a new paralogue of XRCC4 in non-homologous end joining DNA repair pathway. *Nat. Commun.* 6, 1–12 (2015).
42. Difilippantonio, M. J. et al. DNA repair protein Ku80 suppresses chromosomal aberrations and malignant transformation. *Nature* 404, 510–514 (2000).
43. Gao, Y. et al. Interplay of p53 and DNA-repair protein XRCC4 in tumorigenesis, genomic stability and development. *Nature* 404, 897–900 (2000).
44. Gu, Y., Jin, S., Gao, Y., Weaver, D. T. & Alt, F. W. Ku70-deficient embryonic stem cells have increased ionizing radiosensitivity, defective DNA end-binding activity, and inability to support V(D)J recombination. *Proc. Natl. Acad. Sci. U. S. A.* 94, 8076–8081 (1997).
45. Woodbine, L., Gennery, A. R. & Jeggo, P. A. The clinical impact of deficiency in DNA non-homologous end-joining. *DNA Repair (Amst.)* 17, 9–20 (2014).
46. Chang, D. J. & Cimprich, K. A. DNA damage tolerance: when it's OK to make mistakes. *Nat. Chem. Biol.* 5, 82–90 (2009).
47. Sharma, S., Helchowski, C. M. & Canman, C. E. The roles of DNA polymerase ζ and the Y family DNA polymerases in promoting or preventing genome instability. *Mutation Research - Fundamental and Molecular Mechanisms of Mutagenesis* 743–744, 97–110 (2013).
48. Sale, J. E., Lehmann, A. R. & Woodgate, R. Y-family DNA polymerases and their role in tolerance of cellular DNA damage. *Nat. Rev. Mol. Cell Biol.* 13, 141–152 (2012).
49. Lee, Y.-S., Gregory, M. T. & Yang, W. Human Pol ζ purified with accessory subunits is active in translesion DNA synthesis and complements Pol η in cisplatin bypass. *Proc. Natl. Acad. Sci. U. S. A.* 111, 2954–9 (2014).
50. Moldovan, G. L., Pfander, B. & Jentsch, S. PCNA, the Maestro of the Replication Fork. *Cell* 129, 665–679 (2007).
51. Hoegel, C., Pfander, B., Moldovan, G.-L., Pyrowolakis, G. & Jentsch, S. RAD6-dependent DNA repair is linked to modification of PCNA by ubiquitin and SUMO. *Nature* 419, 135–141 (2002).
52. Davies, A. A., Huttner, D., Daigaku, Y., Chen, S. & Ulrich, H. D. Activation of Ubiquitin-Dependent DNA Damage Bypass Is Mediated by Replication Protein A. *Mol. Cell* 29, 625–636 (2008).
53. Ulrich, H. D. Regulating post-translational modifications of the eukaryotic replication clamp PCNA. *DNA Repair* 8, 461–469 (2009).
54. Yang, W. & Woodgate, R. What a difference a decade makes: insights into translesion DNA synthesis. *Proc. Natl. Acad. Sci. U. S. A.* 104, 15591–15598 (2007).
55. Gan, G. N., Wittschieben, J. P., Wittschieben, B. Ø. & Wood, R. D. DNA polymerase zeta (pol zeta) in higher eukaryotes. *Cell Res.* 18, 174–183 (2008).
56. Makarova, A. V & Burgers, P. M. Eukaryotic DNA polymerase Zeta. *DNA Repair (Amst.)* XXX, XXX (2015).
57. Kunkel, T. A. Balancing eukaryotic replication asymmetry with replication fidelity. *Current Opinion in Chemical Biology* 15, 620–626 (2011).
58. Clauson, C., Schärer, O. D. & Niedernhofer, L. Advances in understanding the complex mechanisms of DNA interstrand cross-link repair. *Cold Spring Harb Perspect Biol* 5, a012732 (2013).
59. Kim, H. & D'Andrea, A. D. Regulation of DNA cross-link repair by the Fanconi anemia/BRCA pathway. *Genes and Development* 26, 1393–1408 (2012).
60. Zou, L. & Elledge, S. J. Sensing DNA damage through ATRIP recognition of RPA-ssDNA complexes. *Science* 300, 1542–1548 (2003).
61. Andreassen, P. R., D'Andrea, A. D. & Taniguchi, T. ATR couples FANCD2 monoubiquitination to the DNA-damage response. *Genes Dev.* 18, 1958–1963 (2004).
62. Smogorzewska, A. et al. Identification of the FANCI Protein, a Monoubiquitinated FANCD2 Paralog Required for DNA Repair. *Cell* 129, 289–301 (2007).
63. McCabe, K. M. et al. ERCC1 is required for FANCD2 focus formation. *Mol. Genet. Metab.* 95, 66–73 (2008).
64. Bhagwat, N. et al. XPF-ERCC1 participates in the Fanconi anemia pathway of cross-link repair. *Mol. Cell Biol.* 29, 6427–6437 (2009).
65. Sato, K. et al. Histone chaperone activity of Fanconi anemia proteins, FANCD2 and FANCI, is required for DNA crosslink repair. *The EMBO Journal* 31, 3524–3536 (2012).
66. Kitao, H. et al. Functional interplay between BRCA2/FancD1 and FancC in DNA repair. *J. Biol. Chem.* 281, 21312–21320 (2006).
67. Long, D. T., Räschle, M., Joukov, V. & Walter, J. C. Mechanism of RAD51-dependent DNA interstrand cross-link repair. *Science* 333, 84–87 (2011).
68. Nijman, S. M. B. et al. The deubiquitinating enzyme USP1 regulates the fanconi anemia pathway. *Mol. Cell* 17, 331–339 (2005).
69. Cohn, M. A. et al. A UAF1-Containing Multisubunit Protein Complex Regulates the Fanconi Anemia Pathway. *Mol. Cell* 28, 786–797 (2007).
70. Miki, Y. et al. A strong candidate for the breast and ovarian cancer susceptibility gene BRCA1. *Science*

- 266, 66–71 (1994).
71. Hall, J. M. et al. Linkage of early-onset familial breast cancer to chromosome 17q21. *Science* 250, 1684–1689 (1990).
 72. Wu, L. C. et al. Identification of a RING protein that can interact in vivo with the BRCA1 gene product. *Nat. Genet.* 14, 430–440 (1996).
 73. Hashizume, R. et al. The RING Heterodimer BRCA1-BARD1 Is a Ubiquitin Ligase Inactivated by a Breast Cancer-derived Mutation. *J. Biol. Chem.* 276, 14537–14540 (2001).
 74. Wu-Baer, F., Lagrazon, K., Yuan, W. & Baer, R. The BRCA1/BARD1 heterodimer assembles polyubiquitin chains through an unconventional linkage involving lysine residue K6 of ubiquitin. *J. Biol. Chem.* 278, 34743–34746 (2003).
 75. Scully, R. et al. Dynamic changes of BRCA1 subnuclear location and phosphorylation state are initiated by DNA damage. *Cell* 90, 425–435 (1997).
 76. Thomas, J. E., Smith, M., Tonkinson, J. L., Rubinfeld, B. & Polakis, P. Induction of phosphorylation on BRCA1 during the cell cycle and after DNA damage. *Cell Growth Differ.* 8, 801–809 (1997).
 77. Scully, R. et al. Association of BRCA1 with Rad51 in mitotic and meiotic cells. *Cell* 88, 265–275 (1997).
 78. Moynahan, M. E., Chiu, J. W., Koller, B. H. & Jasint, M. Brca1 controls homology-directed DNA repair. *Mol. Cell* 4, 511–518 (1999).
 79. Xia, B. et al. Control of BRCA2 Cellular and Clinical Functions by a Nuclear Partner, PALB2. *Mol. Cell* 22, 719–729 (2006).
 80. Sy, S. M. H., Huen, M. S. Y. & Chen, J. PALB2 is an integral component of the BRCA complex required for homologous recombination repair. *Proc. Natl. Acad. Sci. U. S. A.* 106, 7155–7160 (2009).
 81. Zhang, F., Bick, G., Park, J.-Y. & Andreassen, P. R. MDC1 and RNF8 function in a pathway that directs BRCA1-dependent localization of PALB2 required for homologous recombination. *J. Cell Sci.* 125, 6049–57 (2012).
 82. Yu, X. & Chen, J. DNA damage-induced cell cycle checkpoint control requires CtIP, a phosphorylation-dependent binding partner of BRCA1 C-terminal domains. *Mol. Cell Biol.* 24, 9478–9486 (2004).
 83. Polato, F. et al. CtIP-mediated resection is essential for viability and can operate independently of BRCA1. *J. Exp. Med.* 211, 1027–1036 (2014).
 84. Reczek, C. R., Szabolcs, M., Stark, J. M., Ludwig, T. & Baer, R. The interaction between CtIP and BRCA1 is not essential for resection-mediated DNA repair or tumor suppression. *J. Cell Biol.* 201, 693–707 (2013).
 85. Cruz-García, A., López-Saavedra, A. & Huertas, P. BRCA1 Accelerates CtIP-Mediated DNA-End Resection. *Cell Rep.* 9, 451–459 (2014).
 86. Huertas, P. DNA resection in eukaryotes: deciding how to fix the break. *Nat. Struct. Mol. Biol.* 17, 11–16 (2010).
 87. Evers, B. & Jonkers, J. Mouse models of BRCA1 and BRCA2 deficiency: past lessons, current understanding and future prospects. *Oncogene* 25, 5885–5897 (2006).
 88. Ludwig, T., Chapman, D. L., Papaioannou, V. E. & Estratiadis, A. Targeted mutations of breast cancer susceptibility gene homologs in mice: Lethal phenotypes of Brca1, Brca2, Brca1/Brca2, Brca1/p53, and Brca2/p53 nullizygous embryos. *Genes Dev.* 11, 1226–1241 (1997).
 89. Xu, X. et al. Genetic interactions between tumor suppressors Brca1 and p53 in apoptosis, cell cycle and tumorigenesis. *Nat. Genet.* 28, 266–271 (2001).
 90. Cao, L. et al. ATM-Chk2-p53 activation prevents tumorigenesis at an expense of organ homeostasis upon Brca1 deficiency. *EMBO J.* 25, 2167–2177 (2006).
 91. Cao, L. et al. A Selective Requirement for 53BP1 in the Biological Response to Genomic Instability Induced by Brca1 Deficiency. *Mol. Cell* 35, 534–541 (2009).
 92. Bunting, S. F. et al. 53BP1 inhibits homologous recombination in brca1-deficient cells by blocking resection of DNA breaks. *Cell* 141, 243–254 (2010).
 93. Bouwman, P. et al. 53BP1 loss rescues BRCA1 deficiency and is associated with triple-negative and BRCA-mutated breast cancers. *Nat. Struct. Mol. Biol.* 17, 688–695 (2010).
 94. Wooster, R. et al. Localization of a breast cancer susceptibility gene, BRCA2, to chromosome 13q12-13. *Science* 265, 2088–2090 (1994).
 95. Lord, C. J., Tutt, A. N. J. & Ashworth, A. Synthetic Lethality and Cancer Therapy: Lessons Learned from the Development of PARP Inhibitors. *Annu. Rev. Med.* 66, 455–470 (2015).
 96. Bryant, H. E. et al. Specific killing of BRCA2-deficient tumours with inhibitors of poly(ADP-ribose) polymerase. *Nature* 434, 913–917 (2005).
 97. Farmer, H. et al. Targeting the DNA repair defect in BRCA mutant cells as a therapeutic strategy. *Nature* 434, 917–921 (2005).
 98. Patel, A. G., Sarkaria, J. N. & Kaufmann, S. H. Non-homologous end joining drives poly(ADP-ribose) polymerase (PARP) inhibitor lethality in homologous recombination-deficient cells. *Proc. Natl. Acad. Sci. U. S. A.* 108, 3406–3411 (2011).
 99. De Lorenzo, S. B., Patel, A. G., Hurley, R. M. & Kaufmann, S. H. The Elephant and the Blind Men: Making Sense of PARP Inhibitors in Homologous Recombination Deficient Tumor Cells. *Front. Oncol.* 3, 228 (2013).
 100. Bouwman, P. & Jonkers, J. Molecular pathways: How can BRCA-mutated tumors become resistant to PARP inhibitors? *Clin. Cancer Res.* 20, 540–547 (2014).
 101. Rottenberg, S. et al. High sensitivity of BRCA1-deficient mammary tumors to the PARP inhibitor AZD2281 alone and in combination with platinum drugs. *Proc. Natl. Acad. Sci. U. S. A.* 105, 17079–17084 (2008).
 102. Jaspers, J. E. et al. Loss of 53BP1 causes PARP inhibitor resistance in BRCA1-mutated mouse mammary tumors. *Cancer Discov.* 3, 68–81 (2013).
 103. Edwards, S. L. et al. Resistance to therapy caused by intragenic deletion in BRCA2. *Nature* 451, 1111–1115 (2008).
 104. Sakai, W. et al. Secondary mutations as a mechanism of cisplatin resistance in BRCA2-mutated cancers.

Nature 451, 1116–1120 (2008).

105. Norquist, B. et al. Secondary somatic mutations restoring BRCA1/2 predict chemotherapy resistance in hereditary ovarian carcinomas. *J. Clin. Oncol.* 29, 3008–3015 (2011).
106. Pettitt, S. J. et al. A Genetic Screen Using the Piggy-Bac Transposon in Haploid Cells Identifies Parp1 as a Mediator of Olaparib Toxicity. *PLoS One* 8, 1–10 (2013).
107. Moynahan, M. E., Pierce, A. J. & Jasin, M. BRCA2 is required for homology-directed repair of chromosomal breaks. *Mol. Cell* 7, 263–272 (2001).
108. Tutt, A. et al. Mutation in Brca2 stimulates error-prone homology-directed repair of DNA double-strand breaks occurring between repeated sequences. *EMBO J.* 20, 4704–4716 (2001).
109. Sharan, S. K. et al. BRCA2 deficiency in mice leads to meiotic impairment and infertility. *Development* 131, 131–142 (2004).
110. Thorslund, T. & West, S. C. BRCA2: a universal recombinase regulator. *Oncogene* 26, 7720–7730 (2007).
111. Pellegrini, L. et al. Insights into DNA recombination from the structure of a RAD51-BRCA2 complex. *Nature* 420, 287–293 (2002).
112. Yang, H. et al. BRCA2 function in DNA binding and recombination from a BRCA2-DSS1-ssDNA structure. *Science* 297, 1837–1848 (2002).
113. Sharan, S. K. et al. Embryonic lethality and radiation hypersensitivity mediated by Rad51 in mice lacking Brca2. *Nature* 386, 804–810 (1997).
114. Davies, A. A. et al. Role of BRCA2 in control of the RAD51 recombination and DNA repair protein. *Mol. Cell* 7, 273–282 (2001).
115. Tarsounas, M., Davies, A. A. & West, S. C. RAD51 localization and activation following DNA damage. *Philos. Trans. R. Soc. Lond. B. Biol. Sci.* 359, 87–93 (2004).
116. Park, J. Y., Zhang, F. & Andreassen, P. R. PALB2: The hub of a network of tumor suppressors involved in DNA damage responses. *Biochimica et Biophysica Acta - Reviews on Cancer* 1846, 263–275 (2014).
117. Tischkowitz, M. & Xia, B. PALB2/FANCN: Recombining cancer and fanconi anemia. *Cancer Research* 70, 7353–7359 (2010).
118. Wilson, J. B. et al. FANCG promotes formation of a newly identified protein complex containing BRCA2, FANCD2 and XRCC3. *Oncogene* 27, 3641–3652 (2008).
119. Hussain, S. et al. Direct interaction of FANCD2 with BRCA2 in DNA damage response pathways. *Hum. Mol. Genet.* 13, 1241–1248 (2004).
120. Ohashi, A., Zdzienicka, M. Z., Chen, J. & Couch, F. J. Fanconi anemia complementation group D2 (FANCD2) functions independently of BRCA2- and RAD51-associated homologous recombination in response to DNA damage. *J. Biol. Chem.* 280, 14877–14883 (2005).
121. Patel, K. J. et al. Involvement of Brca2 in DNA repair. *Mol. Cell* 1, 347–357 (1998).
122. Goggins, M. et al. Germline BRCA2 gene mutations in patients with apparently sporadic pancreatic carcinomas. *Cancer Res.* 56, 5360–5364 (1996).
123. Chen, J. et al. Stable interaction between the products of the BRCA1 and BRCA2 tumor suppressor genes in mitotic and meiotic cells. *Mol. Cell* 2, 317–328 (1998).
124. Chen, P.-L. et al. The BRC repeats in BRCA2 are critical for RAD51 binding and resistance to methyl methanesulfonate treatment. *Proc. Natl. Acad. Sci. U. S. A.* 95, 5287–5292 (1998).
125. Xia, F. et al. Deficiency of human BRCA2 leads to impaired homologous recombination but maintains normal nonhomologous end joining. *Proc. Natl. Acad. Sci. U. S. A.* 98, 8644–8649 (2001).
126. Kee, Y. & D'Andrea, A. D. Molecular pathogenesis and clinical management of Fanconi anemia. *J. Clin. Invest.* 122, 3799–806 (2012).
127. Bogliolo, M. et al. Mutations in ERCC4, encoding the DNA-repair endonuclease XPF, cause Fanconi anemia. *Am. J. Hum. Genet.* 92, 800–806 (2013).
128. D'Andrea, A. D. Susceptibility pathways in Fanconi's anemia and breast cancer. *N. Engl. J. Med.* 362, 1909–1919 (2010).
129. Levitus, M. et al. The DNA helicase BRIP1 is defective in Fanconi anemia complementation group J. *Nat. Genet.* 37, 934–935 (2005).
130. Litman, R. et al. BACH1 is critical for homologous recombination and appears to be the Fanconi anemia gene product FANCI. *Cancer Cell* 8, 255–265 (2005).
131. Meindl, A. et al. Germline mutations in breast and ovarian cancer pedigrees establish RAD51C as a human cancer susceptibility gene. *Nat. Genet.* 42, 410–414 (2010).
132. Vaz, F. et al. Mutation of the RAD51C gene in a Fanconi anemia-like disorder. *Nature genetics* 42, 406–409 (2010).
133. Howlett, N. G. et al. Biallelic inactivation of BRCA2 in Fanconi anemia. *Science* 297, 606–609 (2002).
134. Xia, B. et al. Fanconi anemia is associated with a defect in the BRCA2 partner PALB2. *Nat. Genet.* 39, 159–161 (2007).
135. Reid, S. et al. Biallelic mutations in PALB2 cause Fanconi anemia subtype FA-N and predispose to childhood cancer. *Nat. Genet.* 39, 162–164 (2007).

Chapter 2

Pathway choice in DNA double strand break repair: observations of a balancing act

Genome Integrity 2012 Nov 27;3(1) p. 9

Inger Brandsma and Dik C. van Gent

Abstract

Proper repair of DNA double strand breaks (DSBs) is vital for the preservation of genomic integrity. There are two main pathways that repair DSBs, Homologous recombination (HR) and Non-homologous end-joining (NHEJ). HR is restricted to the S and G2 phases of the cell cycle due to the requirement for the sister chromatid as a template, while NHEJ is active throughout the cell cycle and does not rely on a template. The balance between both pathways is essential for genome stability and numerous assays have been developed to measure the efficiency of the two pathways. Several proteins are known to affect the balance between HR and NHEJ and the complexity of the break also plays a role. In this review we describe several repair assays to determine the efficiencies of both pathways. We discuss how disturbance of the balance between HR and NHEJ can lead to disease, but also how it can be exploited for cancer treatment.

Introduction

Genomic integrity and faithful replication are essential to prevent mutations and chromosomal rearrangements, which may otherwise lead to diseases and in some cases even death. DNA damage is generated by several different genotoxic agents such as reactive oxygen species, UV light from the sun and mutagenic chemicals¹. These agents cause many types of DNA damage, ranging from base damage to double strand breaks (DSBs). To protect the genome from the deleterious effects of these lesions, several mechanisms have evolved that detect and repair DNA damage. Together with mechanisms that regulate cell cycle progression and cell death pathways this is known as the DNA damage response (DDR).

In this review we concentrate on DSBs, which are among the most cytotoxic types of DNA damage. The therapeutic effect of several commonly used cancer treatment

modalities, such as ionizing radiation and the chemotherapeutic doxorubicin, are based on the cell killing effect of DSBs. However, DSBs are also the initiating lesion of disease-causing chromosomal translocations in cancer. Therefore, it is important to understand the intricate regulation of the DDR upon DSB formation. We mainly concentrate on the two main DSB repair pathways, Non-homologous end joining (NHEJ) and Homologous recombination (HR), with a special emphasis on the balance between both repair mechanisms in health and disease.

NHEJ

NHEJ is a relatively simple DSB repair pathway (Figure 1). Both ends of the break are first bound by the Ku70/Ku80 heterodimer, which then recruits the catalytic subunit of the DNA dependent protein kinase (DNA-PKcs)². If necessary, the ends can be trimmed by nucleases (such as Artemis) or filled in by DNA polymerases (such as Pol μ or Pol λ) to create compatible ends³. Finally, the ligation complex, consisting of DNA ligase IV, X-ray cross-complementation group 4 (XRCC4) and XRCC4 like factor (XLF)/Cernunnos ligates the ends^{4,5}. NHEJ can take place throughout the cell cycle. For an extensive review on NHEJ see³.

HR

HR uses a sequence similar or identical to the broken DNA as a template for accurate repair. The sister chromatid is used as an identical template in the S and G2 phases of the cell cycle, when the DNA has been replicated. HR is restricted to these cell cycle phases in higher eukaryotes to prevent recombination between (repetitive) non-identical sequences. Spurious HR can lead to loss of heterozygosity (when HR takes place between paternal and maternal chromosomes) or insertions/deletion (when repeats are not aligned properly).

The HR pathway starts with resection of the broken DNA ends (Figure 1) by the MRN-complex^{6,7}, together with CtBP-

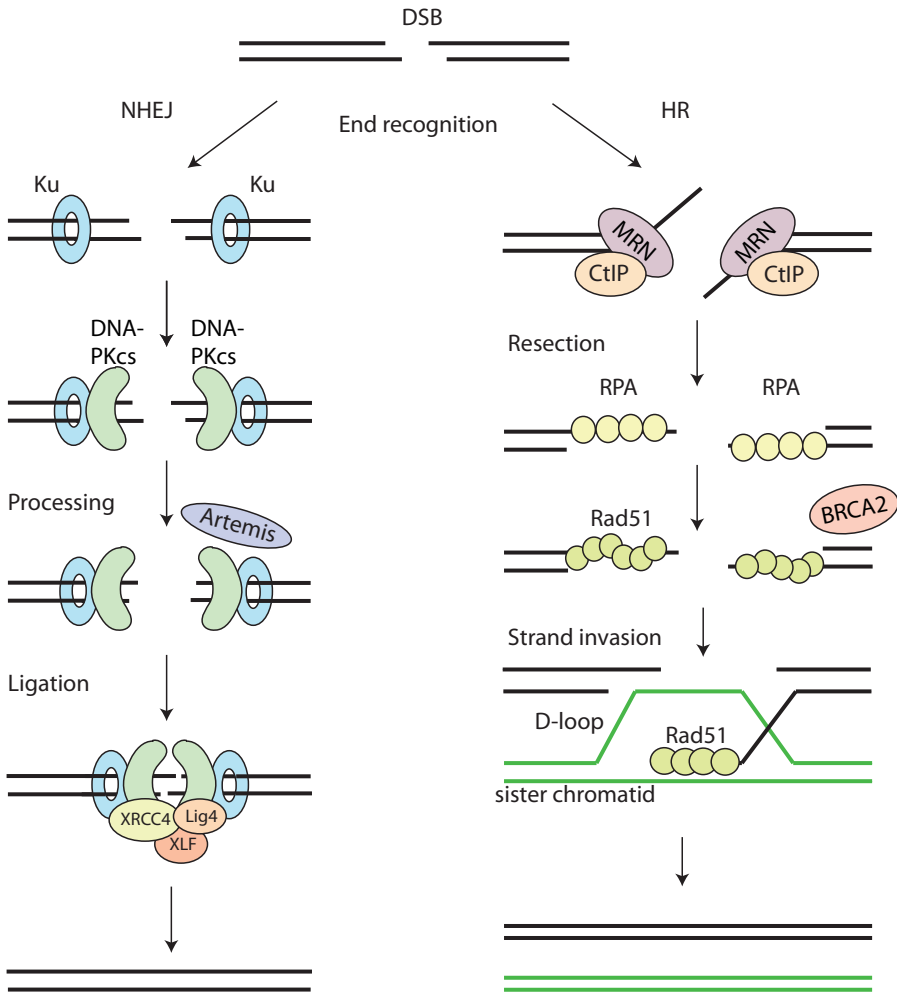


Figure 1 HR and NHEJ.

NHEJ) NHEJ starts with recognition of the DNA ends by the Ku70/80 heterodimer, which recruits DNA-PKcs. If the ends are incompatible, nucleases such as Artemis can trim the ends. The XRPC4-DNA Ligase IV-XLF ligation complex seals the break. **HR)** The MRN CtIP- complex starts resection on the breaks to generate single stranded DNA (ssDNA). After resection the break can no longer be repaired by NHEJ. The ssDNA is first coated by RPA, which is subsequently replaced by Rad51 with the help of BRCA2. These Rad51 nucleoprotein filaments mediate strand invasion on the homologous template. Extension of the D-loop and capture of the second end lead to repair.

interacting protein (CtIP)^{8,9} and other exonucleases, generating 3'-single stranded DNA (ssDNA)^{9,10}. The ssDNA tail is coated by Replication protein A (RPA) to remove secondary structure¹¹. Subsequently, BRCA2 mediates the replacement of RPA by RAD51, to form a nucleoprotein filament that searches for the homologous sequence on

the sister chromatid. After strand invasion, catalyzed by RAD51 and many other proteins, the DNA end is extended using the intact sequence as a template. After restoration of any lost sequence information, the second end of the broken DNA is captured and the junctions are resolved to give a precisely repaired DSB¹². This resolution step can be

accomplished via formation of two Holliday junctions, which are subsequently resolved to give crossover or non-crossover products (the double Holliday junction model). An alternative HR model, the synthesis dependent strand annealing (SDSA) model, does not involve Holliday junctions and results in non-crossover products only¹³.

Foci

Microscopically, DSBs can be visualized as local spots of repair protein accumulation (also called foci) in the nucleus. For example, histone H2AX is phosphorylated locally around the DSB and 53BP1, RPA and RAD51 accumulate in foci after ionizing radiation. Changes in the number of foci per nucleus in time can be quantified to analyze the dynamics of DNA repair¹⁴. Not all repair proteins accumulate in sufficient numbers to form foci. For example Ku70/80 does not form foci, although it is recruited to DNA damage^{15,16}.

Alternative DSB repair pathways

In addition to classical HR, several subpathways result in slightly different products. For example the single strand annealing (SSA) pathway uses directly repeated stretches of homology to repair DSBs. After resection of the break (as described above for HR) complementary stretches in the ssDNA anneal and the intervening sequence and one of the repeats is deleted¹⁷. Since HR and SSA use the same substrate, these pathways compete when repeats are present on both sides of the break and SSA should be suppressed to prevent its mutagenic effect.

Alternative end-joining pathways can also join DSBs in an error-prone manner, especially when classical NHEJ is impaired by deletion of essential components. The genetics of this pathway are not well defined and there may even be several alternative end-joining pathways. A dependence on DNA ligase III, Xrcc1 and PARP1 has been found in genetic assays^{18,19}. However, in another assay the repair of I-SceI induced DSBs in XRCC4-

deficient pro-B cell lines did not require Xrcc1²⁰. Alternative pathways show increased DSB joining using microhomologies (stretches of 1–6 bp of direct repeat at the junction), possibly to stabilize the synapsed ends³.

Although these alternative DSB repair pathways can work in specific experimental settings, they probably do not play a major role in repair of most DSBs in wild type cells. Therefore this review will focus on the balance between the classical forms of HR and NHEJ.

Repair assays

To study the balance between HR and NHEJ, one would ideally measure both types of repair at the same time using a defined chromosomal site. Unfortunately such an assay is not yet available. There are, however, many assays to measure HR and NHEJ separately. A good understanding of these assays is indispensable for correct interpretation of the results obtained using these different approaches. We therefore review the major assay systems and discuss their merits and drawbacks.

Assays to measure NHEJ

NHEJ can be measured in many different ways. The simplest version is transfection of linearized DNA into wild type and mutant cells. Joining of the ends can be monitored by cloning out individual plasmids or PCR amplification followed by sequencing or digestion of the junction²¹ (Figure 2a). Recircularization can also be monitored by following the restoration of expression of a reporter gene, such as an antibiotic resistance gene or a fluorescent marker (Figure 2b). A major disadvantage of these assays is that the linear DNA is extrachromosomal and NHEJ cannot be measured in the normal context of chromatin. However, it is a simple assay that can monitor decreased activity of the core NHEJ machinery as a shift towards microhomology use at the newly formed junctions.

Another type of NHEJ assays uses two I-SceI restriction sites. These sites can

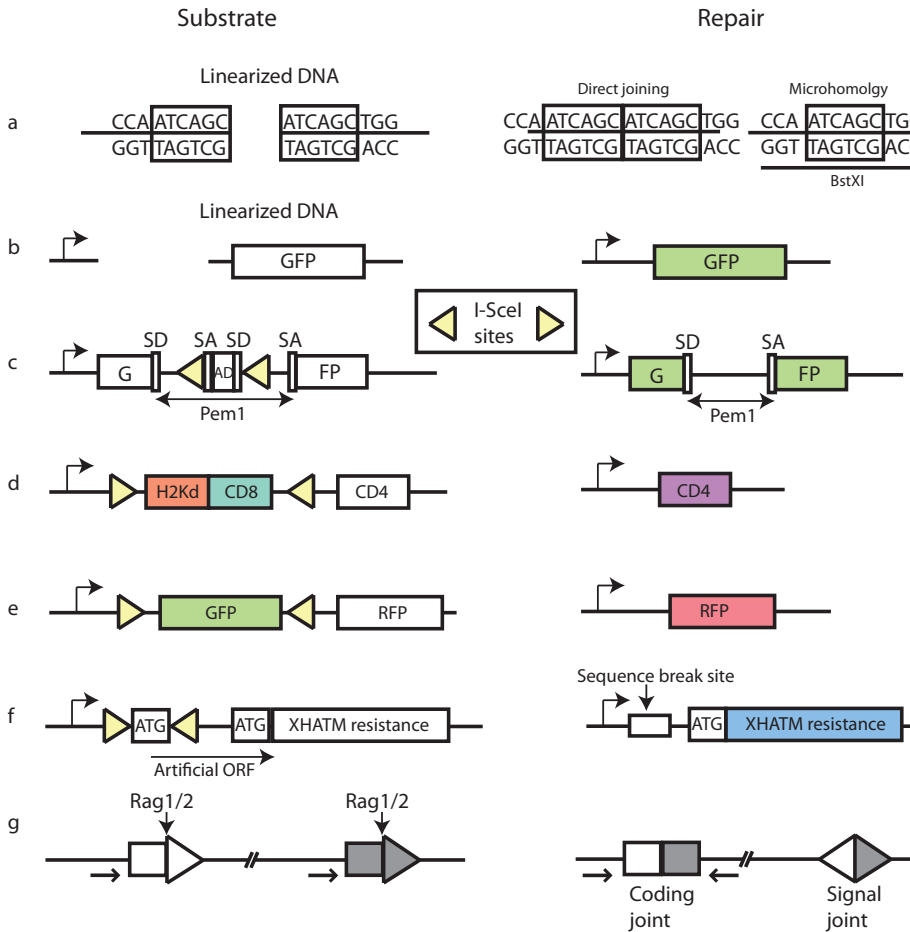


Figure 2 NHEJ repair assays.

a) Linear plasmid DNA with 6 bp repeats at the ends is joined after transfection. The joints are amplified by PCR and digested using BstXI to distinguish between direct repair and microhomology mediated repair²¹. b) Repair of linearized plasmid DNA results in restoration of GFP expression. c) Cleavage by I-SceI and subsequent repair lead to loss of the middle splice donor and acceptor sites (SD and SA) and the adenoviral exon (AD), resulting in the expression of active GFP²². d) H2Kd fused to CD8 is expressed from the intact substrate. Repair of the oppositely oriented I-SceI breaks results in loss of H2Kd-CD8 and allows expression of CD4²³. e) Similar to d), the intact substrate expresses GFP, while the repaired substrate allows expression of RFP and loses GFP expression²⁴. f) Between the opposite I-SceI sites, a translation start site is located, preventing translation of the XHATM resistance gene. Repair of the I-SceI breaks and loss of the intervening ATG results in XHATM resistance. The sequence around the breaks can be sequenced to monitor loss of nucleotides²⁵. g) V(D)J recombination assay. Cleavage by the Rag1/2 endonuclease at the recombination signal sequences induces inversion of the intervening sequence. Small arrows indicate location of PCR primers to amplify joints²¹.

be in the same or opposite orientation, generating compatible or incompatible ends, respectively. These constructs are generally integrated into the genome. The general theme of all these assays is restoration of expression of a marker gene, in some cases

accompanied by inactivation of another gene. Mao et al. interrupted the GFP gene with an intron containing an adenoviral exon (AD) flanked by two I-SceI sites (Figure 2c). Repair of the two I-SceI induced DSBs leads to loss of the intervening exon and expression

2 of functional GFP²². Guirouilh-Barbat et al. developed a similar assay (Figure 2d) with compatible or incompatible I-SceI sites, but they used surface antigens as a read-out for repair²³. Coleman and Greenberg also used a comparable assay (Figure 2e) with GFP between the I-SceI sites and RFP downstream, resulting in loss of GFP and expression of RFP after repair of the I-SceI induced DSBs²⁴. In these assays with a double I-SceI site it is also possible to sequence the joints and to determine the loss of nucleotides around the breaks²⁵ (Figure 2f).

A disadvantage of these assays using I-SceI restriction sites is that the individual I-SceI break has compatible ends and can recreate an I-SceI site if it is repaired precisely by NHEJ. Therefore, several cycles of cleavage and repair can happen before the site is lost due to inaccurate repair and these assays cannot measure the NHEJ efficiency accurately. However, sequencing of the junctions can provide interesting information about imprecise end-joining events. To avoid the cut-and-paste cycle problem of the I-SceI sites, some assays use transposon excision to create a break. Repair of transposon induced DSBs can reveal details of efficiency as well as precision of NHEJ^{26,27}. In principle, transposons would also be useful to study HR, although their DSB formation efficiency is generally lower than endonucleases.

The immune system depends on end-joining for V(D)J and class switch recombination (CSR). Pan-Hammarstrom and colleagues studied CSR by PCR amplification and sequencing of the junctions in normal individuals and patients. They found that patients with mutations in NHEJ components, such as DNA ligase IV, showed an increased dependence on longer microhomology stretches at the junctions²⁸. An advantage of this assay is that repair is measured on endogenous substrates. However, it is not clear whether these loci are representative for other types of DSBs.

V(D)J recombination also depends on NHEJ factors to repair the breaks induced by the RAG1 and RAG2 proteins. This type of

repair can be assayed using a specific repair substrate containing Recombination Signal Sequences, the recognition sites for Rag1 and Rag2²¹ (Figure 2g). The V(D)J recombination assay gives a clear phenotype for defects in proteins involved in DNA end-processing, such as the Artemis nuclease²⁹. The major disadvantage of these types of assays is the special nature of the DSBs formed by the RAG-proteins, which may shuttle the breaks towards NHEJ³⁰.

Assays to measure HR

The most commonly used assay to measure HR is the DR-GFP assay developed by Pierce and Jasin³¹ (Figure 3). The reporter construct can be inserted by gene targeting or random integration. It contains two GFP sequences separated by a selection marker. The 5' GFP sequence is inactivated by an I-SceI site and internal stop codons, preventing GFP expression. The 3' truncated GFP serves as a template for repair after DSB induction by I-SceI. Repair of the break by gene conversion using the downstream GFP sequence leads to restoration of the GFP gene and the percentage of GFP expressing cells can be determined by FACS analysis.

This HR assay has been used successfully to characterize defects in various (repair) mutant genetic backgrounds. An important advantage of this HR assay is that it measures repair using a chromatinized reporter construct in the chromosome. However, the template for repair is downstream of the break, whereas the normal template for HR is the equivalent position on the sister chromatid. Furthermore, the I-SceI site can be subject to several cycles of cleavage and repair by precise NHEJ or restoration of the sequence using the sister chromatid as a repair template, which leaves a high degree of uncertainty about the relative levels of HR and NHEJ.

Expression of I-SceI is usually induced by transfection of an expression plasmid into an asynchronously growing cell population. This creates DSBs in the reporter substrate throughout the cell cycle, whereas HR

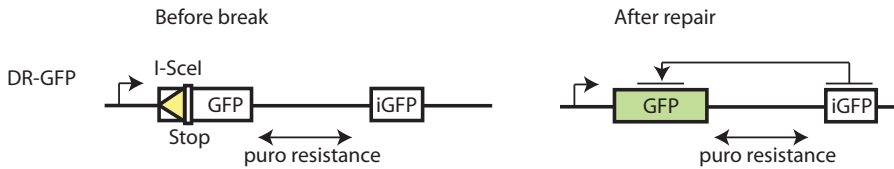


Figure 3 HR Assay.

The 5' GFP is inactivated by several in frame stop codons and contains an I-SceI site. A downstream truncated GFP, lacking the I-SceI sites and stops, serves as a template. Accurate repair via HR results in GFP expression.

only takes place in the S and G2 phases. To overcome this problem, Hartlerode et al. developed an I-SceI fusion protein that is drugactivatable. Enriching cells in a certain phase of the cell cycle then allows restricted activation of I-SceI³².

HR can also be estimated by scoring sister chromatid exchanges (SCEs). In this assays a nucleotide analog is added in the first cell cycle to allow incorporation into the newly synthesized strand in S phase. After a second replication round, only one of the sister chromatids is labeled, which allows visualization of recombination between the sister chromatids in metaphase spreads by staining for the incorporated nucleotide analog. SCEs can be formed in S phase during the repair of collapsed replication forks as well as in G2 phase at two-ended DSBs³³.

A completely different method to assess the efficiency of DSB repair is monitoring the disappearance of γ H2AX foci. These foci form within a few minutes after DSB formation and disappear slowly as repair takes place. By comparing the kinetics of several known HR and NHEJ mutants, the efficiency and likely repair pathway can be determined. For a review on the advantages and potential pitfalls of this assay, see³⁴.

As a more sophisticated approach, the formation and disappearance of 53BP1-YFP and Rad52-Cherry foci has been followed to estimate the use of HR and NHEJ in single cells throughout the cell cycle³⁵. Karanam et al. found that there is a gradual increase in HR at the beginning of S phase. The number of Rad52 foci increases till mid S phase and then decreases towards the end of S phase. In G2, very few Rad52 foci were observed, showing

that HR is not the predominant pathway in G2. This is consistent with data from Beucher et al., who demonstrated that NHEJ repairs approximately 85% of all IR-induced DSBs in G2, as measured by γ H2AX foci kinetics³⁶.

Balancing HR and NHEJ

The presence of large numbers of highly repetitive sequences in the DNA of higher eukaryotes makes HR between sequences other than sister chromatids prone to misalignment of the homologous sequences. Therefore, HR generally dominates in organisms with a small genome (with low abundance of repetitive sequences), whereas mammals mainly rely on NHEJ for DSB repair^{35,37}. However, even in highly complex genomes, HR is used as the preferred DSB repair mechanism to deal with DSBs that are formed during replication. This necessitates intricate control mechanisms to prevent access of the wrong repair pathway to the DSB.

Resection & cell cycle

HR can only safely be used to repair breaks in the S and G2 phases of the cell cycle. The first mechanism to regulate this depends on S/G2 specific cyclin dependent kinases (CDKs). DNA end resection requires phosphorylation of CtIP on a CDK consensus sequence^{9,38,39}. Proteasome-mediated degradation of the CtIP protein in G1⁴⁰ adds an additional layer of regulation at the resection step.

CDK1/CyclinB also phosphorylates the NBS1 component of the MRN complex on Serine 432 during the S, G2 and M phases, which is required for resection and efficient HR. However, IR sensitivity was not affected in

the Ser432Ala NBS1 mutant, consistent with the notion that NHEJ is the major DSB repair pathway in mammals⁴¹.

Although activation of HR proteins in a cell cycle dependent manner helps to restrict their activity, it is insufficient to ensure safe use of HR. While replication is ongoing in the S phase, parts of the genome have not yet been replicated and recombination of these parts should be avoided to prevent loss of heterozygosity and non-allelic recombination. Therefore, another layer of regulation is provided by the structural maintenance of chromosomes (SMC) proteins such as Cohesin, Condensin and SMC5/6: they are able to confine repair to the sister chromatid and prevent HR between other sequences^{42,43}.

Complexity of the break

Whether HR or NHEJ is used also depends on DSB complexity. This phenomenon has been studied in detail in the G2 phase of the cell cycle, when both HR and NHEJ contribute to DSB repair. Treatment of cells with the topoisomerase II inhibitor Etoposide results in breaks with a 4 bp 5'-overhang with covalently attached protein⁴⁴. The large majority of these breaks are repaired rapidly by NHEJ. The remaining 10% of the Etoposide induced breaks is repaired with slow kinetics via HR⁴⁵. High linear energy transfer (LET) carbon ions, on the other hand, induce highly complex clusters of DSBs and other types of DNA damage⁴⁶, because this type of radiation causes a high number of ionizations in a small volume. These breaks are frequently resected and their repair takes place via HR with slow kinetics⁴⁵. From the breaks induced by low LET ionizing irradiation (IR), which causes less complex DSBs, only 20-30% is resected and their repair is much less dependent on HR^{36,45}.

The chromatin structure around the DSB affects repair as well. Breaks in heterochromatin are repaired more slowly than breaks in euchromatin⁴⁷ probably because euchromatin is more easily accessible for repair and requires less or no remodeling. Repair of breaks in heterochromatin requires

ATM⁴⁷. ATM phosphorylates transcriptional corepressor Krüppel-associated box (KRAB)-associated protein (KAP)-1⁴⁸, which disrupts the interaction between KAP-1 and CHD3⁴⁹. CHD3 is an ATP-dependent nucleosome remodeling enzyme and its dispersion allows chromatin relaxation, facilitating DSB repair in heterochromatin. Furthermore, the ATPdependent chromatin remodeler SMARCAD1 can also be recruited to sites of DNA damage where it facilitates resection⁵⁰.

Genetic factors influencing pathway choice

The core HR and NHEJ machineries have been conserved from yeast to mammals⁵¹. However, several genes have been added to optimize or regulate both pathways in higher eukaryotes. For example, NHEJ has acquired DNA-PKcs and HR added several RAD51 paralogs. Furthermore, several additional genes in higher eukaryotes regulate DSB repair pathway choice without direct participation in the catalytic steps of the repair reaction.

53BP1

The p53 binding protein 1 (53BP1) is recruited to DSBs, where it has functions in cell cycle checkpoint maintenance and double strand break repair⁵². The fast phase in DSB repair is normal in the absence of 53BP1, but repair of breaks in heterochromatin is severely impaired, probably as a result of impaired KAP1 phosphorylation^{49,53}.

A deeper understanding of the 53BP1 function has been gained from studies in the immune system. During class switch recombination, highly repetitive DNA segments are recombined to generate the different classes of antibodies. DSBs generated during this recombination reaction can be repaired via NHEJ or alternative end joining. In the absence of 53BP1, resection increases and microhomology mediated alternative end-joining takes over from classical NHEJ⁵⁴. In V(D)J recombination, Variable (V), Diversity (D) and Joining (J) segments are recombined to create a large variety of functional coding

sequences for immunoglobulins and T-cell receptors. DSBs created by RAG1/2 are repaired via NHEJ. 53BP1 prevents extensive degradation and it promotes synapsis of DNA ends and stabilizes long-range interactions, not only between breaks created during V(D)J recombination⁵⁵, but also between deprotected telomeres⁵⁶.

BRCA1 and associated proteins

In contrast to the NHEJ promoting effect of 53BP1, the tumor suppressor BRCA1 is required for efficient HR⁵⁷ and formation of RAD51 foci after DSB induction⁵⁸. BRCA1 is an E3-ubiquitin ligase that forms a complex with the E2 enzyme BARD1 via its RING domain. This interaction is required for the ligase activity, as well as protein stability and nuclear localization⁵⁹. Although several RING-domain mutations have been found in patients, it is currently unknown how the HR defect is related to the E3-ligase function and BARD1 interaction. Drost et al. recently showed that the RING-domain is necessary for tumor suppression, but not required for the development of resistance to chemotherapeutics. Tumors with a C61G mutation in the RING-domain rapidly develop resistance to platinum drugs and the PARP inhibitor Olaparib, while retaining this mutation⁶⁰.

In addition to its function as a ubiquitin ligase, BRCA1 may also function as a scaffold protein that associates with many interaction partners, such as Abraxas, BACH1 and BRCA2/PALB2⁵⁹. For efficient resection of DNA ends, its interaction with CtIP and the MRN complex is probably important^{39,61}. BRCA1 also interacts with RAP80 and the BRCA1/RAP80 complex is recruited to ubiquitylated chromatin around DSBs⁶²⁻⁶⁴. In contrast to the BRCA1 interactions described above, the RAP80-BRCA1 interaction decreased HR: depletion of Rap80 stimulated recruitment of CtIP and Mre11 and thereby resection²⁴. The BRCA1 interactions with CtIP and RAP80 are mutually exclusive, indicating that competition for this BRCA1 binding site affects resection and thereby pathway

choice. For replication-associated breaks, BRCA1 clearly tips the balance towards HR.

Genetic interactions of BRCA1 and 53BP1

Recently, some unexpected genetic interactions between BRCA1 and 53BP1 shed new light on their function in balancing DSB repair pathways. Deletion of BRCA1 causes embryonic lethality, but this can be rescued by deletion of 53BP1⁶⁵. Unexpectedly, deletion of 53BP1 also restored HR and RAD51 foci formation in BRCA1 deficient cells^{66,67}, implying that both factors influence HR in opposite directions and that inactivation of both genes largely restores the balance. Inactivation of 53BP1 in BRCA1^{-/-} ES cells led to an increase in both nucleolytic DNA end processing and RPA phosphorylation⁶⁷. ATM inhibition in BRCA1^{-/-} 53BP1^{-/-} cells reduced RPA phosphorylation and Rad51 foci formation, indicating that ATM-dependent resection allows partial restoration of HR⁶⁷.

Figure 4 presents a plausible model to accommodate these findings. One-ended DSBs that are formed during replication require BRCA1 to stimulate resection. In BRCA1 deficient cells, 53BP1 prevents resection of DNA ends, leading to aberrant diversion of breaks to NHEJ. This creates dead-end products (if only one DNA end is present) or inappropriate joining to distant sequences causing chromosomal translocations (if a DNA end combines with an unrelated other DNA end). Two-ended DSBs, on the other hand, require 53BP1 to limit resection and allow efficient NHEJ. Overactive resection in 53BP1^{-/-} cells may result in aberrant HR reactions (such as single-strand annealing) or alternative end-joining pathways, creating microhomology-mediated translocations and/or junctions with excessive deletions^{68,69}.

Further insight into the role of BRCA1 and 53BP1 in repair pathway choice was recently obtained using super resolution microscopy of IR induced foci (IRIF). The core of the focus contained mainly 53BP1 molecules in the G1 phase of the cell cycle, probably representing repair via NHEJ. In S phase, however, the core of the IRIF was filled with BRCA1 and 53BP1

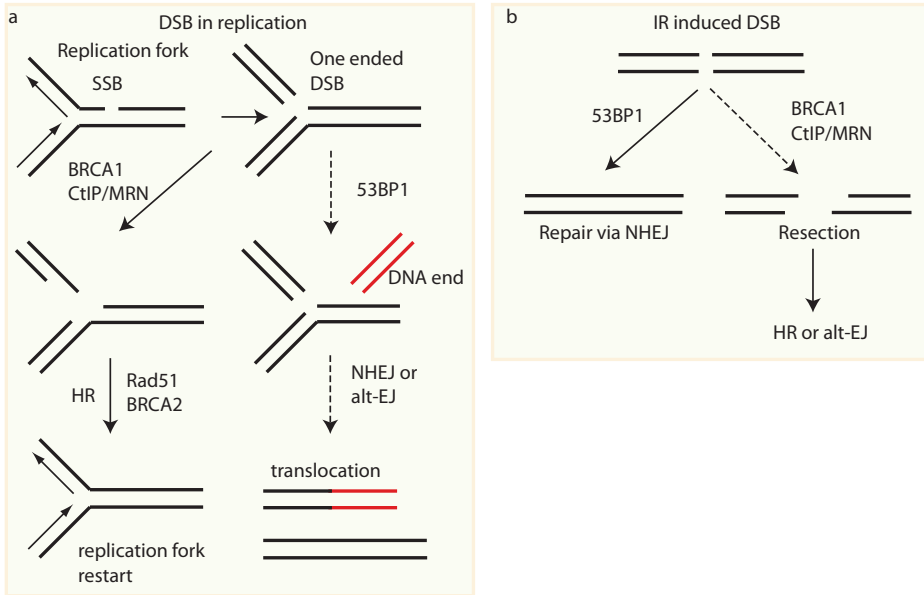


Figure 4 BRCA1 and 53BP1 in DSB repair.

a) Repair of replication associated breaks requires HR. 53BP1 blocks resection of the one-ended break in BRCA1 deficient cells, preventing repair via HR. The breaks are either left unrepaired or repaired via NHEJ using other random DNA ends, which leads to chromosomal rearrangements and genomic instability. In the absence of 53BP1, resection of the DNA ends can take place, allowing faithful repair via HR. b) IR induced two ended DSBs are mainly repaired via NHEJ, however part of the breaks is repaired via HR or alternative end-joining (alt-EJ). Repair via HR or alt-EJ increases when classical NHEJ is impaired by a mutation in one of the core NHEJ genes or 53BP1.

formed a ring around this core, suggesting that BRCA1 physically excludes 53BP1 from the break to allow repair via HR⁷⁰.

BRCA1 deficient cells are exquisitely sensitive to PARP inhibitors, which inhibit single strand break repair^{71,72}. The rationale for this observation is that replication of DNA with single strand breaks results in formation of single DNA ends, which require HR for their repair (Figure 4). As described above, deletion of 53BP1 in BRCA1-deficient cells rescues embryonic lethality. However, loss of 53BP1 also leads to resistance to PARP inhibition^{66,73}. In the BRCA1-deficient cells that have also lost 53BP1, the number of chromosome and chromatid breaks is decreased and checkpoint activation is diminished compared to cells that are only BRCA1 deficient⁶⁶, suggesting that the regained HR capacity in these cells is largely sufficient to restore genomic stability. A subset BRCA1 and BRCA2 mutant tumors shows loss of 53BP1, indicating that therapy

resistance via loss of 53BP1 may be clinically relevant⁶⁶.

Ubiquitylation and sumoylation

Ubiquitin and the small ubiquitin-like modifier (SUMO) are small polypeptides that can be attached to proteins as a posttranslational modification. After activation of ubiquitin or SUMO by an E1 enzyme, they are transferred to an E2 conjugating enzyme. With the help of a ubiquitin (or SUMO) ligase (E3) the modification is attached to the substrate. Deubiquitylating enzymes (DUBs) can reverse the ubiquitin modification.

Many proteins involved in the DDR can be ubiquitylated or sumoylated^{2,74-76}. For the sake of simplicity, we will focus on one part of the DDR signaling cascade as an example. Upon DSB formation, histone H2AX is phosphorylated by ATM or DNA-PK. MDC1 is recruited to this phosphorylated histone

(γ H2AX) and is in turn phosphorylated by ATM. This attracts the E3 ligase RNF8 which ubiquitylates H2A and H2AX. Subsequent action of the E3 ligase RNF168 leads to more extensive ubiquitylation of the chromatin around the break, creating a recruitment platform for many other repair proteins, including 53BP1 and BRCA1⁷⁷. These ubiquitylation events are also required for phospho-KAP-1 foci formation and thereby chromatin relaxation at sites of damage⁵³.

In addition to an effect on recruitment of repair proteins, ubiquitylation can also affect release of proteins from the lesion. The transient binding of Ku at DNA ends affects pathway choice. Ku binds in all phases of the cell cycle and must be removed to allow resection^{78,79}. This removal can be facilitated via ubiquitylation of Ku by the E3 ligase RNF8 and an unknown E2 conjugating enzyme, leading to proteasome-dependent Ku degradation⁸⁰. Since ubiquitylation is a very abundant modification on DDR proteins, it is likely that more modifications affecting pathway choice will be discovered in the future.

Concluding remarks

A unifying model for DSB repair pathway choice should take into account that NHEJ is relatively fast, while resection is a slow process that probably creates a point of no return. Therefore, it is to be expected that NHEJ initially tries to repair all DSBs and only if this repair pathway fails to repair the lesion, the chance that resection takes place increases over time, necessitating repair via HR. This is consistent with the observation that the binding of the Ku heterodimer to DNA ends is a very fast process, but the assembly of end-joining complexes is dynamic and may in the long run give way to proteins mediating resection if they are active¹⁶. This means that initiation of HR will mainly be restricted to the S and G2 phases of the cell cycle, when CtIP is active. Indeed, a subfraction of DSBs in G2 requires BRCA2 for their repair, but knock-down of both CtIP

and BRCA2 alleviates this repair defect⁴⁵, suggesting that avoiding resection prevents HR and allows repair of these DSBs by NHEJ. Replication associated breaks, on the other hand, should be channeled to HR, which is the only pathway that can restart a replication fork from a single broken DNA end.

The study of the balance between HR and NHEJ is important for the prediction of treatment responses upon inhibition of these pathways in various genetic backgrounds. Combined treatments might backfire when the balance is tipped the wrong way. For example, the treatment of BRCA1 and BRCA2 deficient cells is most effective when NHEJ is functional, whereas impaired NHEJ prevents lethal genomic instability and cytotoxicity, which counteracts the effect of PARP inhibitors in HR deficient cells^{73,81}.

The balance between HR and NHEJ is heavily regulated, but the wiring and hierarchy of this regulatory network is still incompletely understood. Development of targeted therapies using DNA damage response defects requires a much more detailed knowledge of the precise network of the cellular responses to DNA damaging treatments. It is to be expected that new assay systems will be developed and that a flurry of novel combinations of chemical inhibitors and genetic defects will increase our understanding of these processes in the near future. This knowledge will then be an invaluable source for developing new targeted therapies for tumors with DNA damage response defects, which should yield more specific and effective therapeutic approaches to combat cancer. Novel tools to characterize tumor-specific (DNA repair gene) mutations, such as whole genome sequencing approaches, should then bring truly personalized medicine for cancer treatment within reach.

Competing interests

The authors declare that they have no competing interests.

Authors' contributions

IB wrote the first draft. IB and DvG wrote the final text. Both authors read and approved the final manuscript.

Acknowledgement

The research leading to these results has received funding from the European Community's Seventh Framework Programme (FP7/2007-2013) under grant agreement No. HEALTH-F2-2010-259893.

Received: 2 October 2012

Accepted: 22 November 2012

Published: 27 November 2012

References

- Friedberg ECW, Siede GC, Wood RD, Schultz RA, Ellenberger T: DNA repair and mutagenesis. Washington, USA: ASM press; 2006.
- Ciccio A, Elledge SJ: The DNA damage response: making it safe to play with knives. *Mol Cell* 2010, 40:179–204.
- Lieber MR: The mechanism of double-strand DNA break repair by the nonhomologous DNA end-joining pathway. *Annu Rev Biochem* 2010, 79:181–211.
- Ahnesorg P, Smith P, Jackson SP: XLF interacts with the XRCC4-DNA ligase IV complex to promote DNA nonhomologous end-joining. *Cell* 2006, 124:301–313.
- Buck D, Malivert L, de Chasseval R, Barraud A, Fondaneche MC, Sanal O, Plebani A, Stephan JL, Hufnagel M, le Deist F, et al: Cernunnos, a novel nonhomologous end-joining factor, is mutated in human immunodeficiency with microcephaly. *Cell* 2006, 124:287–299.
- Heyer WD, Ehmsen KT, Liu J: Regulation of homologous recombination in eukaryotes. *Annu Rev Genet* 2010, 44:113–139.
- Stracker TH, Petrini JH: The MRE11 complex: starting from the ends. *Nat Rev Mol Cell Biol* 2011, 12:90–103.
- Limbo O, Chahwan C, Yamada Y, de Bruin RA, Wittenberg C, Russell P: Ctp1 is a cell-cycle-regulated protein that functions with Mre11 complex to control double-strand break repair by homologous recombination. *Mol Cell* 2007, 28:134–146.
- Sartori AA, Lukas C, Coates J, Mistrik M, Fu S, Bartek J, Baer R, Lukas J, Jackson SP: Human CtIP promotes DNA end resection. *Nature* 2007, 450:509–514.
- Wyman C, Kanaar R: DNA double-strand break repair: all's well that ends well. *Annu Rev Genet* 2006, 40:363–383.
- Sugiyama T, Zaitseva EM, Kowalczykowski SC: A single-stranded DNA-binding protein is needed for efficient presynaptic complex formation by the *Saccharomyces cerevisiae* Rad51 protein. *J Biol Chem* 1997, 272:7940–7945.
- Pardo B, Gomez-Gonzalez B, Aguilera A: DNA repair in mammalian cells: DNA double-strand break repair: how to fix a broken relationship. *Cell Mol Life Sci* 2009, 66:1039–1056.
- Maher RL, Branagan AM, Morrical SW: Coordination of DNA replication and recombination activities in the maintenance of genome stability. *J Cell Biochem* 2011, 112:2672–2682.
- Polo SE, Jackson SP: Dynamics of DNA damage response proteins at DNA breaks: a focus on protein modifications. *Genes Dev* 2011, 25:409–433.
- Kim JS, Krasieva TB, Kurumizaka H, Chen DJ, Taylor AM, Yokomori K: Independent and sequential recruitment of NHEJ and HR factors to DNA damage sites in mammalian cells. *J Cell Biol* 2005, 170:341–347.
- Mari PO, Florea BI, Persengiev SP, Verkaik NS, Bruggenwirth HT, Modesti M, Giglia-Mari G, Bezstarosti K, Demmers JA, Luider TM, et al: Dynamic assembly of end-joining complexes requires interaction between Ku70/80 and XRCC4. *Proc Natl Acad Sci USA* 2006, 103:18597–18602.
- Stark JM, Pierce AJ, Oh J, Pastink A, Jasin M: Genetic steps of mammalian homologous repair with distinct mutagenic consequences. *Mol Cell Biol* 2004, 24:9305–9316.
- Audebert M, Salles B, Calsou P: Involvement of poly(ADP-ribose) polymerase-1 and XRCC1/DNA ligase III in an alternative route for DNA double-strand breaks rejoining. *J Biol Chem* 2004, 279:55117–55126.
- Wang M, Wu W, Wu W, Rosidi B, Zhang L, Wang H, Iliakis G: PARP-1 and Ku compete for repair of DNA double strand breaks by distinct NHEJ pathways. *Nucleic Acids Res* 2006, 34:6170–6182.
- Boboila C, Oksenysh V, Gostissa M, Wang JH, Zha S, Zhang Y, Chai H, Lee CS, Jankovic M, Saez LM, et al: Robust chromosomal DNA repair via alternative end-joining in the absence of X-ray repair cross-complementing protein 1 (XRCC1). *Proc Natl Acad Sci USA* 2012, 109:2473–2478.
- Verkaik NS, Esvelde-van Lange RE, van Heemst D, Bruggenwirth HT, Hoeijmakers JH, Hoeijmakers MZ, van Gent DC: Different types of V(D)J recombination and end-joining defects in DNA double-strand break repair mutant mammalian cells. *Eur J Immunol* 2002, 32:701–709.
- Mao Z, Bozzella M, Seluanov A, Gorbunova V: Comparison of nonhomologous end joining and homologous recombination in human cells. *DNA Repair (Amst)* 2008, 7:1765–1771.
- Guirouilh-Barbat J, Huck S, Bertrand P, Pirzio L, Desmaze C, Sabatier L, Lopez BS: Impact of the KU80 pathway on NHEJ-induced genome rearrangements in mammalian cells. *Mol Cell* 2004, 14:611–623.
- Coleman KA, Greenberg RA: The BRCA1-RAP80 complex regulates DNA repair mechanism utilization by restricting end resection. *J Biol Chem* 2011, 286:13669–13680.
- Schulte-Uentrop L, El-Awady RA, Schliecker L, Willers H, Dahm-Daphi J: Distinct roles of XRCC4 and Ku80 in non-homologous end-joining of endonuclease-

- and ionizing radiation-induced DNA double-strand breaks. *Nucleic Acids Res* 2008, 36:2561–2569.
26. van Heemst D, Brugmans L, Verkaik NS, van Gent DC: End-joining of blunt DNA double-strand breaks in mammalian fibroblasts is precise and requires DNA-PK and XRCC4. *DNA Repair (Amst)* 2004, 3:43–50.
 27. Yant SR, Kay MA: Nonhomologous-end-joining factors regulate DNA repair fidelity during Sleeping Beauty element transposition in mammalian cells. *Mol Cell Biol* 2003, 23:8505–8518.
 28. Pan-Hammarstrom Q, Jones AM, Lahdesmaki A, Zhou W, Gatti RA, Hammarstrom L, Gennery AR, Ehrenstein MR: Impact of DNA ligase IV on nonhomologous end joining pathways during class switch recombination in human cells. *J Exp Med* 2005, 201:189–194.
 29. van der Burg M, Verkaik NS, den Dekker AT, Barendregt BH, Pico-Knijnenburg I, Tezcan I, van Dongen JJ, van Gent DC: Defective Artemis nuclease is characterized by coding joints with microhomology in long palindromic-nucleotide stretches. *Eur J Immunol* 2007, 37:3522–3528.
 30. Lee GS, Neiditch MB, Salus SS, Roth DB: RAG proteins shepherd doublestrand breaks to a specific pathway, suppressing error-prone repair, but RAG nicking initiates homologous recombination. *Cell* 2004, 117:171–184.
 31. Pierce AJ, Johnson RD, Thompson LH, Jasin M: XRCC3 promotes homology-directed repair of DNA damage in mammalian cells. *Genes Dev* 1999, 13:2633–2638.
 32. Hartlerode A, Odate S, Shim I, Brown J, Scully R: Cell cycle-dependent induction of homologous recombination by a tightly regulated I-SceI fusion protein. *PLoS One* 2011, 6:e16501.
 33. Conrad S, Kunzel J, Loblrich M: Sister chromatid exchanges occur in G2-irradiated cells. *Cell Cycle* 2011, 10:222–228.
 34. Loblrich M, Shibata A, Beucher A, Fisher A, Ensminger M, Goodarzi AA, Barton O, Jeggo PA: gammaH2AX foci analysis for monitoring DNA double-strand break repair: strengths, limitations and optimization. *Cell Cycle* 2010, 9:662–669.
 35. Karanam K, Kafri R, Loewer A, Lahav G: Quantitative live cell imaging reveals a gradual shift between DNA repair mechanisms and a maximal Use of HR in Mid S phase. *Mol Cell* 2012, 47:320–329.
 36. Beucher A, Birraux J, Tchouandong L, Barton O, Shibata A, Conrad S, Goodarzi AA, Krempler A, Jeggo PA, Loblrich M: ATM and Artemis promote homologous recombination of radiation-induced DNA double-strand breaks in G2. *EMBO J* 2009, 28:3413–3427.
 37. Lamarche BJ, Orazio NI, Weitzman MD: The MRN complex in doublestrand break repair and telomere maintenance. *FEBS Lett* 2010, 584:3682–3695.
 38. Huertas P, Jackson SP: Human CtIP mediates cell cycle control of DNA end resection and double strand break repair. *J Biol Chem* 2009, 284:9558–9565.
 39. Yun MH, Hiom K: CtIP-BRCA1 modulates the choice of DNA doublestrand- break repair pathway throughout the cell cycle. *Nature* 2009, 459:460–463.
 40. Germani A, Prabel A, Mourah S, Podgorniak MP, Di Carlo A, Ehrlich R, Gisselbrecht S, Varin-Blank N, Calvo F, Bruzzoni-Giovanelli H: SIAH-1 interacts with CtIP and promotes its degradation by the proteasome pathway. *Oncogene* 2003, 22:8845–8851.
 41. Falck J, Forment JV, Coates J, Mistrik M, Lukas J, Bartek J, Jackson SP: CDK targeting of NBS1 promotes DNA-end resection, replication restart and homologous recombination. *EMBO Rep* 2012, 13:561–568.
 42. Cortes-Ledesma F, de Piccoli G, Haber JE, Aragon L, Aguilera A: SMC proteins, new players in the maintenance of genomic stability. *Cell Cycle* 2007, 6:914–918.
 43. Covo S, Westmoreland JW, Gordenin DA, Resnick MA: Cohesin Is limiting for the suppression of DNA damage-induced recombination between homologous chromosomes. *PLoS Genet* 2010, 6:e1001006.
 44. Spitzner JR, Chung IK, Gootz TD, McGuirk PR, Muller MT: Analysis of eukaryotic topoisomerase II cleavage sites in the presence of the quinolone CP-115,953 reveals drug-dependent and -independent recognition elements. *Mol Pharmacol* 1995, 48:238–249.
 45. Shibata A, Conrad S, Birraux J, Geuting V, Barton O, Ismail A, Kakarougkas A, Meek K, Taucher-Scholz G, Loblrich M, Jeggo PA: Factors determining DNA double-strand break repair pathway choice in G2 phase. *EMBO J* 2011, 30:1079–1092.
 46. Hada M, Georgakilas AG: Formation of clustered DNA damage after high-LET irradiation: a review. *J Radiat Res* 2008, 49:203–210.
 47. Goodarzi AA, Noon AT, Deckbar D, Ziv Y, Shiloh Y, Loblrich M, Jeggo PA: ATM signaling facilitates repair of DNA double-strand breaks associated with heterochromatin. *Mol Cell* 2008, 31:167–177.
 48. Ziv Y, Bielopolski D, Galanty Y, Lukas C, Taya Y, Schultz DC, Lukas J, Bekker-Jensen S, Bartek J, Shiloh Y: Chromatin relaxation in response to DNA double-strand breaks is modulated by a novel ATM- and KAP-1 dependent pathway. *Nat Cell Biol* 2006, 8:870–876.
 49. Goodarzi AA, Kurka T, Jeggo PA: KAP-1 phosphorylation regulates CHD3 nucleosome remodeling during the DNA double-strand break response. *Nat Struct Mol Biol* 2011, 18:831–839.
 50. Costelloe T, Louge R, Tomimatsu N, Mukherjee B, Martini E, Khadaroo B, Dubois K, Wiegant WW, Thierry A, Burma S, et al: The yeast Fun30 and human SMARCAD1 chromatin remodellers promote DNA end resection. *Nature* 2012, 489(7417):581–584.
 51. Sonoda E, Hocheegger H, Saberi A, Taniguchi Y, Takeda S: Differential usage of non-homologous end-joining and homologous recombination in double strand break repair. *DNA Repair (Amst)* 2006, 5:1021–1029.
 52. Rappold I, Iwabuchi K, Date T, Chen J: Tumor suppressor p53 binding protein 1 (53BP1) is involved in DNA damage-signaling pathways. *J Cell Biol* 2001, 153:613–620.
 53. Noon AT, Shibata A, Rief N, Loblrich M, Stewart GS, Jeggo PA, Goodarzi AA: 53BP1-dependent robust localized KAP-1 phosphorylation is essential for heterochromatic DNA double-strand break repair. *Nat Cell Biol* 2010, 12:177–184.

54. Bothmer A, Robbiani DF, Feldhahn N, Gazumyan A, Nussenzweig A, Nussenzweig MC: 53BP1 regulates DNA resection and the choice between classical and alternative end joining during class switch recombination. *J Exp Med* 2010, 207:855–865.
55. Difilippantonio S, Gapud E, Wong N, Huang CY, Mahowald G, Chen HT, Kruhlak MJ, Callen E, Livak F, Nussenzweig MC, et al: 53BP1 facilitates longrange DNA end-joining during V(D)J recombination. *Nature* 2008, 456:529–533.
56. Dimitrova N, Chen YC, Spector DL, de Lange T: 53BP1 promotes nonhomologous end joining of telomeres by increasing chromatin mobility. *Nature* 2008, 456:524–528.
57. Moynahan ME, Chiu JW, Koller BH, Jasin M: Brca1 controls homologydirected DNA repair. *Mol Cell* 1999, 4:511–518.
58. Chen JJ, Silver D, Cantor S, Livingston DM, Scully R: BRCA1, BRCA2, and Rad51 operate in a common DNA damage response pathway. *Cancer Res* 1999, 59:17525–17565.
59. Ohta T, Sato K, Wu W: The BRCA1 ubiquitin ligase and homologous recombination repair. *FEBS Lett* 2011, 585:2836–2844.
60. Drost R, Bouwman P, Rottenberg S, Boon U, Schut E, Klarenbeek S, Klijn C, van der Heijden I, van der Gulden H, Wientjens E, et al: BRCA1 RING function is essential for tumor suppression but dispensable for therapy resistance. *Cancer Cell* 2011, 20:797–809.
61. Chen L, Nievera CJ, Lee AY, Wu AY: Cell cycle-dependent complex formation of BRCA1.CtIP.MRN is important for DNA double-strand break repair. *J Biol Chem* 2008, 283:7713–7720.
62. Kim H, Chen J, Yu X: Ubiquitin-binding protein RAP80 mediates BRCA1- dependent DNA damage response. *Science* 2007, 316:1202–1205.
63. Sobhian B, Shao G, Lilli DR, Culhane AC, Moreau LA, Xia B, Livingston DM, Greenberg RA: RAP80 targets BRCA1 to specific ubiquitin structures at DNA damage sites. *Science* 2007, 316:1198–1202.
64. Wang B, Matsuoka S, Ballif BA, Zhang D, Smogorzewska A, Gygi SP, Elledge SJ: Abraxas and RAP80 form a BRCA1 protein complex required for the DNA damage response. *Science* 2007, 316:1194–1198.
65. Cao L, Xu X, Bunting SF, Liu J, Wang RH, Cao LL, Wu JJ, Peng TN, Chen J, Nussenzweig A, et al: A selective requirement for 53BP1 in the biological response to genomic instability induced by Brca1 deficiency. *Mol Cell* 2009, 35:534–541.
66. Bouwman P, Aly A, Escandell JM, Pieterse M, Bartkova J, van der Gulden H, Hiddingh S, Thanasoula M, Kulkarni A, Yang Q, et al: 53BP1 loss rescues BRCA1 deficiency and is associated with triple-negative and BRCAmutated breast cancers. *Nat Struct Mol Biol* 2010, 17:688–695.
67. Bunting SF, Callen E, Wong N, Chen HT, Polato F, Gunn A, Bothmer A, Feldhahn N, Fernandez-Capetillo O, Cao L, et al: 53BP1 inhibits homologous recombination in Brca1-deficient cells by blocking resection of DNA breaks. *Cell* 2010, 141:243–254.
68. Nik-Zainal S, Alexandrov LB, Wedge DC, Van Loo P, Greenman CD, Raine K, Jones D, Hinton J, Marshall J, Stebbings LA, et al: Mutational processes molding the genomes of 21 breast cancers. *Cell* 2012, 149:979–993.
69. Morales JC, Franco S, Murphy MM, Bassing CH, Mills KD, Adams MM, Walsh NC, Manis JP, Rassidakis GZ, Alt FW, Carpenter PB: 53BP1 and p53 synergize to suppress genomic instability and lymphomagenesis. *Proc Natl Acad Sci USA* 2006, 103:3310–3315.
70. Chapman JR, Sossick AJ, Boulton SJ, Jackson SP: BRCA1-associated exclusion of 53BP1 from DNA damage sites underlies temporal control of DNA repair. *J Cell Sci* 2012, 125:3529–3534.
71. Bryant HE, Schultz N, Thomas HD, Parker KM, Flower D, Lopez E, Kyle S, Meuth M, Curtin NJ, Helleday T: Specific killing of BRCA2-deficient tumours with inhibitors of poly(ADP-ribose) polymerase. *Nature* 2005, 434:913–917.
72. Farmer H, McCabe N, Lord CJ, Tutt AN, Johnson DA, Richardson TB, Santarosa M, Dillon KJ, Hickson I, Knights C, et al: Targeting the DNA repair defect in BRCA mutant cells as a therapeutic strategy. *Nature* 2005, 434:917–921.
73. Bunting SF, Callen E, Kozak ML, Kim JM, Wong N, Lopez-Contreras AJ, Ludwig T, Baer R, Faryabi RB, Malhowski A, et al: BRCA1 functions independently of homologous recombination in DNA interstrand crosslink repair. *Mol Cell* 2012, 46:125–135.
74. Dou H, Huang C, Van Nguyen T, Lu LS, Yeh ET: SUMOylation and de-SUMOylation in response to DNA damage. *FEBS Lett* 2011, 585:2891–2896.
75. Selvarajah J, Moumen A: Role of ubiquitination in the DNA damage response: proteomic analysis to identify new DNA-damage-induced ubiquitinated proteins. *Biochem Soc Trans* 2010, 38:87–91.
76. Al-Hakim A, Escribano-Diaz C, Landry MC, O'Donnell L, Panier S, Szilard RK, Durocher D: The ubiquitous role of ubiquitin in the DNA damage response. *DNA Repair (Amst)* 2010, 9:1229–1240.
77. Stewart GS, Panier S, Townsend K, Al-Hakim AK, Kolas NK, Miller ES, Nakada S, Ylanko J, Olivarius S, Mendez M, et al: The RIDDLE syndrome protein mediates a ubiquitin-dependent signaling cascade at sites of DNA damage. *Cell* 2009, 136:420–434.
78. Shao Z, Davis AJ, Fattah KR, So S, Sun J, Lee KJ, Harrison L, Yang J, Chen DJ: Persistently bound Ku at DNA ends attenuates DNA end resection and homologous recombination. *DNA Repair (Amst)* 2012, 11:310–316.
79. Postow L, Ghenoiu C, Woo EM, Krutchinsky AN, Chait BT, Funabiki H: Ku80 removal from DNA through double strand break-induced ubiquitylation. *J Cell Biol* 2008, 182:467–479.
80. Feng L, Chen J: The E3 ligase RNF8 regulates KU80 removal and NHEJ repair. *Nat Struct Mol Biol* 2012, 19:201–206.
81. Patel AG, Sarkaria JN, Kaufmann SH: Nonhomologous end joining drives poly(ADP-ribose) polymerase (PARP) inhibitor lethality in homologous recombination-deficient cells. *Proc Natl Acad Sci USA* 2011, 108:3406–3411

¹Division of Molecular Oncology, The Netherlands Cancer Institute, Plesmanlaan 121, 1066CX Amsterdam, The Netherlands. ²The Wellcome Trust Centre for Human Genetics, Roosevelt Drive, Oxford OX3 7BN, UK. ³Department of Genetics, Erasmus, University Medical Center, 3000 CA Rotterdam, The Netherlands. ⁴Department of Experimental Radiation Oncology, University of Texas MD Anderson Cancer Center, Houston, Texas 77030, USA. ⁵Institute of Molecular and Translational Medicine, Faculty of Medicine and Dentistry, Palacky University, 779 00 Olomouc, Czech Republic. ⁶Division of Molecular Pathology, The Netherlands Cancer Institute, Plesmanlaan 121, 1066CX Amsterdam, The Netherlands. ⁷Danish Cancer Society Research Center, 2100 Copenhagen, Denmark. ⁸Division of Cell Biology, The Netherlands Cancer Institute, Plesmanlaan 121, 1066CX Amsterdam, The Netherlands. ⁹Protein Facility, The Netherlands Cancer Institute, Plesmanlaan 121, 1066CX Amsterdam, The Netherlands. ¹⁰Deep Sequencing Core Facility, The Netherlands Cancer Institute, Plesmanlaan 121, 1066CX Amsterdam, The Netherlands. ¹¹Division of Molecular Carcinogenesis, The Netherlands Cancer Institute, Plesmanlaan 121, 1066CX Amsterdam, The Netherlands. ¹²DNA Damage Response Laboratory, London Research Institute, Cancer Research UK, Clare Hall, South Mimms, Hertfordshire EN6 3LD, UK. ¹³Institute of Animal Pathology, Vetsuisse Faculty, University of Bern, Laengasstrasse 122, 3012 Bern, Switzerland.

Chapter 3

REV7 counteracts DNA double-strand break resection and affects PARP inhibition

Nature 2015 May 28;521(7553):541-4

Guotai Xu¹, J. Ross Chapman^{2*}, Inger Brandsma^{3*}, Jingsong Yuan⁴, Martin Mistrik⁵, Peter Bouwman⁶, Jirina Bartkova⁷, Ewa Gogola¹, Daniël Warmerdam⁸, Marco Barazas¹, Janneke E. Jaspers¹, Kenji Watanabe⁷, Mark Pieterse⁶, Ariena Kersbergen¹, Wendy Sol¹, Patrick H. N. Celie⁹, Philip C. Schouten⁶, Bram van den Broek⁸, Ahmed Salman², Marja Nieuwland¹⁰, Iris de Rink¹⁰, Jorma de Ronde¹¹, Kees Jalink⁸, Simon J. Boulton¹², Junjie Chen⁴, Dik C. van Gent³, Jiri Bartek^{5,7}, Jos Jonkers⁶, Piet Borst¹ & Sven Rottenberg^{1,13}

*These authors contributed equally to this work.

Abstract

Error-free repair of DNA double-strand breaks (DSBs) is achieved by homologous recombination (HR), and BRCA1 is an important factor for this repair pathway¹. In the absence of BRCA1-mediated HR, the administration of PARP inhibitors induces synthetic lethality of tumour cells of patients with breast or ovarian cancers^{2,3}. Despite the benefit of this tailored therapy, drug resistance can occur by HR restoration⁴. Genetic reversion of BRCA1-inactivating mutations can be the underlying mechanism of drug resistance, but this does not explain resistance in all cases⁵. In particular, little is known about BRCA1-independent restoration of HR. Here we show that loss of REV7 (also known as MAD2L2) in mouse and human cell lines re-establishes CTIP-dependent end resection of DSBs in BRCA1-deficient cells, leading to HR restoration and PARP inhibitor resistance, which is reversed by ATM kinase inhibition. REV7 is recruited to DSBs in a manner dependent on the H2AX-MDC1-RNF8-RNF168-53BP1 chromatin pathway, and seems to block HR and promote end joining in addition to its regulatory role in DNA damage tolerance⁶. Finally, we establish that REV7 blocks DSB resection to promote non-homologous end-joining during immunoglobulin class switch recombination. Our results reveal an unexpected crucial function of REV7 downstream of 53BP1 in coordinating pathological DSB repair pathway choices in BRCA1-deficient cells.

To identify mechanisms of BRCA1-independent restoration of the HR pathway, we carried out a loss-of-function short hairpin RNA (shRNA) screen using the KB1P-B11 and KB1P-G3 cell lines that we previously derived from *Brca1*^{-/-}*p53*^{-/-} (*p53* is also known as *Trp53*) mouse mammary tumours⁷ (Fig. 1a and Supplementary Table 1). Resistant cells were selected with a high concentration of olaparib

(500nM, about 100-fold the half-maximal inhibitory concentration(IC50)), which killed cells of the empty vector control. Sequencing of the olaparib-surviving colonies revealed a reproducible enrichment of various individual hairpins targeting *Rev7* or *53bp1* (also known as *Trp53bp1*). To validate the *Rev7* hit, we introduced two different hairpins into the KB1P-B11 and KB1P-G3 cell lines; these substantially inhibited *Rev7* expression (Fig. 1b, c and Extended Data Fig. 1a). Despite the role of *REV7* in metaphase-to-anaphase transition⁸, the level of *Rev7* inhibition in these cells did not affect proliferation (Extended Data Fig. 1b, c), allowing long-term clonogenic survival assays. We confirmed that loss of *Rev7* resulted in increased resistance to the PARP inhibitors (PARPi) olaparib and AZD2461 (ref. 7) in both cell lines (Fig. 1d and Extended Data Fig. 1d–g). Resistant cells that survived olaparib treatment (*Rev7* sh1/2-ola) yielded even lower *REV7* expression levels and increased numbers of colonies after PARPi treatment (Fig. 1b–d and Extended Data Fig. 1h). When we reconstituted the *Rev7*-depleted cells with shRNA-resistant *Rev7* complementary DNA resulting in similar *REV7* protein levels (Extended Data Fig. 1i), we successfully re-sensitized the tumour cells to PARPi (Fig. 1e, f).

Tumours derived from the *Brca1*^{-/-}*p53*^{-/-} cells with stable *Rev7* inhibition also showed olaparib resistance *in vivo*, in contrast to the empty vector controls (Fig. 1g and Extended Data Fig. 1j–l). In addition, we found that *Rev7* loss explains some cases of *in vivo* acquired PARPi resistance in BRCA1-deficient mouse mammary tumours (data not shown). *REV7* depletion also resulted in PARPi resistance of the human BRCA1-deficient cell line SUM149PT (Extended Data Fig. 2). Together, these data strongly indicate that inhibition of *Rev7* confers PARPi resistance in BRCA1-deficient tumour cells.

Together with the catalytic subunit *REV3*, *REV7* forms the translesion synthesis polymerase ζ (Pol ζ), and it interacts with *REV1* (ref. 9). We therefore investigated whether loss of *REV1* or *REV3* also confers

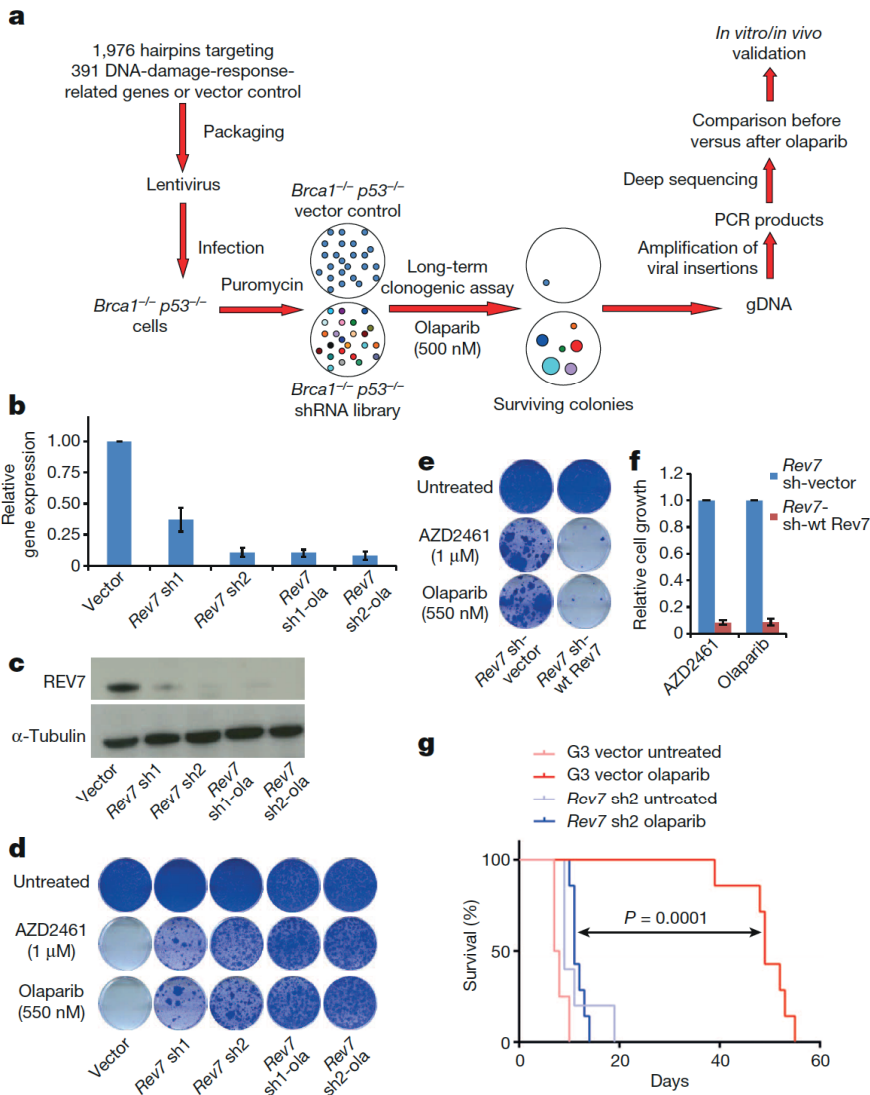


Figure 1 Identification of loss of Rev7 in PARPi-resistant *Brca1^{-/-}p53^{-/-}* mammary tumour cells.

a, Design of the functional shRNA screen. gDNA, genomic DNA. b, c, Quantification of *Rev7* transcript (b) or protein (c) levels in KB1P-G3 cells transduced with *Rev7*-targeting shRNAs or the vector control. *Hprt* was used as a control for transcript expression, and β -tubulin was used as a control for protein expression. The data represent the mean \pm s.d. d, e, Long-term clonogenic assay using KB1P-G3 cells transduced with the indicated constructs (wt *Rev7* stands for pLenti6-wt *Rev7*) and treatments. f, Quantification of the clonogenic assay in e by determining the absorbance of crystal violet at 590 nm. All the groups were normalized to the absorbance of the vector control. The data represent the mean \pm s.d. g, Overall survival of mice with KB1P-G3-derived *Rev7*-depleted or control tumours treated with one regimen of 50 mg olaparib per kilogram daily for 28 days or left untreated. The *P* value was calculated using the log-rank test.

PARPi resistance in *Brca1^{-/-}p53^{-/-}* cells. A 60% inhibition of *Rev1* or *Rev3* transcripts did not cause olaparib resistance (Extended Data

Fig. 3a–d). Moreover, we studied various shRNA-resistant REV7 mutants that lack REV1 (Leu186Ala/Gln200Ala/Tyr202Ala and

3

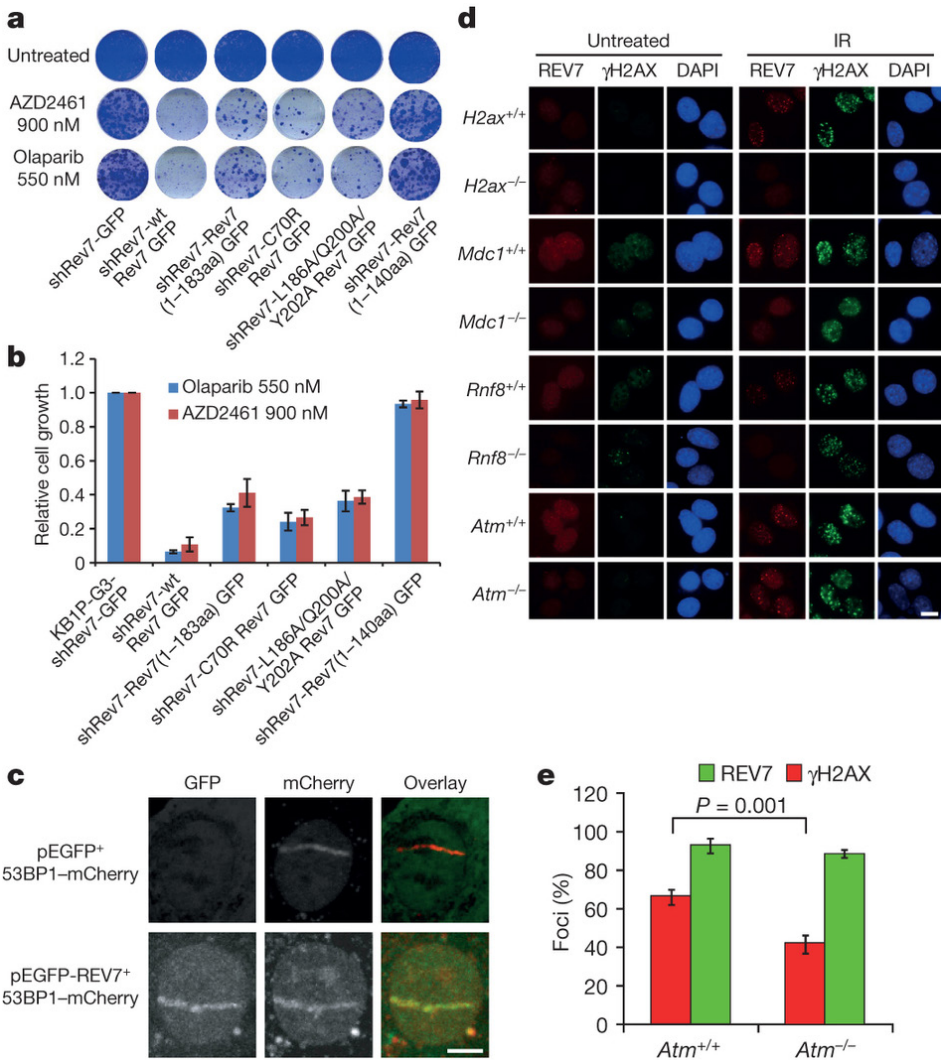


Figure 2 | Dissection of REV7 function and its dependent factors.

a, b, Long-term clonogenic assay (a) and quantification (b) using KB1P-G3 cells transduced with the indicated constructs (wt Rev7 stands for pMSCVGFp-wt *Rev7*) and treatments. All groups were normalized to the absorbance of the shRev7-GFP control. The data represent the mean \pm s.d. c, GFP-REV7 recruitment to sites of DNA damage (visualized by 53BP1-mCherry) was observed 5 min after 405nm laser exposure (0.99mW, 60% laser power, 50 s) in KB1P-B11 cells. pEGFP denotes a mammalian expression vector containing enhanced GFP. Scale bar, 5 μ m. d, REV7 foci formation in *H2ax*^{-/-} (also known as *H2afx*^{-/-}), *Atm*^{-/-}, *Mdc1*^{-/-} and *Rnf8*^{-/-} mouse embryonic fibroblast (MEF) cells and their corresponding controls before and 4 h after 10 Gy ionizing radiation (IR). DAPI, 49,6-diamidino-2-phenylindole. Scale bar, 10 μ m. e, Quantification of REV7 foci formation (>8 foci per cell) in *Atm*^{-/-} and *Atm*^{+/+} MEF cells. The quantification of foci-positive cells was performed by counting a total of 100 cells per sample. Data are presented as mean \pm s.d. from three different experiments. *P* value calculated using the t-test.

a 1-183-amino-acids truncated protein) or REV3 (Cys70Arg) binding sites^{10,11}. In contrast to the truncated 1-140-amino-acid REV7 protein, these mutants are recruited

to DNA damage sites (Extended Data Fig. 3e-g), and their expression in *Rev7* shRNA KB1P-B11 and KB1P-G3 cells significantly restored the sensitivity to PARPi to a degree

approaching that of wild-type REV7 (Fig. 2a, b; $P=0.001$, t-test). The remaining differences of the Leu186Ala/Gln200Ala/Tyr202Ala or Cys70Arg mutants with wild-type REV7 may be explained by unequal expression levels (Extended Data Fig. 3f). These data suggest that the REV1 or REV3 interaction is not absolutely required for the REV7-mediated function in this context. We observed that green fluorescent protein (GFP)-tagged REV7 colocalizes with 53BP1 shortly after DNA damage induction, suggesting that REV7 acts directly at the site of DNA damage (Fig. 2c). REV7 recruitment depends on H2AX, MDC1, RNF8, RNF168 and partly ATM, in both mouse and human cells (Fig. 2d, e and Extended Data Fig. 4a–d). To examine whether PARPi resistance in *Rev7*-depleted *Brca1*^{-/-}*p53*^{-/-} tumour cells is due to HR restoration, we investigated RAD51 focus formation after 10 Gy ionizing radiation. As shown in Fig. 3a, b and Extended Data Fig. 4e, f, *Rev7* loss resulted in the restoration of RAD51 foci formed after DNA damage. To exclude potential off-target effects of the hairpins, we reconstituted *Rev7* shRNA1 and shRNA2 cells with shRNA-resistant mouse or human REV7–GFP fusion proteins (Extended Data Fig. 4g). REV7 re-expression abolished RAD51 focus formation after DNA damage in GFP-positive cells (Fig. 3b). We confirmed the re-appearance of RAD51 foci after tumour irradiation *in vivo* using computed tomography (CT)-guided high precision cone beam irradiation of animals carrying PARPi-resistant KB1P(M) tumours with low *Rev7* gene expression (Fig. 3c).

We then tested whether the processing of broken DNA ends requires ATM in *Rev7*-depleted cells, and found that inhibition of ATM using KU55933 efficiently suppresses DNA damage-induced RAD51 foci and increases olaparib sensitivity (Extended Data Fig. 4h, i). Hence, the partial restoration of RAD51 focus formation in *Brca1*-deficient mammary tumour cells after DNA damage by inhibition of *Rev7* is ATM dependent.

In contrast to the results with BRCA1-deficient cells, *Rev7* depletion in BRCA2-

deficient cells did not result in PARPi resistance (Extended Data Fig. 5a–f). Furthermore, we did not observe increased PARPi resistance after *Rev7* inhibition in the BRCA1/2-proficient *p53*^{-/-} tumour cell line KP3.33 (Extended Data Fig. 5g–i). This indicates that REV7 works upstream of BRCA2 and is antagonized by BRCA1. We therefore tested whether DNA end resection is altered in the absence of *Rev7* in BRCA1-deficient cells. Accumulation of the single-strand binding protein, RPA, was used as a marker for the generation of singlestranded DNA (ssDNA). Cells were exposed to α -particles¹², and BRCA1-deficiency resulted in a marked decrease in RPA-positive α -tracks compared to BRCA1-proficient cells (Fig. 3d, e). REV7 depletion in the *Brca1*^{-/-}*p53*^{-/-} cells largely suppressed this defect in both KB1P-G3 and KB1P-B11 cells (Fig. 3e and Extended Data Fig. 6a). In addition to coating resected DNA ends, RPA also interacts with ssDNA gaps (for example, during replication)¹³. To exclude that the observed RPA accumulation reflected interaction with internal ssDNA gaps, we prevented DNA end resection (without influencing replication) by knocking down CTIP (ref. 14). This eliminated the increase in RPA-positive tracks induced by *Rev7* knockdown in *Brca1*^{-/-}*p53*^{-/-} cell lines (Fig. 3f and Extended Data Fig. 6b), without affecting cell cycle distribution (Extended Data Fig. 6c). We therefore conclude that increased resection and not binding to ssDNA gaps is responsible for RPA accumulation.

As *Rev7* loss could restore end resection in BRCA1-deficient cells, we analysed whether its depletion could restore full HR proficiency in this context. Using mouse embryonic stem (mES) cells with a *Brca1* selectable conditional knockout allele¹⁵, we observed that *Rev7* loss indeed prevented cell death of mES cells after BRCA1 deletion, and restored RAD51 focus formation upon DNA damage (Extended Data Fig. 6d–h). Moreover, we reproducibly observed a partial restoration of HR function in the DR–GFP reporter assay for homologous recombination¹⁶ when *Rev7* was depleted in BRCA1-deficient mES cells (Fig. 3g).

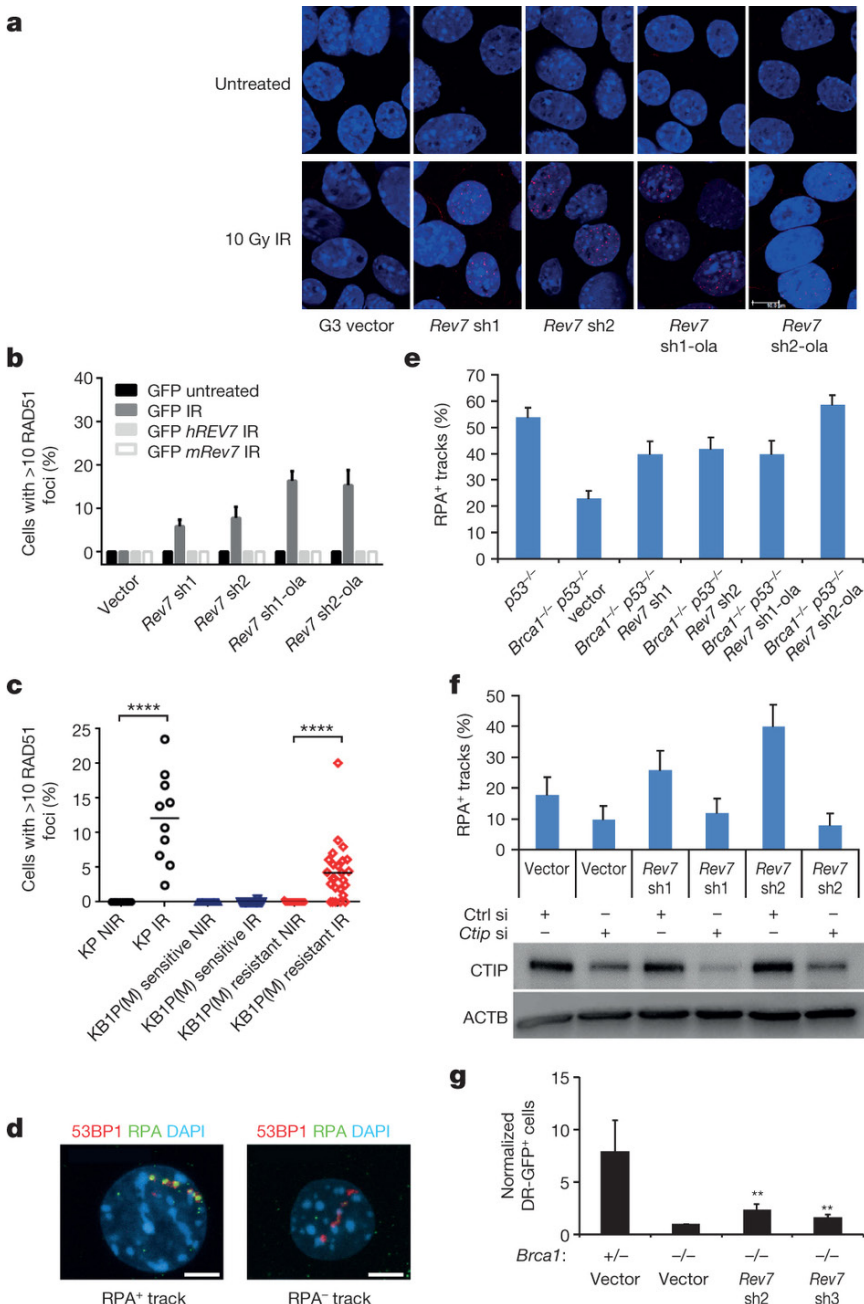


Figure 3 The effect of REV7 inhibition on RAD51 and RPA focus formation of *Brca1*^{-/-}*p53*^{-/-} cells.

a, RAD51 focus (red) formation in KB1P-G3 cells before and 5 h after 10 Gy ionizing radiation. Scale bar, 10 μ m. b, Quantification of RAD51 foci in KB1P-G3 cells (with or without REV7 depletion) transfected with an empty vector (GFP) or vectors containing mouse or human *Rev7* or REV7, respectively. At least 150 GFP-positive cells were analysed per group in three independent experiments each. The data represent the mean \pm s.d. IR denotes 5 h after 10 Gy ionizing radiation. c, In situ analysis of RAD51 foci in PARPi-resistant KB1P(M) tumours with low *Rev7* gene expression. KP (KP3.33) denotes mouse mammary tumour cell line (*p53*^{-/-}); IR denotes 2 h after 15 Gy ionizing radiation; NIR denotes no ionizing radiation. *****P*=0.0001, Mann–Whitney U test. Legend continues on next page.

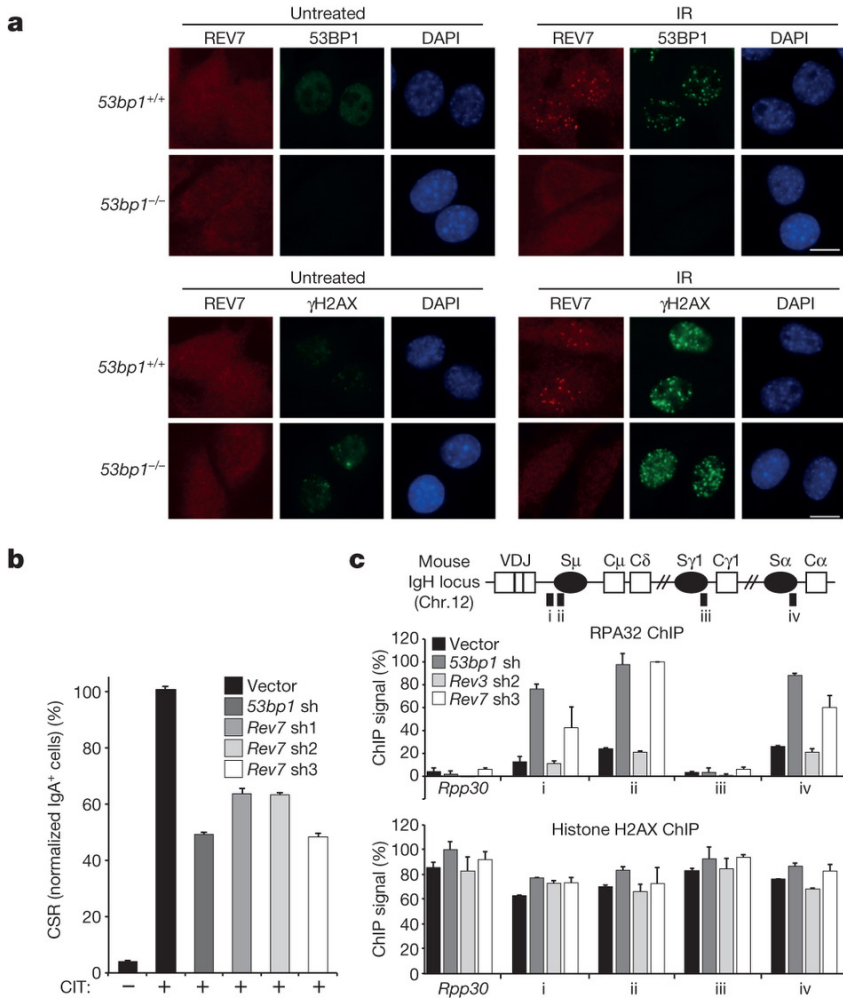


Figure 4 REV7 is a downstream effector of 53BP1 on inhibiting end resection and promoting CSR.

a, REV7 foci formation in *53bp1*^{-/-} and *53bp1*^{+/+} MEF cells before and 4 h after 10 Gy ionizing radiation. Scale bar, 10 μ m. b, Quantification of CSR to IgA of shRNA-transduced CH12 cells 40 h after stimulation (CIT denotes CD40 antibody, IL-4 and TGF- β 1). Data represent mean \pm s.d. from two independent experiments performed in triplicate. c, Schematic of IgH locus shows relative positions of quantitative PCR amplicons used in ChIP experiments. A control non-IgH locus (*Rpp30*) was also examined. Indicated CH12 cell lines stimulated for 30 h with CIT were subjected to ChIP with IgG (control), histone H2AX and RPA32 monoclonal antisera. After background subtraction, values were normalized to the DNA input signals, followed by the maximum value in each data set. Mean signals, two replicates \pm s.e.m.

Figure 3 continued

d, e, Representative images of 53BP1-labelled α tracks in cells positive or negative for RPA (d) and quantification of RPA-positive tracks 2 h after ionizing radiation (e). KP (*p53*^{-/-}) or KB1P-G3 cells with or without Rev7-targeting shRNAs were tested. Scale bar, 5 μ m. f, Quantification of RPA- and 53BP1-positive α tracks in KB1P-G3 cells transfected with non-targeting control (ctrl) short interfering RNAs (siRNAs) or siRNAs against mouse *Ctip*. CTIP protein expression of the indicated groups was checked by western blotting, with β -actin (ACTB) as a loading control. g, Quantification of HR using the DR-GFP reporter assay. GFP-positive cells normalized to the vector-transduced *Brca1*^{-/-} p53 shRNA cells are shown. The data represent mean \pm s.d. ***P*=0.01, two-tailed t-test.

Our data for REV7 are reminiscent of previous findings that 53BP1 loss occurs in subsets of human breast carcinomas¹⁵ and can also restore HR to BRCA1-deficient cells^{7,15,17}. As with 53BP1, we found a frequent aberrant reduction or loss of the REV7 protein in human triple-negative breast carcinomas (Extended Data Fig. 7). Addressing the relationship between REV7, 53BP1 and the 53BP1 non-homologous end-joining (NHEJ) effector protein, RIF1 (ref. 18), we found that *Rev7* deficiency did not compromise the formation of endogenous 53BP1 or RIF1 foci (Extended Data Fig. 8a–d). By contrast, endogenous REV7 foci or laser induced stripes were absent in 53BP1-depleted mouse and human cells (Fig. 4a and Extended Data Fig. 4c, d), strongly suggesting that REV7 acts downstream of 53BP1. This is also consistent with our results that PARPi resistance is not increased when both *Rev7* and *53bp1* are depleted (data not shown). Despite such strong evidence for a cooperative role for REV7 and 53BP1, we did not detect REV7 in 53BP1 immunocomplexes isolated from untreated cell lysates, or ATM-phosphorylated 53BP1 immunocomplexes containing RIF1 that were induced by DNA damage¹⁹ (Extended Data Fig. 8e and data not shown). Although the intricacies of the interactions remain to be determined, REV7 recruitment to DNA damage sites by 53BP1 may result from indirect interactions or an activity elicited by 53BP1 protein complexes in chromatin at DSB sites.

To examine whether REV7, like 53BP1 (ref. 18), also promotes NHEJ of DSBs during class switch recombination (CSR), we depleted *Rev7* transcripts in the mouse CH12 B-cell line, which after stimulation undergoes CSR from IgM to IgA at a high rate²⁰. Efficient *Rev7* knockdown was achieved using several shRNAs, reducing CSR to levels comparable with 53BP1-depleted cells when compared to control-depleted cells (Fig. 4b and Extended Data Fig. 9a, b). Moreover, these defects were not accompanied by defects in cell proliferation, *Aid* (also known as *Aicda*), or germ-line transcript (μ GLT/ α GLT) expression (Extended Data Fig. 9c–e). Conditional REV3-

ablation has been reported to reduce CSR efficiency in B lymphocytes²¹, suggesting that distinct from 53BP1, REV7 might participate in CSR through Pol ζ function. This considered, we reasoned that we might separate the function of REV7 from that of Pol ζ during CSR, at the level of DSB resection inhibition. To this end, RPA enrichment was measured by chromatin immunoprecipitation (ChIP) at control and several IgH loci in control, 53BP1-, REV3- or REV7-depleted CH12 lines stimulated to undergo CSR. Consistent with the role of 53BP1 in resection inhibition, 53BP1-depletion was accompanied by a 3–5-fold enrichment of RPA ChIP signal specifically in donor (S_{μ}) and acceptor (S_{α}) IgH switch (S) regions where DSBs occur during IgM to IgA CSR, but not at an IgH Sc1 locus or a control non-IgH Rpp30 locus (Fig. 4c). Notably, these defects were closely mimicked after REV7 depletion, whereas shRNA-mediated REV3 depletion yielded no detectable increase in RPA IgH S-region enrichment, despite diminishing CSR efficiency (Extended Data Fig. 9f) as expected²¹. Importantly, at each locus equivalent ChIP signals for total histone were obtained between cell lines. Thus, our data support a Pol ζ -independent function of REV7 in inhibiting the nucleolytic processing of DSBs generated during CSR.

Our data uncover a crucial role for REV7 in regulating DSB repair. REV7 depletion restores homology-directed DNA repair of BRCA1-deficient cells resulting in PARPi resistance. We attribute this result to the inhibitory effect of REV7 on DNA end resection. Like 53BP1 together with RIF1 and PTIP (ref. 18), REV7 may function as a NHEJ factor that performs a regulatory role in DSB repair pathway choice. This provides new insight into the versatile functions of REV7 in addition to its role in translesion synthesis^{9,22}, and helps to explain how HR can be partially restored in the absence of BRCA1.

Received 17 February 2014;

Accepted 13 February 2015.

Published online 23 March 2015.

References

- Roy, R., Chun, J. & Powell, S. N. BRCA1 and BRCA2: different roles in a common pathway of genome protection. *Nature Rev. Cancer* 12, 68–78 (2012).
- Lee, J.-M., Ledermann, J. A. & Kohn, E. C. PARP Inhibitors for BRCA1/2 mutation-associated and BRCA-like malignancies. *Ann. Oncol.* 25, 32–40 (2013).
- Farmer, H. et al. Targeting the DNA repair defect in BRCA mutant cells as a therapeutic strategy. *Nature* 434, 917–921 (2005).
- Lord, C. J. & Ashworth, A. Mechanisms of resistance to therapies targeting BRCA mutant cancers. *Nature Med.* 19, 1381–1388 (2013).
- Ang, J. E. et al. Efficacy of chemotherapy in BRCA1/2 mutation carrier ovarian cancer in the setting of PARP inhibitor resistance: a multi-institutional study. *Clin. Cancer Res.* 19, 5485–5493 (2013).
- Chun, A. C.-S., Kok, K.-H. & Jin, D.-Y. REV7 is required for anaphase-promoting complex-dependent ubiquitination and degradation of translesion DNA polymerase REV1. *Cell Cycle* 12, 365–378 (2013).
- Jaspers, J. E. et al. Loss of 53BP1 causes PARP inhibitor resistance in Brca1- mutated mouse mammary tumors. *Cancer Discov* 3, 68–81 (2013).
- Listovsky, T. & Sale, J. E. Sequestration of CDH1 by MAD2L2 prevents premature APC/C activation prior to anaphase onset. *J. Cell Biol.* 203, 87–100 (2013).
- Gan, G. N., Wittschieben, J. P., Wittschieben, B. Ø. & Wood, R. D. DNA polymerase zeta (pol zeta) in higher eukaryotes. *Cell Res.* 18, 174–183 (2008).
- Hara, K. et al. Crystal structure of human REV7 in complex with a human REV3 fragment and structural implication of the interaction between DNA polymerase zeta and REV1. *J. Biol. Chem.* 285, 12299–12307 (2010).
- Khalaj, M. et al. A missense mutation in Rev7 disrupts formation of Pol ζ , impairing mouse development and repair of genotoxic agent-induced DNA lesions. *J. Biol. Chem.* 289, 3811–3824 (2014).
- Stap, J. et al. Induction of linear tracks of DNA double-strand breaks by alpha particle irradiation of cells. *Nature Methods* 5, 261–266 (2008).
- Fanning, E., Klimovich, V. & Nager, A. R. A dynamic model for replication protein A (RPA) function in DNA processing pathways. *Nucleic Acids Res.* 34, 4126–4137 (2006).
- Sartori, A. A. et al. Human CtIP promotes DNA end resection. *Nature* 450, 509–514 (2007).
- Bouwman, P. et al. 53BP1 loss rescues BRCA1 deficiency and is associated with triple-negative and BRCA-mutated breast cancers. *Nature Struct. Mol. Biol.* 17, 688–695 (2010).
- Pierce, A. J., Johnson, R. D., Thompson, L. H. & Jasin, M. XRCC3 promotes homology-directed repair of DNA damage in mammalian cells. *Genes Dev.* 13, 2633–2638 (1999).
- Bunting, S. F. et al. 53BP1 inhibits homologous recombination in Brca1-deficient cells by blocking resection of DNA breaks. *Cell* 141, 243–254 (2010).
- Zimmermann, M. & de Lange, T. 53BP1: pro choice in DNA repair. *Trends Cell Biol.* 24, 108–117 (2014).
- Chapman, J. R. et al. RIF1 is essential for 53BP1-dependent nonhomologous end joining and suppression of DNA double-strand break resection. *Mol. Cell* 49, 858–871 (2013).
- Muramatsu, M. et al. Class switch recombination and hypermutation require activation-induced cytidine deaminase (AID), a potential RNA editing enzyme. *Cell* 102, 553–563 (2000).
- Schenten, D. et al. Pol ζ ablation in B cells impairs the germinal center reaction, class switch recombination, DNA break repair, and genome stability. *J. Exp. Med.* 206, 477–490 (2009).
- Kikuchi, S., Hara, K., Shimizu, T., Sato, M. & Hashimoto, H. Structural basis of recruitment of DNA polymerase ζ by interaction between REV1 and REV7 proteins. *J. Biol. Chem.* 287, 33847–33852 (2012).
- Evers, B. et al. Selective inhibition of BRCA2-deficient mammary tumor cell growth by AZD2281 and cisplatin. *Clin. Cancer Res.* 14, 3916–3925 (2008).
- Fradet-Turcotte, A. et al. 53BP1 is a reader of the DNA-damage-induced H2A Lys15 ubiquitin mark. *Nature* 499, 50–54 (2013).
- Watanabe, S. et al. JMJD1C demethylates MDC1 to regulate the RNF8 and BRCA1-mediated chromatin response to DNA breaks. *Nature Struct. Mol. Biol.* 20, 1425–1433 (2013).
- Doil, C. et al. RNF168 binds and amplifies ubiquitin conjugates on damaged chromosomes to allow accumulation of repair proteins. *Cell* 136, 435–446 (2009).
- Stewart, G. S. et al. The RIDDLE syndrome protein mediates a ubiquitin-independent signaling cascade at sites of DNA damage. *Cell* 136, 420–434 (2009).
- Stap, J. et al. Induction of linear tracks of DNA double-strand breaks by a-particle irradiation of cells. *Nature Methods* 5, 261–266 (2008).
- de Jager, M. et al. DNA-binding and strand-annealing activities of human Mre11: implications for its roles in DNA double-strand break repair pathways. *Nucleic Acids Res.* 29, 1317–1325 (2001).
- Bouwman, P. et al. A high-throughput functional complementation assay for classification of BRCA1 missense variants. *Cancer Discov.* 3, 1142–1155 (2013).
- Bartkova, J. et al. DNA damage response as a candidate anti-cancer barrier in early human tumorigenesis. *Nature* 434, 864–870 (2005).

Acknowledgements

We thank B. Gerritsen, P. Halonen, B. Morris, T. Halaizonetis and O. Kallioniemi for advice on the DDR shRNA library, A. Gasparini and G. Borst for their assistance with the cone beam micro-irradiator, R. Kanaar for his RAD51 antibody, J. Jacobs for the pMSCV-GFP vector, and M. O'Connor for olaparib and AZD2461. This work was supported by the Netherlands Organization for Scientific Research (NWO-Toptalent to J.E.J. and NWO-VIDI to S.R.), the Dutch Cancer Society, CTMM Breast Care, the Swiss National Science Foundation, and the European Union (EU) FP6 Integrated Project CHEMORES and FP7 Project

DDRresponse. Work in J.R.C.'s group is funded by the Wellcome Trust. The work in the J.B.'s laboratories was funded by the Danish Cancer Society, the Danish Council for Independent Research, the Lundbeck Foundation and the Czech National Program of Sustainability. S.J.B. is funded by Cancer Research UK and an ERC Advanced Investigator Grant (RecMitMei) and is a Royal Society Wolfson Research Merit Award Holder.

Author Contributions

G.X. and S.R. designed the study, performed experiments and wrote the manuscript; I.B. and D.C.v.G. designed and performed the RPA foci analysis; J.R.C., A.S. and S.J.B. performed and planned the CSR assay and RIF1-associated data; J.C. and J.Y. designed and performed the experiments using MEFs; J.E.J., A.K. and W.S. assisted with the mouse intervention studies; E.G. established the *in vivo* RAD51 analysis that K.J. and B.v.d.B. quantified; P.H.N.C. designed and M.B. helped in generating the REV7 mutants; Pe.B., M.P. and J.J. helped in designing the shRNA screen and performed experiments using mES cells; M.M. performed the laser stripe assays, and K.W. performed co-immunoprecipitations. D.W. helped to visualize GFP-REV7 recruitment; M.N., I.d.R. and J.d.R. carried out the RNA sequencing (RNA-seq) data analysis, Jirina B. established, carried out and evaluated the REV7 immunohistochemistry, P.C.S. helped with the analysis of the immunohistochemistry data, Jiri B. and Pi.B. advised on experiments and manuscript revisions, and all authors discussed and approved the manuscript.

METHODS

Cell culture and reagents. KB1P-B11 (B11) and KB1P-G3 (G3) cell lines were derived from a *Brcal*^{-/-} *p53*^{-/-} mouse mammary tumour as described⁷. KB2P-1.21 and KB2P-3.4 cell lines originate from a *Brcal*^{-/-} *p53*^{-/-} mouse mammary tumour, and KP3.33 cell line from a *p53*^{-/-} mouse mammary²³. These cell lines were cultured in DMEM/F-12 (Life Technologies) supplemented with 10% FCS, 50 Uml⁻¹ penicillin, 50 ng ml⁻¹ streptomycin, 5 mg ml⁻¹ insulin (Sigma), 5 ng ml⁻¹ epidermal growth factor (Life Technologies) and 5 ng ml⁻¹ cholera toxin (Gentaur) under low oxygen conditions (3% O₂, 5% CO₂, 37°C). SUM149PT cells were grown in RPMI1640 (Life Technologies) supplemented with 10% FCS, under normal oxygen conditions (21% O₂, 5% CO₂, 37°C). U2OS, phoenix, 293T cells were cultured in DMEM (Life Technologies) supplemented with 10% FCS, under normal oxygen conditions (21% O₂, 5% CO₂, 37°C). mES cells with a selectable conditional BRCA1 deletion (*R26*^{CreERT2/wt}; *Brcal*^{1^{Scor}D})¹⁵ were cultured on gelatin-coated plates in 60% buffalo red liver cell-conditioned medium supplied with 10% FCS, 0.1 mM β-mercaptoethanol (Merck) and 1 × 10³ Uml⁻¹ ESGROLIF (Millipore) under normal oxygen conditions (21% O₂, 5% CO₂, 37°C). CH12 cells (CH12F3-2) were cultured in RPMI-1640 medium (Sigma) supplemented with 10% FBS, 5% NCTC 109 medium (Sigma), 50 μM β-mercaptoethanol, 50 Uml⁻¹ penicillin and 50 ng ml⁻¹ strepto-

mycin under normal oxygen conditions. Olaparib and AZD2461 were provided by AstraZeneca; KU-55933 (KuDOS) was bought from Selleckchem (S1092).

Lentivirus-based transduction of cells with shRNA.

Glycerol stocks of shRNA hairpins were obtained from the Sigma Mission library (TRC 1.0) and isolation of plasmids was carried out with the high pure plasmid Mini Kit or Genopure maxi kit (Roche). 293T cells were seeded 16 h before transfection. For each 10-cm dish, 0.5 ml 2xHBS (8.18 g NaCl, 0.2 g Na₂HPO₄·7H₂O, 5.95 g HEPES in 500 ml MilliQ water at pH7.01) was added into a sterile falcon tube. In another sterile falcon tube, 6 μg plasmid DNA of interest, 2 μg pHCMV-G envelope vector (pMD.G), 2 μg pRSV-Rev, 2 mg packaging vector pMDLg/pRRE, 250 ml 0.5M CaCl₂ and distilled water were added to bring up to 0.5 ml. The CaCl₂/plasmid DNA mix was added to the 2xHBS and incubated for 20 min and then added to the cells. Medium was refreshed after 6 h and another 18 h, respectively. The supernatant of 293T cells containing lentivirus was collected after 24 h to infect cells with polybrene (6 mg ml⁻¹) for 12 h. The medium was refreshed after lentivirus infection and the cells were selected with puromycin.

Individual shRNA vectors used were collected from the TRC library.

Mouse *Rev7*: sh1: TRCN0000012844_C CAGTGGAGAAGTTGTCTTT; sh2: TRCN 0000012846_CATCTTCCAGAAGCGCAAGAA; sh3: TRCN0000012847_GAT ACAGTTCATCAAGGACTT; human *REV7*: sh1: TRCN0000006569_CCCTGA TTCCAAGTGCTCTTA; sh2: TRCN0000006570_CCCGGAGCTGAATCAGTATAT; sh3: TRCN0000006571_CCCAGTGGAGAAATTCGCTCTT; sh4: TRCN0000006573_CATCTTCCAGAAACGCAAGAA; mouse *53bp1*: (puromycin) sh: TRCN0000081778_GCTATTGTGGAGATTGTGTGTTT; (neomycin) sh: same sequences as above; human *53BP1*: sh1: TRCN0000018866_C CAGTGTGATTAG ATTGATT; sh2: TRCN0000018865_GATACTTGGTCTTACTGGTTT; mouse *p53*: (neomycin) TRCN0000054551_AGAGTATTCACCTCAAGAT; mouse *Rev1*: sh1: TRCN0000120298_GCGAGATCAACTATGGAATA; sh2: TRCN 0000120297_CAGCAGTGCTTGTGAGGATT; mouse *Rev3*: sh1: TRCN0000119969_CCGTCACATTAGTGAGACTAT; sh2: TRCN0000119970_GCCAC ATACACTTCTTCTT.

Loss-of-function screen. In total, 1,976 lentiviral hairpins (pLKO.1) from the Sigma Mission library (TRC Mm 1.0) that target 391 mouse genes involved in the DNA damage response were selected (see Supplementary Table 1). This library was used to generate pools of lentiviral shRNA in 293T cells to infect target cells. After infection, the cells stably expressing integrated shRNA were selected with puromycin. Cells with HR restoration were selected with a high concentration of olaparib (500 nM, about 100-fold the IC₅₀), which killed cells of the empty vector group. Surviving cells were pooled and genomic DNA was extracted using the Genra Puregene kit according to the manufacturer's protocol (Qiagen). shRNA inserts were retrieved from 50 ng genomic DNA by PCR amplification (PCR1 and PCR2) using the following conditions: (1) 95 °C, 5 min; (2) 95 °C, 30 s; (3) 60 °C, 30 s; (4) 72 °C, 1 min; (5) go to step (2), 20 cycles; (6) 72 °C, 5 min; (7) 4 °C. The PCR reaction system

were as follows: 0.6 μ l DMSO, 4.0 μ l phusion HF buffer 5x, 0.4 μ l dNTPs, 1.0 μ l primer f (10mM), 1.0 μ l primer r (10mM), 11.8 μ l mQ, 0.2 μ l phusion, 1.0 μ l gDNA for PCR1 or 1 μ l PCR1 products for PCR2. Adaptors and indexes for deep sequencing (Illumina HiSeq 2000) were incorporated into PCR primers as follows: PCR1 forward: PCR1_01_PLKO1_f_Integration_determination_1, 5'-AC ACTCTTCCCTACACGACGCTCTTCGATCTCGTATCTTGTGGAAAGGACGAAACACCGG-3'; PCR1_02_PLKO1_f_Integration_determination_2, 5'-ACACTCTTCCCTACACGACGCTCTTCCGATCTGTAGCCCTTGTGGAAAGGACGAAACACCGG-3'; PCR1_03_PLKO1_f_untreated_1, 5'-ACACTCTTCCCTACACGACGCTCTTCCGATCTGTGTTGGAAAGGACGAAACACCGG-3'; PCR1_04_PLKO1_f_untreated_2, 5'-ACACTCTTCCCTACACACTCTTCCCTACACGACGCTCTTCCGATCTGTAGCCCTTGTGGAAAGGACGAAACACCGG-3'; PCR1_03_PLKO1_f_untreated_1, 5'-ACACTCTTACGACGCTCTTCCGATCTATTGGCCTTGTGGAAAGGACGAAACACCGG-3'; PCR1_05_PLKO1_f_olaparib_1, 5'-ACACTCTTCCCTACACGACGCTCTTCCGATCTGATCTGTTGGAAAGGACGAAACACCGG-3'; PCR1_06_PLKO1_f_olaparib_2, 5'-ACACTCTTCCCTACACGACGCTCTTCCGATCTTCAAGTCTTGTGGAAAGGACGAAACACCGG-3'; PCR1_07_PLKO1_f_olaparib_3, 5'-ACACTCTTCCCTACACGACGCTCTTCCGATCTCTGATCCTTGTGGAAAGGACGAAACACCGG-3'; PCR1_08_PLKO1_f_olaparib_4, 5'-ACACTCTTCCCTACACGACGCTCTTCCGATCTAAGCTACTTGTGGAAAGGACGAAACACCGG-3'; PCR1 reverse: P7_plKO1_r, 5'-CAAGCAGAAGACGGCATAAGATTCTTCCCTGCACTGTACCC-3'; PCR2 forward: P5_illuSeq, 59-AATGATACGGCACCACCGAGATCTCACTCTTCCCTACACGACGCTCTTCCGATCT-3'; PCR2 reverse: P7, 5'-CAAGCAGAAGACGGCATAAGAT-3'. PCR2 products were purified using the PCR purification kit from Qiagen. The shRNA stem sequence was segregated and aligned to the TRClibrary. The reads of different hairpins were counted and the following criteria were used to select the top hits for further validation: (1) hairpins targeting the same gene in survival clones should have at least 13104 reads (total 6×10^6 reads); (2) at least two different hairpins targeting the same gene should be present; (3) hairpins in resistant clones should be highly enriched (0.8-fold) in cells after olaparib selection; and (4) hairpins should be present in 4 out of 4 independent screens.

PARPi treatment study. Long-term clonogenic assay: on day 0, 1.5×10^4 (B11) or 1×10^4 (G3, KB2P.1.21 or KB2P.3.4) or 6×10^3 (KP3.33) cells were seeded per well with PARPi (or untreated control) into six-well plates. The medium of the PARPi treatment groups was refreshed with PARPi every 4 days. On day 5, the untreated control group was stopped and the PARPi treatment groups were stopped after another 2–3 weeks and stained with 0.1% crystal violet. Using the SUM149PT cells, 4×10^4 cells were seeded per well with olaparib (or untreated control) into 12-well plates. The medium of the PARPi treatment groups was refreshed with olaparib every 4 days. On day 6, the untreated control group was stopped and the olaparib treatment groups were

stopped on day 8 and stained with 0.1% crystal violet. Quantification of the clonogenic assay was done by determining the absorbance of crystal violet at 590 nm.

Short-term clonogenic assay: on day 0, 43102 (G3) cells were seeded per well with olaparib (or untreated control) into 6-well plates. On day 4, the medium was refreshed with olaparib or untreated control. On day 8, all the groups were stained with Leishman dye and quantification was done by the relative colony numbers.

ATM and PARP inhibitor combination study. On day 0, 1×10^4 (G3) cells were seeded per well into 6-well plates and then ATM inhibitor or olaparib or their combination was added. The medium was refreshed every 3 days with the different drugs. For the combination therapy groups, ATM inhibitor was applied for 6 days. On day 5, ATM inhibitor alone and untreated control groups were stopped and the other groups were stopped on day 12 and stained with 0.1% crystal violet.

Constructs. Human REV7 was amplified by PCR using Platinum Taq polymerase (Invitrogen) from U2OS cDNA using the following primers 5'-ATAGAATTCATGAC-CACGCTCACACGACAAGAC -3' and 5'-ATATGGTACCAT-CAGC TGCCCTTATGAGCGCGC-3'. Mouse *Rev7* was amplified from mouse lung cDNA in two parts to introduce silent mutations, making it resistant to *Rev7* shRNA2 (*mRev7R*). The following primers were used for part A: [IB11m] 5'-ATATGAATTCGATGACCACCCTCACGCGC-3' [IB14m] 5'-TACTTCTCCGTTTCTGAAAGATGCCACCGG-GTA-3' and part B: [IB12m] 5'-ATATGGTACCATGCTGTCT-TATCGCTCGCT-3' [IB13m] 5'-GGGCATCTTTCAGAAACGG AAGAAGTACAACGTGC-3'. Equal parts of both PCR reactions were mixed and used for aPCR using IB11m and IB12m to create the complete mouse *Rev7* sequence including the silent mutations. The PCR product and pEGFP-C1 vector were digested using *EcoRI* and *KpnI* and ligated using the T4 DNA Ligase (Roche) to generate pEGFP-hREV7 and pEGFP-mREV7R. Using pEGFP-mREV7R as a template, pEGFP-C1-based REV7 truncated constructs was amplified by PCR using the following primers: forward: 5'-ATATGAATTCGATGAC-CACCCTCACGCGC-3'; reverse: mREV7R (1–55aa): 5'-ATATGGTACCGGACATCTGAACCGGCAC-3'; mREV7R (1–81aa): 5'-ATATGGTACCCTCCACATCGTTCTTCTCCAGG-3'; mREV7R (1–110aa): 5'-ATATGGTACCAGATGGACAG-CAAGGGAGGC-3'; mREV7R (1–140aa): 5'-ATATGGTACCCTTGTGATCCAGGACAGC-3'; mREV7R (1–183aa): 5'-ATATGGTACCCTGCTGATGTTGGACATCCTG-3'. pEGFP-REV7 mutants (shRNA-resistant) were ordered as gBlocks (IDT) and cloned into the pEGFP-C1 vector using *EcoRI* and *KpnI* restriction enzymes and quick ligase (NEB). The DNA sequences that were ordered as gBlocks are: mREV7_shRNAresistant (mREV7R): CGCCGCG AATCCGCCACCATGACCACCCTCACGCGCAAGACCT-CAACTTTGGCCAAGTGGTGGCTGACGTGCTCTCCGAGT-TCCTGGAGGTGGCCCTGCACCTGATTTCTATGTGCGC-GAGGTCTACCCGGTGGGCATCTTTCAGAAACGGAAGAA-GTACAACGTGCCGTTTCAGATGCTCTGTACCCGGAGCTG AACCAGTACATCCAGGACACACTCCACTGCGTCAAACCTCTCTGGAGAGAAGACGATGTGGAGAAGGTGGTGGTGGTATTTGGATAAGGAACACCGCCAGTG-GAGAAGTTTGTCTTTGAGATCACTACGCTCCCTTGCT-

GTCCATCAATTCAGACTCCCTCCTGTCTCATGTG-
GAGCAGCTGCTTCGAGCCTTCATCCTTAAGATT-
AGTGTGTGTGATGCTGTCTCGATCACAACC
CTCCAGGCTGCACATTTACAGTCTCGTGCACAAA-
GCAAGCTGCTACTCGAAACATGGAGAAGATACAG-
GTCATCAAGGACTTCCATGATCCTGGCAGATGAA-
CAGGATGTCCACATGCACGACCCCGCTTGATACC
CTAAAAACCATGACGTCGGACATTTAAAGATG-
CAGTCTACGTTGAAGAGCGAGCGCATAAGAACAGCT-
GAGTACCCCGG; mREV7_shRNA resistant_L186A/
Q200A/Y202A: CGCCGCGAATTCGCCACCATGAC-
CACCTCACGCGCAAGACCTCAACTTTGGCCAAGT-
GGTGGCTGACGTGCTCTCCGAGTTCCTGGAGTGGC-
CGTGACCTGATTCTATGTGCGGAGGCTACCCG-
CTGGGCATTTTCAGAAACGGAAGAAGTACAACGTGCC
GGTTTCAGATGCTGTACCCGAGACTGAAC-
CAGTACATCCAGGACACACTCCACTGCGT-
CAAACCTCTCCGAGAGAAGCATGTGGAGAAGG
TGGTGGTGGTATTGGATAAGGAACCCGCCAGTG-
GAGAAGTTGTCTTGAGATCACTAGCTCCCTCTGCT-
GTGCAATTCAGACTCCCTCTGTCTCATGTGGAG-
CAGCTGCTTCGAGCCTTCATCCTTAAGATTAGTGTGT-
GATGCTGTCCGATCACAACCCTCCAGCTGCACATTAC
AGTCTCGTGCACACAAGAGAAGCTGCTACTCGAAA-
CATGGAGAAGATACAGCTCATCAAGGACTTCCCAT-
GGATCTTGGCAGATGAACAGGATGTCCACATG-
CACGACCCCGCGTATAACCCATAAAACCATGACGTCG-
GACATTTAAAGATGGCTCTCGCTGTGAAGAGCGAG-
CGCATAAGAAGCTGAGGTACCCCGG; mREV7_
shRNAresistant_C70R: CGCCGCGAATTCGCCACCAT-
GACCACCTCACGCGCCAAGACTCAACTTTGGCCA
AGTGTGTGCTGACGTGCTCTCCGAGT-
TCTCTGAGGTGGCCGTGCACCT
GATTCTCATGTGCGGAGGTTACCCGGTGGGCATCT-
TTCAGAAACGGAAGAAGTACAACGTCCGGTTCAGAT-
GCTCTGTACCCCGGAGCTGAACCATGATCCAGGA-
CACACTCCACCGCTCAAACCTCTCTGGAGAAGAAC-
GATGTGGAGAAGTGGTGGTGGTATTGGATAAG-
GAACACCCGAGTGGAGAAGTTGTCTTTGAGATCACT-
CAGCTCCCTCTGTGCTCAATTCAGACTCCCTCTCT-
GTCTCATGTGGAGCAGCTCTTCGAGCCTTCATCCTTAA-
GATTAGTGTGTGATGCTGTCTGGATCACAACCCTC-
CAGGCTGCACATTTACAGTCTCTGTGCACACAA-
GAGAAGCTGCTACTCGAAACATGGAGAAGATACAGGCAT-
CAAGGACTTCCCATGGATCTGGCAGATGAACAGGAT-
GTCCACATGCACGACCCCGCTTGATACCCCTAAAAAC-
CATGACGTGCGACATTTAAAGATGACGCTCTACGTTGAA
GAGCGAGCGCATAAGAAGCTGAGGTACCCCGG.Using
pEGFPmREV7R, C70R and L186A/Q200A/Y202A
mutants as templates, Gateway compatible pMSCV-GFP or
pLenti6-UBC(Invitrogen)-based REV7 truncated orREV7
mutated constructs were amplified by PCR using the
following primers: forward: 5'-GGGGACAACCTTTGTA-
CAAAAAGTTGGCATGACCACCTCACGCGCCAA-3';
reverse: mREV7R (full-length for wt REV7, C70R REV7,
L186A/Q200A/Y202A REV7): 5'-GGGGACAACCT-
TTGTACAAGAAAGTTGGGTATTACGCTGTTCTTATG-
CGCTCGCTC-3'; mREV7R(1-140aa): 5'-GGGGACAACCTT
GTACAAGAAAGTTGGGTATTACGTTGTGATCCAGGA-
CAGC-3'; mREV7R (1-183aa): 5'-GGGGACAACCTTG-
TACAAGAAAGTTGGGTATTACGTCGTGCATGTGGA-

CATCCTG-3'. PCR products were purified using PCR
purification kit (Roche) and then subjected to BP (BP-
clonase II, Invitrogen) and LR (LRClonase II, Invitrogen)
reaction according to manufacturer's instructions. Wildtype
53BP1 and 53BP120AQ constructs were previously de-
scribed¹⁹. All the constructs were verified by sequencing.
siRNA, cDNA transfection and cDNA transduction.
SMARTpool siRNAs targeting mouse *Ctip* (siGENOME:
M-055713-02, Thermo Scientific) and non-targeting-
control were transfected into cells using Dharmacon1
transfection reagent (Thermo Scientific). After 48 h,
cells were subjected to western blot and a track assay.
siRNAs against *53bp1*, *Rnf8* or *Rnf168* were transfected
into cells using Lipofectamine RNAiMax according to
the manufacturer's instruction. The sequences of
53bp1 siRNA: 5'-GAGAGCAGAUGAUCCUUUA-3' (ref.
24); *Rnf8* siRNA: 5'-GGCAUUUUGGACAACAATT-3'
(ref. 25); *Rnf168* siRNA: 5'-GGCGAAGAGCGAUGGAG-
GAtt-3' (ref. 26); GFP siRNA: 5'-GGCUACGUCCAGGAG-
CGCACCTT-3'. Immunofluorescence and western
blotting analysis was done 64 h after transfection.

For pEGFP-based constructs, transient
transfection was done using X-treme GENE HP
DNA transfection reagent (Roche) according to the
manufacturer's manual. GFP-positive cells were
sorted by flow cytometry and subjected to west-
ern blotting and immunofluorescence staining.

For pMSCV-GFP (retrovirus)-based constructs,
transient transfection was done using X-treme GENE
HP DNA transfection reagent in phoenix cells and the
medium was refreshed after 24 h. Retroviruses were
collected 48 h after transfection, and then target cells
were infected for two consecutive periods of 12 h using
fresh virus. The medium was refreshed after retrovirus
infection and the cells were selected with blasticidin.

For pLenti6-UBC(lentivirus) based constructs,
together with the packaging plasmids p59, p60 and p61,
transient transfection was done using X-treme GENE HP
DNA transfection reagent in 293T cells and the medium
was refreshed after 24 h. Lentiviruses were collected 48
h after transfection and then target cells were infected
for two consecutive periods of 12 h using fresh vi-
rus. The medium was refreshed after lentivirus in-
fection and the cells were selected with blasticidin.

**Mouse, generation of PARPi-resistant mouse mam-
mary tumours.** All mouse experiments were ap-
proved by the Animal Experiments Review Board
of the Netherlands Cancer Institute (Amsterdam),
complying with Dutch legislation. Olaparib resistant
KB1P(M)- and AZD2461-resistant KB1P mouse mam-
mary tumours were generated as described⁷. In this
study we analysed a total of 55 PARPi-resistant and
52 PARPi-sensitive tumours derived from 13 individ-
ual KB1P(M) and 10 individual KB1P donor tumours.

To generate mouse mammary tumours
from cell lines, 5×10^5 cells were orthotopically trans-
planted into 6-week-old female wild-type FVB/N_
Ola129 mice as reported previously⁷. Mice were ran-
domized to the PARPi or untreated control groups.
RT-qPCR. Total RNA was isolated from cells using the
high pure RNA isolation kit (Roche). cDNA was made

from 1 µg RNA with the GoScript Reverse Transcription system (Promega). For the quantitative PCR cDNA, Primer Fw&Rv (400nM) and Lightcycler 480 SYBRGreenMaster (Roche) were applied in a Lightcycler 480 96-well plate (Roche). The SYBR green signals were measured with Lightcycler 480 II (Roche). The Cp value of the gene of interest was subtracted from the housekeeping gene. This value was put in the power of 2 and this was also done for the s.d. The primer sequences used in this study are as follows: Mouse *Hprt* forward: 5'-CTGGT-GAAAAGACCTCTCG-3'; mouse *Hprt* reverse: 5'-TGAA-GTACTCATTATAGCAAGGGCA-3'; mouse *Rev7* forward: 5'-ACACTCCACTGCGTCAAACC-3'; mouse *Rev7* reverse: 5'-AAAGACAAACTTCTCCACTGGGC-3'; mouse *Rev1* forward: 5'-ACAGGATTGCTTGGTGCCTGTG-3'; mouse *Rev1* reverse: 5'-TGAAGTCCGCGTTGCTCTTTC-3'; mouse *Rev3* forward: 5'-AAGAGATGTCACAGACAGGCC-3'; mouse *Rev3* reverse: 5'-AGTTAGACAGCCGCTGTTGTGC-3'; mouse α GLT forward: 5'-GACATGATCACAGGCACAGG-3'; mouse α GLT reverse: 5'-TTCCCAAGTACATTCATCGT-3'; mouse μ GLT forward: 5'-TAGTAAGCGAGGCTTAAAAG-CAT-3'; mouse μ GLT reverse: 5'-AGAACAGTCCAGT-GTAGCAGTAGA-3'; mouse *Aid* forward: 5'-GAAA-GTACGCTGGAGACCG-3'; mouse *Aid* reverse: 5'-TCT-CATGCCGTCCTTGG-3'. Human HPRT-P1 (primers pair 1) forward: 5'-GCAGACTTGTCTTCTTGG-3'; human HPRT-P reverse: 5'-ACACTTCGTGGGGTCTT-3'; human HPRT-P2 forward: 5'-TGCTCGAGAT-GTGATGAAGG-3'; human HPRT-P2 reverse: 5'-AATC-CAGCAGGTACGCAAG-3'; human REV7-P1 forward: 5'-TGCTGTCCATCAGCTCAGAC-3'; human REV7-P1 reverse: 5'-TCTTCTCCATGTTGCGAGTG-3'; human REV7-P2 forward: 5'-GCTCACACGACAAGACCTCA-3'; human REV7-P2 reverse: 5'-GACCCGACGTTGTACTTCT-3'; mouse *53bp1* forward: 5'-TCAGCCAACAGGACAAGCA-3'; mouse *53bp1* reverse: 5'-GCAGAATCTTACAGCAGCAAGG-3'.

Western blotting. Cells were washed with ice-cold PBS and lysed on ice for 30 min with RIPA lysis buffer supplemented with three protease inhibitors (P8340, P5726, P0044; Sigma-Aldrich). Protein concentration was determined by the Bradford Protein Assay Kit (Bio-Rad) and a calibration standard curve created from the BSA. The samples were prepared for loading by adding 4x sample buffer (Invitrogen) and heating the samples at 70 °C for 10 min. Total proteins were separated by SDS-PAGE on 3–8% Tris-acetate (for 53BP, RIF1) or 4–12% Bis-Tris gradient gels (all others). Next, proteins in the gel were electrophoretically transferred to PVDF membrane (Millipore) (for REV7, ACTB, α -tubulin) or to NC membranes (Invitrogen) (all others) and then the membrane was blocked in 5% milk with Tris-buffered saline Triton X-100 buffer (100mM Tris, pH7.4, 500mM NaCl, 0.1% Triton X-100) (TBS-T0.1%). Membranes were incubated with primary antibodies in 5% milk in TBS-T0.1% overnight at 4 °C. Horseradish peroxidase (HRP)-conjugated secondary antibody incubation was performed for 1 h at room temperature in 5% milk in TBS-T0.1% and signals were visualized by ECL. Primary antibodies used in this study were as follows: mouse anti-REV7 (612266, BD Biosciences), 1:5,000 dilution; rabbit anti-53BP1 (NB100-304, Novus), 1:1,000 dilution; rabbit anti-53BP1

(A300-272A, Bethyl), 1:5,000 dilution; rabbit anti-CTIP (ab70163, Abcam), 1:1,000 dilution; mouse anti- α -tubulin (T6074, Sigma), 1:5,000 dilution; mouse anti-ACTB (MAB1501R, Millipore), 1:5,000 dilution; rabbit anti-mouse RIF1 (SK1316) (ref. 19), 1:2,000 dilution; mouse anti-RNF8 (B-2, Santa Cruz), 1:1,000 dilution; rabbit anti-RNF168 (ref. 27), 1:5,000 dilution; mouse anti-GAPDH (1D4, GeneTex) 1:1,000 dilution. Secondary antibodies used in this study were as follows: polyclonal rabbit anti-mouse immunoglobulins/HRP (P0161, Dako), 1:10,000 dilution; polyclonal swine anti-rabbit immunoglobulins/HRP (P0217, Dako), 1:10,000 dilution. **Immunofluorescence.** Cells were grown on glass coverslips (12mm) in 24-well plates. To induce ionizing radiation-induced foci, cells were γ -irradiated (10Gy) and compared to non-irradiated controls 5 h after ionizing radiation. For this purpose the cells were pre-extracted using cold CSK buffer (10mM HEPES-KOH, pH7.9, 100mM NaCl, 300mM sucrose, 3mM MgCl₂, 1mM EGTA and 0.5% (v/v) Triton X-100) on ice for 5 min and then cold CSS buffer (10mM Tris, pH7.4, 10mM NaCl, 3mM MgCl₂, 1% (v/v) Tween and 0.5% (w/v) sodium deoxycholate) on ice for 5 min. Cells were washed with PBS++ (PBS with 1mM CaCl₂ and 0.5mM MgCl₂) and fixed using 2% PFA/PBS++ for 20 min at room temperature. Fixed cells were washed three times with PBS++ and stored at 4 °C. The cells were incubated 20 min in 0.2% Triton X-100/PBS++ to be permeabilized. Then the cells were washed three times in staining buffer (PBS++: 1% BSA, 0.15% glycine, 0.1% Triton X-100), incubated for 30 min in staining buffer at room temperature, incubated with the first antibody for 2 h at room temperature in staining buffer, washed three times in staining buffer, incubated with the second antibody for 1 h at room temperature in staining buffer and washed three times in staining buffer. Next, the cells were counter-stained with DAPI for 5 min, washed in staining buffer, washed in PBS++, mounted in Vectashield and sealed with nail polish. Primary antibodies used in this study were as follows: rabbit anti-RAD51 (70-001, BioAcademia), 1:20,000 dilution; rabbit anti-53BP1 (A300-272A, Bethyl), 1:4,000 dilution. Secondary antibodies used in this study were as follows: Alexa Fluor 568 F(ab')₂ Fragment goat anti-rabbit (A21069, Invitrogen), 1:1,000 dilution; Alexa Fluor 488 anti-mouse antibody (A11001, Invitrogen), 1:1,000 dilution.

For REV7 staining in MEF cells, cells cultured on coverslips were treated with 10 Gy IR and allowed to recover for 4 h. Cells were then washed with PBS, pre-extracted with 0.5% Triton X-100 solution for 3 min and fixed with 3% paraformaldehyde for 12 min. Coverslips were washed with PBS and then immunostained with REV7 antibody (612266, BD Biosciences, 1:200 dilution) and anti-ch2AX or anti-53BP1 in 5% goat serum for 1 h at room temperature. Coverslips were washed and incubated with secondary antibodies conjugated with rhodamine or FITC for 30min at room temperature. Cells were then stained with DAPI to visualize nuclear DNA. The coverslips were mounted onto glass slides with anti-fade solution. For RIF1 staining in MEF cells, wild-type-MEFs stably transduced with indicated shRNA expressing

lentiviruses were examined for RIF1 foci following neocarzinostatin treatment. Automated quantification of RIF1 foci following mock and neocarzinostatin treatment was performed using Cell-Profiler software (Broad Institute).

Laser irradiation of human cells and immunofluorescence staining. Cells were grown on plastic disks (17mm diameter) that were cut using CNC cutter from the bottom of standard 10-cm cultivation dish (TPP) ultraviolet-sterilized and placed inside the wells of a 12-well plate. BrdU (0.5 mM) was added into siRNA-transfected cells 40 h after the transfection to pre-sensitize cells towards UV-A wavelength. Twenty-four hours after BrdU addition, the plastic disks with cells were removed and covered by a coverslip and immediately placed inside Zeiss AxioObserver Z.1 inverted microscope combined with LSM 780 confocal module. Cells were irradiated at 20 °C via 40x water immersion objective (ZeissC-Apo 403/1.2WDICIII), using 355nm 65mW laser set on 100% power. The total laser dose that can be further manipulated by the amount of irradiation cycles was empirically set to six irradiation cycles. Laser track was pre-defined to cover all the cells within the acquisition area with at least one stripe across the nucleus. After the irradiation process the coverslip was gently removed and plastic disk was quickly placed back into the same well of the 12-well plate and incubated for another 45 min at standard cultivation conditions. The plastic disks with laser-irradiated cells were first processed by pre-extraction at 4 °C. It involves washing by PBS (4 °C), equilibration for 2 min in sucrose buffer 1 (10mM PIPES, pH6.8, 100mM NaCl, 1.5mM MgCl₂ and 300mM sucrose) on ice and then pre-extraction for 15 min on ice, on slowmoving shaker using sucrose buffer 2 (10mM PIPES, pH6.8, 100mMNaCl, 1.5mM MgCl₂, 300mM sucrose, 0.5% Triton X-100, 5 mg ml⁻¹ leupeptin, 2 mg ml⁻¹ aprotinin, 0.1mM phenylmethanesulfonylfluoride (PMSF), 1mM dithiothreitol (DTT)). After the pre-extraction cells were washed by PBS (4 °C) and fixed by 4% paraformaldehyde (PFA) for 15 min at room temperature. PFA was washed out three times by PBS. The disks were further processed as standard coverslips (that is, blocking in blocking solution (DMEM plus 20% FCS) for 1 h followed by incubation with primary antibodies involving REV7 (BDBioscience,mouse, 1:200), pS139-H2AX (Cell Signaling, 20E3, rabbit, 1:300) and 53BP1 (Santa Cruz, H-300, rabbit 1:400) for 2 h, and with appropriate secondary antibodies coupled to Alexa Fluor 488 and Alexa Flour 568 fluorophores (dilution 1:1,000) (Life Technologies). Both primary and secondary antibodies were dissolved in the blocking solution. After washes in PBS, the disks were incubated in 1 mg ml⁻¹ DAPI in dH₂O at room temperature for 5 min and air dried. Dried disks were placed on a standard microscopy glass (cell layer face up) and anchored by two rubber bands laced over the glass. Stained cells were mounted using VectaShield (Vector Labs) mounting medium and covered by a coverslip. The samples were examined using Zeiss AxioObserver Z.1 inverted microscope combined with LSM 780 confocal module using x40 oil objective (Zeiss EC PlnN 403/1.3 Oil DICII). It means that after the first

acquisition the plastic disk and themicroscopy glass-wasmarked by diamond cutter (to ensure same positioning of the disk in the future), the coverslip was gently removed and disk was washed three times in PBS, 0.5% Tween to remove the mounting medium. Next, the disk was incubated in the 1xRe-Blot solution (Re-Blot Plus Mild, Millipore) for 30 min on a slow moving shaker. The solution was washed out three times in PBS. Such sample was ready for new staining procedure involving new set of primary and secondary antibodies following the same protocol as described above.

In situ analysis of RAD51 foci formation. Five matched PARPi-resistant and -sensitive KB1P(M)tumours were orthotopically transplanted into wild-type FVB/N recipient mice. When tumours reached 500mm³ in volume, the mice were randomized to be either irradiated (dose: 15 Gy) using a CT-guided high precision cone beam micro-irradiator (X-RAD 225Cx) or left untreated. As a positive control a BRCA1-proficient KP tumour was taken along. Two hours after irradiation the tumours were taken out and fixed in 4% formalin. Immunofluorescence staining was performed on FFPE slides. RAD51foci were detected using a non-commercial antibody provided by R. Kanaar in a dilution of 1:5,000. 53BP1 foci were detected using rabbit anti-53BP1 (A330-272A, Bethyl), diluted 1:500. As a secondary antibody goat-anti rabbit-Alexa Fluor568 (Invitrogen) was used at a dilution of 1:1,000 (2 mg ml⁻¹). Images were taken by a 'blinded' investigator using a confocal microscope (Leica SP5, LeicaMicrosystemsGmbH), equipped with a3100 objective. For each tumour five random areas (246x246 µm) were imaged. Image stacks (~four slices) were analysed in ImageJ, using an in-house developed macro to automatically and objectively evaluate the RAD51 foci. In brief, nuclei were segmented by thresholding the (median-filtered)DAPI signal, followed by a watershed operation to separate touching nuclei. For every z-stack the maximum-intensity projection of the foci signal was background-subtracted using a difference of gaussians method. Next, for each nucleus, foci candidates were identified as locations where the resulting pixel values exceeded the background by a factor (typically tenfold) times the median standard deviation of all nuclei in the image. In combination with additional filters discriminating for foci size and absolute brightness this procedure yielded a robust and reliable foci count for all nuclei. Results were validated by visual inspection.

REV7 recruitment to local laser-induced DNA damage sites. pEGFP-REV7 or pEGFP and 53BP1-mCherry were co-transfected into *Brcal*^{-/-}*p53*^{-/-} cells using X-treme GENE HP DNA Transfection Reagent according to the manufacturer's manual. GFP and mCherry double-positive cells were sorted by flowcytometry and seeded onto coverslips. Cells were sensitized by pre-incubationwith Hoechst33342 and were subsequently irradiated using a 405-nm diode laser (363 objective, 0.99mW, 60% laser power, 50 s) on a Leica SP5 confocal microscope equipped for live-cell imaging. EGFP-REV7 and 53BP1-mCherry recruitment in living cells was monitored by time-lapse imaging.

Alpha track assay. Cells were seeded in dishes with a mylar surface as previously described²⁸, allowing α -particle irradiation through the bottom of the dish. One or two hours after irradiation three times for 30 s with a ²⁴¹americium source, cells were washed once in ice-cold PBS. Subsequently, cells were extracted with cold CSK buffer (10mM HEPES-KOH, pH 7.9, 100mM NaCl, 300mM sucrose, 3mM MgCl₂, 1mM EGTA, 0.5% (v/v) Triton X-100) and cold CSS buffer (10mM Tris, pH 7.4, 10mM NaCl, 3mM MgCl₂, 1% (v/v) Tween 20, 0.5% (w/v) sodium deoxycholate) for 5 min each before fixation in 4% PFA in PBS for 20 min at room temperature. Fixed cells were washed five times in PBS plus 0.1% Triton X-100 and washed once in blocking solution (0.5% BSA plus 0.15% glycine in PBS). Primary antibodies were diluted in blocking solution and cells were incubated overnight at 4 °C. After incubation, cells were washed five times with PBS plus 0.1% Triton X-100 and washed once in blocking solution. Secondary antibodies were diluted in blocking solution and cells were incubated at room temperature for at least 1 h. Afterwards, cells were washed five times in PBS plus 0.1% Triton X-100 and once in PBS. Finally, mylar films were glued on glass slides and cells were mounted using Vectashield with DAPI. For quantification, at least 100 53BP1 or MRE11-positive tracks were scored for the presence of RPA. Primary antibodies used in this study were as follows: rabbit anti-53BP1 (NB100-304, Novus), 1:1,000 dilution; mouse anti-RPA2 (Ab2175, Abcam), 1:500 dilution; MRE11 antibody²⁹, 1:200 dilution. Secondary antibodies used in this study were as follows: Alexa Fluor 594 goat anti rabbit IgG (A 31631, Invitrogen), Alexa Fluor 488 goat anti-mouse IgG (A11001, Invitrogen).

BrdU propidium iodide cell cycle assay. Cells were seeded in 6-cm dishes and attached overnight. The next day, cells were incubated for 15 min with 5 mM BrdU in growth medium, trypsinized, washed in PBS and fixed in 70% ethanol overnight. Fixed cells were washed in PBS, resuspended in pepsin solution (5 mg pepsin in 10 ml 0.1N HCl) and incubated for 20 min at room temperature. Subsequently blocking solution (0.5% Tween, 0.1% BSA in PBS) was added to wash. Next, cells were resuspended in 2N HCl and incubated 12 min at 37°C. To neutralize, 100mM borate buffer (pH8.5) was added and cells were pelleted. Anti-BrdU-FITC antibody (347583, BD Bioscience) was diluted in blocking solution, added to cells and incubated for 2 h on ice. Stained cells were washed once with blocking solution and resuspended in 500 ml PBS plus 12.5 ml RNaseA and 1 ml propidium iodide (P3566, Invitrogen). Cell cycle analysis was performed the next day.

Survival assay of mES cells. *R26^{CreERT2/wt}; Brca1^{ScD}* mES cells¹⁵ were infected with hairpins targeting *Rev7* or the vector control and selected with puromycin. Expression of mouse *Brca1* was switched off by overnight incubation with 0.5 mM 4-hydroxytamoxifen. Four days after switching, 5,000 cells of the indicated groups were seeded per well into 6-well plates and assayed for growth. Surviving colonies were fixed in formalin and stained with crystal violet.

DR-GFP for HR assay. *R26^{CreERT2/wt}; Brca1^{ScD}* mES cells

were targeted with a modified version of the p59X DR-GFP construct as described³⁰. To allow experiments on a p53-deficient background, cells were infected with a lentiviral p53 shRNA (5'-AGAGTATTTCCACCTCAAGAT-3') using a pLKO1 vector provided with a neomycin resistance marker. A G418-selected p53-deficient clone was subsequently infected with hairpins targeting *Rev7* or the vector control and selected with puromycin. Expression of mouse *Brca1* was switched off by overnight incubation with 0.5mM 4-hydroxytamoxifen to measure the effect of *Rev7* loss on HR. HR reporter assays were performed by Lipofectamine 2000 (Invitrogen) transfection of the I-SceI-mCherry plasmid, which was generated by providing the cBasI-SceI expression plasmid with CMV-mCherry (Clontech). Forty-eight hours after transfection, mCherry/GFP double-positive cells were monitored by flow cytometry as described¹⁵.

53BP1 pull-down. 53BP1 pull-downs were performed as described¹⁹. Flag pull-downs were performed from 2 mg lysate prepared from MEFs following mock or neocarzinostatin treatment (2 h at 250 ng μ l⁻¹). Control, 53BP1 and 53BP120AQ immunoprecipitates were then treated with sequential low-salt (150mM) and high salt (500mM) RIPA buffer washes, before re-equilibration in nuclear extract buffer (20mM HEPES, pH7.9, 100mM KCl, 0.2mM EDTA, 20% glycerol, 0.5mM PMSF, 0.5mM DTT and protease inhibitors (Roche, Complete)). After incubation in Hela Nuclear Extract (2mg), control, 53BP1 and 53BP120AQ complexes were washed four times in nuclear extract buffer, then eluted with triple-Flag peptide (Sigma).

Immunoglobulin CSR. CH12 cells were either mock-treated or stimulated with agonist anti-CD40 antibody (0.5 mg ml⁻¹; eBioscience; HM40-3), mouse IL-4 (5 ng ml⁻¹; R&D Systems) and TGF- β 1 (1.25 ng ml⁻¹; R&D Systems). Cell-surface IgA expression was determined by flow cytometry, immunostaining with biotinylated anti mouse IgA antibody (eBioscience; 13-5994), and Alexa488-streptavidin conjugate (Life Technologies).

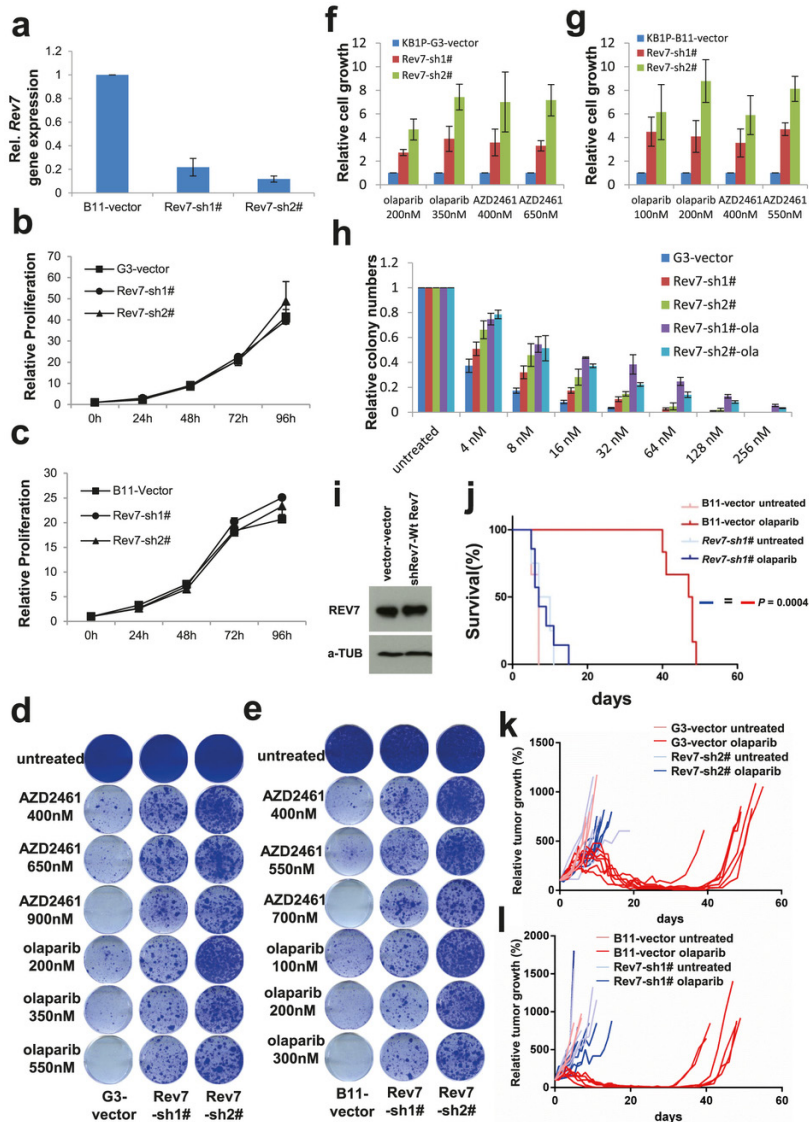
Carboxyfluorescein succinimidyl ester assay. Cell proliferation was assessed in stimulated CH12 cells using carboxyfluorescein succinimidyl ester (CFSE) according to manufacturer's instructions (CellTrace; Life Technologies).

Chromatin immunoprecipitation. Each ChIP was performed from chromatin prepared from 1×10^7 CH12 cells stimulated for 30 h with agonist CD40 antibody, IL-4 and TGF- β 1 essentially as described¹⁹. For each individual ChIP, 4 μ g of RPA34-20 (Ab-3, Calbiochem), 2 μ g H2AX (3522-1, Epitomics), or 4 μ g control mouse anti-IgG (sc-2025; Santa Cruz) coupled to 25 μ l Protein-G Dynabeads (Life Technologies, 10003D) was used. Quantities of immunoprecipitated chromatin were calculated relative to total input chromatin by quantitative PCR in duplicate on an CFX96 Real-Time Analyzer (Biorad) with the use of iQ SYBR Green (Biorad) for each primer pair (see below). Rpp30: forward, 5'-TCCAGTGTGCAAGAAAGCTAAATG-3'; reverse, 5'-GGCAGTGCCTGGAGACTCA-3'; A (target IgH S μ): forward, 5'-CAATGTGGTTAATGAATTTGAAGTTGCCA-3'; reverse, 5'-TCTCACACTCACCTTGATCTAAGCACTGT-3'; B (target IgH S μ): forward,

5'-GCTAAACTGAGGTGATTACTCTGAGGTAAG-3'; reverse, 5'-GTTTAGCTTAGCGGCCAGCTCATCCAGT-3'; C (target IgH Sc1): forward, 5'-AGTGTGGGAACCCAGTCAAA-3'; reverse, 5'-GTACTCTCACCGGGATCAGC-3'; D (target IgH Sa): forward, 5'-TGAAAAGACTTTGGATGAAATGTGAACCAA-3'; reverse, 5'-GATACTAGGTTGCATGGCTCCATTCACACA-3'.

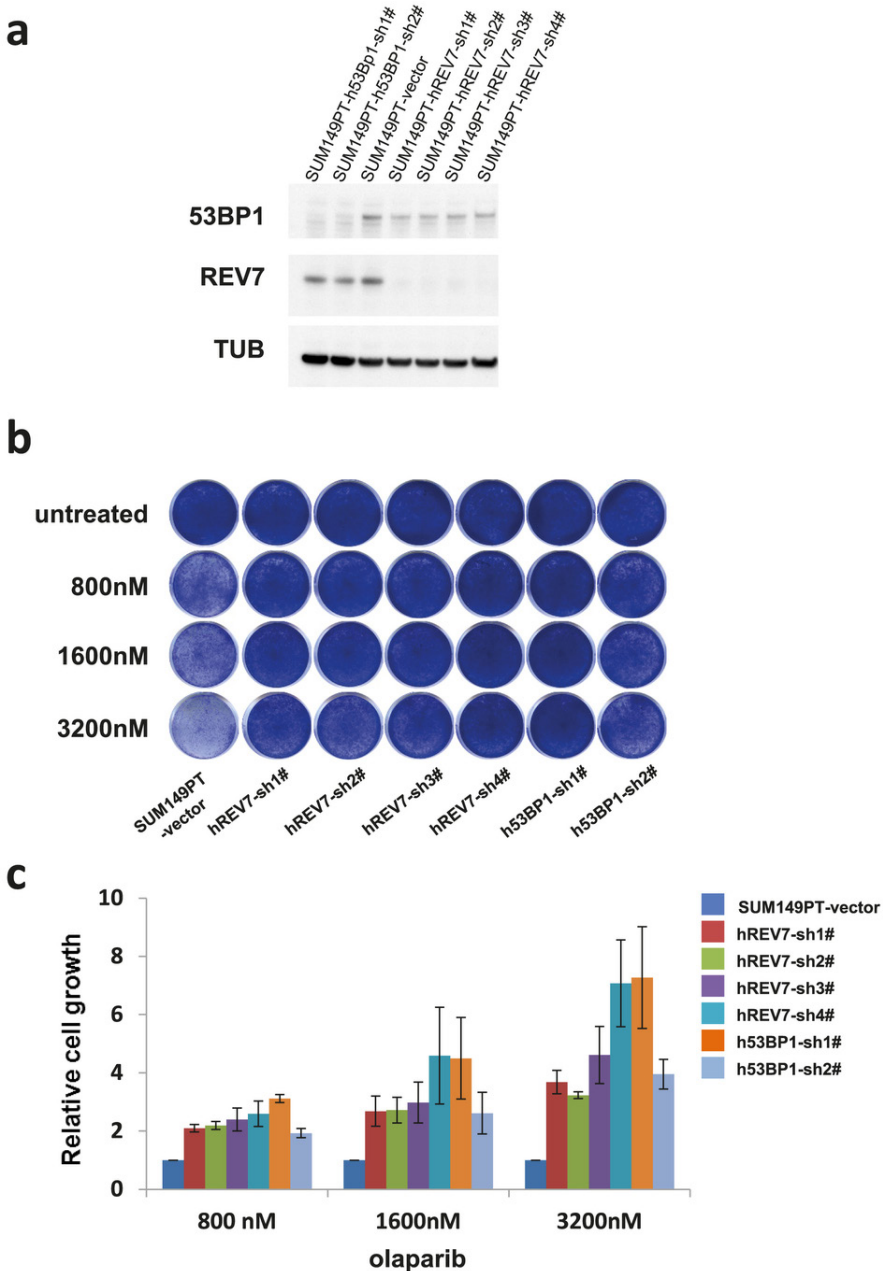
Immunohistochemistry on paraffin sections. The panel of formalin-fixed, paraffin-embedded archival specimens from a series of 50 human primary breast carcinomas was examined, surgically resected before any chemotherapy or radiotherapy. In parallel, sections from ten specimens of formalin-fixed, paraffin-embedded histologically normal human breast tissues were used as normal tissue controls, for immunohistochemical analysis of REV7 expression patterns. The breast carcinomas were all of the triple-negative type, defined in this cohort as having fewer than 1% tumour cells positive in standard immunohistochemical staining for oestrogen and progesterone receptor proteins, and lacking amplification of the HER2 (also known as ERBB2) gene. For the immunohistochemical analysis, 4- μ m-thick sections were cut from representative blocks of the tumour tissues, the sections were deparaffinized and processed for sensitive immunoperoxidase staining with the primary mouse monoclonal antibody to REV7 (BD Biosciences, 612266, diluted 1:100). The staining procedure was essentially as described¹⁵, with antigen unmasking in citrate buffer, pH 6.0, for 15–20 min in a microwave oven, and overnight incubation with the primary antibody, followed by the Vectastain Elite kit (Vector Laboratories) and nickel sulfate enhancement without nuclear counterstaining³¹. Mouse normal serum and antibody to γ H2AX served as negative and positive controls, respectively. Evaluation of the staining patterns was performed by two independent observers (with very similar outcomes), including a senior oncopathologist with more than 20 years of experience with breast cancer pathology. The results were scored in the following categories, based on comparison of cancer cells with the series of normal breast tissue controls, and also the normal of cells present within each of the tumour sections. As normal breast epithelium showed reproducible positivity for REV7 protein in over 90% of cells, we considered as aberrantly decreased expression in a tumour when fewer than 70% of cancer cells were positive. In addition to the percentage of stained tumour cells, staining intensity was classified as either normal (comparable with the intensity of normal cells present on each section) or aberrantly low (clearly below the intensity seen in adjacent normal cells, and up to undetectable in some cases). Overall, while 6 out of 47 informative cases showed concomitantly aberrant fraction of REV7-stained cells and reduced intensity of staining, 12 additional cases showed less pronounced defects limited to either staining intensity or reduced percentage of cancer cells, respectively. As the primary goal of these analyses was to establish a detection assay for REV7 on archival tissue specimens and to assess the frequency of potentially REV7-deficient breast tumours, correlation analyses with clinical parameters including treatment outcome remain to be performed on larger cohorts of patients in the future.

Statistics. Statistical tests used were log-rank test, t-test and Mann–Whitney U test, with $P, 0.05$ as the significance level. No statistical methods were used to predetermine sample size.



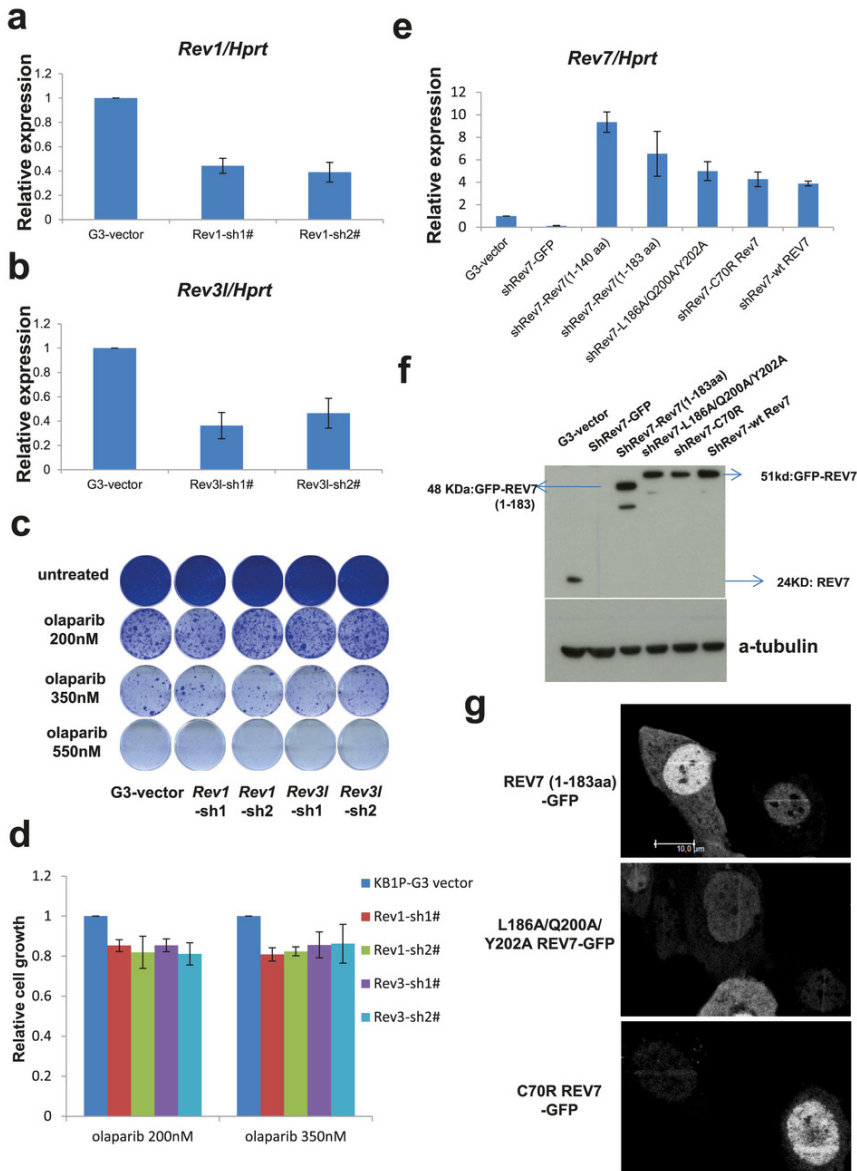
Extended Data Figure 1 Loss of Rev7 causes PARPi resistance in vitro and in vivo.

a, Quantification of *Rev7* transcript levels in KB1P-B11 cells transduced with *Rev7*-targeting shRNAs or the vector control. *Hprt* was used as a control for transcript expression. The data represent mean \pm s.d. b, c, Cell proliferation rates in KB1P-G3 (b) or KB1P-B11 (c) cells analysed using the MTT assay. d–g, Long-term clonogenic survival assays and quantification of KB1P-G3 (d, f) or KB1P-B11 (e, g) cells transduced with the indicated constructs and treatments. All the groups were normalized by the absorbance of the vector control. The data represent mean \pm s.d. h, Quantification of the real colony numbers from the short-term clonogenic survival assay of KB1P-G3 cells with or without *Rev7* loss exposed to olaparib. i, REV7 protein levels were determined by western blotting of lysates derived from KB1P-G3 cells transduced with the indicated constructs. j, Overall survival of mice with KB1P-B11-derived *Rev7*-depleted or control tumours treated with one regimen of 50 mg kg⁻¹ olaparib daily for 28 days or left untreated. The P value was calculated using the log-rank test. k, l, Relative tumour growth of individual KB1P-G3- (k) and KB1P-B11- (l) derived *Rev7*-depleted or control tumours treated with one regimen of 50 mg kg⁻¹ olaparib daily for 28 days or left untreated.



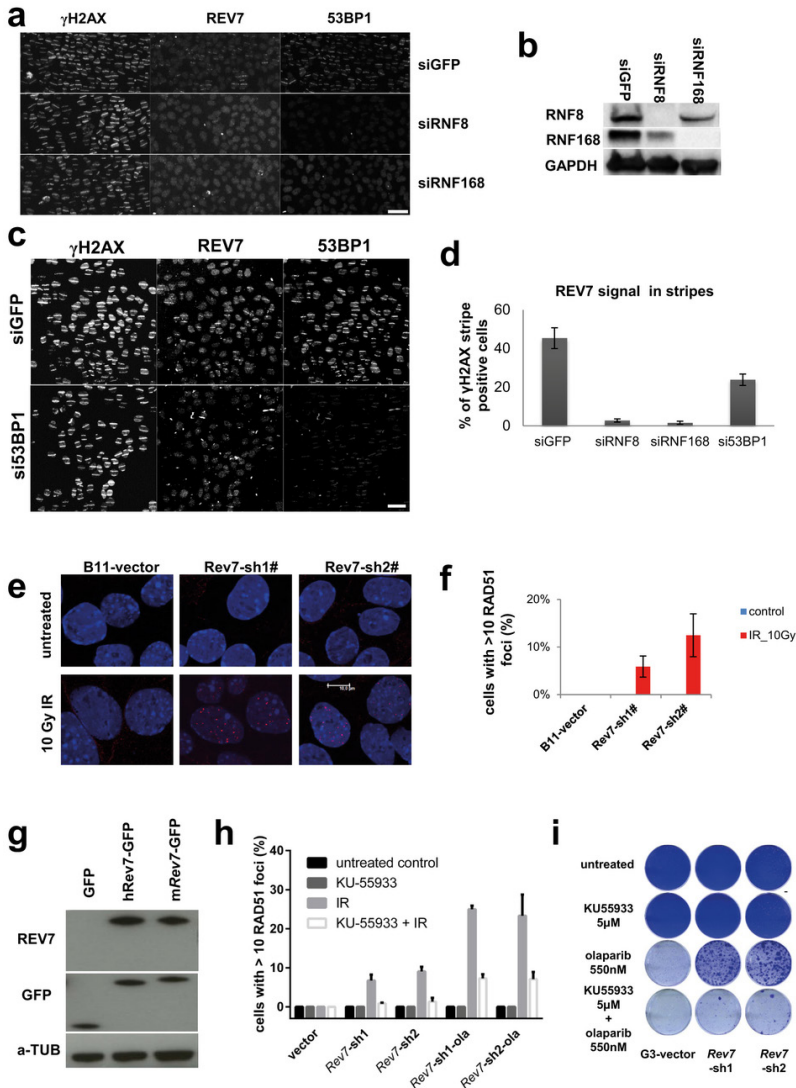
Extended Data Figure 2 Loss of REV7 causes olaparib resistance in BRCA1-deficient SUM149PT cells.

a, Western blotting analysis of REV7 or 53BP1 expression in SUM149PT cells transduced with REV7- or 53BP1-targeting hairpins or the vector control. b, Example of a long-term clonogenic survival assay using the indicated hairpins and olaparib concentrations. c, Quantification of the clonogenic assays using absorbance of crystal violet at 590 nm. The data represent mean \pm s.d. All the groups were normalized by the absorbance of the vector control and showed significant differences to the control (P<0.01, t-test).



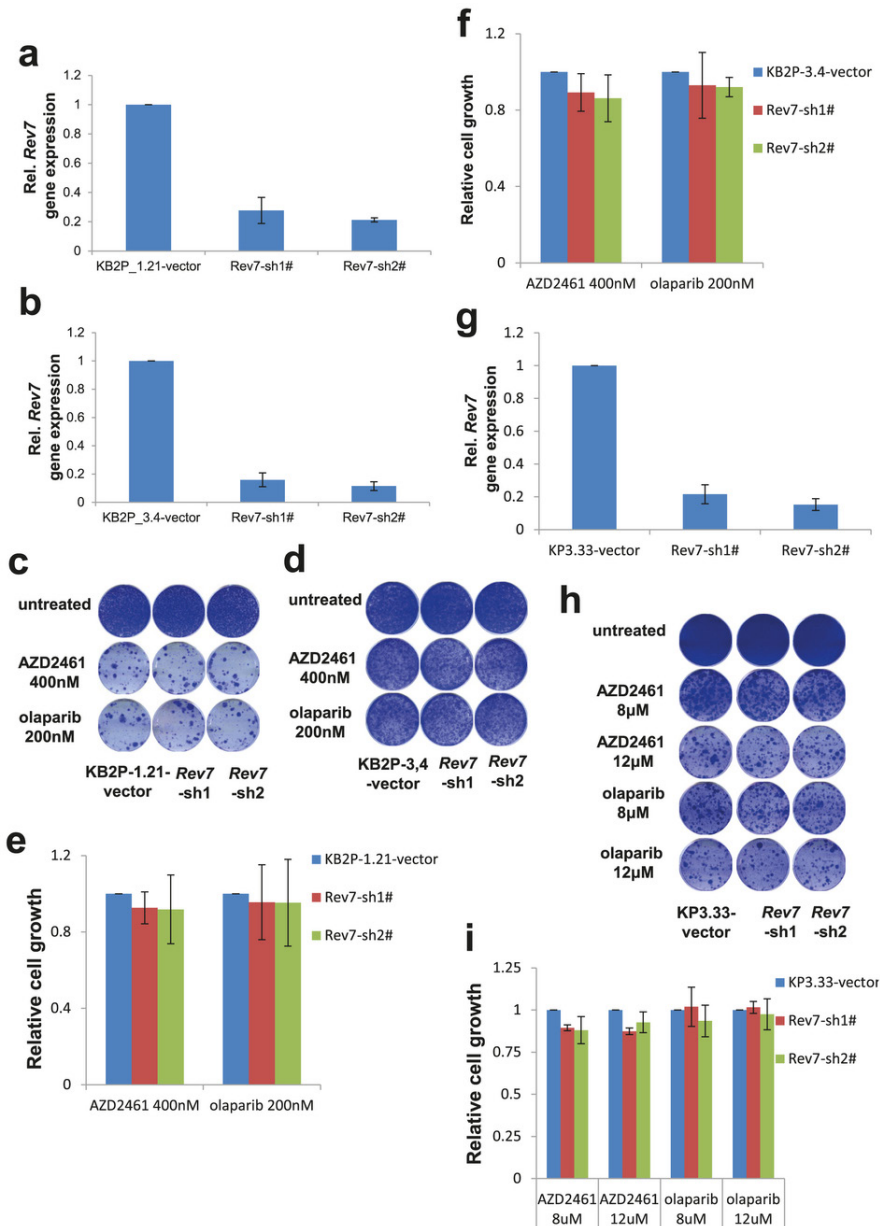
Extended Data Figure 3 *Rev1* or *Rev3* inhibition and PARPi sensitivity of *Brca1*^{-/-}*p53*^{-/-} mammary tumour cells.

a, b, Quantification of *Rev1* (a) or *Rev3* (b) transcript levels in KB1P-G3 cells transduced with *Rev1*- or *Rev3*-targeting shRNAs or the vector control. *Hprt* was used as a control for transcript expression. The data represent the mean \pm s.d. c, Long-term clonogenic survival assays of KB1P-G3 cells exposed to the indicated PARP inhibitors. d, Quantification of the clonogenic assay by determining the absorbance of crystal violet at 590nm. All the groups were normalized by the absorbance of the vector control. The data represent the mean \pm s.d. e, f, Quantification of *Rev7* transcript (e) or protein (f) levels in KB1P-G3 cells transduced with *Rev7*-targeting shRNAs or the vector control. *Hprt* was used as a control for transcript expression; α -tubulin as a control for protein expression. The data represent mean \pm s.d. g, GFP-tagged *REV7* mutants recruitment to sites of DNA damage was observed 5 min after 405nm laser exposure (0.99mW, 60% laser power, 50 s) in KB1P-B11 cells. Scale bar, 10 μ m.



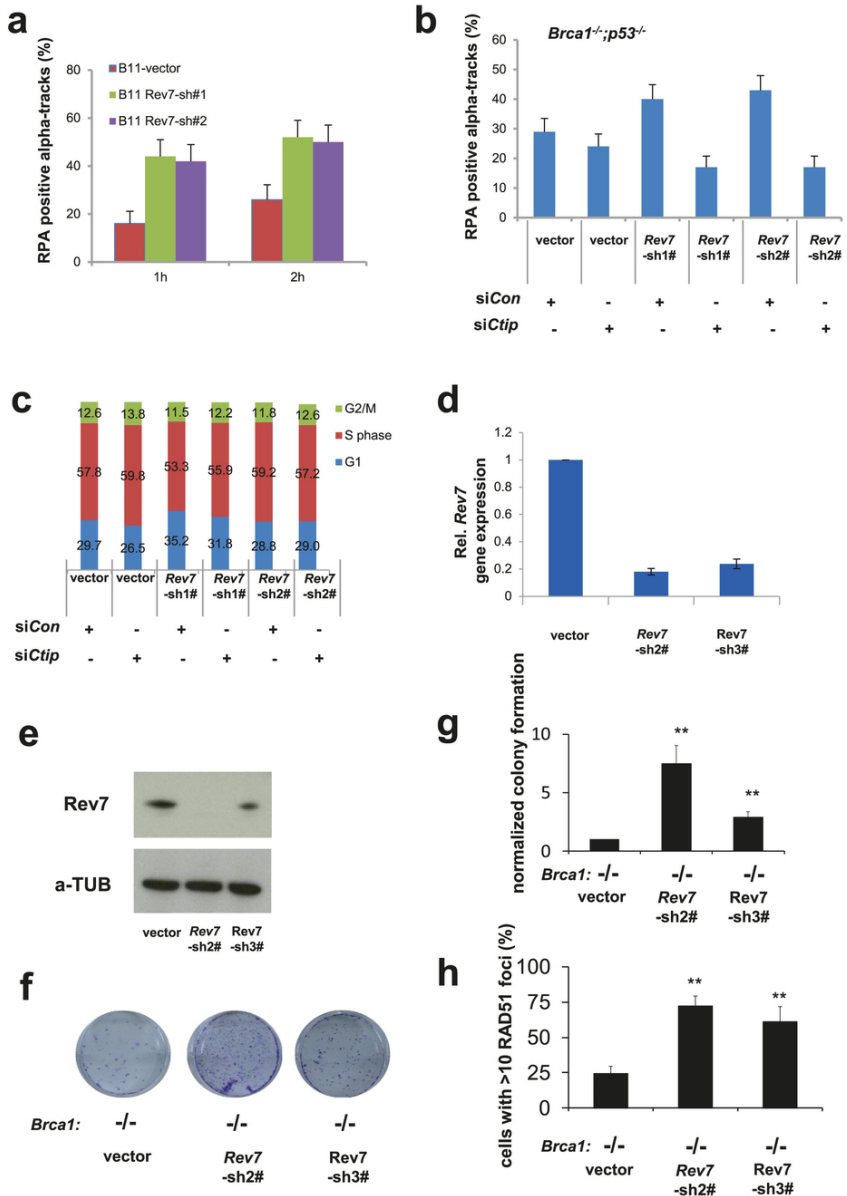
Extended Data Figure 4 REV7 recruitment to the DNA damage sites in human cells.

a–c, Human REV7 recruitment to sites of laser-induced DNA damage was analysed in U2OS cells transfected with siRNAs targeting RNF8 (siRNF8), RNF168 (siRNF168) (a), 53BP1 (si53BP1) (c) and GFP (siGFP). RNF8 and RNF168 protein levels were determined by western blotting (b) using lysates derived from U2OS cells transfected with the indicated siRNAs. d, For the quantification of the REV7 signal within laser-induced DNA damage stripes, a minimum of 100 striped (that is, γ H2AX-positive) cells were analysed for the presence of the REV7 signal in two independent experiments. Scale bars, 50 μ m. e, RAD51 focus (red) formation in KB1P-B11 cells before and 5 h after 10 Gy ionizing radiation. Scale bar, 10 μ m. f, Quantification of RAD51 foci in KB1P-B11 cells in the presence or absence of REV7 depletion. At least 150 cells were analysed per group in three independent experiments each. Error bars indicate s.d.; IR denotes 5 h after 10 Gy ionizing radiation. g, Western blotting analysis of REV7-depleted KB1P-G3 cells transfected with human REV7-GFP or Rev7-shRNA-resistant mouse REV7-GFP fusion proteins. h, Same as in e and f using the ATM inhibitor KU5933 with or without IR (5 h after 10 Gy ionizing radiation). i, Long-term clonogenic survival assay of KB1P-G3 cells exposed to olaparib in the presence or absence of KU5933 pre-treatment.



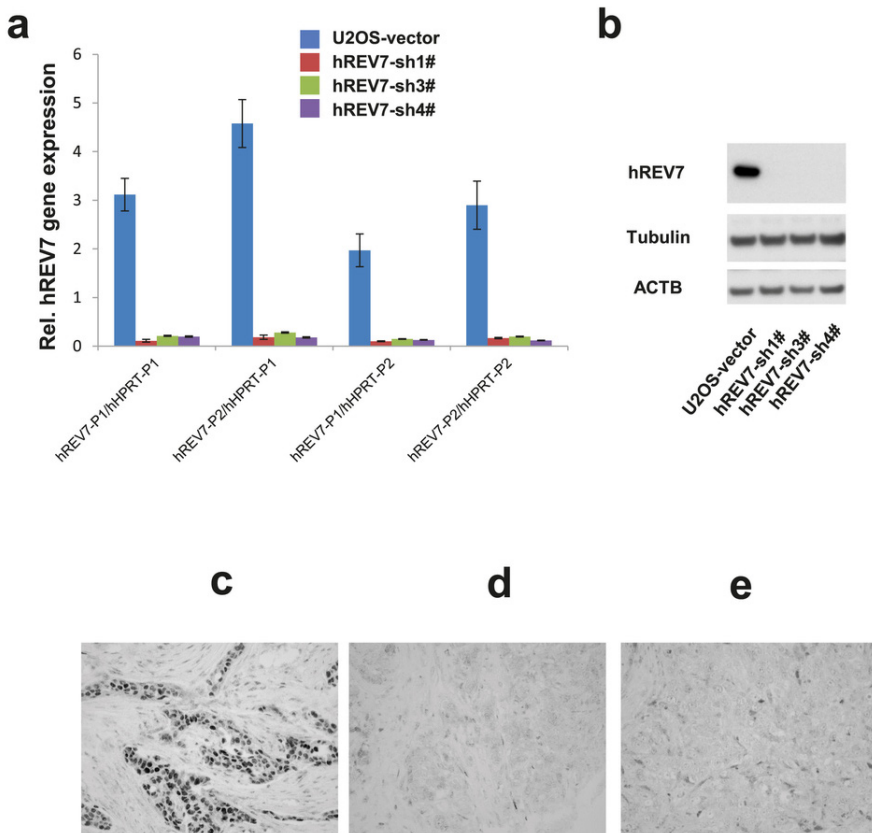
Extended Data Figure 5 Loss of Rev7 does not cause PARPi resistance in *Brca2*^{-/-} *p53*^{-/-} or *p53*^{-/-} mammary tumour cells in vitro.

a, b, Quantification of Rev7 transcript levels in *Brca2*^{-/-} *p53*^{-/-} (KB2P-1.21 or KB2P-3.4) cells transduced with *Rev7*-targeting shRNAs or the vector control. *Hprt* was used as a control for transcript expression. The data represent the mean±s.d. c–f, Long-term clonogenic survival assays and quantification of KB2P-1.21 or KB2P-3.4 cells with or without *Rev7* depletion exposed to the indicated treatments. All the groups were normalized by the absorbance of the vector control. The data represent mean±s.d. g, Quantification of *Rev7* transcript levels in *p53*^{-/-} (KP3.33) cells transduced with the indicated constructs. *Hprt* was used as a control for transcript expression and the data represent the mean±s.d. h, i, Long-term clonogenic survival assays and quantification of KP3.33 cells exposed to the indicated treatments. The data represent the mean±s.d.



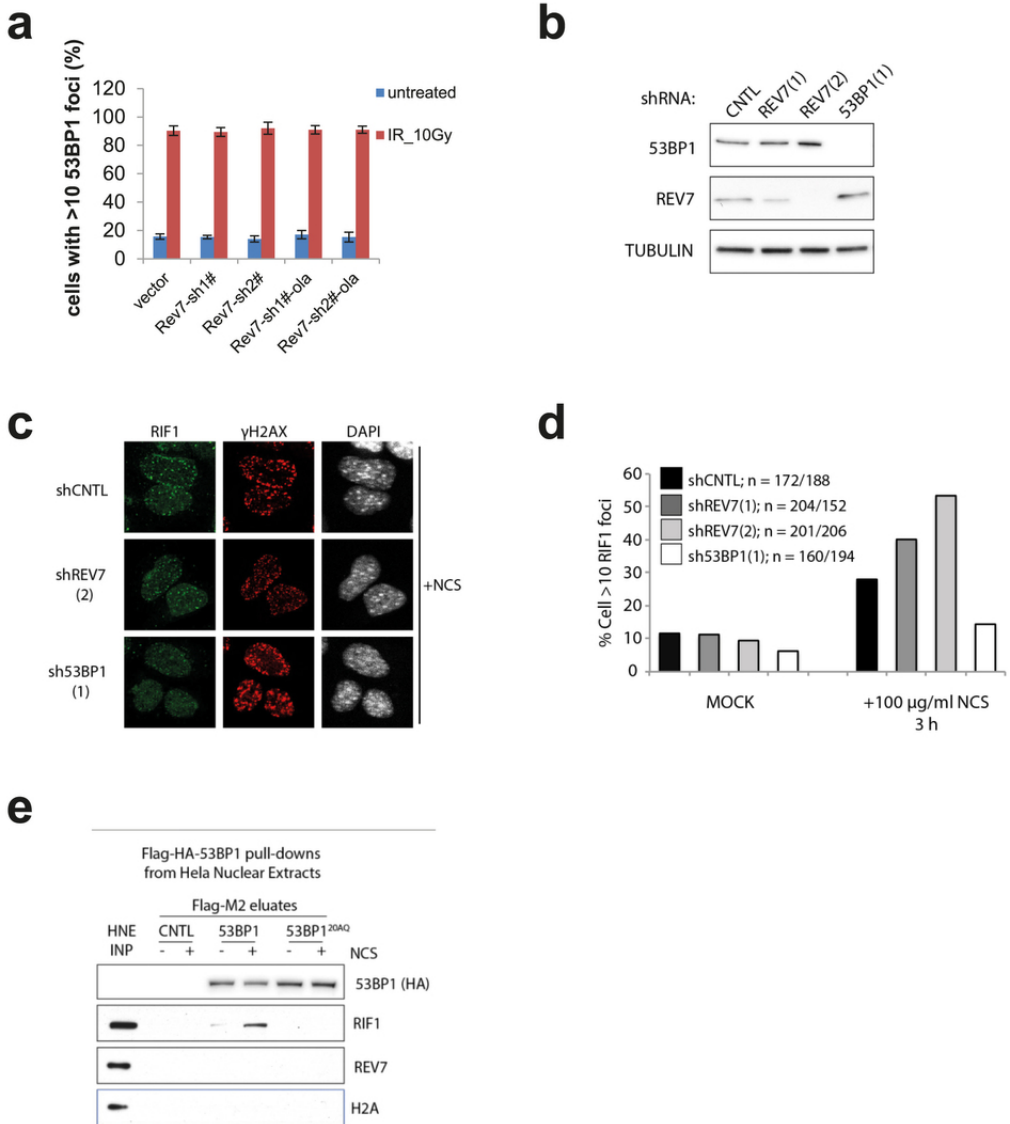
Extended Data Figure 6 Rev7 loss promotes end resection at DSBs in BRCA1-deficient cells after ionizing radiation.

a, Quantification of RPA positive α tracks in KB1P-B11 cells 1 or 2 h after irradiation with a particles. b, Quantification of RPA- and 53BP1-positive α tracks in KB1P-B11 cells transfected with non-targeting control siRNAs or siRNAs against *Ctip*. c, Cell cycle analysis (BrdU incorporation and propidium iodide labelling) of KB1P-B11 cells transduced with the indicated constructs and siRNAs. d, e, Quantification of *Rev7* transcript (d) or protein (e) levels in BRCA1-deficient mES cells transduced with *Rev7*-targeting shRNAs or the vector control. *Hprt* was used as a control for transcript expression, α -tubulin as a control for protein expression. The data represent mean \pm s.d. f, Representative images of surviving colonies of *Brca1*^{-/-} mES cells transduced with an empty vector control or *Rev7*-targeting shRNAs. g, Quantification of colony formation normalized to the vector control. h, Quantification of RAD51 foci in *Brca1*^{-/-} mES cells that were transduced with the indicated constructs.



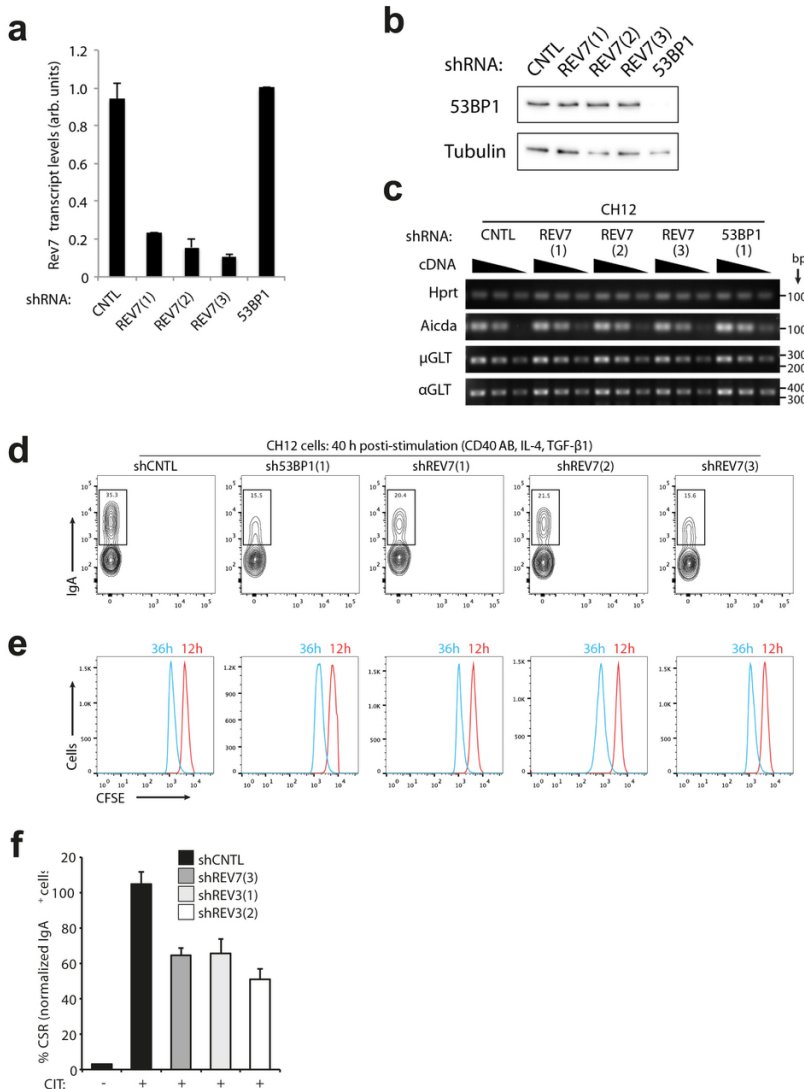
Extended Data Figure 7 REV7 loss frequently occurs in triple-negative breast cancer.

a, b, Quantification of human REV7 transcript levels (a) and protein levels (b) in U2OS cells transduced with indicated constructs. Two different pairs of primers for REV7 or HPRT were used for the quantification of REV7 transcript levels. c–e, Examples of aberrantly reduced REV7 protein expression in triple-negative human breast carcinomas. Immunohistochemical detection of REV7 in human breast carcinomas shows moderate to high nuclear expression in normal human breast tissue (data not shown), and most invasive breast tumours (c). Aberrant reduction of REV7 with less than 70% of cancer cells that show nuclear positivity (d, e) was observed in 18 out of 50 cases.



Extended Data Figure 8 REV7 is a downstream effector of 53BP1.

a, Quantification of 53BP1 foci in KB1P-G3 cells in the presence or absence of REV7 depletion. At least 100 cells were analysed per group in three independent experiments each. Error bars indicate s.d.; IR denotes 5 h after 10 Gy ionizing radiation. b, REV7 or 53BP1 protein levels were determined by western blotting of lysates derived from MEF cells transduced with the indicated control (CNTL) or *Rev7*- and *53bp1*-targeting shRNA constructs. c, d, RIF1 foci formation (c) after neocarzinostatin (NCS) treatment and quantification of RIF1 foci (d) in MEF cells in the presence or absence of REV7 or 53BP1 depletion. e, Flag pull-downs were performed from 2 mg lysate prepared from *53bp1*^{-/-}, *53bp1*^{-/-} plus 53BP1 and *53bp1*^{-/-} plus 53BP120AQ MEFs after mock or neocarzinostatin treatment. Control, 53BP1 and 53BP120AQ immunoprecipitates were incubated in HeLa nuclear extract (HNE, 2 mg) and then eluted with triple-Flag peptide. HA, haemagglutinin.



Extended Data Figure 9 The effect of REV7 inhibition on CSR after antigenic stimulation of CH12 cells.

a, Rev7 messenger RNA levels determined by qRT-PCR were normalized against β -actin (Actb) transcripts in the indicated shRNA-transduced CH12 cell lines. The data represent the mean \pm s.e.m. from two primer sets specific for Rev7 transcript. CNTL, control. b, 53BP1 protein of each group normalized to vector-transduced cells (CH12) was analysed by western blotting. c, IgH μ and α germ-line transcripts (GLT) and *Aid* mRNA were estimated by semi-quantitative RT-PCR using twofold serial dilutions of cDNA made from indicated CH12 cell lines 40 h after stimulation. *Hprt* was used as a control for transcript expression. d, Representative flow cytometric profiles of shRNA-transduced CH12 B cells stained with anti-IgA antibody 40 h after stimulation with the indicated cytokines. e, Cells (CH12) were labelled with CFSE immediately before cytokine stimulation as in Fig. 4d, and cell proliferation was assessed by flow cytometry at indicated time points. f, Quantification of CSR to IgA of shRNA-transduced CH12 cells 40 h after stimulation with CD40 antibody, IL-4 and TGF- β 1 (CIT). Data represent the mean \pm s.d. from two independent experiments performed in triplicate.

4

Chapter 4

Mechanistic insight into PARP inhibitor resistance due to REV7 loss in BRCA1-deficient cells

Inger Brandsma, Guotai Xu, Mattia Siragusa, Bart Geverts, Dick Dekkers, Karel Bezstarosti, Nicole Verkaik, Jeroen Demmers, Adriaan Houtsmuller, Sven Rottenberg, Dik van Gent

Abstract

Cells and tumours deficient in homologous recombination are exquisitely sensitive to PARP inhibitors. Unfortunately, a fraction of the tumours treated with PARP inhibitors eventually becomes resistant. In BRCA1-deficient cells resistance can be caused by restoration of homologous recombination due to loss of REV7 expression. REV7 (MAD2B or MAD2L2) plays a role in translesion synthesis together with REV3, is involved in regulation of cell cycle progression via the anaphase-promoting complex and has been linked to several other processes via other interaction partners. Here we investigate which roles and interaction partners of REV7 are important for PARP inhibitor resistance in BRCA1-deficient cells. The role of REV7 in cell cycle progression seems to be dispensable for restoration of homologous recombination, but the interaction between REV3 and REV7 is possibly involved.

Introduction

Breast cancer is one of the most common types of cancer in women¹. Carriers of mutations in the tumour-suppressor genes BRCA1 and BRCA2 have a strongly increased lifetime risk of developing breast cancer. The BRCA1 and BRCA2 proteins play a role in homologous recombination (HR), a pathway to repair DNA double strand breaks in an error-free manner. Double strand breaks can be caused by ionizing radiation or they are formed during the repair of DNA crosslinks. To repair a double strand break, the broken DNA is first resected, generating single-stranded DNA overhangs, which are bound by replication protein A (RPA). RPA is then replaced by RAD51 forming nucleo-protein filaments. RAD51 helps to pair the damaged DNA with the homologous sequence on the sister chromatid. The intact DNA on the sister chromatid is then used as a template for accurate repair of the broken DNA. Failure to repair DNA breaks in this reliable manner

can cause mutations, translocations and chromosomal aberrations, which eventually can lead to cancer.

Women with breast cancer are commonly treated with chemotherapy, which has severe side effects because the chemotherapeutics target all dividing cells in the patient's body. Recently a new treatment strategy has been developed that reduces side effects by targeting specifically the tumour cells with a defect in homologous recombination^{2,3}. Cells deficient in homologous recombination are extremely sensitive to inhibition of Poly [ADP-ribose] polymerase 1 (PARP1), which is required for the efficient repair of single-strand breaks in the DNA. When these breaks are repaired inefficiently due to PARP inhibition, replication forks collapse at these sites of damage, resulting in DNA double strand breaks. To repair these breaks, BRCA1 and BRCA2 are needed. In tumours where these proteins are not functioning properly, DNA damage accumulates, eventually leading to cell death.

Unfortunately, although the treatment of BRCA1- and BRCA2-deficient tumours with PARP inhibitors such as Olaparib is very promising, tumours often eventually become resistant⁴. Resistance has various causes such as overexpression of a drug-efflux pump⁵, loss of 53BP1⁶ or reversion of the mutation in BRCA1 or BRCA2^{7,8}. However, these mechanisms do not explain all cases of resistance.

Recently, Xu et al. described loss of REV7 as a resistance mechanism in BRCA1-deficient cells and tumours⁹. In BRCA1-deficient cells, loss of REV7 restored CtIP-dependent resection and thereby homologous recombination, causing PARP inhibitor resistance. REV7 (also known as MAD2B or MAD2L2) and REV3 form the translesion polymerase Zeta (Polζ), a low-fidelity polymerase that plays a role in the bypass of replication-blocking lesions such as DNA crosslinks or damaged bases. REV3 contains the polymerase domain of Polymerase ζ and REV7 is an accessory subunit. Apart from functioning in trans lesion synthesis

(TLS), REV7 has been linked to end-joining as well. Boersma et al. showed that when TRF2 is inactivated and telomeres become uncapped, telomeres no longer fuse when REV7 is absent¹⁰.

REV7 has also been shown to be involved in cell-cycle progression through the anaphase-promoting complex. The anaphase-promoting complex/cyclosome (APC/C) is an E3-ubiquitin ligase that controls progression through mitosis by targeting key mitotic factors for degradation at specific points during the cell cycle. During mitosis, APC/C is activated by CDC20 and from late mitosis to the G1/S transition, APC/C is activated by CDH1¹¹. REV7 (MAD2B) and MAD2 are both inhibitors of the APC/C, but REV7 targets APC/C-CDH1 while MAD2 inhibits APC/C-CDC20^{12,13}.

As described above, REV7 loss results in Olaparib resistance in BRCA1-deficient cells due to restoration of resection and thereby homologous recombination. To be able to prevent resistance or to treat resistant tumours, it is important to understand how this resistance mechanism works. As it is still unclear whether the Olaparib resistance observed in BRCA1-deficient cells after REV7 loss is due to the role of REV7 in TLS (i.e. dependent on REV3), we generated several point mutants in REV7 that disturb the interaction with REV3. Additionally we used mass spectrometry to identify the main interacting partners of wild-type REV7 and the C70R mutant. We found that mutations in REV7 also lead to the loss of interaction with POGZ and CHAMP1 and investigated whether loss of those proteins had any effect in HR in BRCA1-deficient cells.

Results

REV7 and the APC/C

Xu et al.⁹ found loss of REV7 as a resistance mechanism in a loss-of-function PARP-inhibitor screen in BRCA1-deficient cells. Another hit from the screen was 53BP1, for which it was already known that its loss causes Olaparib resistance. REV7 has been

linked to cell cycle progression and is known to be an inhibitor of the APC/C. Another example of an inhibitor of the APC/C is EMI1. REV7 only inhibits APC/C-CDH1, while EMI1 inhibits APC/C-CDH1 and APC/C in complex with CDC20^{14,15}. To test whether the APC/C regulatory function of REV7 and EMI1 is important for restoring RAD51 focus formation, we depleted REV7 and EMI1 in BRCA1-deficient mouse mammary tumour cells (G3 cells). Unfortunately, EMI1 could not be knocked down using shRNA for more than 60% (data not shown) as measured on mRNA level. EMI1 is essential for precise mitotic progression and EMI1 knockout embryos are not viable¹⁶. EMI1 depletion might therefore be very poorly tolerated, hampering our analysis of the connection of REV7 and APC/C with PARP inhibitor resistance.

The APC/C complex can also be inhibited pharmacologically with the proTAME inhibitor¹⁷. G3 cells transfected with a scrambled shRNA or shRNA targeting REV7 or 53BP1 were treated with proTAME for 5 hours, irradiated with 5Gy one hour after the inhibitor was added and stained for RAD51 foci (Fig 1A). 53BP1-depleted cells were taken along as a control, since the APC/C complex is not expected to play a role in restoration of homologous recombination in those cells. Treatment with proTAME had no effect on the formation of RAD51 foci in BRCA1-deficient G3+ shREV7 cells. 4 hours after 5 Gy, these cells were still able to form RAD51 foci in S-phase cells to a similar extent as DMSO treated cells (Fig1B). In G3 cells or G3 cells + sh53BP1 the addition of proTAME before irradiation did not affect the RAD51 focus formation either. As expected, BRCA1-deficient cells (G3 Scr) were still unable to form RAD51 foci after irradiation in the presence of proTAME.

To verify that the inhibitor was active, cells were stained for mitosis marker phospho-histone H3 (pH3) after incubation with proTAME for three, five, eight or 24 hours. As expected, cells accumulated in mitosis after proTAME treatment, resulting in increased numbers of pH3-positive cells compared to DMSO-treated cells (Fig1C,D). After 24 hours

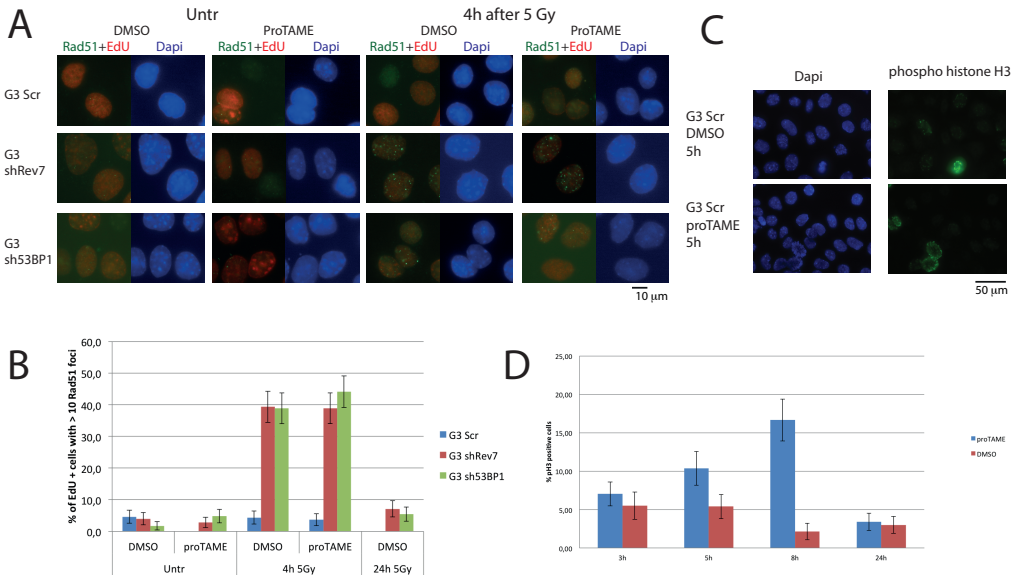


Figure 1 Inhibition of the APC/C does not affect RAD51 foci formation in BRCA1-deficient G3 cells

(A) Incubation with proTAME does not affect RAD51 focus formation in EdU positive (S-phase) cells after irradiation. Indicated cell lines were incubated with proTAME or vehicle (DMSO), irradiated with 5 Gy and stained for RAD51. (B) Quantification of RAD51 focus formation in BRCA1-deficient G3 cells + indicated shRNAs treated with proTAME or vehicle (DMSO). The number of S-phase cells with more than 10 RAD51 foci was quantified. Bars represent average \pm SEM. At least 100 nuclei were counted per sample. (C,D) Incubation with proTAME results in an increase in mitotic cells. (C) Examples of phospho histone H3 (pH3) positive cells after incubation with proTAME or DMSO. (D) Quantification of the percentage of pH3 positive cells. At least 150 nuclei were counted per sample. Bars represent average \pm SEM.

the effect of the proTAME inhibitor was no longer visible, probably because cells that were arrested in mitosis for a prolonged period died.

Inhibition of the APC/C does not reverse the restoration of RAD51 focus formation in BRCA1-deficient cells with a depletion of REV7. This indicates that the APC/C has no effect on the restoration of RAD51 focus formation in REV7-depleted BRCA1-deficient cells.

Disturbing the interaction between REV7 and REV3

REV3 and REV7 form the DNA Polymerase ζ complex, which can bypass DNA lesions during translesion synthesis. Currently it is still unclear whether the REV3-REV7 interaction is required for restoration of HR in BRCA1-deficient cells. REV3 deletion or knock-down is poorly tolerated in mammalian cells¹⁸, so

as an alternative point mutants in REV7 that disturb the interaction with REV3 were used. Khalaj et al. recently found that the C70R point mutation caused infertility in mice¹⁹. Based on the crystal structure of REV7 in complex with a REV1 or REV3 peptide Hara et al. designed several other REV1 and REV3 interaction mutants²⁰. The C70R (Cys70Arg) and 2A (Y63A / W171A) mutants were chosen to disturb the interaction between REV3 and REV7 and the 3A (Leu186Ala / Gln200Ala / Tyr202Ala) mutant to disturb the interaction between REV1 and REV7.

An immunoprecipitation of GFP-REV7 (wild-type or point-mutants) with MBP-REV3 was used to verify that the REV7 mutants are defective in their interaction with REV3. All mutants and wild-type REV7 were cloned into a GFP-vector and transiently overexpressed in HEK293T cells co-transfected with MBP-REV3. All GFP-REV7 constructs were expressed at

similar levels, but MBP-REV3 expression was not detectable in the input, probably due to low levels, as has been observed previously²¹. After immunoprecipitation of the GFP-constructs using GFP-beads, wild-type REV7 and the 3A mutant pulled down MBP-REV3, while the 2A and C70R showed a decreased interaction with REV3 (Fig 2A).

REV7 mutants partially restore homologous recombination

REV7 depletion causes restoration of resection and thereby HR in BRCA1-deficient cells⁹. Re-expression of wild-type REV7 abrogates this restoration. To investigate whether the interaction between REV7 and REV1 or REV7 and REV3 is required for

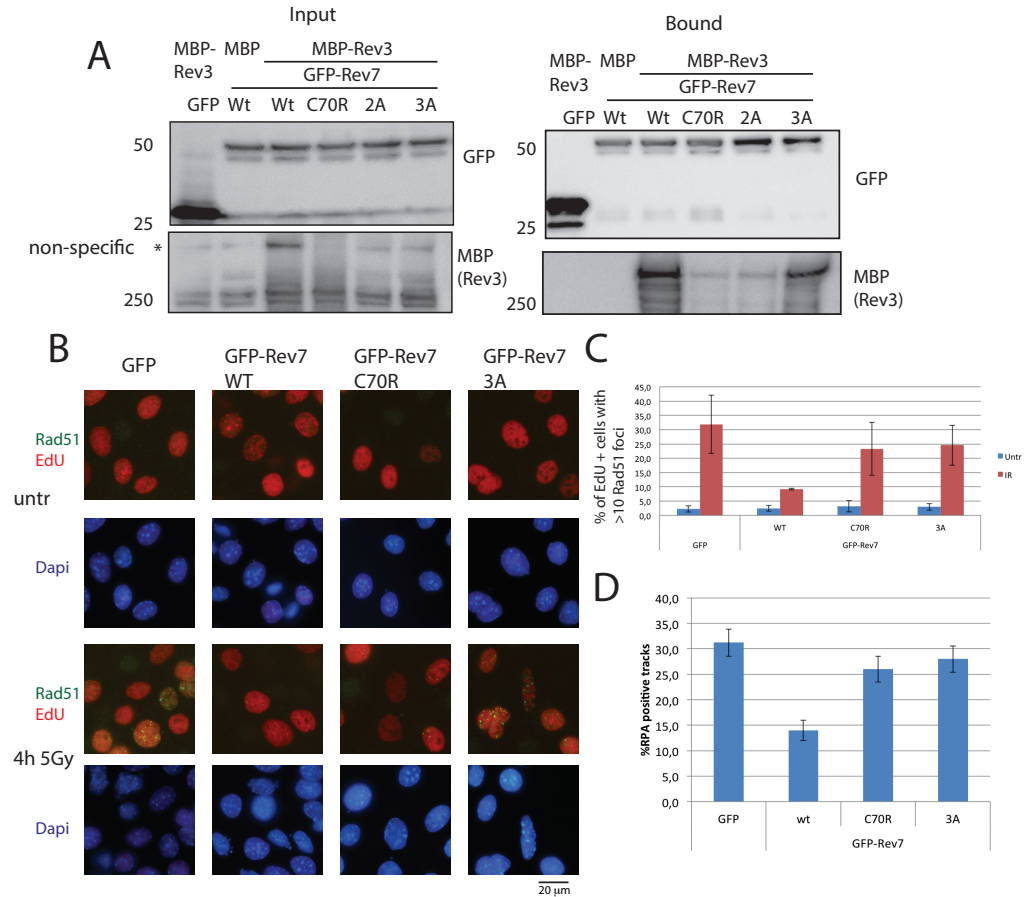


Figure 2 REV7 point mutants affect RAD51 foci formation and resection.

(A) REV7 point mutants C70R and 2A show a decreased interaction with REV3. Immunoblot of input and bound fractions using MBP and GFP antibodies. MBP-REV3 was co-immunoprecipitated using wild-type GFP-REV7 or the point mutants. Both MBP-REV3 and the GFP-REV7 constructs were transiently overexpressed in HEK293T cells and immunoprecipitated using GFP-beads. MBP-REV3 is not detectable in the input. (B) Examples of RAD51 foci (green) in G3 cells expressing GFP or GFP-REV7 constructs. S-phase cells were labeled using EdU incorporation (Red). (C) Quantification of the number of S-phase cells with more than 10 RAD51 foci. At least 300 nuclei in 3 experiments were counted per sample. Bars represent average \pm SEM. (D) G3 cells expressing REV7 point mutants were damaged using alpha particles and stained for RPA and 53BP1 tracks. 300 tracks were counted over 3 experiments and bars represent average \pm SEM.

4

the restoration of HR, G3 cells expressing shRNA-resistant GFP-tagged wild-type REV7 or the point mutants were generated. Endogenous REV7 was depleted with the stable expression of a shRNA. As the 2A mutant was not expressed in G3 cells, it was left out of the analysis (Fig S1A). These cells were irradiated and stained for RAD51 foci 4 hours later, as a surrogate marker for homologous recombination (Fig 2B). EdU incorporation was used to label S-phase cells and the number of S-phase cells with more than 10 RAD51 foci was quantified (Fig 2C). As expected, re-expression of GFP-REV7 results in a reduction of RAD51 foci after damage in BRCA1-deficient cells. Expression of the two REV7 mutants still allowed RAD51 focus formation and their phenotype is more similar to GFP-expressing G3 cells than to REV7-expressing cells. This suggests that the mutants are not able to function as wild-type REV7.

Loss of REV7 also increases DNA end resection in BRCA1-deficient cells⁹. As a measure for resection, cells were damaged with alpha particles, the tracks of DNA damage were stained for RPA and 53BP1 and the number of RPA-positive tracks was quantified. Re-expression of wild-type shRNA-resistant REV7 in G3 cells+shREV7 results in a decrease in the number of RPA-positive tracks compared to G3+shREV7 cells expressing GFP. Expression of the REV7 interaction mutants on the other hand, only resulted in a minor decrease in resection compared to the expression of GFP (Fig 2D). This intermediate phenotype suggests that the interactions between REV7 and REV1 and REV3 play a role in the prevention of end resection. However, in survival experiments with Olaparib treatment, expression of the REV7 point mutants does not result in a strong resistance phenotype⁹. The BRCA1-deficient cell lines expressing mutant REV7 are only slightly more resistant than cell lines expressing wild-type REV7.

Dynamic behaviour of the REV7 mutants

REV7 is known to be recruited to sites

of IR induced DNA damage⁹. To study how the recruitment to sites of damage affects the dynamic behavior of stably overexpressed GFP-REV7, FRAP experiments were performed after UV and IR damage. After DNA damage caused by UV (10 J/m²) or IR (5Gy), wild-type REV7 does not become immobilized compared to untreated cells (Fig 3A). The reduction in fluorescence compared to the pre-bleach intensity is partly due to the bleached volume. However, wild-type REV7 also seems to be more immobilized compared to the point mutants. This suggests that only a small fraction of REV7 is bound at sites of damage and that the bulk continues to diffuse freely through the nucleus.

FRAP experiments were also performed with the GFP-REV7 mutants to study whether they behave differently from wild-type GFP-REV7 *in vivo*. Wild type and GFP-REV7 mutants were expressed in U2OS cells in which endogenous REV7 was depleted by shRNA targeting the 3'-UTR (Fig 3B, S1B). In undamaged cells, the recovery after photobleaching is faster for the mutants than for wild-type REV7 (Fig 3C), indicating decreased binding to sites of damage or faster diffusion of the mutants because the proteins are no longer part of a larger complex.

The FRAP data for the mutants and wild-type REV7 were further analyzed by fitting the curves using a Monte Carlo simulation²² to determine the long and short bound fractions as well as the residence time, which are related to the rate constants for the interactions. Both short and long bound fractions were included in the modeling, since the behavior of many DNA-binding proteins and transcription factors can be characterized by initial short binding to random targets and subsequent stable binding to specific targets.

Since it is unknown what fraction of REV7 is in complex with REV3 (forming a larger complex with slower diffusion) the data was fitted using three different diffusion constants ($dc=0.25 \mu\text{m}^2/\text{s}$, $dc=1.0 \mu\text{m}^2/\text{s}$, $dc=2.5 \mu\text{m}^2/\text{s}$). A dc of 0.25 corresponds to a very large complex in the range of megadaltons, while the diffusion constant of GFP is $7-9 \mu\text{m}^2/\text{s}$.

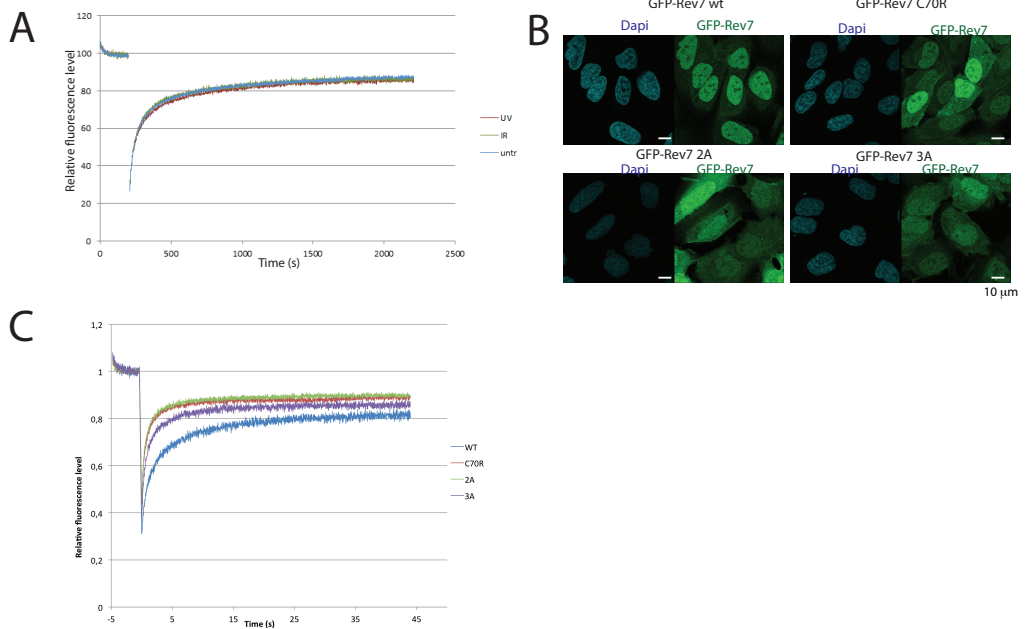


Figure 3 Dynamics of wild-type and mutant REV7

(A) FRAP analysis of U2OS cells stably expressing an shRNA against the REV7 3'-UTR and GFP-REV7 wild type in undamaged cells or cells treated with UV (10 J/m^2) or IR (5Gy). FRAP measurement were performed directly after UV damage and 3-4 hours after IR damage. Graphs represent the average of 20 cells and were normalized to the pre-bleach intensity. (B) Examples of GFP-REV7 wild type or mutant expressing cells used for FRAP analysis. Wild type and GFP-REV7 mutants were expressed in U2OS cells in which endogenous REV7 was depleted by shRNA targeting the 3'-UTR. Scale bar represents $10 \mu\text{m}$. (C) FRAP analysis of U2OS cells stably expressing an shRNA against the REV7 3'-UTR and GFP-REV7 wild type or mutants. Cells were not damaged and the recovery was normalized to the average pre-bleach value. Graphs represent average of 20 cells.

The best fitting curve for wild type REV7 had a diffusion constant of $1 \mu\text{m}^2/\text{s}$, a long immobile fraction of approximately 21% percent (82 seconds immobilized) and a short immobile fraction of 29% (Table 1 and Fig S2). The residence time of the short immobilized fraction was set to 1 second for all mutants. All REV7 mutants showed a decreased long and short immobilized fraction compared to wild type REV7. Furthermore, for the point mutants, the fits are even better with a diffusion constant of $2.5 \mu\text{m}^2/\text{s}$, indicating that the diffusion of these proteins is faster than of wild-type GFP-REV7 (Table 1).

REV7 contains a HORMA domain²³ that could directly or indirectly bind to chromatin. REV7 was found in the cytoplasmic, nuclear and chromatin fractions (Fig S3). The

interaction with chromatin could be via REV1 and REV3, but it might also be via another interaction partner. The differences in the dynamic behavior between the wild-type and mutant REV7 might be due to their inability to form a complex with REV3, but since the REV1 interaction mutant (the 3A mutant) shows a similar increase in recovery after photobleaching as the other point mutants (Fig 3C), it is also possible that other interaction partners are disturbed as well. Also, the intermediate phenotypes in the RAD51 and alpha track assay for different mutants suggest that another common interaction partner might be disturbed. We therefore sought to identify the main interaction partners of wild type REV7 and the C70R mutant.

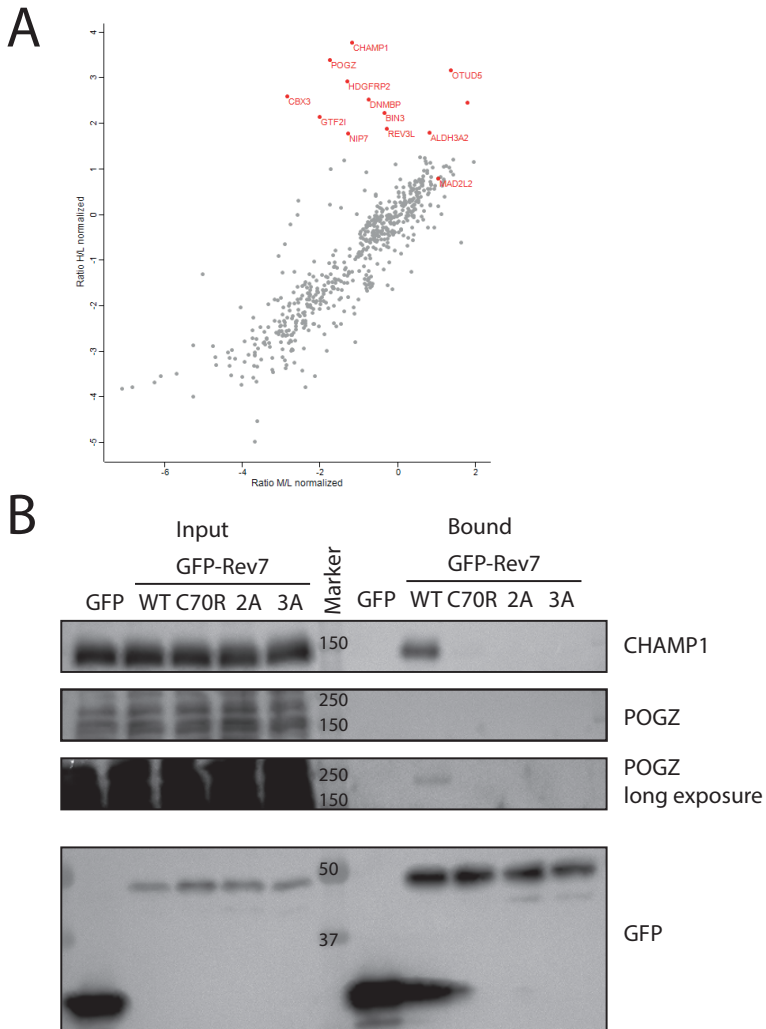


Figure 4 REV7 interacts with POGZ and CHAMP1

(A) Scatterplot showing the SILAC ratios of the proteins in the bound fractions after GFP immunoprecipitation of U2OS cells expressing GFP-REV7 wild type (Heavy), C70R (Medium) and 3A (Light). See also supplementary table 1; MAD2L2 is REV7. (B) Point mutations in REV7 disturb the interaction between GFP-REV7 and endogenous CHAMP1 and POGZ. Immunoprecipitation of GFP or GFP-REV7 wild type or mutants transiently overexpressed in U2OS cells.

REV7 interaction partners CHAMP1 and POGZ

A SILAC-based mass spectrometry analysis of immunoprecipitated GFP-REV7 wild type and mutants was used to investigate whether the interaction partners of the 3A and C70R mutants are different from wild-type REV7 (Fig 4A). As expected, the interaction between REV3 and REV7 C70R is decreased compared

to REV3 and wild-type REV7 (SILAC Ratio:1.3, Log₂ converted ratio 0.45). However, the interaction partners that change most when comparing wild-type REV7 to the C70R mutant are CHAMP1 (C13orf8, ZNF828) and POGZ (Suppl table 1). The same is true when comparing wild-type REV7 to the 3A mutant (table not shown).

A complex between REV7, CHAMP1 and

POGZ has previously been identified in a screen for readers of epigenetic histone marks²⁴. The complex might also contain the HP1 isoforms CBX1, CBX3 and CBX5, which bind to the repressive histone modification H3K9me3. POGZ (Pogo transposable element with ZNF domain) contains a transposase-derived DDE domain and interacts with LEDGF/p75, a transcriptional co-activator that is the main interaction partner of HIV-1 integrase, via this DDE-domain²⁵. Additionally, POGZ has been shown to play a role in modulating the dissociation of HP1 α (Heterochromatin protein 1 α) from mitotic chromosome arms through Aurora B activation²⁶. CHAMP1 (CAMP) also contains a zinc finger motif and is involved in kinetochore–microtubule attachment²⁷.

Immunoprecipitations on wild-type GFP REV7 or the C70R, 2A or 3A mutant in U2OS cells showed that only wild-type GFP-REV7 interacts with POGZ and CHAMP1 (Fig 4B) and all point mutants have lost the interaction. In fractionated cells, endogenous REV7 and GFP-REV7 are present in the cytoplasm, nucleus and chromatin fraction. POGZ is mostly chromatin bound, while CHAMP1 is mainly nuclear but also found in the cytoplasm and on chromatin. Depletion of endogenous REV7 or overexpression of GFP-REV7 did not affect

the localization of CHAMP1. Depletion of REV7 seems to decrease the nuclear fraction of POGZ (Fig S3).

To establish whether these interaction partners of REV7 play a role in mediating PARP inhibitor resistance in BRCA1-deficient cells, shRNAs were used to deplete POGZ in G3 cells (Fig 5B). Unfortunately, depletion of POGZ was inefficient in most clones, even after isolation of single clones. Selected clones with the most efficient depletion of POGZ were used to measure PARP inhibitor sensitivity in clonogenic survivals and RAD51 focus formation after IR. REV7 and 53BP1-depleted G3 cells were used as controls. Loss of REV7 or 53BP1 results in restoration of RAD51 focus formation after irradiation and PARP inhibitor resistance^{9,28,29}. Although the depletion of POGZ was poor, one clone (81-5) showed PARP inhibitor resistance comparable to G3 cells with REV7 or 53BP1 depletion (Fig 5A). Since it was found only in one clone, it could be an off target effect. Depletion of POGZ did not lead to restoration of RAD51 focus formation in G3 cells with stable knock-down of POGZ, even in the clone that was Olaparib resistant (Fig S4 A,B).

As an alternative siRNAs were used to transiently deplete POGZ and CHAMP1 in G3 cells. The transfection with siRNA targeting

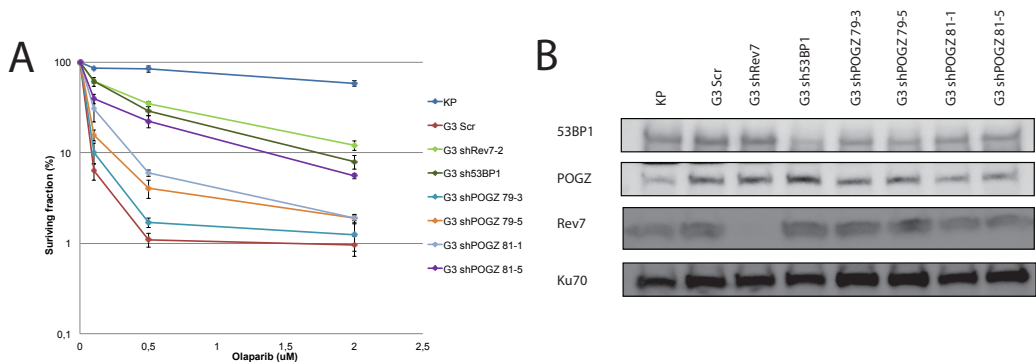


Figure 5 Stable POGZ depletion BRCA1-deficient cells

(A) Depletion of POGZ results in Olaparib resistance in one clone with POGZ depletion (81-5). KP (BRCA1-proficient), G3 shScrambled (Scr, BRCA1-deficient) or G3 cells induced with indicated shRNAs were used for a clonogenic survival assay in the presence of increasing doses of Olaparib. Data represent average \pm SD. (B) Immunoblot of cell lines used in panel (A) with indicated antibodies. Ku70 was used as a loading control.

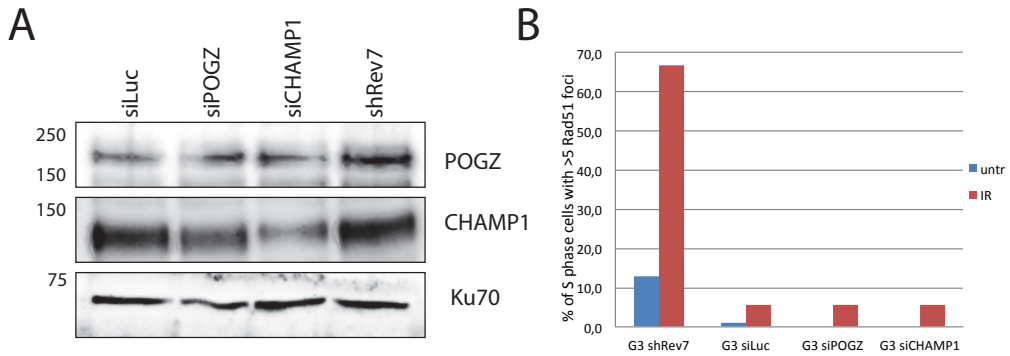


Figure 6 Transient depletion of POGZ and CHAMP1 in G3 cells

(A) Western blot of G3 cells transfected with indicated siRNAs. Ku70 was used to ensure equal loading. (B) Quantification of the number of S-phase cells with more than 5 RAD51 foci. At least 100 nuclei were counted per sample.

POGZ had little effect on POGZ expression (Fig 6A) and there was no restoration of RAD51 focus formation in G3 cells transfected with this siRNA (Fig 6B). CHAMP1 could be knocked down partially with siRNA. However, also in G3 cells transfected with CHAMP1 siRNA, there was no increase in the formation of RAD51 foci after irradiation compared to G3 cells transfected with siRNA targeting Luciferase. This suggests that at least CHAMP1 does not have an effect on RAD51 focus formation in BRCA1-deficient cells. For POGZ a better depletion would be required to draw any conclusions.

Discussion

REV7 is a multifunctional protein that has been linked to trans lesion synthesis, cell cycle progression and transcriptional activation. Each of these functions could theoretically be important in mediating PARP inhibitor resistance in BRCA1-deficient cells. The role of REV7 in cell cycle progression does not seem to be important for the restoration of homologous recombination, but the interaction between REV3 and REV7 is likely to play a role.

In the absence of REV7, mitotic aberrations such as lagging chromosomes and anaphase bridges occur more frequently³⁰. Loss of REV7 could lead to pre-mature or over-activation

of the APC/C, disturbing the tight regulation of mitotic progression. To try to reverse the effect of REV7 loss, we inhibited the APC/C pharmacologically with the inhibitor proTAME¹⁷. Inhibition of the APC/C in BRCA1-deficient cells, with or without REV7 depletion, had no effect on RAD51 focus formation. Therefore, the role of REV7 as inhibitor of the APC/C does not appear to be important for restoring HR in BRCA1-deficient cells. APC/C activation is tightly controlled, not only by REV7, but also by MAD2, EMI1 and several other proteins¹¹, so loss of only REV7 might not result in over-activation of the complex. Also mechanistically, it is difficult to explain why proteins involved in mitosis would restore HR in BRCA1-deficient cells.

The role of REV7 in TLS is more likely to be important. REV7 has been linked to HR³¹ and a flexible polymerase such as Polymerase ζ could be involved in taking care of resected DNA ends that cannot be used for HR, by refilling the resected DNA for example. If the TLS role of REV7 (i.e. Polymerase ζ) would be important for mediating PARP inhibitor resistance, REV3 depletion should have the same phenotype (HR restoration and PARP inhibitor resistance) as REV7 depletion in BRCA1-deficient cells. Unfortunately, REV3 depletion is poorly tolerated in most mammalian cells¹⁸. As an alternative to REV3 depletion, we made point mutations

in REV7 that have been reported to disturb the interaction with REV3 or REV1. The interaction of the C70R and 2A mutants with MBP-REV3 is indeed decreased, although not completely lost. The C70R mutant has been shown to completely lose interaction with a REV3 peptide¹⁹, but the interaction between full length REV7 and REV3 proteins might not be restricted to this region.

The REV7 point mutants show an intermediate phenotype for RAD51 focus formation or RPA recruitment on alpha tracks. This could be due to partial loss of the interaction with REV1 and REV3 or another process might be important for PARP inhibitor resistance as well. We found that the REV7 point mutants also lose their interaction with CHAMP1 and POGZ. The loss of this interaction could also contribute to the intermediate phenotype. Likewise, the phenotype of the repro-22 mouse in which the C70R mutation was found, is completely ascribed to the loss of the interaction between REV3 and REV7, but the loss of CHAMP1 and POGZ interaction could also contribute to infertility and the development of ovarian cancers^{19,32}.

Partial depletion of POGZ in BRCA1-deficient mouse cells did not lead to restoration of RAD51 focus formation after IR. Only in one single clone resistance to Olaparib comparable to REV7 depletion was observed. This could be due to an off-target effect or via an unknown mechanism. In this clone the expression of 53BP1 or REV7 was not affected and in the G3 cell line restoration of BRCA1 expression is not possible because a large part of the BRCA1 coding region (exon 5-13) is deleted³³. Additionally, no RAD51 foci were formed after irradiation, while this is the case for REV7 and 53BP1-depleted G3 cells. POGZ has been shown to be essential for normal mitotic progression²⁶ and it is therefore possible that POGZ depletion is poorly tolerated. Knockout of POGZ or CHAMP1 in BRCA1-deficient cells using the CRISPR/Cas9 system could help to solve the problem of poor knockdown, if loss of their expression is not lethal. Transient depletion of CHAMP1

did not affect RAD51 focus formation either, suggesting that this interaction partner of REV7 is not important for restoring HR.

Several models could explain how REV7 loss leads to restoration of homologous recombination. Boersma et al showed that REV7 promotes NHEJ mediated fusion of uncapped telomeres and inhibits 5'-end resection¹⁰. How REV7 inhibits resection remains unclear. REV7 could block access of nucleases, but in proteomics analysis no interaction between REV7 and any of the nucleases known to be involved in resection or any NHEJ proteins was found (data not shown). REV7 also did not interact directly with 53BP1. Another possibility is that Polymerase ζ reverses resection by filling in the ssDNA gap formed during resection. For this to be possible, a hairpin or a piece of dsDNA or RNA-DNA hybrid would be required to serve as a primer at the DNA end. To be able to distinguish between these models it is necessary to know what the phenotype of REV3 deletion in BRCA1-deficient cells is. Both BRCA1 and REV3 deletion are poorly tolerated in most mammalian cells. Chicken DT40 cells are an exception since both BRCA1 and REV3 knock-outs have been generated^{34,35}. We tried to create *BRCA1^{-/-}REV7^{-/-}* and *BRCA1^{-/-}REV3^{-/-}* DT40 cells. *BRCA1* knock-out *REV7^{-/-}* cells were viable and loss of REV7 in BRCA1-deficient DT40 cells restored RAD51 focus formation (data not shown). *BRCA1^{-/-}REV3^{-/-}* cells could not be generated, suggesting that this double knockout might be lethal. A conditional deletion version of *BRCA1* could circumvent this problem and more experiments are needed to determine whether *REV3* loss in *BRCA1*-deficient cells restores homologous recombination.

References

1. Siegel, R. L., Miller, K. D. & Jemal, A. Cancer Statistics, 2015. *CA Cancer J Clin* 65, 5–29 (2015).
2. Bryant, H. E. et al. Specific killing of BRCA2-deficient tumours with inhibitors of poly(ADP-ribose) polymerase. *Nature* 434, 913–917 (2005).
3. Farmer, H. et al. Targeting the DNA repair defect in BRCA mutant cells as a therapeutic strategy. *Nature* 434, 917–921 (2005).
4. Bouwman, P. & Jonkers, J. Molecular pathways: How

- can BRCA-mutated tumors become resistant to PARP inhibitors? *Clin. Cancer Res.* 20, 540–547 (2014).
5. Rottenberg, S. et al. High sensitivity of BRCA1-deficient mammary tumors to the PARP inhibitor AZD2281 alone and in combination with platinum drugs. *Proc. Natl. Acad. Sci.* 105, 17079–84 (2008).
 6. Jaspers, J. E. et al. Loss of 53BP1 causes PARP inhibitor resistance in BRCA1-mutated mouse mammary tumors. *Cancer Discov.* 3, 68–81 (2013).
 7. Sakai, W. et al. Secondary mutations as a mechanism of cisplatin resistance in BRCA2-mutated cancers. *Nature* 451, 1116–1120 (2008).
 8. Edwards, S. L. et al. Resistance to therapy caused by intragenic deletion in BRCA2. *Nature* 451, 1111–1115 (2008).
 9. Xu, G. et al. REV7 counteracts DNA double-strand break resection and affects PARP inhibition. *Nature* 521, 541–4 (2015).
 10. Boersma, V. et al. MAD2L2 controls DNA repair at telomeres and DNA breaks by inhibiting 5' end resection. *Nature* (2015). doi:10.1038/nature14216
 11. Peters, J. M. The anaphase promoting complex/cyclosome: a machine designed to destroy. *Nat. Rev. Mol. Cell Biol.* 7, 644–656 (2006).
 12. Chen, J. & Fang, G. MAD2B is an inhibitor of the anaphase-promoting complex. *Genes Dev.* 15, 1765–1770 (2001).
 13. Fang, G., Yu, H. & Kirschner, M. W. The checkpoint protein MAD2 and the mitotic regulator CDC20 form a ternary complex with the anaphase-promoting complex to control anaphase initiation. *Genes Dev.* 12, 1871–1883 (1998).
 14. Reimann, J. D. R., Gardner, B. E., Margottin-Goguet, F. & Jackson, P. K. Emi1 regulates the anaphase-promoting complex by a different mechanism than Mad2 proteins. *Genes Dev.* 15, 3278–3285 (2001).
 15. Reimann, J. D. R. et al. Emi1 is a mitotic regulator that interacts with Cdc20 and inhibits the anaphase promoting complex. *Cell* 105, 645–655 (2001).
 16. Lee, H. et al. Mouse emi1 has an essential function in mitotic progression during early embryogenesis. *Mol. Cell Biol.* 26, 5373–5381 (2006).
 17. Lara-Gonzalez, P. & Taylor, S. S. Cohesion Fatigue Explains Why Pharmacological Inhibition of the APC/C Induces a Spindle Checkpoint-Dependent Mitotic Arrest. *PLoS One* 7, (2012).
 18. Lange, S. S., Wittschieben, J. P. & Wood, R. D. DNA polymerase zeta is required for proliferation of normal mammalian cells. *Nucleic Acids Res.* 40, 4473–4482 (2012).
 19. Khalaj, M. et al. A missense mutation in Rev7 disrupts formation of Pol, impairing mouse development and repair of Genotoxic Agent-induced DNA Lesions. *J. Biol. Chem.* 289, 3811–3824 (2014).
 20. Hara, K. et al. Crystal structure of human REV7 in complex with a human REV3 fragment and structural implication of the interaction between DNA polymerase ζ and REV1. *J. Biol. Chem.* 285, 12299–12307 (2010).
 21. Lee, Y.-S., Gregory, M. T. & Yang, W. Human Pol ζ purified with accessory subunits is active in translesion DNA synthesis and complements Pol η in cisplatin bypass. *Proc. Natl. Acad. Sci. U. S. A.* 111, 2954–9 (2014).
 22. Geverts, B., van Royen, M. E. & Houtsmuller, A. B. in *Advanced Fluorescence Microscopy: Methods and protocols, Methods in Molecular Biology* vol. 1251 109–133 (2015).
 23. Aravind, L. & Koonin, E. V. The HORMA domain: a common structural denominator in mitotic checkpoints, chromosome synapsis and DNA repair. *Trends Biochem. Sci.* 23, 284–286 (1998).
 24. Vermeulen, M. et al. Quantitative Interaction Proteomics and Genome-wide Profiling of Epigenetic Histone Marks and Their Readers. *Cell* 142, 967–980 (2010).
 25. Bartholomeeusen, K. et al. Lens epithelium-derived growth factor/p75 interacts with the transposase-derived DDE domain of pogZ. *J. Biol. Chem.* 284, 11467–11477 (2009).
 26. Nozawa, R. S. et al. Human POGZ modulates dissociation of HP1alpha from mitotic chromosome arms through Aurora B activation. *Nat. Cell Biol.* 12, 719–727 (2010).
 27. Itoh, G. et al. CAMP (C13orf8, ZNF828) is a novel regulator of kinetochore-microtubule attachment. *EMBO J.* 30, 130–144 (2011).
 28. Bouwman, P. et al. 53BP1 loss rescues BRCA1 deficiency and is associated with triple-negative and BRCA-mutated breast cancers. *Nat. Struct. Mol. Biol.* 17, 688–695 (2010).
 29. Bunting, S. F. et al. 53BP1 inhibits homologous recombination in brca1-deficient cells by blocking resection of DNA breaks. *Cell* 141, 243–254 (2010).
 30. Listovsky, T. & Sale, J. E. Sequestration of cdh1 by mad2l2 prevents premature apc/c activation prior to anaphase onset. *J. Cell Biol.* 203, 87–100 (2013).
 31. Sharma, S. et al. REV1 and polymerase ζ facilitate homologous recombination repair. *Nucleic Acids Res.* 40, 682–691 (2012).
 32. Abbasi, A. et al. Lack of Rev7 function results in development of tubulostromal adenomas in mouse ovary. *Mol. Cell. Endocrinol.* 412, 19–25 (2015).
 33. Liu, X. et al. Somatic loss of BRCA1 and p53 in mice induces mammary tumors with features of human BRCA1-mutated basal-like breast cancer. *Proc. Natl. Acad. Sci. U. S. A.* 104, 12111–12116 (2007).
 34. Sonoda, E. et al. Multiple roles of Rev3, the catalytic subunit of polzeta in maintaining genome stability in vertebrates. *EMBO J.* 22, 3188–3197 (2003).
 35. Martin, R. W. et al. RAD51 up-regulation bypasses BRCA1 function and is a common feature of BRCA1-deficient breast tumors. *Cancer Res.* 67, 9658–9665 (2007).
 36. Tan, T. L. R. et al. Mouse Rad54 affects DNA conformation and DNA-damage-induced Rad51 foci formation. *Curr. Biol.* 9, 325–328 (1999).
 37. Rodrigue, A. et al. Interplay between human DNA repair proteins at a unique double-strand break in vivo. *EMBO J.* 25, 222–231 (2006).

Acknowledgements

We would like to thank Wei Yang for providing the MBP-REV3 construct. This research has received funding from the European Community's Seventh Framework Programme (FP7/2007-2013) under grant agreement No. HEALTH-F2-2010-259893 (DDRResponse) and the Dutch Cancer Society (KWF) grant nr. 2011-5030.

Materials and Methods

Cell culture, transfections and treatments

HEK293FT cells were grown at 37°C in 5% CO₂ in Dulbecco's modified Eagle medium (DMEM) (Sigma) supplemented with 10% fetal bovine serum (Biowest), penicillin, streptomycin, 1x non-essential amino acids (Lonza) and 1 mM sodium pyruvate (Lonza). U2OS cells were grown under the same conditions in a mixture of DMEM and Ham's F10 (1:1) (Sigma) supplemented with 10% fetal bovine serum (Biowest), penicillin and streptomycin. G3 cells were cultured in DMEM/F12 (1:1) (Life technologies) supplemented with 10% fetal bovine serum (Biowest), penicillin and streptomycin, 5 mg/ml insulin (Sigma), 5 ng/ml epidermal growth factor (Life Technologies) and 5 ng/ml cholera toxin (Sigma) under low oxygen conditions (3% O₂, 5% CO₂, 37°C).

HEK cells were transfected using calcium phosphate precipitations and U2OS plasmid transfections were carried out using Xtremegene HP (Roche). U2OS lines stably expressing mutants were generated by plasmid transfection and subsequent G418 di-sulphate selection (ForMedium).

For treatments with proTAME (I-440, Boston Biochem), G3 cells were incubated with 20 μM proTAME or equal amounts of DMSO (vehicle).

For clonogenic survivals, KP and G3 cells were seeded at low density and treated with Olaparib (AstraZeneca) the next day. Olaparib was refreshed every 4 days. Colonies were fixed and stained 10 days after seeding and counted manually.

siRNA transfections on G3 cells were carried out using Dharmafect 1 (Dharmacon) using a single transfection according to manufacturer's instructions and cells were analysed 48 hours after transfection. Four siRNAs per gene were mixed at equimolar ratios and transfected as a pool for POGZ or CHAMP1.

siRNAs (Dharmacon): siLuciferase sense sequence (CGUACGCGAAUACUUCGAdTdT) siPOGZ ON-TARGETplus set of 4, J059516-09 target sequence (GAGCAGAUUUAGACACGUU), J059516-10 target sequence (CACCGAAGGUAGCGUCAGA), J059516-11 target sequence (CUUAAAUGUCCACGUGUA), J059516-12 target sequence (CUGAGGAGGAGAU CGCAA). siCHAMP1 ON-TARGETplus set of 4, J056406-09 target sequence (CGGCUGAACACUUCGAAA), J056406-10 target sequence (CCAGGACGGUGGACGGAAA), J056406-11 target sequence (GGAUUGUGCUAACGUACA), J056406-12 target sequence (ACGUAGAACUUGAUCAACA)

Lentiviral transduction with shRNA

ShRNA expression constructs were obtained from the Sigma mission library (TRC 1.5). Lentiviral packaging

plasmids (pMDLg/pRRE, pRSV-REV and pMD2.G) and shRNA expression constructs were transfected into HEK293FT cells using calcium phosphate precipitations. 24h after transfection the medium was changed and 48h after transfection the supernatant of the HEK cells was added to U2OS, G3 or B11 cells. This process was repeated the next day. 48 hours after the second transduction, cells were selected using puromycin (Invivogen). Creation of G3 cell lines with shRNAs targeting REV7 or 53BP1 has been described before⁹. The following shRNA constructs were used for lentiviral transduction in human or mouse cells. Human: shNT32 no insert; shREV7 3'-UTR TRCN0000006569_CCCTGATCCAAGTGCTCTTA Mouse: REV7 sh2 TCRN0000012846_CATCTCCAGAAGCGCAAGAA; 53BP1 TCRN0000081778_GCTATTGTG-GAGATTGTGTTT POGZ sh79 TRCN0000098926_GCCAA-CAACAATGCTGGTAAT POGZ sh81 TRCN0000098928_CGCACTCACTTGTCAGAAGAA

Cloning

Cloning of GFP-REV7 and the point mutants has been described before⁹. The MBP-REV3 construct was kindly provided by Wei Yang²¹.

FRAP

For FRAP experiments cells were seeded on 24 mm glass coverslips at low density, such that single cells did not touch. All experiments were performed on a Leica SP5 confocal microscope equipped with a 37°C chamber and CO₂ supply (5% CO₂). Cells were imaged and bleached with a 488 nm Argon laser using a 63x oil immersion objective. FRAP analysis was performed on a 16 pixel wide strip spanning the short axis of an ellipsoid nucleus. Pre-bleach, 200 frames were scanned using a 22ms interval, after which the ROI was bleached at maximum laser power for 100 ms. Subsequently the intensity in the ROI was measured with 22 ms intervals for 45 seconds to follow recovery of the fluorescence. A ROI outside the nucleus was measured to correct for the background. All curves were normalized to the pre-bleach intensity and averaged (n=20 cells).

FRAP data were analyzed using a Monte Carlo simulation based program described before²². The error of the fit was calculated using the formula: $\text{Error} = \frac{\sum(\text{measured data} - \text{data-fitted data})^2}{\text{total number of points fitted}}$.

Immunofluorescence

Cells were grown on glass coverslips and fixed in 4% paraformaldehyde for 15 min. For RAD51 staining, cells were extracted before fixation for 1 min in cold Triton X-100 buffer (0.5% Triton X-100, 20 mM HEPES-KOH pH 7.9, 50 mM NaCl, 3 mM MgCl₂, 300 mM Sucrose). PBS+0.1% Triton X-100 was used for all washing steps and PBS+ (0.5% BSA, 0.15% Glycine in PBS) was used for blocking and dilution of primary and Alexa conjugated secondary antibodies (Invitrogen). Stained coverslips were mounted using Vectashield+dapi (Vectorlabs).

Alpha track experiments were performed as described previously⁹.

Antibodies

CHAMP1 (SAB1408469, Sigma), MBP (maltose-binding protein) (Ab 9084, Abcam), GFP (clones 7.1 and 13.1, Roche), Ku70 (C-19, Sc1486, Santa Cruz), POGZ (ARP 39173_P050, Aviva systems biology), RAD51 (2307, home-made 36), REV7 (612266, BD transduction laboratories) and (EPR13657, Abcam), RPA (9H8, Abcam), 53BP1 (NB100-304 Novus Biologicals).

Immuno precipitation

Cells were washed in PBS and lysed for 5 min on ice in NETT buffer (100 mM NaCl, 50 mM Tris-HCl pH 7.5, 5 mM EDTA, 0.5% Triton X-100) supplemented with protease inhibitor cocktail (Roche) and Pefa-bloc (Roche). Lysates were cleared by centrifugation (1200 rcf, 15 min at 4°C), the supernatant was added to GFP-trap agarose beads (Chromo-Tek) in NETT buffer and incubated for 4-5h on a rotating wheel at 4°C. Beads were washed 3x in NETT buffer+ protease inhibitors+Pefa-bloc and eluted by boiling in 2x SDS-PAGE sample buffer.

Mass spectrometry

For SILAC labelling, cells were grown in DMEM medium for SILAC (Thermo Scientific) without lysine or arginine and supplemented with dialysed serum, L-arginine and L-lysine (Light: K_0R_0 , Medium: K_4R_0 , Heavy: K_8R_{10}) for 2 weeks. Amino acids for SILAC (K_4 : L-LYSINE:2HCL (4,4,5,5-D4, 96-98%), K_8 : L-LYSINE:2HCL (13C6, 99%), R_6 : L-ARGININE:HCL (13C6, 99%), R_{10} : L-ARGININE:HCL (13C6, 99%; 15N4, 99%) were obtained from Cambridge Isotope Laboratories.

IPs were performed for each state separately in NETT buffer (100 mM NaCl, 50 mM Tris HCl pH 7.5, 5 mM EDTA, 0.5% Triton X100) supplemented with protease inhibitor cocktail (Roche) and Pefa-bloc (Roche). After Immunoprecipitation, bound proteins of all three states were mixed and were digested 'on-bead'. Briefly, beads were transferred to a Pierce spin column and washed at least five times with cold 50mM ammoniumbicarbonate (ABC). The columns were plugged and 100µl of 2.4mM sodium deoxycholate (SDC), 2.4mM sodium N-lauroylsarcosinate (SLS) in 0.1M Tris-HCl pH 8.5 was added. Proteins were reduced by addition of 5µl 100mM DTT and incubation at 50°C in a shaker for 30 minutes and subsequently alkylated by addition of 5µl 200mM 2-chloroacetamide (CAA) and incubation at room temperature for 30 minutes on a shaker in the dark. After addition of 100µl 50mM ABC and 2µl 100mM CaCl₂ 0.5µg trypsin (TPCK trypsin, Thermo Fisher Scientific) was added. Proteins were digested at 30°C overnight on a shaker. After collection of the supernatant the beads were washed with 50µl 50mM ABC and trifluoroic acid (TFA) was added to the digest to a final concentration of 0.5%. An equal volume of water-saturated ethylacetate was added and after mixing vigorously for 1 minute and spinning the upper phase was removed and the same wash was repeated. Sample volume was reduced in a SpeedVac and pH was adjusted with 10% TFA if necessary (pH < 4) and purified on a home-made C18 column (a 1.4mm diameter punch from a 3M Empore octadecyl C18 extraction disk in a 200ul tip) similar to the ZipTip C18 procedure (Sigma). The

peptide eluate was dried in a SpeedVac and the residue was dissolved in 3% acetonitril (ACN), 0.5% formic acid (FA) and briefly sonicated. A fraction was injected onto a Waters nanoAcquity LC equipped with a Waters 20mm x 180um nanoACQUITY UPLC Symmetry C18 Trap Column with 5µm particles and a home-made 40cm x 75µm fused silica analytical column with Waters 3.5µm Xbridge BEH C18 particles. Peptides were separated using a 90 or 120 minute gradient from 99%A to 65%A (A= 0.1% FA, B=0.1% FA in ACN) at 0.3µl/min and 50°C and analyzed on a Thermo Orbitrap Fusion mass spectrometer using a nanoESI source and a TopSpeed DDA method with 3 seconds cycle time, full scan detection at 120K resolution in the orbitrap, HCD fragmentation of selected peaks and fragment detection in the ion trap. Each sample was injected twice using either a maximal intensity first or a minimal intensity first DDA method. Data was analysed using MaxQuant and Perseus.

Western blot

Cell extracts were prepared in 2x Leammli buffer (0.8% SDS, 4% glycerol, 280 mM β-mercaptoethanol, 25 mM Tris-HCl pH 6.8). Proteins were separated by SDS-PAGE and then transferred to either nitrocellulose or PVDF membrane. Blots were probed using the specified primary antibodies in blocking buffer (3% milk in PBS+ 0.05% Tween-20) and secondary antibodies coupled to HRP (Jackson ImmunoResearch). Membranes were washed in PBS+0.05% Tween-20. Proteins were detected by ECL.

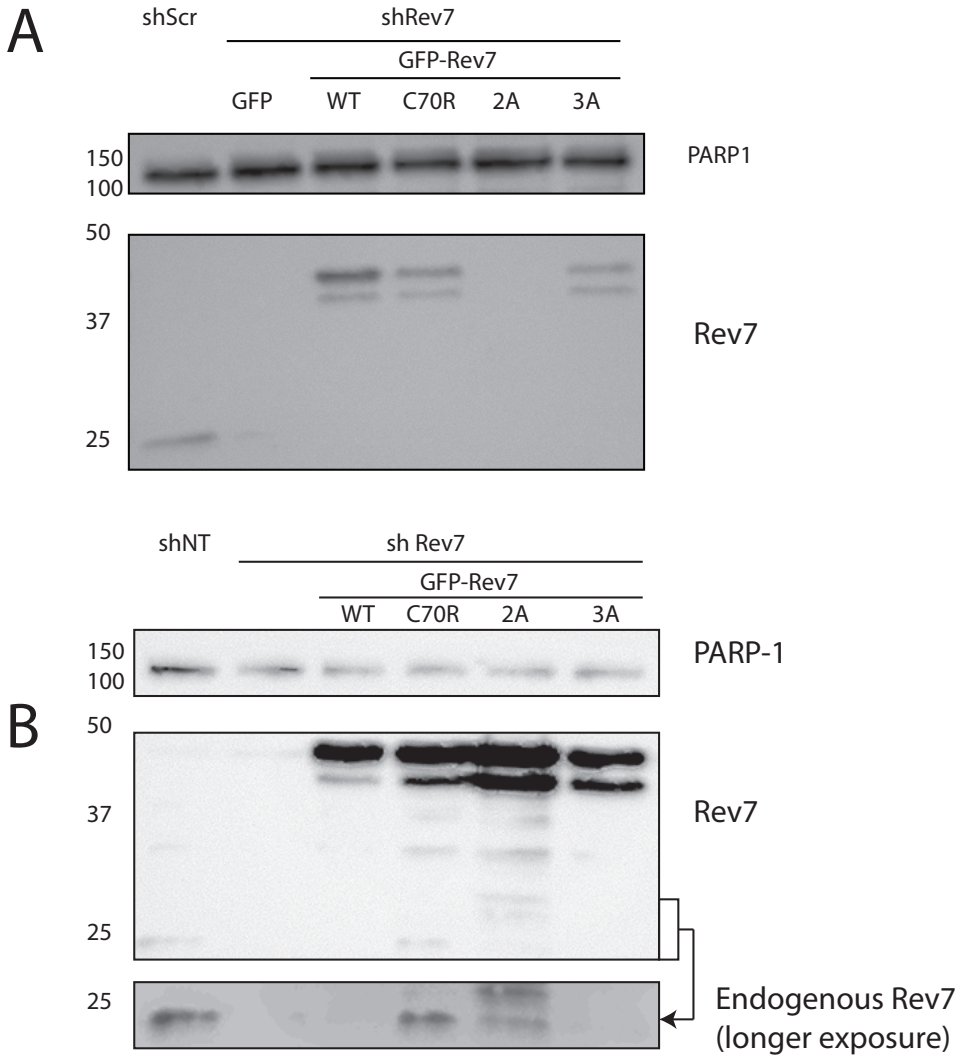
Fractionation

For fractionations, cells were washed in PBS and trypsinized. Cells were counted and per sample 1 million cells were used. Fractionations were performed as described before³⁸.

Table 1

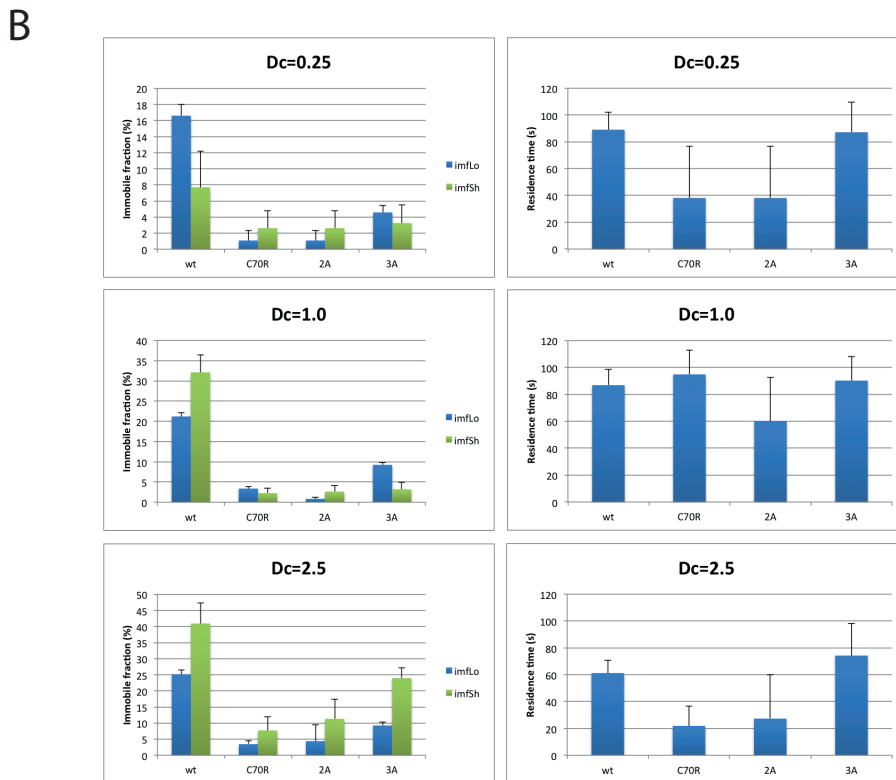
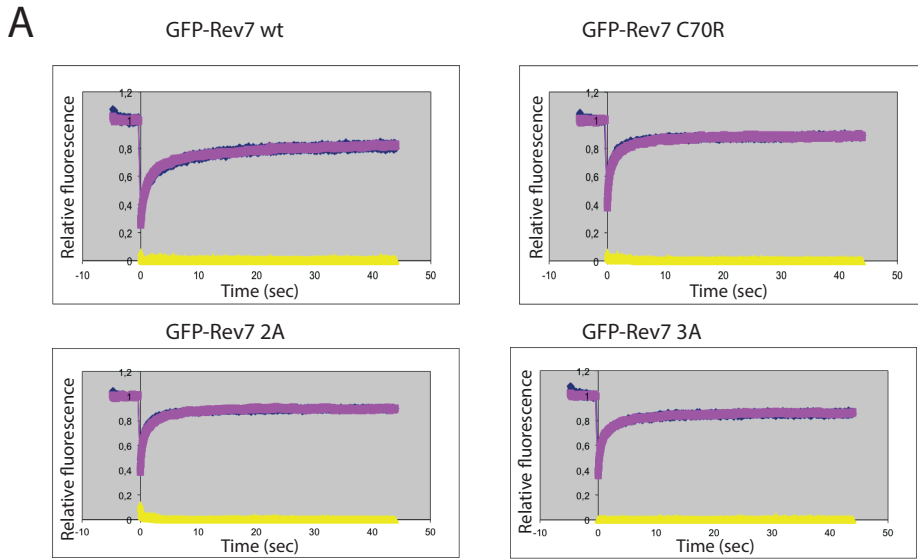
	Long		Short			
	Immobile fraction	Residence time (sec)	Immobile fraction	Residence time (sec)	Diffusion constant ($\mu\text{m}^2/\text{s}$)	Error best fit
WT	17%	79.88	10.5%	1.0	0.25	0.000173313
C70R	0.53%	29.56	0.25%	1.0	0.25	0.001596048
2A	0.53%	29.55	0.25%	1.0	0.25	0.001812122
3A	4.3%	103.12	1.46%	1.0	0.25	0.000838836
	Long		Short			
	Immobile fraction	Residence time (sec)	Immobile fraction	Residence time (sec)	Diffusion constant ($\mu\text{m}^2/\text{s}$)	Error best fit
WT	21.3%	81.94	29.4%	1.0	1.0	0.000150538
C70R	3.1%	78.7	0.64%	1.0	1.0	0.000145077
2A	0.66%	110.11	1.04%	1.0	1.0	0.000159326
3A	8.4%	109.55	3.9%	1.0	1.0	0.000100401
	Long		Short			
	Immobile fraction	Residence time (sec)	Immobile fraction	Residence time (sec)	Diffusion constant ($\mu\text{m}^2/\text{s}$)	Error best fit
WT	25.9%	52.2	35.5%	1.0	2.5	0.000171998
C70R	3.4%	14.88	5.9%	1.0	2.5	5.85241E-05
2A	10.8%	29.33	8.6%	1.0	2.5	9.69721E-05
3A	8.9%	57.33	19.3%	1.0	2.5	0.000103614

Values for best fits per Dc. Residence time for the short immobile fraction was set to 1 sec in the model.



Supplementary figure 1

(A) Western blot showing the expression of GFP-tagged REV7 wild type or mutants in BRCA1-deficient mouse G3 cells. The 2A mutant was not expressed. (B) Western blot showing the expression of GFP-tagged REV7 wild type or mutants in U2OS cells. Cells were transduced with a shRNA targeting the 3'-UTR of endogenous REV7. PARP1 was used as a loading control.

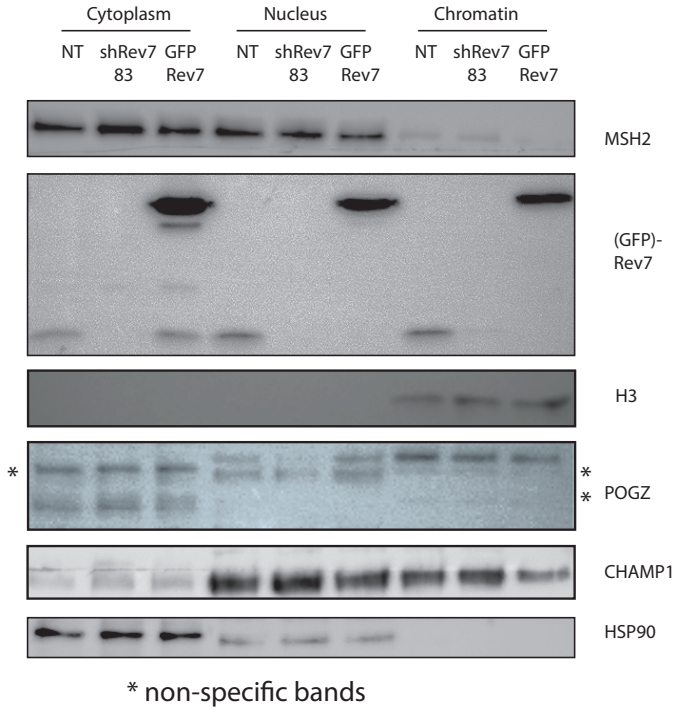


Supplementary figure 2

(A) Best fitting curves with a diffusion constant of 1 ($dc=1.0$) from Monte Carlo simulation of FRAP from data GFP-REV7 wild-type or mutants. Experimental data in blue, fitted data in purple and residual (difference between experimental en fitted data) in yellow. (B) Average values from 10 best fits for the short (imfSh) and long immobile (imfLo) fractions and residence time for three different values for the diffusion constant ($dc=0.25;1.0;2.5$).

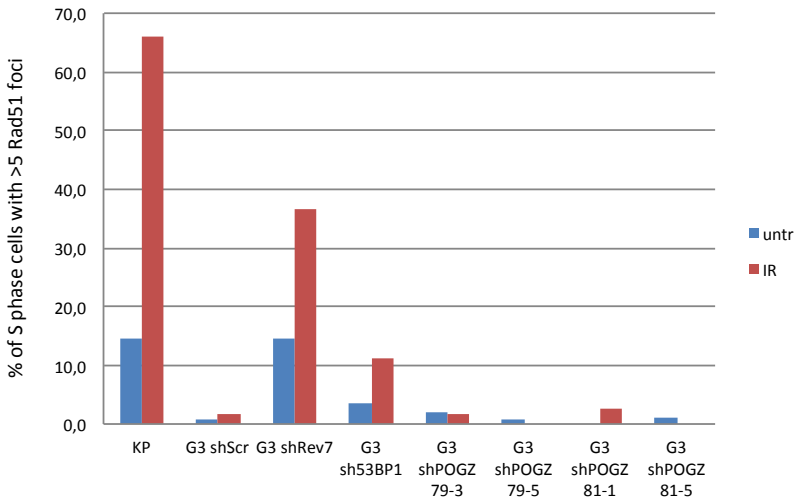
4

4



Supplementary figure 3

Immunoblot of fractionated U2OS cells with depletion of REV7 or overexpression of GFP-REV7 using indicated antibodies. Depletion or overexpression of REV7 does not affect the localization of POGZ and CHAMP1.



Supplementary figure 4

Quantification of the number of EdU positive cells with more than 5 RAD51 foci. Cells were irradiated with 5 Gy and incubated with EdU to label S-phase cells. At least 100 nuclei were counted in this experiment and the experiment was performed twice.

Supplementary Table 1: MS SILAC Ratio's

Results of a SILAC experiment using U2OS cells expressing GFP-tagged wild-type or mutant REV7 to analyze their interacting proteins. The top 150 hits are shown. L: GFP-REV7 3A mutant, M: GFP-REV7 C70R mutant, H: GFP-REV7 wild type. All ratios in this table are Log2 converted. Data is sorted on normalized H/M ratio. A H/M ratio higher than 0 means that a protein is more abundant in the GFP-REV7 wild-type pull down than in the GFP-REV7 C70R pull-down. In essence, the protein interacts (indirectly or directly) more strongly with wild-type REV7 than the point mutant.

Gene names	Ratio M/L normalized	Ratio H/L normalized	Ratio H/M normalized	Peptides	Sequence coverage (%)
POGZ	-1.746713	3.38405	8.718841	34	39.4
CBX3	-2.847466	2.598603	5.084489	6	42.6
CHAMP1	-1.183605	3.767231	5.010467	26	43.2
HDGFRP2	-1.299099	2.919264	4.085085	3	7.2
CBX1	-1.370564	1.186754	3.867106	4	26.6
H2AFV	-5.018071	-1.300129	3.609046	4	31.2
DNMBP	-0.7372301	2.518283	3.156332	13	12.6
HIST2H3PS2	-6.828445	-3.794197	2.940355	2	13.2
HIST1H4A	-7.088786	-3.827625	2.924651	12	61.2
NIP7	-1.273727	1.775388	2.787516	3	28.9
SCAI	-2.560472	0.3070788	2.672697	3	5.4
GLG1	-1.730919	1.000793	2.664415	3	5.3
CAPRIN1	-2.569522	-0.01547628	2.523311	3	8.4
GTF2I	-2.00127	2.147437	2.512657	8	10.7
BIN3	-0.3341343	2.221289	2.448267	2	15.6
ADNP	-2.752826	-0.2124004	2.435469	3	3.4
HIST1H2AC	-6.088335	-3.547763	2.421318	5	35.4
HIST1H2BL	-6.258701	-3.675415	2.36779	5	35.7
BANF1	-5.267455	-2.867121	2.258519	7	56.2

Supplementary Table 1: MS SILAC Ratio's continued

Gene names	Ratio M/L normalized	Ratio H/L normalized	Ratio H/M normalized	Peptides	Sequence coverage (%)
OTUD5	1.373843	3.161678	2.198243	5	20.3
FXR1	-2.909743	-0.6412211	2.125585	5	12.8
VIM	-5.690256	-3.48733	2.065124	46	82.4
PDCD11	-3.056971	-0.9113156	2.049247	12	10.9
BCAS2	-1.751708	0.2087669	1.844747	3	24
PSIP1	-4.035875	-2.031504	1.836369	7	16
RBM8A	-4.762074	-2.894108	1.667892	3	32.2
CSNK2A1	-0.806897	0.9237196	1.639417	5	22.1
SMARCA4	-2.958925	-1.272925	1.571094	6	5.2
ELAVL1	-3.715448	-3.580474	1.493494	7	29.1
POLD2	-1.453597	0.1415635	1.482384	5	16.6
HNRNPUL2	-3.707115	-2.253532	1.367427	4	8
NHP2L1	-4.328957	-3.140253	1.343692	4	32
HNRNPC	-5.257542	-3.991094	1.341872	12	33.2
FAM35A	-0.05866828	1.108625	1.339935	5	9.3
RANBP2	-2.6631	-1.252192	1.297074	11	5.9
HMGA1	-4.670061	-3.303864	1.290837	3	41.1
HEATR1	-2.671991	-1.700404	1.273695	8	5.3
HIST1H1C	-4.686053	-3.128093	1.251022	9	27.7
THY1	-3.329058	-1.973582	1.218719	2	19.7
RPL23A	-0.8451834	0.5293712	1.206268	3	26.3
H1FO	-4.26141	-2.973922	1.173383	2	11.3

Supplementary Table 1: MS SILAC Ratio's continued

Gene names	Ratio M/L normalized	Ratio H/L normalized	Ratio H/M normalized	Peptides	Sequence coverage (%)
LIMA1	-3.37713	-2.71577	1.1644	3	8.2
NOP58	-4.183821	-3.158558	1.080453	10	28.7
RBM25	-3.726615	-2.538178	1.05797	3	5.9
ACIN1	-3.004508	-1.826233	1.043205	6	7.6
ERH	-3.742825	-2.720707	1.004753	3	41.3
NTPCR	-0.5713217	0.4151096	0.9950141	5	35.8
NES	-2.798968	-2.007638	0.9922609	12	10.4
FSCN1	-2.153414	-1.033097	0.9919707	1	3.2
DDB1	-0.9302154	-0.4999934	0.9835318	11	14.9
ALDH3A2	0.8196682	1.797013	0.9833128	4	14
NONO	-4.320861	-3.311435	0.9705592	16	38.9
JUP	-2.991255	-2.563625	0.9374951	17	35.8
CPSF1	-2.667859	-1.95506	0.9330438	8	7.4
NUMA1	-1.299418	-1.505246	0.9290335	23	17.5
NUP93	-1.055531	0.009920342	0.916553	8	16.6
DEK	-2.549029	-2.081614	0.9143348	3	10.4
PNN	-3.638061	-2.734371	0.9112697	4	7.7
RPL7L1	-3.323834	-2.475054	0.8970855	3	16.7
HIST1H1A	-3.537106	-2.462833	0.8951474	8	27
BRIX1	-3.948419	-2.782993	0.891808	6	23.5
HNRNPA0	-2.363865	-1.48221	0.8850276	3	17
NUP155	-2.567297	-1.579491	0.8790784	3	4.9

Supplementary Table 1: MS SILAC Ratio's continued

Gene names	Ratio M/L normalized	Ratio H/L normalized	Ratio H/M normalized	Peptides	Sequence coverage (%)
KPRP	-4.359372	-3.03174	0.874679	11	33.9
RALY	-3.935205	-3.238953	0.8603669	4	23.6
OCIAD2	0.07710631	0.7650254	0.8563882	1	5.8
KHDRBS1	-3.161395	-2.324383	0.8551924	3	6.1
HNRNPL	-2.659996	-3.255529	0.8489584	12	36.8
TUBA4A	-0.5610898	0.4487953	0.8459918	21	54.2
HNRPDL	-3.681677	-3.086323	0.8401208	8	24.8
SNRPD1	-2.27425	-1.300093	0.8303365	2	28.6
POLR2B	-1.612461	-1.044806	0.8277377	9	11.9
HLA-B	-0.9783497	-0.4199896	0.8168864	4	19.3
PRPF8	-3.089881	-1.886299	0.8127036	20	12.6
RSL1D1	-3.613379	-3.330828	0.7962655	9	26.1
HIST1H1E	-3.83218	-3.081186	0.7762725	10	26.9
POLR2H	-2.94586	-2.043111	0.7584738	2	21.6
PRPF6	-2.401406	-1.539645	0.75745	2	2
NOC2L	-2.77962	-1.949087	0.7302269	3	4.8
CSTB	-2.2283	-1.590875	0.7167714	2	24.5
MYO1B	-2.445283	-1.567981	0.716069	8	12.5
IMMT	-1.564862	-1.175957	0.7144873	4	7.9
RPL8	-0.5256003	0.1894135	0.6999069	3	23.4
CKAP4	-0.4338765	0.2447654	0.6882251	6	13.6
DDX27	-1.909797	-1.693621	0.6651199	6	9.8

Supplementary Table 1: MS SILAC Ratio's continued

Gene names	Ratio M/L normalized	Ratio H/L normalized	Ratio H/M normalized	Peptides	Sequence coverage (%)
GNAI2	-2.575873	-1.866857	0.6617496	9	34.1
CPSF6	-1.653991	-0.8935981	0.660381	2	7.5
CPSF7	-2.250577	-1.663465	0.6556266	3	14.2
TMPO	-1.788813	-1.499973	0.6548937	5	22.5
CD44	-1.762583	-1.067243	0.6428402	1	6.6
DDX47	-1.849752	-1.925823	0.6391395	4	15.8
HNRNPF	-2.166956	-1.365574	0.6374712	8	33.5
RANGAP1	-1.625845	-1.129513	0.6325474	3	6.8
RPL13A	-0.5895721	-0.03269853	0.6305919	3	13.3
H2AFY	-3.304149	-2.81624	0.6300327	9	39.5
DHX9	-3.413069	-2.850793	0.6277002	24	26.5
HNRNPA2B1	-4.03122	-3.728354	0.620211	14	50.4
PTBP1	-3.133021	-2.599637	0.6193661	12	42
RPL7A	-0.765842	-0.1585904	0.6052098	7	26.3
LMNA	-3.676909	-3.026558	0.6001746	18	35.2
RPS16	-0.7118895	-0.225565	0.5984604	4	30.1
HNRNPAB	-3.061661	-2.620601	0.5971259	7	32.9
PLBD2	-0.2662986	-0.08303428	0.5967444	3	5.8
KIAA0020	-3.040972	-2.34161	0.5932103	4	8.3
RPL14	-0.6033802	-0.244839	0.587173	3	26.6
TPM4	-2.262088	-1.523338	0.5744406	9	43.1
SNRPA1	-0.02718976	0.5964581	0.5742468	8	32.9

Supplementary Table 1: MS SILAC Ratio's continued

Gene names	Ratio M/L normalized	Ratio H/L normalized	Ratio H/M normalized	Peptides	Sequence coverage (%)
CSTF1	-2.458148	-1.771766	0.5736653	2	6.5
RCC1	-2.611667	-2.386619	0.5702686	9	36.1
ACTG1	-3.447501	-2.822962	0.5692967	21	70.7
RPSA;	-0.7277378	-0.05790221	0.5558162	1	6.5
HNRNPU	-2.304505	-1.731254	0.5479433	16	27.3
PES1	-3.672359	-2.846947	0.5459684	4	8.8
WDR12	-2.553596	-1.932967	0.5365503	3	10.9
HNRNPH1	-2.93115	-2.324094	0.5318679	8	28.5
NUP50	-2.331627	-1.595489	0.5285713	2	6.2
HDAC2	-1.940589	-1.331118	0.5245653	3	8.4
RPL10A	-0.552389	0.06073913	0.5222567	6	33.2
HNRNPR;	-3.679883	-3.069876	0.51924	18	31
ILF2	-3.05122	-2.561835	0.5189379	10	34.4
NOP16	-2.081553	-1.446698	0.5185351	3	27
AP2M1	-1.383642	-1.047517	0.5184344	5	17.7
HNRNPA1;	-3.594156	-2.938652	0.5130864	17	52.8
RPL4	-0.8059381	-0.2853544	0.5080228	14	36.1
RPL27	-0.5771642	-0.1849329	0.506805	5	41.9
RPL13	-0.7359561	-0.1770333	0.5067034	5	24.2
S100A2	-0.4590007	0.1489992	0.503654	1	17.9
SPTAN1	-2.331699	-1.870545	0.5029415	11	7.3
MYO1C	-2.779323	-2.107741	0.5003942	16	19.2

Supplementary Table 1: MS SILAC Ratio's continued

Gene names	Ratio M/L normalized	Ratio H/L normalized	Ratio H/M normalized	Peptides	Sequence coverage (%)
MYBBP1A	-2.077163	-1.614403	0.4998842	6	7.1
RPL18	-0.8865662	-0.3179661	0.498353	3	22.6
SAFB	-3.428162	-2.797263	0.4968203	8	14.3
FBL	-3.211699	-3.46234	0.4963089	8	30.8
HNRNPM	-3.006942	-2.431209	0.4918019	15	28.6
RPL27A	-0.7470032	-0.2211858	0.4882064	4	42.6
HIST1H2A variants	-4.293925	-3.525463	0.4873835	6	35.9
TPR	-2.072179	-1.683576	0.485736	6	3
PPP2R1A	0.03689012	0.4882064	0.4817122	4	11.9
HNRNPK	-2.910393	-2.374	0.4803685	12	44.5
CHD4	-2.278024	-1.793307	0.4766409	11	10
RPL36	-0.7881655	-0.2628324	0.4720718	3	21.9
HADHB	-1.239702	-0.9098782	0.4673838	8	33.5
RPS26	-0.5186598	-0.05812744	0.4642501	2	23.5
ACTB	-3.020575	-2.45419	0.4635179	21	70.7
SFPQ	-3.222027	-3.410551	0.4616333	16	26.3
RPL6	-0.5810868	-0.1512339	0.4598512	7	33.7
RPL30	-0.4255206	-0.01791363	0.458067	4	51.8
DSP	-3.16592	-1.857626	0.455439	22	10.7
REV3L	-0.2832812	1.877116	0.4518573	15	6.9

5

Chapter 5

Overexpression of HSF2BP, a new BRCA2 interactor, results in a Fanconi anemia-like phenotype

Inger Brandsma, Hanny Odijk, Anneke Oostra, Dick Dekkers, Karel Bezstarosti, Nathalie van den Tempel, Jeroen Demmers, Josephine Dorsman, Dik van Gent, Roland Kanaar, Alex Zelensky

Abstract

We identified Heat Shock Factor 2 Binding Protein (HSF2BP) as a novel protein directly interacting with the BRCA2 tumor suppressor. Overexpression, but not genetic deletion of HSF2BP, results in hypersensitivity to the interstrand DNA crosslinker mitomycin C (MMC) and increased MMC-induced chromosomal instability. This phenotype is similar to that of Fanconi anemia (FA) patient cells. HSF2BP, thus, represents an example where overexpression of a wild-type protein is associated with an FA-like phenotype. HSF2BP overexpression does not lead to homologous recombination deficiency as measured by functional assays but increases the kinetics of clearance of RAD51 foci induced by ionizing radiation. FANCD2 ubiquitylation is not affected, indicating that the repair of interstrand crosslinks is disrupted at a downstream step. In conclusion, we demonstrate for the first time that ectopic expression of a wild-type protein, HSF2BP, can cause hypersensitivity to an interstrand DNA-crosslinker.

Introduction

Breast cancer type 2 susceptibility protein (BRCA2) is essential for the repair of DNA double strand breaks via homologous recombination (HR) and thereby maintenance of genomic stability^{1,2}. BRCA2 binds RAD51 and promotes the assembly of RAD51 onto single-stranded DNA (ssDNA)³⁻⁵, a critical obligatory intermediate in HR. Heterozygous mutations in *BRCA2* predispose to breast and ovarian cancer, while certain hypomorphic homozygous mutations cause Fanconi anemia (FA), explaining the genetic defect in complementation group D1⁶.

FA is a rare genetic disease characterized by congenital skeletal and renal anomalies, growth retardation, haematological abnormalities, bone marrow failure and predisposition to leukaemia and a variety of other cancers^{7,8}. The FA pathway is required

for repair of interstrand DNA crosslinks (ICLs) and cells from FA patients are hypersensitive to interstrand crosslinking agents such as mitomycin C (MMC). Classically, FA was diagnosed by exposing patient cells to these agents, which results in increased levels of chromosomal aberrations compared to cells from a healthy control⁹, due to the defect in ICL repair.

When a replication fork encounters an ICL, replication stalls and FANCM is recruited together with FAAP24 and MHF1/2. This triggers accumulation of the FA core complex, consisting of FANCA, B, C, E, F, G, L, M, FAAP20, FAAP24 and MHF1/2. Assembly of this complex is required for monoubiquitination of FANCD2 and FANCI by FANCL and Ube2T^{10,11}, a critical and highly conserved step in ICL repair. Ubiquitinated FANCD2 acts as a recruitment platform for nucleases involved in ICL excision¹². Incision on both sides of the ICL results in unhooking of the lesion, which can then be bypassed by translesion synthesis, which restores one of the broken DNA strands. Because the remaining broken DNA strand was part of a replication fork, the break can be repaired via HR. Resection of the break and RAD51 nucleoprotein filament formation appears to be independent of the FA core complex^{13,14}. The remaining unhooked ICL is no longer an obstacle for replication and can be removed by nucleotide excision repair. Both HR and the FA pathway are required for ICL repair and mutations in several HR proteins give an FA phenotype. For example FANCI is BRIP1/BACH1^{15,16}, FANCO is RAD51C^{17,18} and BRCA2 is also known as FANCD1⁶.

Here we describe HSF2BP as a novel interactor of BRCA2. HSF2BP is expressed in human cancer cell lines and overexpression results in a phenotype that is similar to FA patient cells: hypersensitivity to DNA crosslinking agents and increased numbers of chromosomal aberrations after exposure to MMC. Because the reported FANCD2-BRCA2 interaction domain partially overlaps with the BRCA2-HSF2BP interaction domain, we hypothesize that the MMC hypersensitivity

of cells overexpressing HSF2BP is due to the disturbance of the interaction between BRCA2 and FANCD2.

Results

HSF2BP interacts with BRCA2

HSF2BP was identified as a novel BRCA2 interactor using semi-quantitative SILAC (stable isotope labeling by amino acids in cell culture) mass spectrometry (Fig 1A). BRCA2 was immunoprecipitated from BRCA2-GFP genomic knock-in mouse embryonic stem (ES) cells¹⁹. The abundance of HSF2BP in BRCA2-GFP immunoprecipitates correlated with the abundance of the BRCA2-GFP protein itself. As an example, changes in the abundance of proteins pulled down by anti-GFP beads from *Brca2*^{GFP/GFP} ES cells after 60 minutes of mild hyperthermia treatment are shown in Fig 1A, which was measured in two independent label-swap experiments (log₂ SILAC ratio). Hyperthermia treatment leads to BRCA2 protein degradation²⁰, so its abundance in the immunoprecipitate from the hyperthermia-treated cells decreases (2.9x-4.4x). Similar changes in SILAC ratios were observed for HSF2BP and for proteins that bind to the beads via BRCA2-GFP, such as the known BRCA2 interactors RAD51, PALB2 and MORF4L1.

HSF2BP-GFP knock-in ES cells (*Hsf2BP*^{wt/GFP}) were created by fusing GFP to the 3' end of one HSF2BP allele using a gene targeting approach. These cells were used to verify the interaction between BRCA2 and HSF2BP. BRCA2 and several of its interaction partners, such as RAD51 and PALB2, were efficiently immunoprecipitated via HSF2BP-GFP as analyzed by mass spectrometry (Fig 1B). RAD51-associated protein 1 (RAD51AP1)-GFP knock-in cells (*Rad51ap1*^{GFP/GFP}) were generated and used as a control, because RAD51AP1 is a nuclear protein with low expression, comparable to HSF2BP.

To verify the BRCA2-HSF2BP interaction in human cells, HEK293T cells were transfected with MBP-BRCA2 and GFP-HSF2BP expression plasmids and an immunoprecipitation (IP)

was performed on GFP-HSF2BP using anti-GFP beads (Fig 1C). MBP-BRCA2 interacted with both mouse and human HSF2BP, but not with GFP.

HSF2BP is expressed in human cell lines and mouse tissue

HSF2BP has originally been described as a testis-specific protein²¹. However, we identified HSF2BP in BRCA2 IPs from mouse ES cells. To test whether HSF2BP is expressed in human cell lines as well, RT-PCR reactions were performed from several commonly used human cancer cell lines from different origins (HeLa – cervical carcinoma, U2OS – osteosarcoma, BLM – melanoma, MCF10A – mammary epithelium) with primer combinations amplifying the HSF2BP coding sequence. Amplification with primers targeting the 5' or 3' halves of the HSF2BP cDNAs resulted in a single PCR fragment for the 5' part (Fig 1D) and several bands for the 3' end (Fig S1C), for most cell lines tested. This suggests that several forms of HSF2BP mRNA are constitutively produced in human cells, and might encode proteins that differ in the C-terminal part. Amplification of HSF2BP with the primer combination spanning the complete CDS resulted in multiple bands close to the predicted size of 1002bp (Fig S1B), which could indicate alternative splicing. Cloning and sequencing of the products allowed us to identify several shorter splice forms of HSF2BP. Supplementary figure S1A shows the exon model of the reference human HSF2BP cDNA sequence and identified splice forms.

Expression of mouse HSF2BP in several mouse tissues was detectable by western blot using the antibody we raised against full-length mouse HSF2BP. As expected, a band matching the size of full-length HSF2BP was detected in testis. Importantly, bands of the same size were detected in the samples from kidney and heart and the band was not visible in our *Hsf2BP* knock-out ES cells (Fig 1E). A strong band running higher than mouse HSF2BP is also detectable in testis, however at this moment we cannot

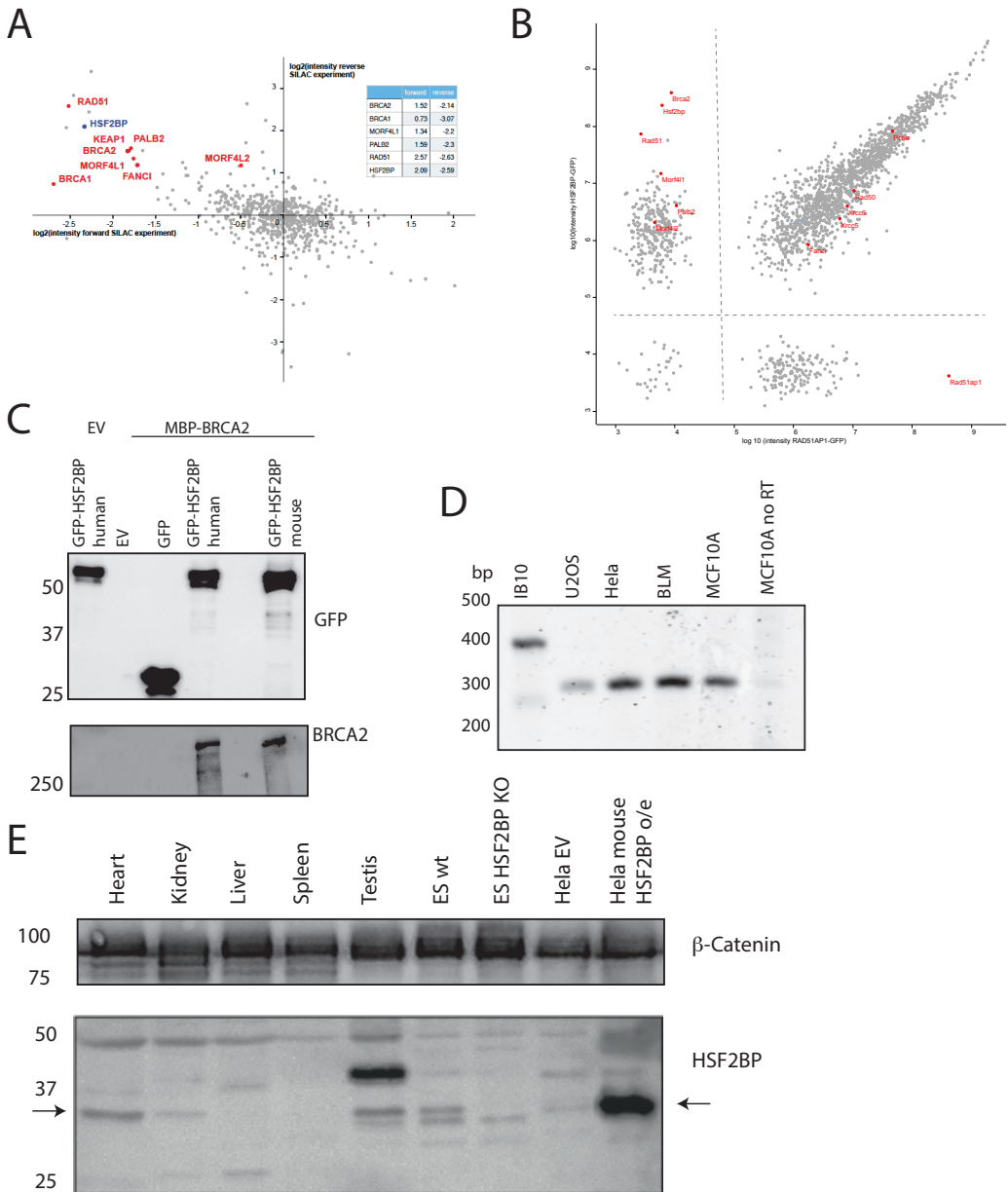


Figure 1 HSF2BP interacts with BRCA2 and its expression is not testis specific

(A) The abundance of HSF2BP correlated with the abundance of the BRCA2-GFP in BRCA2-GFP immunoprecipitates in multiple quantitative mass-spectrometry experiments. Changes in the abundance of proteins pulled down by anti-GFP beads from *Brca2^{GFP/GFP}* mES cells after 60 minutes of mild hyperthermia treatment is plotted, measured in two independent label-swap SILAC experiments (log₂ SILAC ratio). (B) The abundance of proteins precipitated with anti-GFP beads from HSF2BP-GFP or RAD51AP1-GFP knock-in mES cell lines. For visualization purposes the missing intensity values for proteins present in only one pull-down were imputed from a normal distribution with a downsift of 3 (i.e. below and left of the dashed line are proteins that were only identified in one pull-down experiment. For the purpose of visualization, a value was given automatically). Legend continued on next page.

discriminate whether it is a larger splice form of HSF2BP or another testis-specific protein that is detected by the antibody. Neither

endogenous nor overexpressed human HSF2BP was detected with the antibody raised against the mouse protein (Fig S2A).

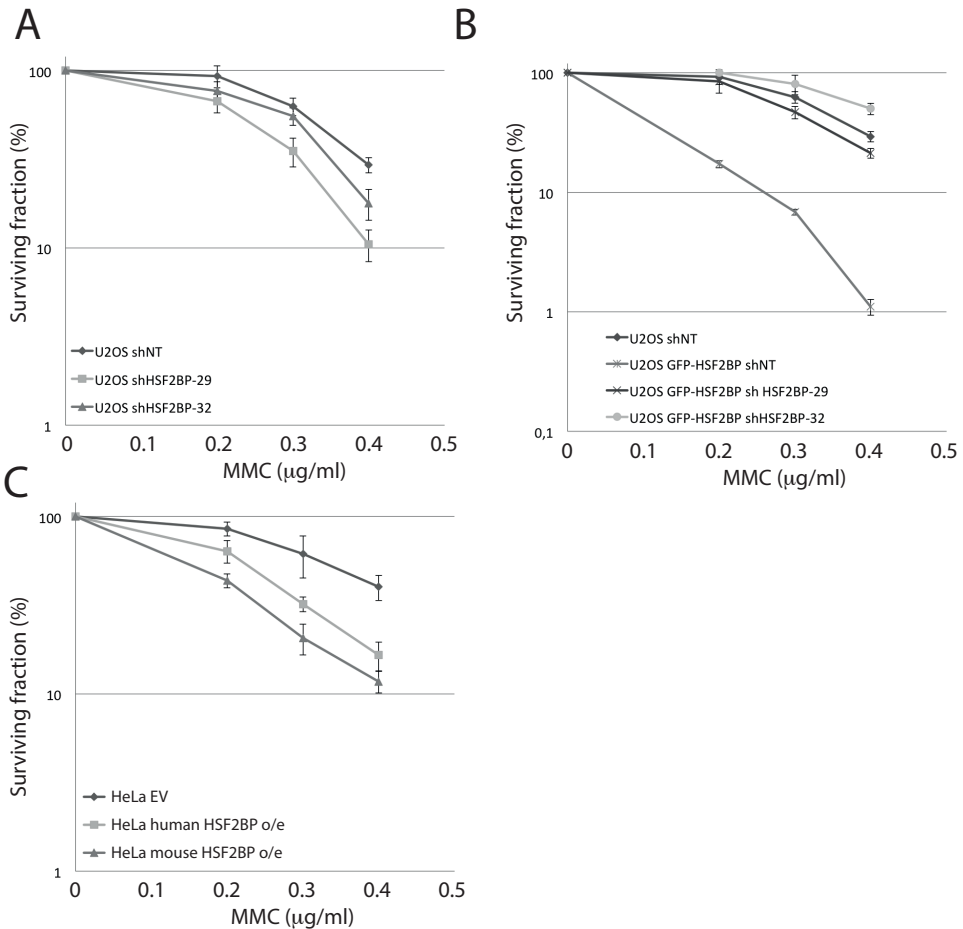


Figure 2 HSF2BP overexpression sensitizes to MMC

(A) Clonogenic survival using U2OS stably transfected with non-targeting shRNA or shRNA targeting HSF2BP treated with increasing doses of MMC. Data represents mean \pm SD. (B) Clonogenic survival using GFP-HSF2BP expressing U2OS cells stably expressing non-targeting shRNA or shRNA targeting HSF2BP (shHSF2BP-29 and-32) treated with increasing doses of MMC. Data represents mean \pm SD. (C) Clonogenic survival using HeLa cells overexpressing (o/e) an empty vector or untagged mouse or human HSF2BP with increasing doses of MMC. Data represents mean \pm SD.

Figure 1 continued

Proteins used in the pull-down and known BRCA2 interactors are indicated. (C) GFP-IP of transiently overexpressed MBP-BRCA2 and GFP constructs. Bound proteins were analysed by immunoblot using MBP and GFP antibodies. EV, empty vector; MBP, maltose binding protein. (D) Isolated total RNA was reverse-transcribed into cDNA and the 5' region of HSF2BP was amplified by PCR, generating a single band for all cell lines tested. A cDNA synthesis reaction without reverse transcriptase was used as negative control. (E) Immunoblot using HSF2BP and β -catenin antibodies showing the expression of HSF2BP in indicated mouse tissues and cell lines. Arrows indicate HSF2BP.

Overexpression of HSF2BP sensitizes cells to MMC damage

Lentivirally-delivered stably expressed shRNAs were used to downregulate HSF2BP in human U2OS cells. Due to the lack of an antibody that could detect the endogenous protein in human cells, knock-down efficiency could not be determined at the protein level. Instead, U2OS cells stably overexpressing GFP-HSF2BP were used to monitor the efficiency of the shRNAs using an anti-GFP antibody. Efficient knock-down of the GFP fusion could be achieved in U2OS cells using two independent shRNAs (Fig S2B). Anti-HSF2BP shRNA expression did not sensitize cells to IR and only marginally to MMC (Fig 2A, S2C). In order to exclude that incomplete knock-down of HSF2BP caused the lack of sensitivity, we inactivated the HSF2BP gene in HeLa cells using CRISPR/Cas9 technology. Again, this did not lead to increased sensitivity to MMC, cisplatin or IR in two clones with complete disruption of the HSF2BP alleles (Fig S3A).

Strikingly, while depletion of HSF2BP did not cause any sensitivity to DNA damage, GFP-HSF2BP overexpression led to a profound sensitization to MMC (Fig 2B). Importantly, counteracting the GFP-HSF2BP overexpression using shRNA reverted the sensitivity close to wild type levels, showing that the phenotype was indeed caused by HSF2BP overexpression. Overexpression of untagged HSF2BP in HeLa cells yielded a similar sensitization (Fig 2C), demonstrating that the phenotype is not caused by the presence of the GFP tag and is not limited to the U2OS cell line. Cells overexpressing untagged HSF2BP also displayed cisplatin sensitivity, although to a lesser extent (Fig S2D). Like cells overexpressing GFP-HSF2BP they were not IR hypersensitive (Fig S2E). In the context of ICL-inducing agents, specific sensitivity to MMC has been observed previously for SNM1²² and HELQ^{23,24} mutant cells, while deficiency in most FA genes results in comparable sensitivity to MMC and cisplatin^{25,26}.

HSF2BP overexpression causes a Fanconi anemia-like phenotype

GFP-HSF2BP localizes predominantly to the cytoplasm (Fig 3A). Although homology searches do not detect strong similarity between HSF2BP and any other known protein sequences, protein fold recognition software²⁷ predicts the presence of armadillo repeats, commonly associated with cytoskeleton interaction and protein trafficking. We therefore investigated whether HSF2BP controls nuclear transport or cytoplasmic retention of BRCA2, similar to its recently described role in transport of its interacting transcription factor basonuclin (BNC1)²⁸. However, biochemical fractionation did not reveal any differences in BRCA2 distribution over cytoplasmic, nuclear and chromatin fractions between HSF2BP-overexpressing and control HeLa cells (Fig 3C) or detectable differences in BRCA2 expression levels (Fig 3B), arguing against this hypothesis.

Acute sensitivity to DNA cross-linking agents is a characteristic of cells deficient in the FA pathway, in which more than 17 proteins have been implicated, including BRCA2 (identified as FANCD1⁶). As FANCD2 mono-ubiquitination is the key event in FA complex activation following cross-link recognition, we compared the efficiency of this protein modification in MMC-treated cells expressing HSF2BP at elevated or endogenous levels (Fig 4A). We did not find a difference in the extent to which FANCD2 was mono-ubiquitinated, suggesting that MMC sensitivity is not caused by disruption of the core FA complex, and is likely to be a direct consequence of BRCA2 dysfunction.

FA cell lines show a characteristic pattern of increased chromosomal aberrations (i.e. increased formation of radials and chromatid breaks) after exposure to DNA crosslinking agents⁷. We therefore exposed HeLa cells overexpressing mouse or human HSF2BP to MMC and prepared metaphase spreads, which were scored for chromosomal aberrations. In untreated cells, HSF2BP overexpression had no effect on the number of chromatid type

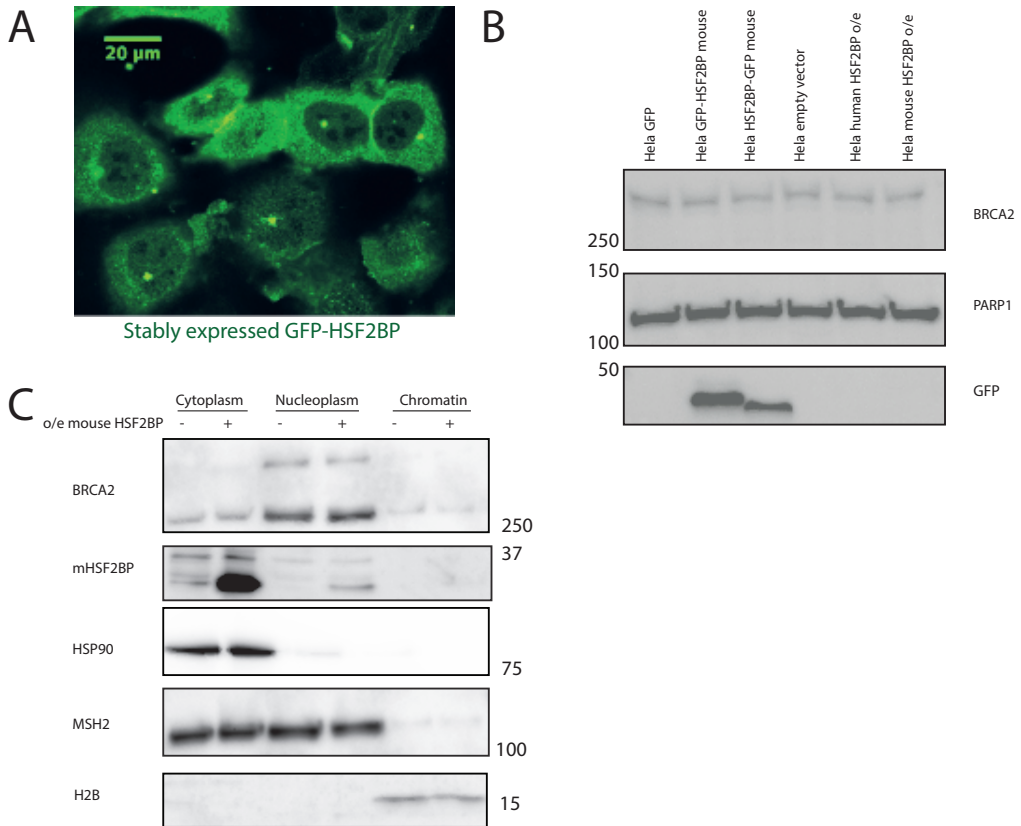


Figure 3 HSF2BP overexpression does not change BRCA2 levels or localization

(A) Ectopically expressed GFP-HSF2BP predominantly localizes to the cytosol in HeLa cells. (B) Immunoblot using antibodies against BRCA2, PARP1 (loading control) and GFP. (C) Fractionation of HeLa cells stably overexpressing mouse HSF2BP or an empty vector. Immunoblot using antibodies against BRCA2, mouse HSF2BP, HSP90, MSH2 and Histone H2B.

breaks per metaphase, but MMC exposure led to an increase in the number of metaphases with 10 or more aberrations from 4% in the controls cells to 32% and 68% in HeLa cells overexpressing human or mouse HSF2BP, respectively (Fig 4B).

HSF2BP overexpression results in a decrease in MMC-induced RAD51 and FANCD2 foci, but no obvious defect in HR

As BRCA2 is required for RAD51 focus formation, a crucial step in HR², HSF2BP overexpression might affect this process. To test whether HSF2BP overexpression had an effect on RAD51 focus formation after crosslinker-induced damage, HeLa cells containing an empty vector or stably

overexpressing mouse or human HSF2BP were treated overnight with a low dose of MMC. Interestingly, HSF2BP overexpression indeed resulted in a reduction of the average number of FANCD2 and RAD51 foci per nucleus (Fig 5A, S4A). This was not due to differences in cell cycle distribution, as all cell lines showed similar cell cycle profiles irrespective of HSF2BP status (Fig S4B).

Subsequently, we investigated whether the decrease in the amount of RAD51 foci correlated with a general reduction in HR capacity. HR efficiency was measured using a U2OS cell line with an integrated gene conversion reporter cassette, where GFP-expression can be activated by HR-mediated repair of a double-strand break generated

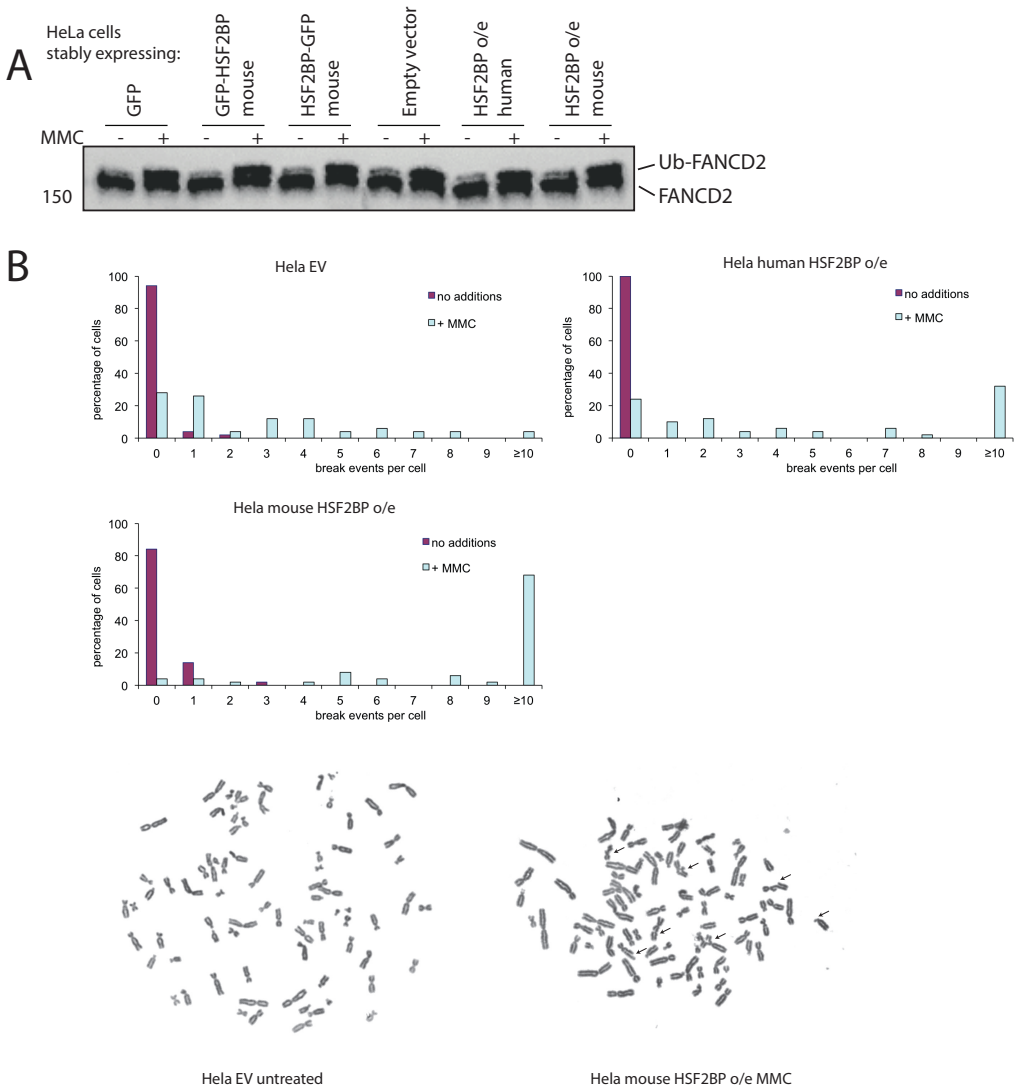


Figure 4 HSF2BP overexpression gives a Fanconi Anemia-like phenotype

(A) HeLa cells stably overexpressing GFP-tagged or untagged HSF2BP were treated overnight with a low dose of MMC (100 nM) and cell extracts were analysed by immunoblot using a FANCD2 antibody. (B) Chromosomal breakage after MMC treatment of HeLa cells expressing an empty vector (EV) or overexpressing mouse or human HSF2BP. Cells were exposed to 50 nM MMC for 48h (blue bars) and compared to untreated cells (purple bars). Percentage of cells with indicated number of chromatid type breaks per cell is shown. 50 metaphases were scored per cell line and treatment. Arrows indicate chromosomal aberrations in example metaphases. o/e, overexpression.

by the I-SceI nuclease²⁹. Overexpression of HSF2BP did not result in HR reduction in this assay (Fig 5B,C). To verify that recombination is reduced in cells in which proteins required for recombination are depleted, the reporter cells were transfected with siRNA targeting

XRCC3. As expected, a reduction in the level of this protein (Fig S5A) resulted in a decrease in the number of GFP-positive cells 5 days after transfection of the double-strand break inducing I-SceI expression construct (Fig S5B).

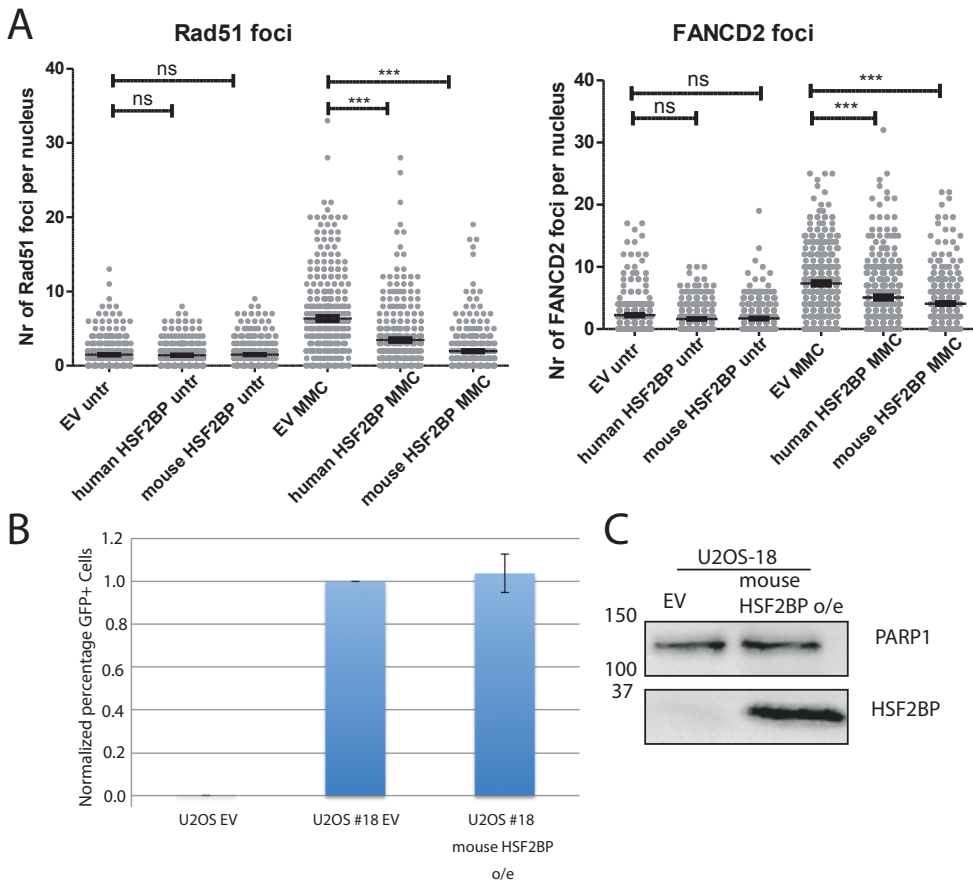


Figure 5 HSF2BP overexpression results in a reduced number of RAD51 and FANCD2 foci per nucleus, but not in a defect in HR mediated repair

(A) The average number of RAD51 and FANCD2 foci per nucleus after MMC treatment (100 nM MMC overnight) in HeLa cells with indicated constructs. Cells were pre-extracted and stained for FANCD2 and RAD51. The number of foci per nucleus is displayed for at least 290 nuclei per condition (from 3 experiments). Line represents average \pm SEM. *** indicates P value < 0.05 as calculated using the Kruskal-Wallis test with Dunn's post test comparing all columns EV, empty vector; ns, not significant. (B) HR function was measured in a U2OS cell line carrying a GFP reporter for gene conversion. Data was normalized to 1 for U2OS #18 empty vector (EV). Bars represent averages of three experiments \pm SD. U2OS EV cells do not contain the HR reporter (C) Immunoblot showing the overexpression of mouse HSF2BP in U2OS #18 cells. o/e, overexpression.

HSF2BP interacts with the C-terminal domain of BRCA2

To map the domain that interacts with HSF2BP, BRCA2 was split into three flag-tagged portions, the N-terminal (B2N, up to Thr939), middle (B2M, Gln940-Glu2198) and the C-terminal (B2C, from Thr2199) part. HeLa cells stably expressing the Flag-tagged BRCA2 versions were transiently transfected with GFP or GFP-HSF2BP expression constructs

and an IP was performed using anti-GFP beads. HSF2BP interacted most effectively with the C-terminal domain of BRCA2 (Fig 6A).

Mass-spectrometry analysis of the proteins co-precipitating with the truncated forms of mouse BRCA2 from ES cells containing GFP-tagged knock-in alleles of BRCA2 revealed that HSF2BP also interacts with BRCA2-GFP lacking the C-terminal DNA binding domain

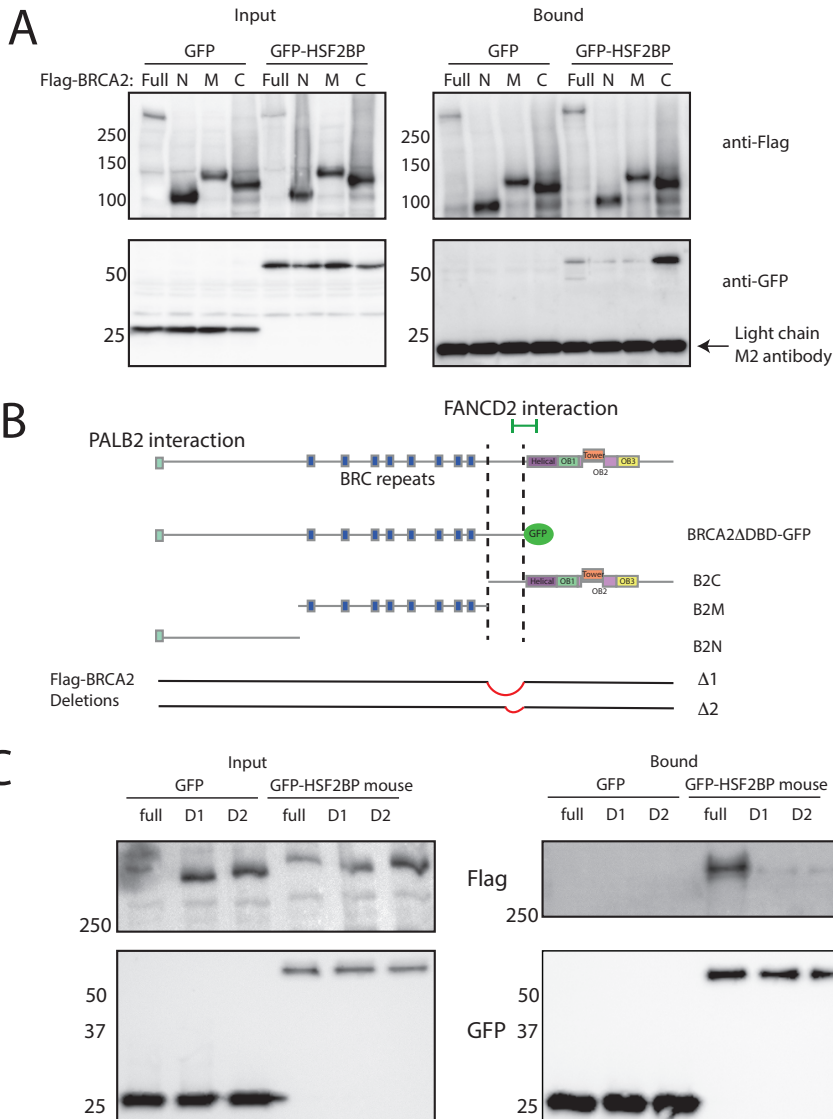


Figure 6 HSF2BP interacts with the C-terminus of BRCA2

(A) Pull-down on Flag-tagged BRCA2 full length or N, M, or C-terminal parts in HeLa cells stably expressing Flag constructs and transiently transfected with GFP or GFP-HSF2BP. Bound proteins were analysed by immunoblot using Flag and GFP antibodies. (B) Schematic overview of BRCA2 and its domains. Area between dashed lines indicates the overlap between HSF2BP-interacting fragments of BRCA2 identified from knock-in studies in mES cells and overexpression of Flag-tagged BRCA2 fragments in HeLa cells. Deleted domains in BRCA2 $\Delta 1$ and $\Delta 2$ constructs shown in red. (C) HeLa cells stably expressing GFP or GFP-HSF2BP were transiently transfected with Flag BRCA2 full length or the BRCA2 $\Delta 1$ and $\Delta 2$ constructs. After an IP using GFP beads, bound proteins were analysed by immunoblot using Flag and GFP antibodies.

(data not shown). The largest deletion (BRCA2- Δ DBD), in which mouse BRCA2 is truncated after Asp2400 (corresponding to Asp2479 in human BRCA2), could still precipitate mouse

HSF2BP. We therefore hypothesized that the HSF2BP-BRCA2 interaction domain is situated between the N-terminal end of the B2C fragment (Thr 2199) and the C-terminus

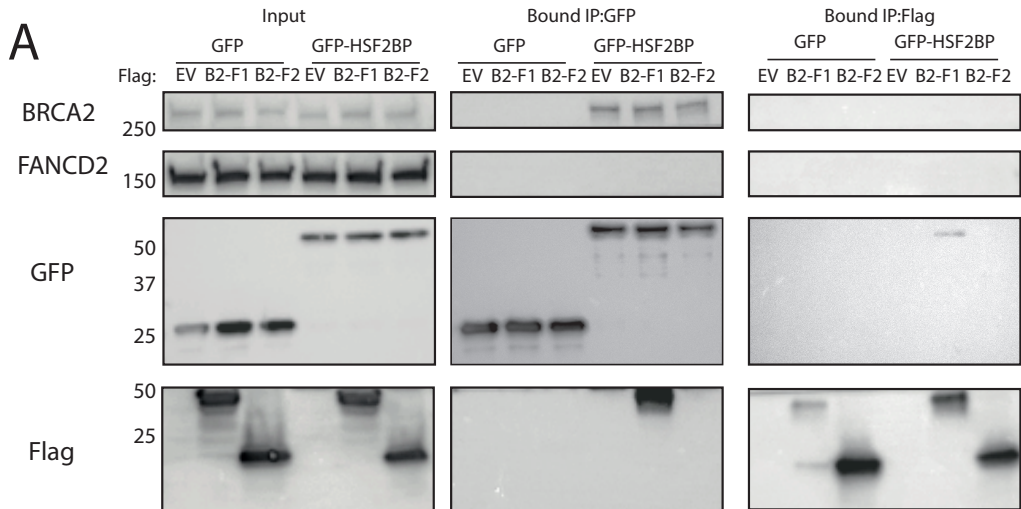


Figure 7 Mapping of the HSF2BP-BRCA2 interacting domain

(A) HeLa cells stably expressing GFP or GFP-HSF2BP were transiently transfected with a Flag empty vector (EV) or the Flag-tagged BRCA2 fragments. After collection of an input sample, the lysate was split in two parts and pull-downs were performed using anti-Flag and anti-GFP beads. Bound fractions were analysed by immunoblot using indicated antibodies.

of the BRCA2- Δ DBD truncation (Asp2479 in human BRCA2). To test our hypothesis, we engineered constructs for the production of Flag-tagged versions of human BRCA2 containing deletions in this region. In the construct Flag-BRCA2 Δ 1 the overlapping region between B2C and BRCA2- Δ DBD is completely deleted and in Flag-BRCA2 Δ 2 only the part of it that overlaps the region previously shown to interact with FANCD2³⁰. Deletion of these regions resulted in a loss of interaction between BRCA2 and HSF2BP (Fig 6C).

Flag-tagged versions of the deleted domain of BRCA2 were also created to verify their interaction with HSF2BP (Table 1, Fig S6B). The proteins were transiently overproduced in HeLa cells stably expressing GFP or GFP-HSF2BP and IPs were performed either on Flag or GFP. The larger BRCA2-F1 fragment interacted with GFP-HSF2BP, but the short BRCA2-F2 fragment did not (Fig 7A).

The putative HSF2BP-BRCA2 interaction domain overlapped the N-terminal part of the BRCA2-FANCD2 interaction domain reported in a previous study³⁰ (Fig 6B). Competition between the overproduced

HSF2BP and the endogenous FANCD2 would provide a straightforward explanation to the FA-like phenotype we observed. However, we were unable to co-immunoprecipitate endogenous FANCD2 and BRCA2 (Fig S6B). In our mass spectrometry experiments, we did not detect FANCD2 in the GFP-BRCA2 pull-downs either, although most, if not all, other previously reported BRCA2 interactors were detected in the precipitate. As an alternative approach to detect an interaction between FANCD2 and BRCA2, we engineered additional constructs to include the complete FANCD2-binding domain of BRCA2: BRCA2-F3 (BRCA2-F1 extended to include the whole of the FANCD2-binding domain); BRCA2-F4 (FANCD2-binding domain alone) and BRCA2-F5. The proteins were transiently overproduced in HeLa cells stably expressing GFP or GFP-HSF2BP and IPs were performed either on Flag or GFP. BRCA2-F3 and -F5 fragments interacted with GFP-HSF2BP (S6A). Also in these IPs we did not detect an interaction between FANCD2 and any of the BRCA2 fragments (Fig S6A).

We also considered the possibility that HSF2BP overexpression disturbs the

interaction between BRCA2 and other proteins required for ICL repair. To test this notion we used an unbiased approach by performing a FLAG IP on HeLa cells transiently expressing Flag-B2-F1 labelled for 3-state SILAC (Schematic shown at the end of table S2). In one state (Light), HSF2BP was overexpressed as a control. Among the proteins that specifically bind to Flag-B2-F1, no FANCD2 proteins were identified (Table 2). The experiment was repeated using the BRCA2-F3, but also in this experiment no FANCD2 was detected. Among the proteins that specifically interacted with the Flag-tagged BRCA2 domains, apart from HSF2BP, we identified GAPDH and several histones including variants of H2A, H2B, H3 and H4, but not H1.

Changes in the kinetics of RAD51 focus formation

As we did not find any connections with proteins directly involved in the repair of ICLs, we reconsidered the possibility that HSF2BP overexpression affected HR in a delicate manner via BRCA2, resulting in subtle changes in HR rather than a complete HR defect. Upon DNA damage induced by MMC or IR, HeLa cells overexpressing HSF2BP form RAD51 foci, but the percentage of cells with more than 10 RAD51 foci per nucleus is lower than in control cells (Fig 8A). To look at the kinetics of RAD51 focus formation, we used IR as damaging agent and quantified the number of S-phase cells with more than 10 RAD51 foci at different time points (Fig 8B). S-phase cells were labelled with EdU for 2 hours directly before fixation. HSF2BP overexpression did not significantly affect the fraction of cells scored as RAD51 focus positive (>10 foci per S-phase cell) at the first time point tested (2 hours after irradiation), but resulted in a reduction in this fraction at the later time points (4 and 8 hours). Also 24 hours after IR, HSF2BP overexpressing cells show fewer nuclei with more than 10 RAD51 foci (Fig 8C). For this time point all cells with more than 10 RAD51 foci were quantified, since EdU staining 24 hours after damage

does not correlate with the cell cycle phase at the time of damage. These data suggest that HSF2BP overexpression results in a faster RAD51 focus clearance.

Discussion

Here we identified HSF2BP as a new BRCA2-interacting protein. Most proteins reported to interact with BRCA2, such as RAD51 and PALB2 have a clear role in HR. However, for several other interactors, for example BRAF35³¹ and USP11³², their function or why they interact with BRCA2 is less clear. The interaction between BRCA2 and HSF2BP could be important for functions in HR as well as other pathways, since overexpression of HSF2BP results in a decrease in RAD51 foci after MMC and IR damage, but not in an overt recombination defect.

HSF2BP overexpression results in MMC hypersensitivity and an increased number of chromatid breaks, reminiscent of a defect in the FA pathway. An essential step in this pathway is the ubiquitination of FANCD2 by the core complex. However, this reaction was not affected by HSF2BP overexpression, suggesting that MMC sensitivity is not caused by disruption of the core FA complex, and is likely to be a direct consequence of BRCA2 dysfunction. This is consistent with previous reports showing that BRCA2 involvement is downstream of FANCD2 mono-ubiquitination^{33,34}.

HSF2BP interacts with BRCA2 in a region that partially overlaps with the reported FANCD2 interacting region of BRCA2³⁰. The most straightforward explanation for the observed phenotype (i.e. hypersensitivity to MMC and increased chromosomal aberrations after MMC exposure) is that overexpression of HSF2BP disturbs the interaction between BRCA2 and FANCD2. However, in our experiments we did not detect an interaction between endogenous FANCD2 and BRCA2 or flag-tagged BRCA2 fragments and we could not test this hypothesis directly.

An alternative model to explain the data is that HSF2BP disturbs a BRCA2-

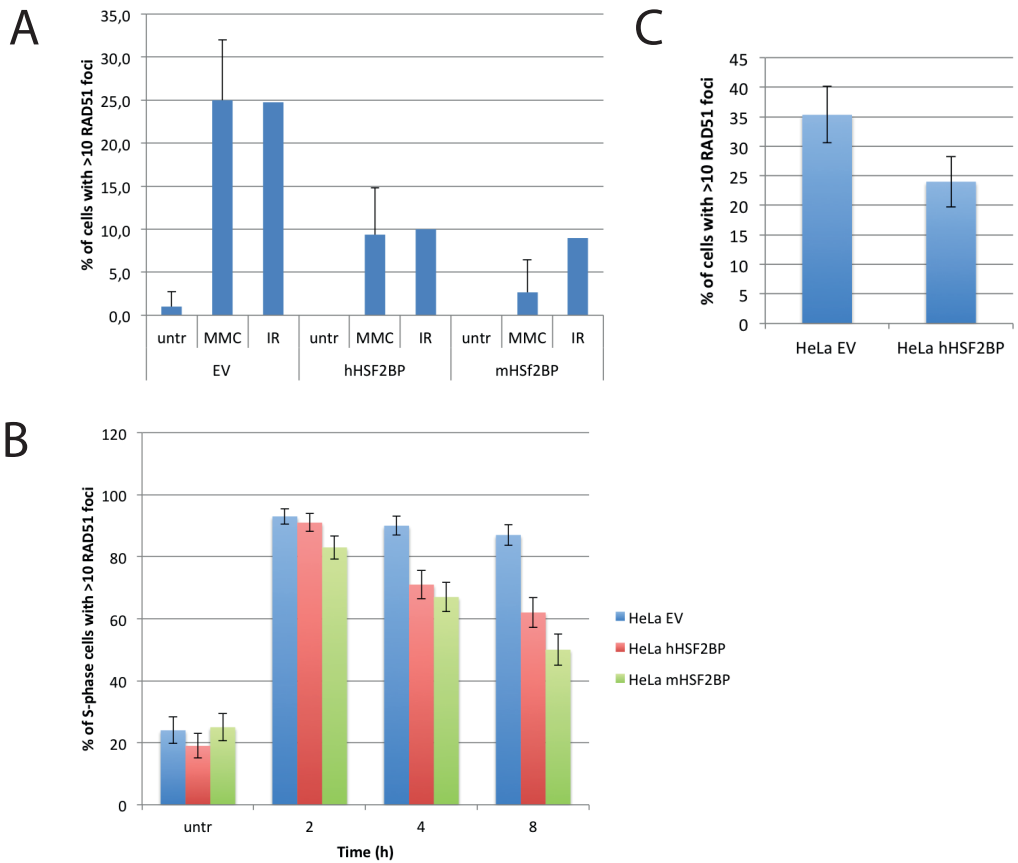


Figure 8 Mapping of the HSF2BP-BRCA2 interacting domain

(A) HeLa cells stably transfected with an empty vector, mouse or human HSF2BP expression constructs were irradiated with 5 Gy and fixed after 4 h or treated overnight with 100 nM MMC and fixed. After fixation cells were stained for RAD51 foci and the number of cells with more than 10 RAD51 foci was quantified. Bars represent mean of 3 experiments \pm SEM. (B) HeLa cells stably transfected with an empty vector, mouse or human HSF2BP expression constructs were irradiated with 5 Gy, pre-extracted and fixed at indicated time points. 2 h before fixation, EdU was added to label S-phase cells. Cells were stained for EdU and RAD51 foci and the number of S-phase cells with more than 10 RAD51 foci was quantified. Bars represent mean \pm SEM. (C) HeLa cells stably transfected with an empty vector or a human HSF2BP expression construct were irradiated with 5Gy, pre-extracted and fixed 24 hours later. Cells were stained for RAD51 foci and the number of cells with more than 10 RAD51 foci was quantified. Bars represent mean \pm SEM.

interaction partner other than FANCD2 that interacts with BRCA2 in the same region. In mass spectrometry experiments, we identified several proteins that specifically interact with the BRCA2-F1 and BRCA2-F3 constructs. One of the strongest candidates is GAPDH (Glyceraldehyde-3-phosphate dehydrogenase). Although it is best known as a metabolic enzyme involved in

glycolysis³⁵, several other functions have been demonstrated for GAPDH, including regulated localisation to the nucleus, and involvement in telomere elongation and base excision repair³⁶⁻³⁹. GAPDH is an abundant protein, and was detected in all mass-spectrometry experiments we performed, including in the negative control IPs. The quantitative proteomics experiments with

BRCA2 fragments provides the first indication that what appeared as a non-specific contaminant may in fact be interacting with BRCA2 in the region to which we mapped HSF2BP binding. The Flag-BRCA2 domains also interact with histones and this interaction is most likely via other chromatin binding proteins since these domains lie outside the BRCA2 DNA binding domain.

Cells overexpressing HSF2BP do not show a defect in an HR assay for intra chromatid gene conversion and although there seem to be fewer RAD51 foci present 2h after IR and after MMC, this defect is not of the same magnitude as for example the defect observed in BRCA1- or BRCA2-deficient cells. However, after IR, the number of nuclei with more than 10 RAD51 foci is decreased and their number also decreases more rapidly in HeLa cells overexpressing HSF2BP. This reduction could be due to the stimulation of HR by HSF2BP or the interference of HSF2BP with the function of proteins that are required for stable accumulation of RAD51 at sites of damage, such as BRCA2⁴⁰. Another possibility is that HSF2BP is involved in the disassembly of protein accumulations at sites of damage and that due to the overexpression of HSF2BP the disassembly takes place faster. Based on the current data, we cannot distinguish between reduced stability or increased disassembly of RAD51 foci.

In several aspects, HSF2BP overexpression causes a FA-like phenotype. However, all FA subtypes described to date are caused by (homozygous) mutations and patients are usually screened by sequencing genomic DNA. In most cases, the mutation needs to be biallelic to cause FA²⁶. Recently two dominant negative RAD51 mutations were identified in FA-like patients^{41,42}. Expression of one of these mutants (T131P) results in a defect in ICL repair, but seems to affect HR to a lesser extent⁴¹. Additionally, it has been shown that overexpression of a FANCC mutant allele causes MMC hypersensitivity⁴³.

HSF2BP knock-out in HeLa cells does not result in increased sensitivity to DNA damaging agents, but overexpression clearly

does. HSF2BP overexpression might therefore serve as a marker for MMC-sensitive tumours. In the GENT (Gene Expression across Normal and Tumour tissue) database⁴⁴, we found that high expression of HSF2BP can occur in several tumour types compared to normal tissue (Fig S7). Thus mechanisms exist that can cause increased expression of HSF2BP.

Overexpression of testis-specific genes in cancer has been observed previously⁴⁵. Due to the misregulation of expression, these cancer/testis (CT) antigens are expressed in a subset of tumours of different types. HSF2BP expression was reported to be testis-specific and on western blot we see the highest expression in testis. HSF2BP mRNA is also detectable in several human cancer cell lines and high expression occurs in cancers. The question remains whether the ectopic expression of these genes is a cause or a consequence of tumorigenesis.

To the best of our knowledge, HSF2BP is the first example where overexpression of a wild-type protein gives a FA-like phenotype. Currently it is still unknown whether there are any cases of HSF2BP overexpression among patients with an unclassified FA subtype. Standard methods such as sequencing of genomic DNA are not suitable to find overexpression of HSF2BP. RNA sequencing or microarray analysis need to be included in the mechanistic analysis of the unassigned FA cases to account for the new paradigm in the FA molecular etiology brought up by our findings on HSF2BP.

References

1. Moynahan, M. E., Pierce, A. J. & Jasin, M. BRCA2 is required for homology-directed repair of chromosomal breaks. *Mol. Cell* 7, 263–272 (2001).
2. Tutt, A. et al. Mutation in Brca2 stimulates error-prone homology-directed repair of DNA double-strand breaks occurring between repeated sequences. *EMBO J.* 20, 4704–4716 (2001).
3. Liu, J., Doty, T., Gibson, B. & Heyer, W.-D. Human BRCA2 protein promotes RAD51 filament formation on RPA-covered single-stranded DNA. *Nat. Struct. Mol. Biol.* 17, 1260–1262 (2010).
4. Thorslund, T. et al. The breast cancer tumor suppressor BRCA2 promotes the specific targeting of RAD51

- to single-stranded DNA. *Nat. Struct. Mol. Biol.* 17, 1263–1265 (2010).
5. Jensen, R. B., Carreira, A. & Kowalczykowski, S. C. Purified human BRCA2 stimulates RAD51-mediated recombination. *Nature* 467, 678–683 (2010).
 6. Howlett, N. G. et al. Biallelic inactivation of BRCA2 in Fanconi anemia. *Science* 297, 606–609 (2002).
 7. Kee, Y. & D'Andrea, A. D. Molecular pathogenesis and clinical management of Fanconi anemia. *J. Clin. Invest.* 122, 3799–806 (2012).
 8. Clauson, C., Scharer, O. D. & Niedernhofer, L. Advances in understanding the complex mechanisms of DNA interstrand cross-link repair. *Cold Spring Harb Perspect Biol* 5, a012732 (2013).
 9. Auerbach, A. D. & Wolman, S. R. Carcinogen-induced chromosome breakage in Fanconi's anemia heterozygous cells. *Nature* 271, 69–71 (1978).
 10. Machida, Y. J. et al. UBE2T Is the E2 in the Fanconi Anemia Pathway and Undergoes Negative Autoregulation. *Mol. Cell* 23, 589–596 (2006).
 11. Smogorzewska, A. et al. Identification of the FANCI Protein, a Monoubiquitinated FANCD2 Paralog Required for DNA Repair. *Cell* 129, 289–301 (2007).
 12. Kim, H. & D'Andrea, A. D. Regulation of DNA cross-link repair by the Fanconi anemia/BRCA pathway. *Genes and Development* 26, 1393–1408 (2012).
 13. Kitao, H. et al. Functional interplay between BRCA2/FancD1 and FancC in DNA repair. *J. Biol. Chem.* 281, 21312–21320 (2006).
 14. Long, D. T., Räschele, M., Joukov, V. & Walter, J. C. Mechanism of RAD51-dependent DNA interstrand cross-link repair. *Science* 333, 84–87 (2011).
 15. Levitus, M. et al. The DNA helicase BRIP1 is defective in Fanconi anemia complementation group J. *Nat. Genet.* 37, 934–935 (2005).
 16. Litman, R. et al. BACH1 is critical for homologous recombination and appears to be the Fanconi anemia gene product FANCI. *Cancer Cell* 8, 255–265 (2005).
 17. Meindl, A. et al. Germline mutations in breast and ovarian cancer pedigrees establish RAD51C as a human cancer susceptibility gene. *Nat. Genet.* 42, 410–414 (2010).
 18. Vaz, F. et al. Mutation of the RAD51C gene in a Fanconi anemia-like disorder. *Nature genetics* 42, 406–409 (2010).
 19. Reuter, M. et al. BRCA2 diffuses as oligomeric clusters with RAD51 and changes mobility after DNA damage in live cells. *J. Cell Biol.* 207, 599–613 (2014).
 20. Krawczyk, P. M. et al. Mild hyperthermia inhibits homologous recombination, induces BRCA2 degradation, and sensitizes cancer cells to poly (ADP-ribose) polymerase-1 inhibition. *Proc. Natl. Acad. Sci. U. S. A.* 108, 9851–9856 (2011).
 21. Yoshima, T., Yura, T. & Yanagi, H. Novel testis-specific protein that interacts with heat shock factor 2. *Gene* 214, 139–146 (1998).
 22. Dronkert, M. L. et al. Disruption of mouse SNM1 causes increased sensitivity to the DNA interstrand cross-linking agent mitomycin C. *Mol. Cell. Biol.* 20, 4553–4561 (2000).
 23. Adelman, C. A. et al. HELQ promotes RAD51 paralog-dependent repair to avert germ cell loss and tumorigenesis. *Nature* 502, 381–4 (2013).
 24. Takata, K., Reh, S., Tomida, J., Person, M. D. & Wood, R. D. Human DNA helicase HELQ participates in DNA interstrand crosslink tolerance with ATR and RAD51 paralogs. *Nat. Commun.* 4, 2338 (2013).
 25. Kratz, K. et al. Deficiency of FANCD2-Associated Nuclease KIAA1018/FAN1 Sensitizes Cells to Interstrand Crosslinking Agents. *Cell* 142, 77–88 (2010).
 26. de Winter, J. P. & Joenje, H. The genetic and molecular basis of Fanconi anemia. *Mutat. Res.* 668, 11–19 (2009).
 27. Kelley, L. A., Mezulis, S., Yates, C. M., Wass, M. N. & Sternberg, M. J. The Phyre2 web portal for protein modeling, prediction and analysis. *Nat. Protoc.* 10, 845–58 (2015).
 28. Wu, Y. et al. HSF2BP represses BNC1 transcriptional activity by sequestering BNC1 to the cytoplasm. *FEBS Lett.* 587, 2099–2104 (2013).
 29. Puget, N., Knowlton, M. & Scully, R. Molecular analysis of sister chromatid recombination in mammalian cells. *DNA Repair (Amst.)* 4, 149–161 (2005).
 30. Hussain, S. et al. Direct interaction of FANCD2 with BRCA2 in DNA damage response pathways. *Hum. Mol. Genet.* 13, 1241–1248 (2004).
 31. Marmorstein, L. Y. et al. A human BRCA2 complex containing a structural DNA binding component influences cell cycle progression. *Cell* 104, 247–257 (2001).
 32. Schoenfeld, A. R., Apgar, S., Dolios, G., Wang, R. & Aaronson, S. A. BRCA2 is ubiquitinated in vivo and interacts with USP11, a deubiquitinating enzyme that exhibits prosurvival function in the cellular response to DNA damage. *Mol. Cell. Biol.* 24, 7444–7455 (2004).
 33. Bruun, D. et al. siRNA depletion of BRCA1, but not BRCA2, causes increased genome instability in Fanconi anemia cells. *DNA Repair (Amst.)* 2, 1007–1013 (2003).
 34. Wang, X., Andreassen, P. R. & Andrea, A. D. D. Functional Interaction of Monoubiquitinated Functional Interaction of Monoubiquitinated FANCD2 and BRCA2 / FANCD1 in Chromatin. *Mol Cell Biol* 24, 5850–62 (2004).
 35. Ercolani, L., Florence, B., Denaro, M. & Alexander, M. Isolation and complete sequence of a functional human glyceraldehyde-3-phosphate dehydrogenase gene. *J. Biol. Chem.* 263, 15335–15341 (1988).
 36. Azam, S. et al. Human glyceraldehyde-3-phosphate dehydrogenase plays a direct role in reactivating oxidized forms of the DNA repair enzyme APE1. *J. Biol. Chem.* 283, 30632–30641 (2008).
 37. Sundararaj, K. P. et al. Rapid Shortening of Telomere Length in Response to Ceramide Involves the Inhibition of Telomere Binding Activity of Nuclear Glyceraldehyde-3-phosphate Dehydrogenase. *J. Biol. Chem.* 279, 6152–6162 (2004).
 38. Demarse, N. et al. Direct binding of glyceraldehyde 3-phosphate dehydrogenase to telomeric DNA protects telomeres against chemotherapy-induced rapid degradation. *J. Mol. Biol.* 394, 789–803 (2009).
 39. Phadke, M. S., Krynetskaia, N. F., Mishra, A. K. & Kry-

- netskiy, E. Glyceraldehyde 3-phosphate dehydrogenase depletion induces cell cycle arrest and resistance to antimetabolites in human carcinoma cell lines. *J. Pharmacol. Exp. Ther.* 331, 77–86 (2009).
40. Tarsounas, M., Davies, A. A. & West, S. C. RAD51 localization and activation following DNA damage. *Philos. Trans. R. Soc. Lond. B. Biol. Sci.* 359, 87–93 (2004).
 41. Wang, A. T. et al. A Dominant Mutation in Human RAD51 Reveals Its Function in DNA Interstrand Crosslink Repair Independent of Homologous Recombination. *Mol. Cell* 59, 478–490 (2015).
 42. Ameziane, N. et al. A novel Fanconi anaemia subtype associated with a dominant-negative mutation in RAD51. *Nat. Commun.* 6, 1–11 (2015).
 43. Youssoufian, H., Li, Y., Martin, M. E. & Buchwald, M. Induction of Fanconi anemia cellular phenotype in human 293 cells by overexpression of a mutant FAC allele. *J. Clin. Invest.* 97, 957–962 (1996).
 44. Shin, G. et al. GENT: Gene expression database of normal and tumor tissues. *Cancer Informatics* 10, 149–157 (2011).
 45. Scanlan, M. J., Gure, A. O., Jungbluth, A. A., Old, L. J. & Chen, Y.-T. Cancer/testis antigens: an expanding family of targets for cancer immunotherapy. *Immunol. Rev.* 188, 22–32 (2002).
 46. Testa, G. et al. BAC engineering for the generation of ES cell-targeting constructs and mouse transgenes. *Methods Mol. Biol.* 256, 123–39 (2004).
 47. Adams, D. J. et al. A genome-wide, end-sequenced 129Sv BAC library resource for targeting vector construction. *Genomics* 86, 753–758 (2005).
 48. Fu, J., Teucher, M., Anastassiadis, K., Skarnes, W. & Stewart, a. F. A recombineering pipeline to make conditional targeting constructs. *Methods in Enzymology* 477, (2010).
 49. Mali, P. et al. RNA-guided human genome engineering via Cas9. *Science* 339, 823–6 (2013).
 50. Essers, J. et al. Disruption of mouse RAD54 reduces ionizing radiation resistance and homologous recombination. *Cell* 89, 195–204 (1997).
 51. Tan, T. L. R. et al. Mouse Rad54 affects DNA conformation and DNA-damage-induced Rad51 foci formation. *Curr. Biol.* 9, 325–328 (1999).
 52. Chalkley, G. E. & Verrijzer, C. P. Immuno-Depletion and Purification Strategies to Study Chromatin-Remodeling Factors In Vitro. *Methods Enzymol.* 377, 421–442 (2004).
 53. Rodrigue, A. et al. Interplay between human DNA repair proteins at a unique double-strand break in vivo. *EMBO J.* 25, 222–231 (2006).
 54. Masuda, T., Saito, N., Tomita, M. & Ishihama, Y. Unbiased quantitation of Escherichia coli membrane proteome using phase transfer surfactants. *Mol. Cell. Proteomics* 8, 2770–2777 (2009).
 55. Cox, J. et al. Andromeda: a peptide search engine integrated into the MaxQuant environment. *J. Proteome Res* 10, 1794–1805 (2011).
 56. Cox, J. et al. A practical guide to the MaxQuant computational platform for SILAC-based quantitative proteomics. *Nat. Protoc.* 4, 698–705 (2009).
 57. Modesti, M. et al. RAD51AP1 Is a Structure-Specific

DNA Binding Protein that Stimulates Joint Molecule Formation during RAD51-Mediated Homologous Recombination. *Mol. Cell* 28, 468–481 (2007).

58. Xu, G. et al. REV7 counteracts DNA double-strand break resection and affects PARP inhibition. *Nature* 521, 541–4 (2015).
59. Oostra, A. B., Nieuwint, A. W. M., Joenje, H. & De Winter, J. P. Diagnosis of fanconi anemia: Chromosomal breakage analysis. *Anemia* 2012, (2012).

Materials and methods

Generation mES cell lines

Hsf2bp^{wt/GFP} mES cells containing a knock-in allele were created by gene targeting using the approach we used previously to engineer the BRCA2-GFP knock-in lines¹⁹. The gene targeting construct was engineered by recombineering⁴⁶, starting with the BAC clone bMQ-430H02 from the Sanger 129/Sv library⁴⁷, homology arms were 3.1 and 6.2 kb long, boundaries defined by the retrieval primers HSF2BP-CG-rtrL and HSF2BP-CG-rtrR, and the GFP-2A-neo cassette¹⁹ was inserted after the last codon of the *Hsf2bp* CDS, using the primers HSF2BP-CG-F and HSF2BP-CG-R. After the completion of selection with 200 µg/ml G418 clones were isolated. Correct targeting was confirmed by Southern blotting on HindIII-digested genomic DNA the probe produced by PCR amplification with the primers HSF2BP-pr5-F and HSF2BP-pr5-R. Two out of the 14 screened clones were identified as *Hsf2bp*^{wt/GFP} (#7 and #14). *Rad51ap1*^{GFP/GFP} cells used as a control in the MS experiment were produced by a similar gene targeting procedure and will be described elsewhere.

Hsf2bp^{-/-} mES cells were created using the “knock-out first conditional allele” strategy⁴⁸ that allows converting the locus into two types of null alleles via an intermediate floxed conditional state using one gene targeting and a series of site specific recombination steps. Exon III was chosen as it is at the beginning of the gene and its deletion leads to a frame shift; the targeting construct is referred to Ce3 (conditional exon 3). The efficiency of the first GT step is facilitated by promotorless selection cassette and was ~25%. Eight independent clones that correctly recombined both homology arms were identified using Southern with 3’ and 5’ probes and one clone (#18) was subjected to a set of recombination steps required to excise the selection cassettes and restore G418 sensitivity, target the second allele, and by Cre recombination excise exon III. Splicing between exon II and IV should lead to a frame-shift. HSF2BP elimination was confirmed by Western Blotting.

Generation of HSF2BP knock-out HeLa cells by CRISPR-Cas9-assisted gene targeting

Oligonucleotides containing sequences for HSF2BP-targeting guide RNAs were cloned into the AflIII-digested gRNA expression vector⁴⁹ using Gibson assembly. Two sgRNA expression constructs were generated targeting regions immediately upstream and immediately downstream of exon 2 (the first coding exon) of HSF2BP (recognition sequences CGCGCCGACGCTCAGCGAACGG and

CTGAGGGGAGCGAATGGCGACGG, PAM underlined). The activity of gRNAs was verified by co-transfection with the Cas9 expression vector⁴⁹ into HEK293T, PCR-amplification of the ~200 bp region surrounding the cut site, and mutation detection using Surveyor[®] kit (Transgenomics). Gene targeting constructs used as donors in CRISPR-Cas9-stimulated gene targeting were engineered by recombineering, starting with a BAC (RP11-349I15). For exon 2 a donor construct was created that replaced the ~1 kb region adjacent to the sgRNA-targeted site(s) with the PGK-hygro selection cassette. Sequences of the oligonucleotides used for BAC recombineering and retrieval into the high copy vector are given in Table S1. The sgRNA expression plasmid(s), Cas9 (wt or catalytically inactive) expression plasmid and the HR donor construct were co-transfected into HeLa cells. Selection with hygromycin B (200 µg/ml) was started one day after transfection and maintained for 8-10 days. Colonies were picked and genotyped using PCR to detect the presence of the wild-type HSF2BP allele. Clones in which no wild-type allele was detected were further analyzed for the presence of the HSF2BP transcript by RT-PCR.

Cell culture, clonogenic survivals and transfections

U2OS cells were grown in Dulbecco's modified Eagle's medium (DMEM) and Ham's F10 (1:1), supplemented with 10% (v/v) FCS (Biowest) and penicillin/streptomycin. HeLa cells were grown in DMEM, supplemented with 10% (v/v) FCS and penicillin/streptomycin. Mouse ES cells were cultured in a 1:1 mixture of DMEM (Lonza) and filtered buffalo rat liver (BRL)-conditioned medium, supplemented with 7.5% fetal calf serum (Biowest), 0.1 mM nonessential amino acids (Lonza), 0.1 mM 2-mercaptoethanol (Sigma-Aldrich), 1,000 U/ml leukemia inhibitory factor, 2 mM ultraglutamine (Lonza) and penicillin/streptomycin. Cells were grown on gelatin-coated (Sigma-Aldrich) Petri dishes. All cells were grown at 37°C and 5% CO₂.

Sensitivity to DNA damaging agents was determined by using a clonogenic survival assay as described⁵⁰.

For plasmid DNA transfections HeLa and U2OS cells were electroporated using a GenePulser XCell (Biorad). For the U2OS #18 HR assay, cells were transfected using XtremeGene (Roche). For siRNA transfections Lipofectamine RNAiMAX (Invitrogen) was used. All transfection reagents were used as per the manufacturers instructions. siRNA and shRNA constructs are described in table S3.

shRNA expression constructs were obtained from the Sigma mission library (TRC 1.5). Lentiviral packaging plasmids (pMDLg/pRRE, pRSV-REV and pMD2.G) and shRNA expression constructs were transfected into HEK-293FT cells using calcium phosphate precipitations. 24h after transfection the medium was changed and 48h after transfection the supernatant of the HEK cells was added to U2OS cells. This process was repeated the next day. 48 hours after the second transduction, cells were selected using puromycin (Invivogen).

Cloning hHSF2BP, BRCA2 fragments

The list of constructs used in the study is presented in

Table S2. Human and mouse HSF2BP CDS were amplified from first-strand cDNA synthesized with SuperScript II RT polymerase using oligo-dT primers from total RNA isolated from U2OS and IB10 cells. The RT-PCR products were cloned into pCR4 TOPO TA (Invitrogen) and sequenced. The clones containing sequences corresponding to full-length HSF2BP CDS present in the NCBI GenBank database (NM_007031 and NM_028902) were used as template for PCRs to re-clone the CDS into C- and N-terminal GFP mammalian expression vectors (pEGFP-N1, pEGFP-C1) and his- or his-GST- bacterial expression vectors (pETM-11 and pETM-30). To facilitate the generation of stable cell lines HSF2BP was cloned into selectable PiggyBac vectors described previously¹⁹ using Gibson assembly. The same vectors were used to generate BRCA2 fragment expression constructs. Flag-tagged full-length hBRCA2 expression construct and various internal deletions were derived from pAZ114¹⁹ by excising a fragment encompassing the region that needs to be deleted using a pair of restriction enzymes uniquely cutting within the region and replacing it with a PCR-generated patch with the desired sequence.

HSF2BP expression detection by RT-PCRs

Total RNA was extracted from pelleted cells using RNeasy mini kit (QIAGEN). First strand cDNA was synthesized with SuperScript II enzyme (Invitrogen) using oligo-dT primer. PCR with primers amplifying either the complete or a part of HSF2BP CDS were performed with Platinum Taq polymerase (Invitrogen).

Antibodies

RAD51 (2307, home-made⁵¹), FANCD2 (NB 100-316, Novus Biologicals), H2B (07-371, Millipore) MSH2 (Ab-2, Oncogene), HSP90 (ab13492, Abcam) BRCA2 (Ab-1, OP95, Calbiochem), FLAG (M2 antibody, Sigma), GFP (clones 7.1 and 13.1, Roche), ORC2 (551178, BD Pharmingen), XRCC3 (ab6494, Abcam).

Mouse HSF2BP: GST-His-mHSF2BP was expressed in bacteria using the his- or his-GST- bacterial expression vectors (pETM-11 and pETM-30) and inclusion bodies were purified. Inclusion bodies were used to immunize rabbits (Eurogentec). Serum was affinity purified using His-mHSF2BP as described previously⁵².

Immunoblot

To prepare lysates, cells were scraped in PBS and lysed in 2x Leamml buffer (120 mM Tris pH 6.8, 4% SDS, 10% Glycerol). Proteins were separated on acrylamide or tris-acetate gels (Novex) and blotted on nitrocellulose or PVDF. Membranes were blocked in 3% milk in PBS+0.05% Tween. After overnight incubation with the primary antibody, membranes were washed in PBS+0.05% Tween and incubated with horseradish peroxidase-conjugated secondary antibodies (Jackson ImmunoResearch). Blots were developed using homemade ECL and detected with the Alliance 4.7 (UVitec).

Fractionations

For fractionations 1 million cells were collected, washed once in ice-cold PBS and fractionated as described⁵³.

Co-immunoprecipitation

Cells were washed twice in ice-cold PBS and lysed in NETT buffer (100 mM NaCl, 50 mM Tris pH 7.5, 5mM EDTA pH 8.0, 0.5% Triton-X100). After 30 min lysis on ice, mixtures were centrifuged and the supernatant (input) was added to washed anti-GFP beads (Chromotec) or anti-Flag M2 affinity gel (A2220, Sigma)). Beads and lysates were incubated 2-4 hours at 4°C while rotating. Bound proteins were washed three times in NETT buffer and bound proteins were eluted by boiling in 2x Sample buffer. For Flag IPs on proteins smaller than 75 kDa Glycine elution according to the manufacturers protocol was used to prevent release of the M2 antibody from the affinity gel.

Co-immunoprecipitation BRCA2 and FANCD2

Fractionations and immunoprecipitations were performed as described³⁴. Briefly, 5 million cells were used per 400 µl of buffer in every step of the fractionation. In the last step of the fractionation, the chromatin fraction was resuspended in 200µl Buffer A+ 250 mM Ammonium Sulphate + Protease inhibitor cocktail (PIC) + Pefa-bloc. The chromatin fraction was pre-cleared with 200 µl 50% protein A sepharose CL-4B beads (GE Healthcare) suspension for 30 min on a rotating wheel at 4°C and the primary antibody was added overnight. Next, 200 µl 50% protA beads was added and incubated another 4 hours. Bound proteins were washed 3x in lysis buffer (20 mM Tris-HCl pH 7.5, 150 mM NaCl, 1mM EDTA, 0,5% NP40 substitute)+PIC+pefabloc and eluted by boiling in 2x sample buffer.

Mass Spectrometry

For SILAC labelling, cells were grown in DMEM medium for SILAC (Thermo Scientific) without lysine or arginine and supplemented with dialysed serum, L-arginine and L-lysine (Light: K0R0, Medium: K4R6, Heavy: K8R10) for 2 weeks. Amino acids for SILAC (K4: L-LYSINE:2HCL (4,4,5,5-D4, 96-98%), K6: L-LYSINE:2HCL (13C6, 99%), R6: L-ARGININE:HCL (13C6, 99%), R10: L-ARGININE:HCL (13C6, 99%; 15N4, 99%) were obtained from Cambridge Isotope Laboratories.

IPs were performed for each state separately in NETT buffer (100 mM NaCl, 50 mM Tris HCl pH 7.5, 5 mM EDTA, 0.5% Triton X100) supplemented with protease inhibitor cocktail (Roche) and Pefa-bloc (Roche). After Immunoprecipitation, bound proteins of all three stated were mixed and were digested 'on-bead', essentially as published⁵⁴. Details of this procedure are available upon request. Data was analysed using the Andromeda search engine within the MaxQuant software package version 1.5.3.8^{55,56}.

Recombination assay

Site specific recombination after DSB induction by I-SceI was measured as described²⁹.

IF Rad51 FANCD2 and confocal microscopy

For FANCD2 and Rad51 staining, cells were treated overnight with 100 mM MMC. Cells were pre-extracted before fixation for 1 min in Triton X-100 buffer and stained as de-

scribed⁵⁷. For the labelling of S-phase cells, cells were incubated for 2 hours with 1 µM EdU before extraction and fixation. EdU staining was performed using the Click-iT® EdU Alexa Fluor 488 Imaging Kit (Thermo Fisher Scientific) according to the manufacturers protocol and before antibody staining. For quantification, experiments were performed in triplicate and per sample 100 nuclei were counted (except figure 8B and 8C, single experiments with at least 100 nuclei). Pictures were taken using a Leica SP5 confocal microscope using a 63x objective and 405, 488 and 594nm lasers. Statistical analysis was performed in Graphpad Prism using a Kruskal-Wallis test with Dunn's post test comparing all columns.

Cell cycle analysis

PI-BrdU labelling was performed as described⁵⁸. Cell cycle distributions were analysed on a FACS Fortessa (BD) and analysed using the FACSDiva software (BD).

Metaphase analysis for chromosomal aberrations

Metaphases analysis was performed as described⁵⁹.

Table 1 Overview of Flag-tagged BRCA2 domains

Construct name	BRCA2 region	MW
B2N	Met 1-Thr 939	107.8 kDa
B2M	Gln 940-Glu 2198	144.3 kDa
B2C	Thr 2199-Ile 3418	141.4 kDa
Flag-BRCA2Δ1	Thr 2198-Asp2478 deleted	345 kDa
Flag-BRCA2Δ2	Thr 2349-Asp 2478 deleted	351 kDa
BRCA2-F1	Thr 2199-Asp2479	35 kDa
BRCA2-F2	Thr 2350-Asp 2479	18 kDa
BRCA2-F3	Thr2199-Ser2546	42.7 kDa
BRCA2-F4	Thr2350-Ser2546	25.6 kDa
BRCA2-F5	Gly2270-Ser2546	34.7 kDa

Table 2 MS data Flag-BRCA2 domains

Gene names	Peptides	±BRCA2 fragment			±HSF2BP overproduction			Sequence coverage [%]
		H/M(n) #1	H/M(n) #2	H/M(n) #3	H/L(n) #1	M/L(n) #2	H/L(n) #3	
BRCA2	19	6,90	-2,46	4,45	0,63	-0,40	0,41	6,3
GAPDH	10	2,46	-1,71	1,60	0,49	1,58	-0,76	45,4
HIST1H2BN;HIST1H	6	2,26	-0,51	1,24	0,87	3,46	-0,04	31,3
HIST2H3A	6	2,24	-0,52	1,18	0,80	3,31	-0,01	48,5
H2AFV;H2AFZ	5	2,04	-0,46	1,02	0,80	2,80	0,00	31,2
LMNB1	13	2,03	-0,55	1,16	0,70	2,54	-0,20	24,1
HIST1H2AC;HIST3H	5	1,95	-0,44	1,49	0,91	3,42	0,06	35,4
RPA1	10	1,94	-0,48	NaN	1,19	2,40	NaN	23,4
ACTA1;ACTC1;ACTC	17	1,84	-0,78	0,94	0,78	2,05	-0,22	33,4
PHGDH	8	1,80	-1,68	NaN	0,70	1,84	NaN	22
ACTN4	25	1,76	-0,90	1,00	0,82	2,56	-0,05	34,7
ACTG1	26	1,75	-0,80	1,06	0,78	2,06	-0,15	76
RACGAP1	10	1,73	-1,28	0,07	0,37	2,82	-0,30	20,7
NHP2L1	4	1,69	-0,44	1,31	0,68	1,51	0,16	31,1
KIF23	12	1,69	-1,88	NaN	0,39	1,81	NaN	17,4
HSP90AB1	15	1,65	-1,26	0,55	0,56	1,90	0,04	22,5
MYH9	100	1,65	-0,58	0,68	1,12	1,93	0,04	50,6
CBX3	4	1,56	-0,76	0,84	0,34	2,37	-0,59	27,3
PPP1CA;PPP1CC	5	1,56	-0,53	NaN	1,02	1,55	NaN	17,9
RAN	7	1,53	-0,87	1,08	0,33	1,76	-0,45	36,5
LIG3	5	1,52	-0,55	NaN	0,79	1,52	NaN	5,9
PPIG	6	1,52	-1,30	NaN	0,96	2,49	NaN	8,4
HSPA9	11	1,52	-0,67	NaN	0,65	1,13	NaN	22,7
EIF4A1	13	1,52	-1,14	0,86	0,64	1,99	0,07	42,9
TUBB	20	1,49	-0,53	0,58	0,37	0,77	-0,28	58,5
DBN1	7	1,49	-0,55	1,16	0,81	1,32	-0,17	17,4
LGALS1	4	1,46	-1,23	0,53	0,59	1,47	-0,16	39,3
RSL1D1	11	1,45	-0,58	0,93	0,66	3,17	0,16	21,6
PKM	9	1,43	-1,70	0,90	0,06	0,98	-0,71	26,6
LIMA1	11	1,43	-0,57	NaN	0,94	-0,40	NaN	24,1
MYL6	6	1,43	-0,51	0,65	1,09	2,04	0,07	49,7
ARL6IP4	4	1,35	-0,97	NaN	0,56	2,47	NaN	23,7
NOP58	9	1,34	-0,53	0,76	0,55	2,52	0,19	22,7
PRPF40A	7	1,33	-1,40	NaN	1,01	2,40	NaN	8,9
DDX21	19	1,33	-0,40	0,87	0,44	2,43	0,02	31,3
FASN	22	1,28	-1,03	NaN	0,45	1,09	NaN	13,5
TUBA1B;TUBA1A;T	19	1,27	-0,96	0,64	0,40	0,81	-0,29	57,4
RBMX;RBMXL1	7	1,22	-0,41	1,17	0,56	1,64	0,08	31,5
RBM39	17	1,22	-1,24	NaN	0,77	1,73	NaN	40,6
PUF60	16	1,21	-1,08	NaN	1,07	2,00	NaN	33,6
PARP2	4	1,21	-1,00	NaN	0,31	1,45	NaN	9,6
RBM25	12	1,20	-1,28	0,26	1,02	2,01	-0,84	16,4
TARDBP	3	1,20	-0,72	NaN	0,23	1,74	NaN	17,3
ATP5B	10	1,19	-1,46	0,18	0,93	1,67	0,18	28,4
SRRM1	8	1,19	-1,26	NaN	0,70	1,30	NaN	12,5
CFL1	9	1,18	-1,18	0,20	0,47	1,51	-0,29	69,3
PPIB	7	1,15	-0,62	1,06	0,74	1,70	-0,38	38,9
HSPD1	8	1,14	-0,98	0,61	0,39	1,43	0,41	15,4
PRC1	5	1,12	-0,94	NaN	0,63	1,68	NaN	13,1
CD59	2	1,12	-0,74	NaN	0,75	1,18	NaN	23,1
SRSF11	4	1,07	-1,14	NaN	1,02	1,97	NaN	15,4
TOP2A	9	1,05	-0,74	0,12	0,27	2,41	-0,68	7,4
SF3A3	7	1,05	-0,64	NaN	0,64	1,67	NaN	18,6
TUBB4B;TUBB4A	22	1,05	-0,56	0,58	0,28	0,58	-0,34	59,8
EIF5A;EIF5A2;EIF5A	4	1,03	-1,75	NaN	0,39	2,00	NaN	45,2
PCBP1	6	1,01	-0,81	NaN	0,58	1,26	NaN	25,6
TUFM	12	1,01	-0,43	0,53	0,46	0,55	0,33	36,7
EEF2	9	1,01	-1,44	NaN	0,25	1,04	NaN	12,6
DEK	14	1,00	-0,78	0,63	0,79	2,50	-0,80	30,1
HADHA	6	0,99	-0,67	0,76	0,67	1,50	0,55	13,8
EFTUD2	9	0,98	-0,45	NaN	0,48	1,84	NaN	11,1
LUC7L3	9	0,97	-0,58	0,49	0,81	1,68	-0,68	25
PRPF38B	7	0,97	-2,18	NaN	0,76	2,04	NaN	20,9
CAPZA1	4	0,96	-0,74	NaN	0,33	1,04	NaN	22
PRKDC	25	0,92	-0,47	1,52	0,61	1,45	0,24	7,8
MMTAG2	3	0,92	-1,44	NaN	0,61	2,12	NaN	15,6
SUB1	10	0,91	-0,54	0,52	0,87	1,63	-0,72	48,8
PRDX1	7	0,86	-0,68	0,46	0,21	0,45	0,03	36,7

SF3A1	6	0,85	-0,68	NaN	0,65	1,05	NaN	9,1
HIST1H1B	11	0,84	-0,51	NaN	0,38	2,79	NaN	27
PSIP1	10	0,73	-0,47	NaN	0,20	2,24	NaN	24,2
DDX46	37	0,73	-0,80	-0,15	0,79	1,53	-0,81	42
YWHAQ;YWHAZ;YV	3	0,67	-0,49	NaN	0,29	0,17	NaN	13,1
HIST1H1C	12	0,66	-0,41	0,69	0,32	2,24	-0,24	28,6
GTPBP4	6	0,65	-0,52	NaN	0,38	1,43	NaN	13,1
EEF1A1;EEF1A1P5	17	0,62	-0,86	0,35	0,26	0,98	0,03	51,5
SSRP1	12	0,60	-1,21	0,94	0,30	2,88	-0,56	20,7
PES1	6	0,60	-0,42	0,46	0,41	1,86	-0,12	12,6
SMARCA5	12	0,59	-0,43	NaN	0,53	1,82	NaN	11,9
SLC25A5	12	0,56	-0,41	-0,04	0,29	0,78	-0,44	36,9
ATAD3A	12	0,55	-0,56	NaN	0,20	0,80	NaN	24,9
ANXA2;ANXA2P2	15	0,55	-0,42	0,46	0,08	0,23	-0,15	51,6
DNAJA3	2	0,53	-1,40	NaN	0,21	2,24	NaN	4,4
HSPA1A	17	0,52	-0,45	NaN	0,15	0,59	NaN	27,3
PARP1	40	0,50	-0,53	0,79	0,31	1,63	-0,47	42,6
FUS	11	0,50	-0,44	0,48	0,26	1,34	-0,23	15,2
LUC7L	12	0,47	-0,43	NaN	0,43	0,29	NaN	31,5
SUPT16H	11	0,45	-1,22	0,59	0,40	3,11	-0,67	12,7
DNAJA1	5	0,45	-0,87	0,41	0,11	1,00	-0,29	18,6
ATAD3A	11	0,41	-0,47	NaN	-0,14	0,19	NaN	22,4
CDC2;CDK1	1	NaN	NaN	NaN	NaN	NaN	NaN	3,7
DNAH8	2	NaN	NaN	NaN	NaN	NaN	NaN	0,5
TAF15	4	NaN	-0,71	NaN	NaN	2,23	NaN	10,9
CHD1L	1	NaN	NaN	NaN	NaN	NaN	NaN	4,5
KHSRP	3	NaN	0,04	NaN	NaN	0,96	NaN	7,3
UHRF1	2	NaN	-0,13	NaN	NaN	1,37	NaN	5,2
PSMD13	1	NaN	NaN	NaN	NaN	NaN	NaN	5,9
MYCBP	2	NaN	0,61	NaN	NaN	-0,32	NaN	33,6
MKI67	4	NaN	-0,84	NaN	NaN	1,80	NaN	2,5
NOP2	6	NaN	-0,35	0,72	NaN	1,28	-0,04	9,4
CLTC	10	NaN	-0,51	0,71	NaN	1,01	-0,19	8,9
TPM3	4	NaN	NaN	NaN	NaN	NaN	NaN	48,4
CCDC88A	2	NaN	NaN	NaN	NaN	NaN	NaN	3,2
COL5A1	1	NaN	-0,92	NaN	NaN	1,95	NaN	0,7
DHX29	2	NaN	NaN	NaN	NaN	NaN	NaN	1,8
PTGES3	1	NaN	NaN	NaN	NaN	NaN	NaN	10,4
KRR1	1	NaN	NaN	NaN	NaN	NaN	NaN	3,5
RBM26	1	NaN	NaN	NaN	NaN	NaN	NaN	8,2
TJP1	2	NaN	NaN	NaN	NaN	NaN	NaN	2,3
DDX52	2	NaN	NaN	NaN	NaN	NaN	NaN	27,8
ZMYM2	1	NaN	NaN	NaN	NaN	NaN	NaN	5,4
USP39	1	NaN	NaN	NaN	NaN	NaN	NaN	2,5
ACAP2	3	NaN	NaN	NaN	NaN	NaN	NaN	4,5
CEBPZ	1	NaN	NaN	NaN	NaN	NaN	NaN	1,7
CDK13;CDK12	1	NaN	NaN	NaN	NaN	NaN	NaN	5,2
MARK3	1	NaN	NaN	NaN	NaN	NaN	NaN	13,2
IFNA6;IFNA1;IFNA1	2	NaN	NaN	NaN	NaN	NaN	NaN	14,2
VDAC2	2	NaN	NaN	NaN	NaN	NaN	NaN	9,9
VAV1	1	NaN	NaN	NaN	NaN	NaN	NaN	1,4
LRIT3	1	NaN	NaN	NaN	NaN	NaN	NaN	4,2
TTN	2	NaN	NaN	NaN	NaN	NaN	NaN	0,1
NOLC1	1	NaN	NaN	NaN	NaN	NaN	NaN	1,6
APTX	1	NaN	NaN	NaN	NaN	NaN	NaN	3,6
IGHV1-45	1	NaN	NaN	NaN	NaN	NaN	NaN	9,4
AKR1C2;AKR1C1	1	NaN	-0,86	NaN	NaN	1,60	NaN	8,5
FDXR	1	NaN	NaN	NaN	NaN	NaN	NaN	8,5
SMARCA4;SMARCA	3	NaN	-0,20	1,03	NaN	1,53	-0,12	2,2
TUBB3	13	NaN	NaN	NaN	NaN	NaN	NaN	14,9
PWP2	1	NaN	0,35	NaN	NaN	1,48	NaN	1,7
MPG	1	NaN	NaN	NaN	NaN	NaN	NaN	12,4
FMR1	4	NaN	NaN	NaN	NaN	NaN	NaN	8,3
AIMP2	1	NaN	NaN	NaN	NaN	NaN	NaN	5
ZNF705F;ZNF705B;	2	NaN	NaN	NaN	NaN	NaN	NaN	6,7
SUN2	2	NaN	NaN	NaN	NaN	NaN	NaN	19,2
APOBEC3B;APOBEC	2	NaN	NaN	0,82	NaN	NaN	-0,67	6,3
MAN1C1	1	NaN	NaN	NaN	NaN	NaN	NaN	2,4
GNB1	2	NaN	NaN	NaN	NaN	1,92	NaN	16,8
EXOSC1	1	NaN	NaN	NaN	NaN	NaN	NaN	11,5



SMARCE1	1	NaN	NaN	NaN	NaN	NaN	NaN	8,3
CCT3	3	NaN	-0,79	NaN	NaN	0,39	NaN	7
CCT5	4	NaN	-0,46	NaN	NaN	0,30	NaN	8,8
CDK11A;CDK11B;CI	2	NaN	-0,68	NaN	NaN	1,73	NaN	3,5
AGPS	1	NaN	NaN	NaN	NaN	NaN	NaN	12,7
SUMO1	1	NaN	NaN	NaN	NaN	NaN	NaN	20,7
TCEB2	1	NaN	NaN	NaN	NaN	NaN	NaN	22,1
IMMT	4	NaN	0,40	1,12	NaN	1,01	0,23	9,3
CMSS1	1	NaN	NaN	NaN	NaN	NaN	NaN	3,6
ARPC1B	1	NaN	NaN	NaN	NaN	NaN	NaN	9,8
NIFK	3	NaN	-0,63	NaN	NaN	1,80	NaN	25,3
EEFSEC	1	NaN	NaN	NaN	NaN	NaN	NaN	4,1
RBM28	1	NaN	NaN	NaN	NaN	NaN	NaN	4,4
ATP5J2-PTCD1;ATP	1	NaN	NaN	NaN	NaN	NaN	NaN	20,4
CAV1;CAV3	2	NaN	NaN	NaN	NaN	NaN	NaN	22,5
CCNL1	1	NaN	-0,01	NaN	NaN	1,13	NaN	2,3
TIPARP	1	NaN	NaN	NaN	NaN	NaN	NaN	3,4
DHRS2	2	NaN	NaN	NaN	NaN	NaN	NaN	11,6
CPLX2	1	NaN	NaN	NaN	NaN	NaN	NaN	37,8
MRPL27	1	NaN	NaN	NaN	NaN	NaN	NaN	16,1
DDX4	3	NaN	NaN	NaN	NaN	NaN	NaN	6,9
POLR1C	1	NaN	NaN	NaN	NaN	NaN	NaN	14,5
CSNK1A1;CSNK1A1	1	NaN	NaN	NaN	NaN	NaN	NaN	5,1
SDHA	2	NaN	NaN	NaN	NaN	NaN	NaN	4,3
EXOSC9	1	NaN	NaN	NaN	NaN	NaN	NaN	2,6
PYCR1;PYCR2	2	NaN	NaN	NaN	NaN	NaN	NaN	12,8
DCTN4	1	NaN	NaN	NaN	NaN	NaN	NaN	9,3
SQSTM1	3	NaN	0,89	NaN	NaN	0,43	NaN	14,6
FLOT2	1	NaN	NaN	NaN	NaN	NaN	NaN	2,8
ADAM22	2	NaN	NaN	NaN	NaN	NaN	NaN	8,8
TCP1	3	NaN	-0,46	NaN	NaN	0,92	NaN	10,5
ACIN1	4	NaN	NaN	NaN	NaN	1,96	NaN	8,9
TCOF1	4	NaN	-0,43	NaN	NaN	0,99	NaN	2,5
ARHGEF4	2	NaN	NaN	NaN	NaN	NaN	NaN	2,8
TOP2B	5	NaN	NaN	NaN	NaN	NaN	NaN	4,8
CP	4	NaN	NaN	NaN	NaN	NaN	NaN	5
MTCH2	1	NaN	NaN	NaN	NaN	NaN	NaN	6,1
PRMT1	4	NaN	0,35	NaN	NaN	-0,51	NaN	16,9
GANAB	1	NaN	NaN	NaN	NaN	NaN	NaN	7,6
IPO7	1	NaN	NaN	NaN	NaN	NaN	NaN	11,5
LMO7	3	NaN	0,17	NaN	NaN	1,13	NaN	3,2
PTS	3	NaN	NaN	NaN	NaN	NaN	NaN	48,1
PUF60	12	NaN	NaN	NaN	NaN	NaN	NaN	50
NUP160	2	NaN	NaN	NaN	NaN	NaN	NaN	2,9
PC	2	NaN	-1,00	NaN	NaN	1,90	NaN	6,3
PFKFB3	7	NaN	1,02	NaN	NaN	-1,30	NaN	18,9
PSMD5	2	NaN	NaN	NaN	NaN	NaN	NaN	30,6
CCT2	3	NaN	NaN	NaN	NaN	NaN	NaN	9,4
DDB1	4	NaN	NaN	0,31	NaN	NaN	-0,24	3,8
RECQL	1	NaN	NaN	NaN	NaN	NaN	NaN	9,2
NOC4L	2	NaN	NaN	NaN	NaN	NaN	NaN	9,3
E2F7	1	NaN	NaN	NaN	NaN	NaN	NaN	2,7
SMARCD1	1	NaN	NaN	0,65	NaN	NaN	-0,19	16,8
CPM	2	NaN	NaN	NaN	NaN	NaN	NaN	12,9
UBAP2L	1	NaN	-0,44	NaN	NaN	1,73	NaN	2,6
IGF2BP2	5	NaN	NaN	-0,25	NaN	NaN	-0,06	12,6
DRC1	1	NaN	NaN	NaN	NaN	NaN	NaN	7,5
HSPB1	1	NaN	NaN	NaN	NaN	NaN	NaN	8,6
ZFP36L1	1	NaN	NaN	NaN	NaN	NaN	NaN	6,2
SNW1	2	NaN	NaN	NaN	NaN	NaN	NaN	7,5
NEMF	2	NaN	NaN	NaN	NaN	NaN	NaN	2,4
ELP4	1	NaN	NaN	NaN	NaN	NaN	NaN	3,6
SMC1A	3	NaN	0,19	NaN	NaN	2,52	NaN	3,1
STAT3	1	NaN	NaN	NaN	NaN	NaN	NaN	3,9
HP;HPR	3	NaN	NaN	0,25	NaN	NaN	-2,15	7,4
DPM1	1	NaN	-0,48	NaN	NaN	1,41	NaN	10
KPNA5;KPNA6;KPN	1	NaN	NaN	NaN	NaN	NaN	NaN	11,5
P4HB	1	NaN	NaN	NaN	NaN	NaN	NaN	6,8
KIF6	1	NaN	NaN	NaN	NaN	NaN	NaN	1,7
UTP15	3	NaN	-0,37	NaN	NaN	1,20	NaN	6,8

PLRG1	3	NaN	NaN	0,18	NaN	NaN	0,04	29,5
VRK1	4	NaN	-0,18	NaN	NaN	1,64	NaN	28
ETFA	1	NaN	NaN	NaN	NaN	NaN	NaN	7,4
SLTM	2	NaN	NaN	NaN	NaN	NaN	NaN	32,3
PSMA4	2	NaN	NaN	NaN	NaN	NaN	NaN	10,5
CDC42BPB	1	NaN	NaN	NaN	NaN	NaN	NaN	1,4
SNRPA1	2	NaN	NaN	NaN	NaN	NaN	NaN	17,6
RNPS1	2	NaN	-0,26	NaN	NaN	1,20	NaN	7,6
PSMD7	1	NaN	-0,29	NaN	NaN	-0,09	NaN	39,5
ZNF598	1	NaN	NaN	-0,15	NaN	NaN	0,07	1,4
CES1	1	NaN	NaN	NaN	NaN	NaN	NaN	5,3
VPS35	1	NaN	NaN	NaN	NaN	NaN	NaN	56,2
TIPIN	1	NaN	NaN	NaN	NaN	NaN	NaN	11,3
RIF1	2	NaN	NaN	NaN	NaN	NaN	NaN	3
ATP5O	1	NaN	NaN	0,44	NaN	NaN	-0,10	18,9
RUVBL1	2	NaN	-1,01	NaN	NaN	1,64	NaN	29
PSMD6	1	NaN	NaN	NaN	NaN	NaN	NaN	10,9
SLC25A11	1	NaN	NaN	NaN	NaN	NaN	NaN	5,4
KDM2A	2	NaN	NaN	NaN	NaN	NaN	NaN	2,1
DDX41	2	NaN	-0,89	NaN	NaN	2,09	NaN	4,5
TBL3	4	NaN	-0,05	NaN	NaN	1,80	NaN	9,5
SMG1	1	NaN	NaN	NaN	NaN	NaN	NaN	0,3
MPRIP	4	NaN	-0,16	NaN	NaN	1,03	NaN	5,7
KPNB1	3	NaN	NaN	NaN	NaN	NaN	NaN	6,5
CHERP	5	NaN	-0,22	NaN	NaN	0,46	NaN	6,6
NIP7	2	NaN	-0,37	NaN	NaN	2,31	NaN	30
SAP30BP	1	NaN	NaN	NaN	NaN	NaN	NaN	4
MYL12A;MYL12B	2	NaN	-0,31	NaN	NaN	1,52	NaN	11,9
COPRS	1	NaN	NaN	NaN	NaN	NaN	NaN	38,2
SON	1	NaN	NaN	NaN	NaN	NaN	NaN	2
NUDT16L1;NUDT1	1	NaN	NaN	NaN	NaN	0,53	NaN	5,6
KANK2	1	NaN	NaN	NaN	NaN	NaN	NaN	5,4
DNMT1	1	NaN	NaN	NaN	NaN	NaN	NaN	14,6
H3F3B;H3F3A;HIST	6	NaN	NaN	NaN	NaN	NaN	NaN	50
MRPL4	3	NaN	NaN	NaN	NaN	NaN	NaN	30,7
LSM12	1	NaN	NaN	NaN	NaN	NaN	NaN	3,9
SF3A2	2	NaN	-0,78	NaN	NaN	0,13	NaN	26,7
TUBB6	7	NaN	NaN	0,63	NaN	NaN	0,75	19,5
ETFB	1	NaN	NaN	NaN	NaN	NaN	NaN	6,7
AP2S1	3	NaN	NaN	NaN	NaN	NaN	NaN	16,7
PHLDB3	1	NaN	NaN	NaN	NaN	NaN	NaN	6,9
DDX39B;DDX39A	2	NaN	NaN	NaN	NaN	NaN	NaN	4,9
TAF4	2	NaN	NaN	NaN	NaN	NaN	NaN	4
CLIC1	1	NaN	NaN	NaN	NaN	NaN	NaN	7,5
POLRMT	2	NaN	NaN	NaN	NaN	NaN	NaN	3
HMGNA4	1	NaN	NaN	NaN	NaN	NaN	NaN	14,4
MPHOSPH10	2	NaN	NaN	NaN	NaN	NaN	NaN	4,4
NDC80	1	NaN	NaN	NaN	NaN	NaN	NaN	1,6
WDR46	2	NaN	NaN	NaN	NaN	NaN	NaN	4,8
CASC3	1	NaN	NaN	NaN	NaN	NaN	NaN	2,1
MRPS12	1	NaN	NaN	NaN	NaN	NaN	NaN	8,7
PPM1G	1	NaN	NaN	NaN	NaN	NaN	NaN	5,5
IPO8	2	NaN	NaN	NaN	NaN	-1,60	NaN	3,1
MAGEB2	3	NaN	NaN	0,01	NaN	NaN	-0,05	11
ZBTB24	1	NaN	NaN	NaN	NaN	NaN	NaN	1,4
MAP3K7	6	NaN	0,67	NaN	NaN	-1,72	NaN	13,9
HNRNPCL1;HNRNP	8	NaN	NaN	NaN	NaN	NaN	NaN	19,5
HSF2BP	4	NaN	NaN	NaN	NaN	NaN	NaN	14,4
FLNB;FLNC	6	NaN	-0,42	NaN	NaN	0,49	NaN	2,7
SNRNP200	16	NaN	-0,11	1,15	NaN	1,71	-0,06	10
BCAS2	1	NaN	0,67	NaN	NaN	0,09	NaN	10,2
DNAJC8	1	NaN	NaN	NaN	NaN	NaN	NaN	10,4
GLS	2	NaN	NaN	0,03	NaN	NaN	-0,14	5,4
ZRANB2	2	NaN	NaN	NaN	NaN	NaN	NaN	7
KIF4A;KIF4B	1	NaN	NaN	NaN	NaN	NaN	NaN	1,4
SGPL1	2	NaN	NaN	-0,16	NaN	NaN	-0,30	5,5
STAU1	4	NaN	NaN	0,07	NaN	NaN	-0,35	12,5
IGKV3-15;IGKV3-7;	2	NaN	NaN	NaN	NaN	NaN	NaN	25
	1	NaN	NaN	NaN	NaN	NaN	NaN	9
IGHG2	1	NaN	NaN	NaN	NaN	NaN	NaN	2,8

COL4A1	3	NaN	NaN	NaN	NaN	NaN	NaN	NaN	2,7
FN1	5	NaN	NaN	NaN	NaN	NaN	NaN	NaN	3,2
HPX	3	NaN	NaN	NaN	NaN	NaN	NaN	NaN	3,7
ANXA1	1	NaN	-0,71	NaN	NaN	NaN	0,89	NaN	12,2
GNAI2;GNAI1;GNA	5	NaN	-0,74	NaN	NaN	NaN	1,67	NaN	18,3
S100A8	2	NaN	0,01	NaN	NaN	NaN	-1,24	NaN	23,7
HSP90AA1	9	NaN	-1,47	NaN	NaN	NaN	1,14	NaN	15,2
PKHD1	2	NaN	NaN	NaN	NaN	NaN	NaN	NaN	0,9
HIST1H1E	12	NaN	NaN	NaN	NaN	NaN	NaN	NaN	27,9
TXN	3	NaN	NaN	NaN	NaN	NaN	NaN	NaN	21
G6PD	4	NaN	NaN	NaN	NaN	NaN	NaN	NaN	9,3
SLC25A6;SLC25A4	9	NaN	-1,19	NaN	NaN	NaN	1,29	NaN	27,9
JUP	5	NaN	NaN	NaN	NaN	NaN	NaN	NaN	7,7
DSP	11	NaN	1,92	NaN	NaN	NaN	-1,73	NaN	4,6
HSPA6;HSPA7	7	NaN	NaN	NaN	NaN	NaN	NaN	NaN	12,6
WARS	2	NaN	NaN	NaN	NaN	NaN	NaN	NaN	5,5
ATP5A1	6	NaN	-0,92	NaN	NaN	NaN	0,64	NaN	13,6
ABCD3	1	NaN	-0,51	NaN	NaN	NaN	0,53	NaN	2,3
PRDX6	2	NaN	NaN	NaN	NaN	NaN	1,06	NaN	12,1
PRDX2	3	NaN	NaN	NaN	NaN	NaN	NaN	NaN	14,6
MCM7	3	NaN	NaN	NaN	NaN	NaN	NaN	NaN	5,4
SHMT2	5	NaN	-0,92	NaN	NaN	NaN	0,23	NaN	17,5
GPC1	1	NaN	-0,42	NaN	NaN	NaN	1,40	NaN	3,2
MYH10	20	NaN	-0,69	NaN	NaN	NaN	1,55	NaN	11,9
GNL1	1	NaN	NaN	NaN	NaN	NaN	NaN	NaN	1,6
RFC5	2	NaN	NaN	NaN	NaN	NaN	NaN	NaN	9,4
PSMC4	1	NaN	NaN	NaN	NaN	NaN	NaN	NaN	2,9
PRRC2A	1	NaN	NaN	NaN	NaN	NaN	NaN	NaN	0,8
NT5C2	2	NaN	NaN	NaN	NaN	NaN	NaN	NaN	23,3
CCT4	1	NaN	-1,14	NaN	NaN	NaN	1,22	NaN	2,4
KPNA2	3	NaN	0,47	0,61	NaN	NaN	1,03	-0,02	10
METAP1	1	NaN	NaN	NaN	NaN	NaN	NaN	NaN	7,8
SLC16A1	1	NaN	NaN	NaN	NaN	NaN	NaN	NaN	4
ALDH18A1	2	NaN	NaN	NaN	NaN	NaN	NaN	NaN	3,5
CSE1L	1	NaN	NaN	NaN	NaN	NaN	NaN	NaN	0,8
MFAP1	2	NaN	NaN	NaN	NaN	NaN	NaN	NaN	6,8
HADHB	5	NaN	-0,27	0,26	NaN	NaN	1,08	-0,01	15,8
ADAR	6	NaN	-0,36	NaN	NaN	NaN	0,79	NaN	6,4
MARS	3	NaN	-0,05	NaN	NaN	NaN	0,07	NaN	3,9
CDC42	1	NaN	NaN	NaN	NaN	NaN	NaN	NaN	8,1
PPP1CB	5	NaN	-0,16	NaN	NaN	NaN	-0,24	NaN	18
SNRPE	1	NaN	-0,35	NaN	NaN	NaN	0,88	NaN	12
SNRPF	1	NaN	NaN	NaN	NaN	NaN	NaN	NaN	15,1
SNRPD2	3	NaN	NaN	NaN	NaN	NaN	NaN	NaN	22,9
GNB2;GNB4	2	NaN	-0,54	NaN	NaN	NaN	1,28	NaN	11,2
RAC1;RAC3;RAC2	2	NaN	-0,41	NaN	NaN	NaN	0,53	NaN	12,5
GNAS	2	NaN	NaN	NaN	NaN	NaN	NaN	NaN	5,1
HIST1H3A	6	NaN	0,35	NaN	NaN	NaN	2,58	NaN	48,5
NOP14	3	NaN	NaN	NaN	NaN	NaN	1,06	NaN	4,6
GTF2I;GTF2IRD2B;C	2	NaN	NaN	NaN	NaN	NaN	-1,94	NaN	3,8
SRPK2;SRPK3	4	NaN	NaN	-0,17	NaN	NaN	NaN	-0,46	8
MRPS6	2	NaN	0,03	NaN	NaN	NaN	-0,04	NaN	18,4
PFKP	3	NaN	NaN	NaN	NaN	NaN	NaN	NaN	4,8
XPC	1	NaN	NaN	NaN	NaN	NaN	NaN	NaN	2,4
DSG1	2	NaN	NaN	NaN	NaN	NaN	NaN	NaN	3,2
HIST1H1A;HIST1H1	6	NaN	NaN	0,42	NaN	NaN	NaN	-0,89	17,7
C1QBP	1	NaN	NaN	NaN	NaN	NaN	NaN	NaN	5
DSC1	3	NaN	NaN	NaN	NaN	NaN	NaN	NaN	5,3
NCBP1	3	NaN	NaN	NaN	NaN	NaN	NaN	NaN	5,4
SPP2	1	NaN	NaN	NaN	NaN	NaN	NaN	NaN	5,7
PSMD2	2	NaN	NaN	NaN	NaN	NaN	NaN	NaN	2,9
GRB10	1	NaN	NaN	NaN	NaN	NaN	NaN	NaN	3
HDAC1;HDAC2	3	NaN	NaN	0,40	NaN	NaN	NaN	-0,14	9,1
CBFB	2	NaN	NaN	NaN	NaN	NaN	NaN	NaN	14,3
BOP1	2	NaN	NaN	NaN	NaN	NaN	NaN	NaN	4
SAFB2	2	NaN	-0,32	NaN	NaN	NaN	0,08	NaN	3,3
DYNC1H1	2	NaN	-0,82	NaN	NaN	NaN	0,75	NaN	0,6
PDCD11	3	NaN	NaN	NaN	NaN	NaN	NaN	NaN	2,1
RRS1	1	NaN	-0,20	NaN	NaN	NaN	2,29	NaN	3,8
KIF14	3	NaN	NaN	NaN	NaN	NaN	NaN	NaN	2,9

WDR43	2	NaN	NaN	NaN	NaN	NaN	NaN	NaN	3,4
KIAA0020	1	NaN	NaN	NaN	NaN	NaN	NaN	NaN	2,2
SAFB	2	NaN	-0,14	NaN	NaN	1,76	NaN	NaN	3
SF1	1	NaN	NaN	NaN	NaN	NaN	NaN	NaN	1,7
TAB1	5	NaN	1,37	NaN	NaN	-1,60	NaN	NaN	9,7
TBR1	2	NaN	NaN	2,22	NaN	NaN	0,02	NaN	5,6
ACTBL2	7	NaN	NaN	NaN	NaN	NaN	NaN	NaN	17,8
DNAJC21	1	NaN	NaN	NaN	NaN	NaN	NaN	NaN	2,4
MOV10	3	NaN	NaN	NaN	NaN	NaN	NaN	NaN	4,6
DNTTIP2	1	NaN	NaN	NaN	NaN	NaN	NaN	NaN	1,9
ODR4	1	NaN	NaN	NaN	NaN	NaN	NaN	NaN	2,6
HNRNPK	19	NaN	0,44	0,05	NaN	-0,40	-0,07	NaN	52,2
KPRP	6	NaN	NaN	NaN	NaN	NaN	NaN	NaN	19,9
LSM14B	1	NaN	NaN	-0,19	NaN	NaN	-0,50	NaN	10,5
PRAMEF16;PRAME	1	NaN	NaN	NaN	NaN	NaN	NaN	NaN	1,5
RPL7L1	3	NaN	-0,60	NaN	NaN	2,39	NaN	NaN	15
PLXDC2	2	NaN	NaN	NaN	NaN	NaN	NaN	NaN	4,2
CD109	1	NaN	NaN	NaN	NaN	NaN	NaN	NaN	1,2
UBN2	2	NaN	NaN	NaN	NaN	NaN	NaN	NaN	3,3
RSRC2	1	NaN	NaN	NaN	NaN	NaN	NaN	NaN	2,5
MYH14	5	NaN	NaN	0,54	NaN	NaN	-0,09	NaN	3
HAPLN4	1	NaN	NaN	NaN	NaN	NaN	NaN	NaN	2
TSPYL5	3	NaN	NaN	0,16	NaN	NaN	0,38	NaN	8,2
WDR75	1	NaN	NaN	NaN	NaN	NaN	NaN	NaN	1,4
FTSJ3	2	NaN	NaN	NaN	NaN	NaN	NaN	NaN	4,6
ASPM	2	NaN	NaN	NaN	NaN	NaN	NaN	NaN	0,8
PRPF38A	2	NaN	-0,42	NaN	NaN	1,59	NaN	NaN	6,1
LEMDD2	2	NaN	NaN	NaN	NaN	NaN	NaN	NaN	10,1
PKD1L1	2	NaN	NaN	NaN	NaN	NaN	NaN	NaN	1,9
NUP210	3	NaN	NaN	NaN	NaN	NaN	NaN	NaN	2,2
PPIL4	1	NaN	NaN	NaN	NaN	NaN	NaN	NaN	2,4
CACTIN	2	NaN	NaN	NaN	NaN	-0,44	NaN	NaN	3,6
PXDN	2	NaN	NaN	NaN	NaN	1,89	NaN	NaN	1,6
SMARCC1;SMARCC	2	NaN	0,15	NaN	NaN	2,23	NaN	NaN	2,3
ZNF622	1	NaN	NaN	NaN	NaN	NaN	NaN	NaN	4,4
CPNE4;CPNE8;CPN	2	NaN	NaN	NaN	NaN	NaN	NaN	NaN	6,1
CMBL	3	NaN	0,37	NaN	NaN	-0,79	NaN	NaN	12,2
PTCD3	2	NaN	NaN	NaN	NaN	NaN	NaN	NaN	4,1
ZFR	3	NaN	NaN	1,03	NaN	NaN	0,49	NaN	4,5
HMCN1	1	NaN	NaN	NaN	NaN	NaN	NaN	NaN	0,3
RSF1	2	NaN	NaN	NaN	NaN	NaN	NaN	NaN	2,8
CDC5L	3	NaN	NaN	0,29	NaN	NaN	-0,15	NaN	5,9
MACROD1	1	NaN	NaN	NaN	NaN	NaN	NaN	NaN	4,3
ESYT1	1	NaN	NaN	NaN	NaN	NaN	NaN	NaN	1,1
DDX23	1	NaN	NaN	NaN	NaN	NaN	NaN	NaN	2
UTP14A	4	NaN	0,05	NaN	NaN	1,53	NaN	NaN	6,4
KIFC1	2	NaN	NaN	-0,46	NaN	NaN	-0,76	NaN	4,8
SF3B5	2	NaN	-0,55	NaN	NaN	0,35	NaN	NaN	18,6
CECR5	1	NaN	NaN	NaN	NaN	NaN	NaN	NaN	4
MAK16	1	NaN	-0,41	NaN	NaN	2,28	NaN	NaN	6
REXO4	1	NaN	NaN	NaN	NaN	NaN	NaN	NaN	2,8
HRH4	1	NaN	NaN	NaN	NaN	NaN	NaN	NaN	2,3
HEATR1	4	NaN	NaN	NaN	NaN	NaN	NaN	NaN	1,9
NOL6	1	NaN	-0,69	NaN	NaN	1,99	NaN	NaN	1,3
RPF2	2	NaN	-0,16	NaN	NaN	2,00	NaN	NaN	9,8
WDR26	2	NaN	NaN	NaN	NaN	NaN	NaN	NaN	5,6
PHAX	1	NaN	NaN	NaN	NaN	NaN	NaN	NaN	4,1
PLXNA4	2	NaN	NaN	NaN	NaN	NaN	NaN	NaN	0,9
XAB2	2	NaN	NaN	NaN	NaN	NaN	NaN	NaN	2,6
IMP3	1	NaN	-0,06	NaN	NaN	1,50	NaN	NaN	9,8
DDX18	6	NaN	0,14	0,61	NaN	1,58	-0,08	NaN	12,8
NHP2	1	NaN	NaN	NaN	NaN	NaN	NaN	NaN	13,1
QPCTL	4	NaN	NaN	NaN	NaN	NaN	NaN	NaN	13,6
GAR1	1	NaN	-0,14	NaN	NaN	1,26	NaN	NaN	6,5
AATF	2	NaN	-0,25	NaN	NaN	2,47	NaN	NaN	5
BCLAF1	16	NaN	NaN	NaN	NaN	NaN	NaN	NaN	22,7
TAB2	2	NaN	NaN	NaN	NaN	NaN	NaN	NaN	3,5
TECR	2	NaN	NaN	NaN	NaN	NaN	NaN	NaN	8,4
RAI14	2	NaN	-0,57	NaN	NaN	2,05	NaN	NaN	3,2
VAPA	1	NaN	NaN	NaN	NaN	NaN	NaN	NaN	6,4

SLAIN2	3	NaN	NaN	0,01	NaN	NaN	-0,13	6,4
HEATR5B	1	NaN	NaN	NaN	NaN	NaN	NaN	0,9
LARS	2	NaN	NaN	NaN	NaN	NaN	NaN	2
ANKFY1	2	NaN	NaN	NaN	NaN	NaN	NaN	2,3
TFIP11	2	NaN	-0,48	NaN	NaN	1,26	NaN	4,2
TJP2	2	NaN	NaN	NaN	NaN	NaN	NaN	3,3
BAZ1B	1	NaN	-0,18	NaN	NaN	2,57	NaN	1,1
PACSIN3	4	NaN	NaN	NaN	NaN	0,75	NaN	13,4
USP24	2	NaN	NaN	NaN	NaN	NaN	NaN	1,5
RUVBL2	2	NaN	NaN	NaN	NaN	NaN	NaN	5,4
STK38L	7	NaN	0,79	NaN	NaN	-0,68	NaN	15,3
WBP11	3	NaN	NaN	0,60	NaN	NaN	-0,47	6,1
RRP15	1	NaN	NaN	NaN	NaN	NaN	NaN	4,6
USP15	3	NaN	NaN	NaN	NaN	NaN	NaN	4
RPA2	3	2,43	NaN	NaN	1,20	NaN	NaN	17,8
HIST1H4A	11	2,30	-0,34	1,17	0,84	3,26	-0,02	55,3
H2AFY	11	2,30	-0,27	1,22	0,87	2,28	-0,10	41,9
VIM	52	2,22	-0,16	1,26	1,08	2,97	0,01	85
HIST2H2BE;HIST1H	6	2,22	-0,22	1,20	0,81	2,47	-0,05	41,3
HIST2H3PS2	4	2,18	-0,35	1,16	0,82	3,44	-0,02	25
HIST1H2AJ;HIST1H:	6	2,17	-0,21	1,17	0,79	3,27	-0,02	35,9
HMG2;HMG3	2	2,05	NaN	NaN	0,53	NaN	NaN	16,7
CBX5	2	1,99	-0,35	NaN	1,23	2,13	NaN	14,7
RPA3	5	1,99	-0,29	NaN	0,83	1,89	NaN	55,4
RCC1	5	1,98	-0,28	NaN	0,70	1,90	NaN	18,5
RALY	5	1,93	NaN	1,22	1,01	NaN	0,07	27
HNRNPC;HNRNPCL	12	1,82	-0,38	1,21	0,75	2,53	0,08	38,9
ARPC4;ARPC4-TTL	2	1,74	NaN	NaN	0,31	NaN	NaN	20,8
BANF1	12	1,73	-0,25	0,24	0,38	2,02	-1,19	76,4
ACTB	26	1,73	-0,29	NaN	0,90	2,01	NaN	76
RBM8A	3	1,64	0,60	NaN	0,59	1,30	NaN	22,4
PPIA	4	1,63	0,40	NaN	0,24	1,71	NaN	31,5
KRT18	26	1,62	-0,15	0,86	0,66	1,85	-0,34	53,3
EMD	6	1,62	-0,36	NaN	0,19	1,61	NaN	30,3
ACTN1	13	1,53	-0,33	NaN	0,70	1,46	NaN	16,3
HNRNP3	4	1,52	-0,31	1,21	0,72	1,58	0,01	18,8
TPM4	4	1,51	-0,39	NaN	0,69	1,51	NaN	18,5
LMNA	50	1,51	-0,13	0,58	0,47	1,60	-0,57	65,1
MYO1C	18	1,50	0,11	0,74	1,14	2,16	-0,13	24,4
NUMA1	12	1,49	-0,29	NaN	0,92	2,32	NaN	8,6
CORO1C	8	1,49	-0,20	1,00	0,17	1,31	-0,35	20,5
XRCC1	5	1,43	NaN	NaN	0,83	NaN	NaN	10,4
PLEC	130	1,39	0,07	0,71	0,72	1,35	-0,11	34,4
TMPO	25	1,38	-0,39	NaN	0,56	1,36	NaN	42,7
ARGLU1	3	1,36	NaN	NaN	0,54	NaN	NaN	9,2
PHB2	2	1,33	NaN	NaN	0,67	NaN	NaN	10,9
MYO1B	7	1,31	-0,08	0,70	1,14	1,45	-0,12	8,4
MATR3	18	1,30	-0,17	0,68	0,53	1,25	-0,03	28
FOLR1	2	1,30	NaN	NaN	0,52	NaN	NaN	9,7
MYL1;MYL3	1	1,27	NaN	0,95	0,90	NaN	0,13	8,2
TMPO	16	1,26	-0,37	NaN	0,44	1,39	NaN	47,6
EIF4A3	6	1,24	0,43	2,28	0,42	1,60	1,03	19,5
TRA2B	4	1,19	-0,29	NaN	0,29	0,92	NaN	15,6
HMG1	6	1,16	NaN	0,64	0,55	NaN	-1,39	41,1
TUBB8	7	1,14	NaN	NaN	0,54	NaN	NaN	18,5
DNAH3	1	1,12	NaN	NaN	1,00	NaN	NaN	0,2
RNMT1	2	1,12	NaN	NaN	1,31	NaN	NaN	15,8
PNN	7	1,09	-0,20	NaN	0,96	1,84	NaN	11,9
SRSF10;SRSF12	4	1,08	0,04	0,92	0,32	-0,50	-0,03	27,3
DKFZp434D199;SN	2	1,08	NaN	NaN	1,15	NaN	NaN	16,5
HLA-A	3	1,07	NaN	NaN	0,50	NaN	NaN	11,2
CIRH1A	2	1,05	NaN	NaN	0,52	NaN	NaN	3,4
HMG1	3	1,03	-0,37	0,73	0,64	2,55	-0,35	41,1
FBL	11	1,02	-0,35	0,79	0,49	2,59	0,16	45,2
DKC1	8	1,02	-0,26	1,32	0,53	2,13	0,22	20,2
HNRNPA2B1	26	1,01	-0,19	0,88	0,46	1,53	0,00	69,1
LMNA	40	1,00	0,01	NaN	0,30	0,17	NaN	66,7
SLC25A3	3	0,98	NaN	NaN	0,37	NaN	NaN	8,3
EIF6	2	0,97	NaN	NaN	0,48	NaN	NaN	29,6
HNRNPA3	18	0,92	-0,27	0,80	0,47	1,84	0,04	40,7



HNRNPUL2;HNRNP	5	0,92	-0,18	NaN	0,39	1,21	NaN	10
PRSS23	2	0,91	NaN	NaN	0,31	NaN	NaN	6,8
MYO1E	8	0,90	NaN	NaN	0,85	NaN	NaN	10
ATP5C1	3	0,88	NaN	NaN	0,55	NaN	NaN	11,1
PGAM5	6	0,84	0,12	0,09	0,56	-0,12	0,21	30,4
SMU1	2	0,80	-0,39	1,08	0,42	1,98	0,08	3,9
ELAVL1	7	0,80	-0,35	0,67	0,53	1,64	0,02	28,2
CHTOP	2	0,76	NaN	NaN	0,23	NaN	NaN	38,2
VARS	5	0,76	NaN	NaN	0,13	NaN	NaN	5,2
PSPC1	3	0,76	-0,12	NaN	0,02	0,92	NaN	8
SPTBN1	30	0,74	0,13	0,05	0,34	0,02	-0,19	19,2
SF3B3	19	0,72	-0,16	0,71	0,52	1,28	-0,17	22,4
NAT10	6	0,72	NaN	NaN	0,51	NaN	NaN	7,9
BUB3	6	0,72	NaN	NaN	0,48	NaN	NaN	27,7
U2SURP	12	0,69	-0,24	NaN	0,37	0,61	NaN	14,5
SPTAN1	31	0,68	0,32	-0,28	0,40	-0,07	-0,88	18,2
SNRPG;SNRPGP15	1	0,67	NaN	0,95	0,39	NaN	0,40	20,3
SMC3	2	0,67	NaN	NaN	0,15	NaN	NaN	2,2
BASP1	1	0,67	NaN	NaN	0,43	NaN	NaN	12,3
TRIM4	1	0,67	NaN	NaN	0,29	NaN	NaN	5,4
LUC7L2;C7orf55-L	16	0,66	-0,37	0,40	0,55	0,77	-0,24	41,1
CLIP2	1	0,65	NaN	NaN	0,22	NaN	NaN	1,6
RBM14	10	0,65	-0,21	0,64	0,37	1,02	-0,07	19,7
LARP4	2	0,62	NaN	NaN	0,62	NaN	NaN	10,1
U2AF1	5	0,62	-0,12	0,39	0,75	1,21	-0,40	26,2
FUBP1	1	0,62	NaN	NaN	-0,01	NaN	NaN	1,2
U2AF2	8	0,61	-0,22	0,59	0,59	1,66	-0,31	29,3
WDR74	2	0,61	NaN	NaN	0,12	NaN	NaN	9,8
H1FO	4	0,60	0,15	0,89	0,55	1,03	-0,22	23,2
CDKN2A;CDKN2B	2	0,60	NaN	NaN	-0,02	NaN	NaN	18,2
HNRNPR	24	0,59	-0,09	0,71	0,27	2,15	0,01	37,3
PRPF8	13	0,59	-0,14	1,67	0,40	0,92	-0,36	6,5
ERH	9	0,58	0,47	0,43	0,27	-0,27	0,14	62,5
HNRNPLL;HNRPLL	4	0,58	NaN	NaN	0,57	NaN	NaN	10,6
ZNF207	2	0,58	NaN	NaN	0,38	NaN	NaN	9,7
SFPQ	32	0,58	-0,16	0,76	0,36	1,44	0,00	43,6
BRIX1	10	0,57	-0,17	NaN	0,39	1,98	NaN	30
SF3B6	1	0,57	-0,20	NaN	0,33	0,60	NaN	11,2
FUBP3	8	0,57	0,19	0,43	0,35	0,87	0,53	21,9
NSRP1;CCDC55	1	0,57	NaN	NaN	0,64	NaN	NaN	8,9
NONO	28	0,56	-0,22	0,79	0,36	1,52	0,08	58,6
SRRM2	11	0,56	-0,15	-0,14	0,50	0,16	-0,60	6,6
MRPS22	3	0,55	NaN	NaN	0,20	NaN	NaN	10,3
DYNLL1;DYNLL2	4	0,54	-0,11	0,32	0,18	0,85	-0,16	40,4
EIF3K	5	0,54	NaN	NaN	-0,10	NaN	NaN	41,6
PLK1	1	0,53	NaN	NaN	0,30	NaN	NaN	11
CYR61	2	0,53	NaN	NaN	0,85	NaN	NaN	7,1
PHF5A	1	0,51	-0,33	NaN	0,31	0,80	NaN	8,2
PRKRA	5	0,51	NaN	-0,21	0,18	NaN	0,27	24
HNRNPDL	8	0,51	-0,03	0,83	0,26	1,11	0,23	24,8
MAT2A	4	0,51	0,53	NaN	0,03	-0,88	NaN	12,4
SRSF7	5	0,51	-0,08	0,30	0,33	0,84	-0,06	42,3
DHX15	15	0,50	-0,16	0,08	0,39	0,81	-0,05	21,1
HNRNPH1	13	0,49	0,00	0,42	0,31	0,55	-0,11	37,7
SART1	6	0,49	NaN	NaN	-0,19	NaN	NaN	9,9
MYBBP1A	15	0,48	0,25	NaN	0,16	1,62	NaN	15
EHD2	9	0,48	-0,07	NaN	0,24	-0,36	NaN	20,4
EBNA1BP2	5	0,48	0,01	NaN	0,29	1,28	NaN	18
S100A10	3	0,48	NaN	NaN	0,48	NaN	NaN	45,4
FRG1	3	0,48	-0,14	NaN	0,54	0,70	NaN	35,3
HNRNPA0	3	0,48	-0,23	NaN	0,18	0,40	NaN	12,8
HP1BP3	3	0,48	NaN	NaN	0,29	NaN	NaN	10,7
PCBP2;PCBP3	6	0,47	-0,23	0,26	0,36	0,61	0,18	28,2
CCDC86	3	0,46	-0,29	NaN	0,29	2,04	NaN	11,9
RRP1	1	0,45	NaN	NaN	0,09	NaN	NaN	2,8
HNRNPH2	7	0,45	NaN	0,42	0,14	NaN	0,15	22
MRT04	8	0,45	NaN	NaN	0,14	NaN	NaN	29,7
RPSA;RPSAP58	5	0,43	-0,03	NaN	0,12	0,96	NaN	31,6
BCLAF1	16	0,43	0,75	0,14	0,24	-0,57	-0,14	23,9
DDX6	2	0,42	0,68	NaN	0,27	0,70	NaN	7,9

USP10	8	0,41	-0,11	NaN	0,26	1,32	NaN	13,9
UPF1	9	0,41	-0,02	NaN	0,31	0,26	NaN	12
DHX30	24	0,41	0,07	0,12	0,15	0,50	-0,24	26,8
SRSF1	11	0,40	0,01	0,52	0,21	0,40	-0,27	41,5
POLR2H	1	0,38	NaN	NaN	0,20	NaN	NaN	8,8
PRPF3	1	0,38	0,01	0,11	0,47	0,52	-0,33	2,6
CPSF6	4	0,37	NaN	0,77	0,30	NaN	-0,09	11,7
HNRNPA1;HNRNPA	21	0,37	-0,09	0,53	0,25	1,12	0,13	60,3
GATAD2B;GATAD2	2	0,37	NaN	NaN	0,47	NaN	NaN	6,1
FXR1	12	0,36	-0,12	0,29	0,19	0,88	0,16	37,4
SRRT	6	0,36	NaN	0,94	0,34	NaN	-0,78	9,5
SF3B2	16	0,36	-0,32	0,23	0,25	0,94	-0,12	25,9
EZR	7	0,35	NaN	NaN	-0,29	NaN	NaN	13,1
DHX9	30	0,35	-0,18	0,62	0,21	1,12	-0,04	29,2
RCL1	4	0,35	NaN	0,99	0,09	NaN	0,19	13,7
HSPA8	25	0,34	-0,29	0,64	0,14	0,50	0,11	40,4
HSPA5	14	0,34	-0,20	-0,30	-0,18	0,06	-0,43	26,3
ATXN2L	17	0,34	-0,35	NaN	0,18	2,18	NaN	21,4
SNRPA	3	0,34	-0,31	NaN	0,18	1,31	NaN	42,5
MTA2	4	0,34	-0,20	NaN	0,36	0,65	NaN	8,8
AP2A1	7	0,34	-0,14	NaN	0,01	0,50	NaN	8,4
SKIV2L2	4	0,34	NaN	NaN	-0,06	NaN	NaN	4,4
PRRC2C	8	0,33	-0,03	NaN	0,17	0,78	NaN	6,3
TFAM	8	0,33	-0,19	0,12	0,32	0,70	0,00	31,7
CAPZB	4	0,33	-0,12	NaN	0,14	0,72	NaN	26,2
DAZAP1	2	0,32	NaN	NaN	0,02	NaN	NaN	11
EIF4E	3	0,32	NaN	NaN	0,15	NaN	NaN	13,1
CAD	3	0,32	0,34	NaN	-0,56	0,61	NaN	1,6
NUFIP2	9	0,31	-0,09	NaN	0,11	1,13	NaN	23,7
EIF5B	33	0,31	-0,61	0,27	0,28	1,19	-0,50	33,9
FXR2	8	0,30	-0,50	NaN	0,17	1,11	NaN	14,7
EXOSC7	2	0,30	0,39	NaN	0,12	0,74	NaN	9,6
IARS	11	0,30	0,17	NaN	0,10	0,20	NaN	11
PABPN1	4	0,30	-0,17	1,15	0,32	1,35	0,12	17
SLC25A1	2	0,30	0,20	NaN	0,18	0,20	NaN	7,4
C14orf166	6	0,30	-0,16	0,14	0,21	1,02	0,04	35,2
SNRPD1	2	0,30	0,33	0,32	0,44	0,27	0,15	20,2
IQGAP1	6	0,29	NaN	NaN	0,31	NaN	NaN	4,8
C9orf114	1	0,28	NaN	NaN	0,11	NaN	NaN	3,6
SNRPN;SNRNPB	3	0,28	0,29	1,12	-0,01	-0,61	0,52	9,5
SMNDC1	2	0,28	NaN	NaN	0,38	NaN	NaN	13,9
SPATS2L	5	0,28	NaN	-0,03	0,65	NaN	-0,07	14,9
HNRNPM	31	0,27	-0,30	0,49	0,14	1,23	-0,10	53,7
PABPC4	25	0,27	-0,03	-0,12	0,18	0,59	0,22	39,5
YTHDF2	2	0,26	NaN	NaN	0,19	NaN	NaN	9,5
CAPRIN1	12	0,26	-0,09	-0,02	0,20	1,25	0,13	23,4
PLBD2	2	0,26	NaN	NaN	-4,59	NaN	NaN	4,1
RTCB	14	0,26	-0,06	0,22	0,17	1,06	0,15	39,4
THRAP3	15	0,26	0,75	0,23	0,11	-0,79	0,70	26,7
HNRNPAB	6	0,25	-0,12	0,50	0,13	1,04	0,23	25,4
BSL	7	0,25	-0,17	NaN	0,00	0,76	NaN	22
UBTF	10	0,25	-0,49	NaN	0,42	1,66	NaN	18,1
DDX3X;DDX3Y	26	0,25	-0,11	0,15	0,14	0,67	0,13	47,6
SF3B1	17	0,25	-0,34	0,19	-0,30	1,06	-0,62	19
PURA	2	0,24	NaN	NaN	0,13	NaN	NaN	5,6
MRPL12	4	0,24	NaN	NaN	-0,07	NaN	NaN	7,7
G3BP2	15	0,23	-0,26	0,09	0,17	1,33	-0,29	37,3
CHD4	10	0,23	-0,26	1,12	-0,13	1,47	0,27	6,9
EMG1	2	0,23	NaN	NaN	0,44	NaN	NaN	11,5
BMS1	5	0,22	NaN	0,05	0,30	NaN	-0,05	5,1
	5	0,22	NaN	NaN	-3,67	NaN	NaN	19,5
PRPF4	3	0,22	NaN	NaN	0,50	NaN	NaN	7,3
HNRNPL	17	0,21	0,33	0,38	0,10	-0,07	0,18	45
PCBP3	4	0,21	NaN	NaN	-0,04	NaN	NaN	15,8
NACA;NACAP1	2	0,21	NaN	0,32	0,00	NaN	-0,84	39,4
AIMP1	2	0,20	NaN	NaN	0,08	NaN	NaN	9,6
EWSR1	5	0,20	0,19	NaN	-0,12	1,99	NaN	14,6
RBM17	3	0,20	-0,41	NaN	0,13	0,75	NaN	9,7
PTBP1	16	0,20	0,11	0,18	0,11	0,44	0,06	43,7
FAM98B	5	0,20	NaN	NaN	-0,06	NaN	NaN	26,1



DDX1	14	0,20	-0,01	0,12	0,19	0,87	0,05	25,6
AP2M1	5	0,19	-0,39	NaN	0,04	0,12	NaN	16,4
PTRF	11	0,19	-0,78	0,01	0,27	1,58	-0,08	34,6
DDX47	7	0,18	-0,37	NaN	0,14	1,33	NaN	22
STRAP	6	0,18	-0,40	NaN	-0,12	0,71	NaN	24,6
LRRC59	6	0,18	-0,38	0,42	0,17	1,03	-0,40	26,4
SRSF2	4	0,18	NaN	0,25	0,12	NaN	-0,58	36,9
SNRNP70	6	0,18	-0,21	0,37	0,18	0,90	-0,48	17,4
SRSF3	7	0,17	0,07	0,36	0,10	0,46	-0,03	41,5
DDX56	1	0,17	NaN	NaN	0,01	NaN	NaN	7,6
DDX17	29	0,17	0,13	0,37	0,13	0,29	0,04	45
TRIM28	5	0,17	NaN	NaN	0,01	NaN	NaN	10,2
EIF4G1	23	0,17	-0,15	-0,08	0,06	0,42	-0,09	21,4
G3BP1	21	0,16	-0,14	0,03	0,12	1,23	-0,01	54,9
PABPC1;PABPC3	27	0,16	0,15	-0,12	0,10	0,38	0,07	45
IGF2BP3	16	0,16	-0,02	NaN	0,28	0,33	NaN	34
FEN1	1	0,16	NaN	NaN	-0,03	NaN	NaN	9,7
ACOT9	2	0,15	NaN	NaN	0,25	NaN	NaN	4,1
RPL38	5	0,15	0,42	0,27	0,17	-1,08	-0,71	54,3
FAM98A	5	0,15	-0,02	NaN	0,14	0,77	NaN	14,3
TRMT112	2	0,15	NaN	NaN	-0,55	NaN	NaN	23,6
CSDE1	4	0,15	NaN	NaN	-0,03	NaN	NaN	4,8
YBX3	14	0,15	0,16	-0,10	0,00	0,14	-0,36	51,3
MBNL1;MBLL;MBN	2	0,15	NaN	NaN	-0,20	NaN	NaN	6,3
RPL22	5	0,15	-0,28	0,04	0,17	0,60	-0,22	41,4
LYAR	3	0,14	NaN	NaN	0,30	NaN	NaN	12,4
MRPS5	2	0,14	NaN	NaN	0,22	NaN	NaN	6
RIOK1	8	0,13	0,80	NaN	0,17	-1,02	NaN	17,1
PRPS2	18	0,13	0,96	NaN	-0,66	-0,91	NaN	56,9
CKAP4	16	0,13	0,16	0,26	0,14	0,19	0,09	38,2
DDX5	32	0,13	0,05	0,13	0,12	0,43	0,06	44,6
FAM120A	13	0,13	0,15	0,01	0,05	0,23	-0,52	16,5
RPL10	15	0,12	NaN	NaN	-0,09	NaN	NaN	63,2
ENO1	2	0,12	-0,89	NaN	-0,41	0,34	NaN	5,8
YBX1	14	0,12	-0,12	0,00	0,12	0,79	0,01	52,8
SYNCRIP	29	0,12	0,10	0,32	0,05	0,24	0,12	44,9
GNL3	10	0,11	-0,45	NaN	-0,01	1,38	NaN	23,5
MRPS34	5	0,11	-0,35	NaN	-0,04	0,29	NaN	25
TOP1	24	0,11	-0,29	0,31	0,23	1,19	-0,51	34,5
MAP7D1	3	0,11	NaN	NaN	-0,12	NaN	NaN	5
KTN1	7	0,11	NaN	-0,07	-0,07	NaN	-0,54	7
HNRNPF	9	0,11	-0,03	0,28	0,16	0,24	-0,15	31,3
RPS27	5	0,10	-0,48	-0,01	-0,06	0,68	-0,80	40,5
MSN	12	0,10	-0,59	NaN	-0,17	-0,33	NaN	28,1
NOP16	4	0,10	NaN	NaN	-0,02	NaN	NaN	31,3
EIF3I	7	0,10	0,63	NaN	-0,04	-0,25	NaN	31,4
FGF2	1	0,09	NaN	NaN	0,04	NaN	NaN	3,5
NUDT21	6	0,09	0,01	0,46	0,23	0,81	0,07	26,4
ILF3	24	0,09	-0,25	0,33	0,06	0,97	0,03	31,7
GRSF1	5	0,08	NaN	NaN	-0,04	NaN	NaN	14,1
MRPS27	4	0,08	NaN	NaN	-0,16	NaN	NaN	13,1
XRN2	8	0,08	0,67	-0,13	-0,16	-0,46	0,04	11,1
EIF2AK2	5	0,08	NaN	NaN	0,09	NaN	NaN	10,2
ILF2	12	0,08	-0,20	0,52	0,08	1,07	0,00	43,2
XRCC5	29	0,08	-0,18	0,14	0,05	0,80	-0,06	41,9
CLNS1A	4	0,07	1,18	0,19	-0,39	-1,25	-0,16	25,7
HNRNPUL1	14	0,07	0,61	-0,31	-0,17	-0,29	0,16	20
QARS	5	0,07	-0,46	NaN	-0,20	-0,22	NaN	8,6
KHDRBS1	8	0,07	0,54	0,05	0,04	-0,56	0,05	23
HLTF	2	0,06	NaN	NaN	-1,24	NaN	NaN	3
RBM3	2	0,06	0,09	0,30	0,06	0,74	-0,01	21
NPM3	3	0,06	-0,56	0,32	-0,04	1,00	0,05	29,2
XRCC6	27	0,06	-0,19	0,08	0,03	0,58	0,01	45,3
HNRNPK	23	0,06	0,66	0,02	-0,01	-0,50	0,05	59
MRPS7	4	0,05	0,09	NaN	-0,02	-0,57	NaN	18,8
DDX24	3	0,05	0,05	NaN	-0,25	1,23	NaN	4
ABCF2	1	0,05	NaN	NaN	0,07	NaN	NaN	6,2
DARS	9	0,05	0,38	0,14	-0,02	0,00	0,14	20,6
LRPPRC	75	0,05	1,09	-0,10	0,09	-0,73	0,47	54,6
SRSF6	8	0,05	0,48	0,18	0,10	0,36	-0,07	20,6

FAU	3	0,05	0,13	-0,14	0,12	-0,18	-0,27	12,2
BOLA2	3	0,04	0,76	NaN	-0,08	-0,87	NaN	51,2
PRP51	18	0,04	0,93	NaN	-0,43	-1,00	NaN	51,6
EIF3H	3	0,04	0,21	NaN	-0,12	-0,23	NaN	12,6
RPS18	17	0,04	0,07	-0,10	0,01	0,13	-0,08	65,1
HNRNPDP	18	0,04	0,08	0,39	0,02	0,49	0,03	44,5
SRPK1	4	0,04	NaN	NaN	0,04	NaN	NaN	8,1
AHNAK	6	0,03	-0,42	NaN	0,41	0,32	NaN	5,7
RPS25	10	0,03	0,13	0,08	0,12	0,10	-0,12	37,6
NPM1	11	0,03	-0,12	0,27	0,00	0,56	0,14	39,1
EXOSC4	3	0,03	NaN	NaN	0,10	0,59	NaN	14,7
PSMD4	2	0,03	0,45	0,08	-0,16	-0,65	0,08	16,3
RPS12	8	0,02	0,17	0,07	0,00	0,22	0,14	54,5
LARP1	15	0,02	0,26	NaN	-0,08	-0,04	NaN	19,5
RPS17L;RPS17	8	0,02	0,01	0,08	0,07	0,40	-0,05	59,3
SLIRP	8	0,02	1,28	-0,12	0,06	-0,93	0,48	78,9
CDKN2AIP	3	0,02	NaN	NaN	-0,05	NaN	NaN	8,8
POLR2A	3	0,02	NaN	NaN	-0,06	NaN	NaN	1,9
DIMT1	2	0,01	NaN	NaN	-0,28	NaN	NaN	18,2
FLNA	84	0,01	0,40	-0,09	-0,13	-0,78	0,81	42,5
IGF2BP1	11	0,01	-0,11	NaN	0,25	0,35	NaN	24,4
ABCF1	21	0,01	-0,28	0,23	0,05	0,42	-0,35	25,3
MCM5	7	0,01	NaN	NaN	-0,06	NaN	NaN	13,2
RARS	7	0,01	0,04	NaN	0,01	0,40	NaN	11,1
ASCC3	3	0,01	NaN	NaN	-0,09	NaN	NaN	1,6
RPS27A	5	0,01	0,36	-0,14	0,09	0,20	-0,05	42,3
C7orf50	5	0,01	NaN	NaN	-0,25	NaN	NaN	24,1
AP2B1	6	0,00	-0,06	0,27	0,16	0,35	0,05	7,6
RPS9	16	0,00	0,26	0,00	-0,02	0,02	0,08	45,9
RPL35	7	-0,01	0,17	-0,03	0,02	-0,12	0,06	38,2
RPL17;RPL17-C18o	11	-0,01	0,03	0,03	-0,02	-0,04	0,01	58,6
PRPF19	6	-0,01	-0,02	0,27	0,14	0,43	0,06	21,8
RPS3	22	-0,01	0,16	-0,06	-0,04	0,08	-0,12	74,1
MAP4	19	-0,01	0,39	-0,16	-0,18	-0,62	-0,42	11,8
DNAJC7	1	-0,01	NaN	NaN	-0,20	NaN	NaN	3
TFB1M	3	-0,01	NaN	NaN	-0,56	NaN	NaN	10,4
RFC4	1	-0,01	NaN	NaN	-0,05	NaN	NaN	7,3
IK	2	-0,01	NaN	NaN	0,17	NaN	NaN	3,8
NSUN2	16	-0,01	-0,02	NaN	-0,04	0,22	NaN	30
SNRPD3	3	-0,01	0,87	0,24	-0,02	-0,95	-0,15	31,7
OTUD4	15	-0,01	0,96	-0,07	-0,35	-1,09	-0,18	17,9
RPS20	7	-0,01	0,23	-0,02	-0,06	-0,16	0,03	38,7
RPS15A	8	-0,01	0,13	-0,01	-0,03	0,17	-0,05	55,4
RPS15	5	-0,02	0,15	-0,13	-0,04	0,37	-0,15	67,9
RPL39P5;RPL39	1	-0,02	0,36	0,00	-0,04	0,36	0,11	19,6
RPS23	6	-0,03	-0,03	0,00	-0,05	0,27	-0,11	30,1
RPS16;ZNF90	12	-0,03	0,00	0,01	-0,01	0,26	-0,09	57,5
RPS28	4	-0,03	NaN	NaN	-0,14	NaN	NaN	50,7
EIF2S2	19	-0,03	0,40	NaN	-0,04	-0,36	NaN	54,4
RPS10;RPS10-NUD	8	-0,04	0,05	0,11	-0,05	0,18	-0,08	46,1
RCC2	16	-0,04	-0,16	0,33	-0,13	0,39	-0,88	33,3
HDLBP	6	-0,04	NaN	-0,13	-0,10	NaN	0,26	7,6
RPS3A	21	-0,04	0,24	-0,01	-0,01	0,09	-0,01	71,6
TRIM25	10	-0,04	NaN	NaN	0,00	NaN	NaN	16,8
EIF3A	28	-0,04	0,41	0,45	-0,15	-0,50	0,00	24,3
SERBP1	22	-0,05	0,33	-0,12	-0,10	-0,36	0,15	58,6
RPS26;RPS26P11	3	-0,05	0,05	-0,08	0,00	0,22	-0,11	31,3
RPS14	11	-0,05	0,18	-0,01	-0,03	0,35	-0,10	43
GPATCH4	5	-0,05	NaN	NaN	0,16	NaN	NaN	22,4
RPS11	14	-0,05	0,13	-0,01	-0,02	0,08	0,06	59,5
RPL11	8	-0,05	0,20	-0,02	-0,09	-0,16	-0,02	45,5
RPS5	11	-0,05	0,07	-0,25	-0,06	0,36	-0,17	47,5
RPS19	12	-0,05	0,22	0,00	-0,08	-0,06	-0,01	57,9
KCTD5	10	-0,05	0,90	-0,13	0,01	-0,94	-0,37	60,7
DRG1	7	-0,05	NaN	NaN	-0,08	NaN	NaN	24
RPS4X	27	-0,06	0,21	-0,03	-0,05	-0,04	-0,05	73,8
MCM3	13	-0,06	NaN	NaN	-0,02	NaN	NaN	20,2
RPL27A	6	-0,06	0,07	0,05	-0,01	0,11	0,04	43,5
RPS2	15	-0,06	0,10	-0,15	-0,04	0,09	-0,05	48,5
ZC3H4	2	-0,06	NaN	NaN	-0,20	NaN	NaN	3,6

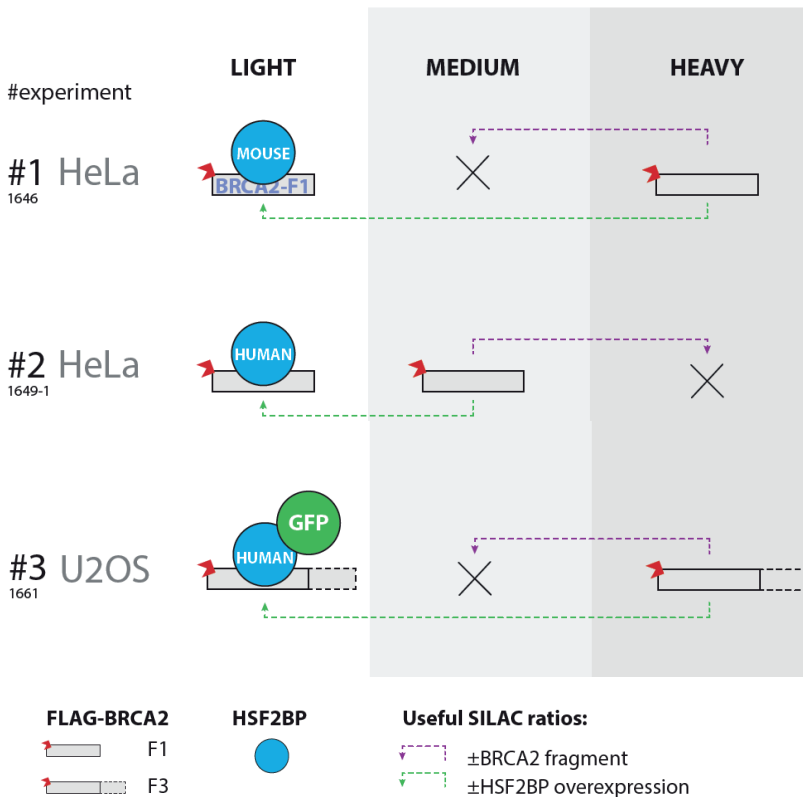


RPL24	7	-0,06	0,18	0,00	-0,05	-0,14	0,10	42,1
HNRNPU	32	-0,06	0,00	0,32	0,01	0,41	0,10	43,3
PRPF31	13	-0,06	0,82	NaN	-0,32	-0,81	NaN	35,9
RPL26;RPL26L1	13	-0,06	0,50	-0,05	-0,09	-0,20	-0,01	49,7
TCEB3	3	-0,06	NaN	NaN	-0,04	NaN	NaN	4,8
RPL23	10	-0,07	-0,16	0,02	-0,10	0,32	-0,32	53,6
RPL14	7	-0,07	0,20	0,02	-0,03	-0,23	0,09	32,1
RPS13	13	-0,07	0,23	0,01	-0,05	0,09	0,01	56,3
RPS29	3	-0,07	0,43	0,01	-0,03	-0,44	0,04	48,2
RPL36A;RPL36A-HN	9	-0,07	NaN	NaN	-0,12	NaN	NaN	35,9
RPL13A;RPL13a	13	-0,07	0,26	0,00	-0,10	-0,28	0,09	46,3
TBL2	2	-0,07	NaN	0,03	-0,28	NaN	0,19	6,1
RPS6	11	-0,08	0,32	-0,02	-0,04	-0,49	-0,02	32,5
RPL23A	14	-0,08	0,17	-0,03	-0,08	0,06	0,04	52,6
TSR1	15	-0,08	NaN	NaN	-0,07	NaN	NaN	23,6
SRSF5	4	-0,08	NaN	NaN	0,02	NaN	NaN	15,1
EIF2S1	14	-0,08	-0,56	0,01	-0,05	0,51	-0,53	47,6
EIF3C;EIF3CL	17	-0,08	0,21	0,06	-0,11	-0,24	0,01	20,7
PHF6	7	-0,08	NaN	NaN	-0,05	NaN	NaN	27,4
RPL30	7	-0,08	0,33	-0,08	-0,01	-0,28	0,06	66,1
EIF3G	4	-0,08	0,31	-0,75	-0,04	0,03	-0,24	20,9
LGALS3	7	-0,08	0,55	-0,34	-0,29	-1,03	-0,06	32,4
GRWD1	6	-0,08	NaN	NaN	-0,16	NaN	NaN	17,9
RPL31	8	-0,09	0,14	-0,10	-0,08	-0,03	0,10	45,6
RPL10A	11	-0,09	0,25	-0,05	-0,09	-0,32	0,09	41
IKBIP	1	-0,09	NaN	NaN	-0,05	NaN	NaN	3,4
RPL18A	13	-0,09	0,25	0,02	-0,03	-0,58	0,11	53,9
RPLP1	3	-0,09	0,36	0,21	-0,04	-0,45	0,18	66,7
RPS7	14	-0,09	0,05	-0,11	-0,14	0,11	-0,27	62,4
RPL21	8	-0,09	0,06	0,05	-0,04	-0,16	0,15	43,8
RPL5	15	-0,09	0,09	0,01	-0,12	-0,26	-0,27	43,8
RPL3	25	-0,09	0,21	-0,10	-0,04	-0,38	0,06	49,6
EIF2S3;EIF2S3L	19	-0,10	0,15	-0,07	-0,05	-0,08	0,14	48,7
RPL15	12	-0,10	0,31	0,02	-0,07	-0,28	0,00	48
PA2G4	15	-0,10	NaN	NaN	-0,24	NaN	NaN	41,6
PNO1	2	-0,10	NaN	NaN	0,22	NaN	NaN	22,1
RPS24	5	-0,10	0,01	-0,05	-0,01	0,15	-0,12	35,9
RPL32	13	-0,10	0,20	-0,05	-0,06	-0,32	0,06	51,1
EIF2A	12	-0,10	NaN	NaN	-0,18	NaN	NaN	28,5
ZNF131	1	-0,10	NaN	NaN	-0,13	NaN	NaN	2,1
RPL35A	8	-0,10	0,53	-0,05	-0,09	-0,69	0,07	47,3
RPL10	17	-0,11	0,23	-0,01	-0,04	-0,28	0,12	55,6
RPL12	6	-0,11	0,41	-0,04	-0,08	-0,59	-0,07	54,5
RPL9	13	-0,11	0,11	-0,03	-0,06	-0,04	0,06	62
RPL18	8	-0,11	0,33	-0,09	-0,09	-0,24	-0,04	42,1
CCAR2	11	-0,11	0,68	0,16	-0,02	-0,62	-0,09	13,3
RPL28	14	-0,11	0,43	-0,07	-0,07	-0,42	0,08	59,1
WIBG	2	-0,11	NaN	NaN	-0,04	NaN	NaN	18,1
RPL6	20	-0,11	0,27	-0,06	-0,09	-0,44	0,01	51,7
EIF3E	7	-0,11	NaN	NaN	-0,23	NaN	NaN	18,4
RPL4	30	-0,11	0,26	-0,03	-0,08	-0,20	0,08	50,8
RPL19	9	-0,11	0,34	-0,14	-0,06	-0,25	0,07	28
POP1	2	-0,12	NaN	NaN	-0,09	NaN	NaN	3,3
RPS8	13	-0,12	0,16	-0,07	-0,12	-0,14	-0,04	59,1
RPL13	14	-0,12	0,46	-0,04	-0,09	-0,62	0,04	47,9
MRPL11	4	-0,12	NaN	NaN	-0,02	NaN	NaN	21,9
EEF1G	15	-0,12	0,19	0,17	-0,01	-0,45	0,00	35,2
RPL7	19	-0,13	0,26	-0,11	-0,09	-0,23	0,04	49,2
COPA	4	-0,13	NaN	NaN	-0,01	NaN	NaN	3,4
CCDC124	3	-0,13	NaN	NaN	-0,33	NaN	NaN	14,8
RPL7A	21	-0,13	0,20	-0,08	-0,07	-0,32	0,02	46,6
RPLP2	10	-0,13	0,49	-0,11	-0,10	-0,65	-0,09	95,7
MAP1B	34	-0,13	0,72	0,06	-0,40	-1,63	-0,16	22,7
CPSF7	4	-0,13	NaN	NaN	0,23	NaN	NaN	12,3
IFI16	7	-0,13	-0,36	NaN	-0,26	0,13	NaN	11,3
KCTD17	2	-0,14	NaN	-0,62	-0,13	NaN	-0,58	12,3
RPL8	13	-0,14	0,34	-0,01	-0,11	-0,57	-0,03	60,7
MRPS23	5	-0,14	-0,20	NaN	-0,11	0,71	NaN	26,8
ZC3H15	4	-0,14	NaN	NaN	-0,11	NaN	NaN	14,8
EIF3F	6	-0,14	NaN	NaN	-0,21	NaN	NaN	22,7

RPL37A	5	-0,14	0,19	NaN	-0,10	-0,44	NaN	58,8
CKAP5	8	-0,14	NaN	0,07	-0,08	NaN	0,17	6,9
RPL27	8	-0,15	0,28	-0,06	-0,10	-0,06	-0,02	49,3
KCTD2	4	-0,15	1,04	-0,39	-0,07	-1,48	-0,94	27
WDR5	2	-0,15	0,16	NaN	-0,07	-0,07	NaN	12
EEF1E1;EEF1E1-BLC	2	-0,15	NaN	NaN	-0,26	NaN	NaN	13,2
RPL36	7	-0,15	0,44	-0,10	-0,06	-0,57	0,08	34,3
EPRS	11	-0,15	0,87	NaN	-0,05	-0,73	NaN	11,3
RPLP0	15	-0,16	0,35	-0,13	-0,10	-0,50	-0,09	63,4
EIF3B	11	-0,16	1,03	0,07	-0,02	-0,85	0,77	18,2
RPL34	8	-0,16	NaN	-0,10	-0,10	NaN	-0,13	38,5
RPL29	3	-0,16	0,26	-0,19	-0,08	-0,50	-0,26	15,1
MAP4K4;MINK1	3	-0,16	NaN	NaN	0,27	NaN	NaN	2,9
NCL	30	-0,16	0,26	0,14	-0,13	-0,21	-0,28	36,3
EIF3M	6	-0,16	-0,06	-0,31	-0,14	0,02	-0,48	24,1
EEF1B2	2	-0,16	0,08	NaN	-0,04	-0,57	NaN	17,3
RBM10	31	-0,17	0,88	0,05	-0,14	-0,82	-0,01	30,1
SSB	4	-0,17	NaN	NaN	-0,39	NaN	NaN	10,8
C11orf98	2	-0,17	NaN	NaN	0,05	NaN	NaN	21,1
MTDH	5	-0,17	NaN	NaN	-0,30	NaN	NaN	10,7
ARHGEF2	3	-0,17	NaN	NaN	-0,35	NaN	NaN	4,3
EEF1D	9	-0,18	0,42	0,03	-0,18	-1,05	0,34	44,4
EIF3D	5	-0,18	0,08	-0,22	-0,23	-0,29	-0,19	8,9
PRPSAP1	14	-0,18	0,93	NaN	-0,50	-0,99	NaN	52,2
TMCO1	1	-0,19	NaN	NaN	0,51	NaN	NaN	14,4
EIF3L	13	-0,19	0,01	NaN	-0,15	-0,24	NaN	25,2
EXOSC5	2	-0,19	NaN	NaN	0,15	NaN	NaN	10,2
DAP3	1	-0,19	0,45	NaN	-0,22	-0,62	NaN	33,3
EXOSC10	3	-0,19	NaN	NaN	0,21	NaN	NaN	4
RBBP4;RBBP7	6	-0,20	-0,21	NaN	-1,64	-0,36	NaN	23,5
ASPH	7	-0,20	-0,04	NaN	-0,03	-0,61	NaN	9,9
SMCHD1	9	-0,20	NaN	-0,12	-0,08	NaN	0,29	6,7
NAP1L1	5	-0,20	0,04	NaN	-0,37	-0,42	NaN	29,3
HSD17B10	15	-0,21	NaN	-0,27	-0,10	NaN	0,16	71,6
MOGS	1	-0,21	NaN	NaN	-0,08	NaN	NaN	1,4
RFC3	4	-0,21	NaN	-0,04	0,02	NaN	-0,24	14,6
SRP9	3	-0,21	0,26	NaN	-0,18	-0,42	NaN	36
WDR77	14	-0,22	1,03	0,02	-0,35	-1,11	-0,11	49,7
UPF3B	2	-0,22	NaN	NaN	0,01	NaN	NaN	5,2
LRRC47	2	-0,22	NaN	NaN	-0,06	NaN	NaN	5
PRMT5	35	-0,22	0,97	-0,02	-0,28	-0,96	-0,10	54,8
SPATS2	1	-0,22	NaN	NaN	-0,07	NaN	NaN	5,1
TMA16	1	-0,22	NaN	NaN	0,07	NaN	NaN	10,4
JAK1	39	-0,22	0,83	NaN	-0,21	-0,74	NaN	44,5
C19orf53	3	-0,23	NaN	NaN	-0,20	NaN	NaN	17,2
TRMT10C	16	-0,23	NaN	-0,85	-0,15	NaN	-0,07	49,9
ALYREF	5	-0,24	-0,11	-0,11	0,00	0,45	-0,50	36,2
SRP14	6	-0,24	0,18	0,06	-0,14	-0,26	0,31	58,8
DHX36	12	-0,25	0,24	NaN	0,00	-0,06	NaN	16,7
KIF2A	6	-0,26	NaN	NaN	-0,12	NaN	NaN	8,8
NOB1	2	-0,28	NaN	NaN	-0,45	NaN	NaN	7,5
GOLGA2	2	-0,28	NaN	NaN	-0,47	NaN	NaN	2,7
STK38	17	-0,29	1,11	-0,34	-0,24	-0,88	-0,07	42,2
EIF4B	24	-0,29	0,79	-0,18	-0,29	-1,02	0,08	42,4
RRBP1	14	-0,30	NaN	-0,17	-0,08	NaN	0,14	21
PPM1B	21	-0,31	1,24	-0,15	-0,33	-1,24	0,24	57,4
QKI	5	-0,32	0,95	-0,49	-0,31	-1,09	-0,73	23,2
ZNF787	2	-0,33	NaN	NaN	-0,49	NaN	NaN	6,5
H1FX	6	-0,34	NaN	-0,10	-0,15	NaN	-0,41	23,5
FRYL	6	-0,34	0,92	NaN	-0,16	-0,62	NaN	2,5
RFC1	4	-0,34	NaN	NaN	-0,06	NaN	NaN	4,8
SPIN1	8	-0,35	0,87	NaN	-0,56	-0,95	NaN	47,3
KIF11	62	-0,36	0,63	-0,36	-0,26	-1,08	-0,47	55,2
ZFP91-CNTF;ZFP91	2	-0,37	NaN	-0,82	0,07	NaN	-1,05	6,4
IVNS1ABP	23	-0,38	1,11	NaN	-0,54	-1,08	NaN	42,5
C11orf84	4	-0,39	0,90	NaN	-0,18	-0,79	NaN	19,2
TXNDC12	9	-0,40	0,70	-0,49	-0,35	-1,01	-0,43	67,4
C8orf33	2	-0,40	0,33	NaN	-0,24	-1,19	NaN	17
NOP56	11	-0,41	-0,66	NaN	0,81	2,63	NaN	21,4
PRPSAP2	12	-0,42	0,97	NaN	-0,79	-0,92	NaN	44,4

PRPF6	1	-0,43	NaN	NaN	-0,31	NaN	NaN	1,6
KARS	3	-0,43	NaN	NaN	-0,18	NaN	NaN	13,3
HEXIM1	2	-0,44	NaN	NaN	-0,19	NaN	NaN	8,6
GEMIN5	2	-0,46	NaN	NaN	-0,15	NaN	NaN	1,6
RPS21	2	-0,48	NaN	NaN	-0,41	NaN	NaN	33,3
NUSAP1	1	-0,53	NaN	NaN	-0,52	NaN	NaN	4,5
TRIM21	28	-0,55	1,30	-0,19	-0,11	-0,99	-0,24	52,4
ZC3HAV1	11	-0,60	NaN	-0,18	-0,13	NaN	0,02	15,9
OASL	5	-1,11	NaN	NaN	0,34	NaN	NaN	12,3
DDX60	3	-1,54	NaN	NaN	-0,45	NaN	NaN	1,9
ANKEF1	1	-5,12	NaN	NaN	-4,68	NaN	NaN	1,2

Three mass-spectrometry experiments (see below) were performed with the FLAG-tagged BRCA2 domain (F1 or F3) produced by transient transfection, and HSF2BP was stably over-produced by the host cell line from PiggyBac integrated construct. Proteins co-immunoprecipitating by anti-FLAG monoclonal antibody (M2) were quantified. The data was purged of contaminants and log₂-transformed. Data was sorted by whether proteins pass a threshold value of 0.4 in all 3 experiments and then by H/M ratio for experiment #1. NaN, not a number. In these cases the protein was not detected in one of the states and no ratio could be calculated.



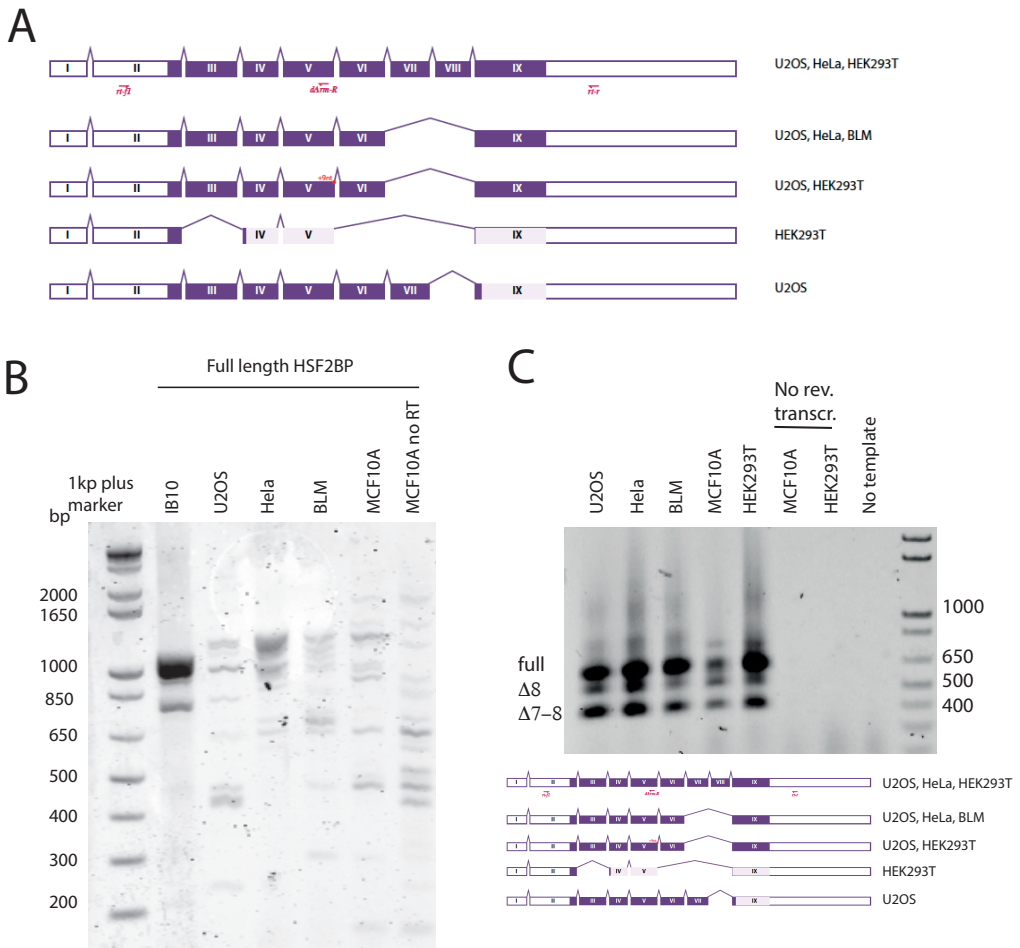


Figure S1 HSF2BP expression in human cell lines

(A) Exon model of the reference human HSF2BP cDNA sequences with the splice variants we identified by sequencing. Amplification of (B) full length (1002 bp) and (C) the 3' end of HSF2BP from cDNA from indicated cell lines. cDNA synthesis reactions without reverse transcriptase enzyme were used as negative controls.

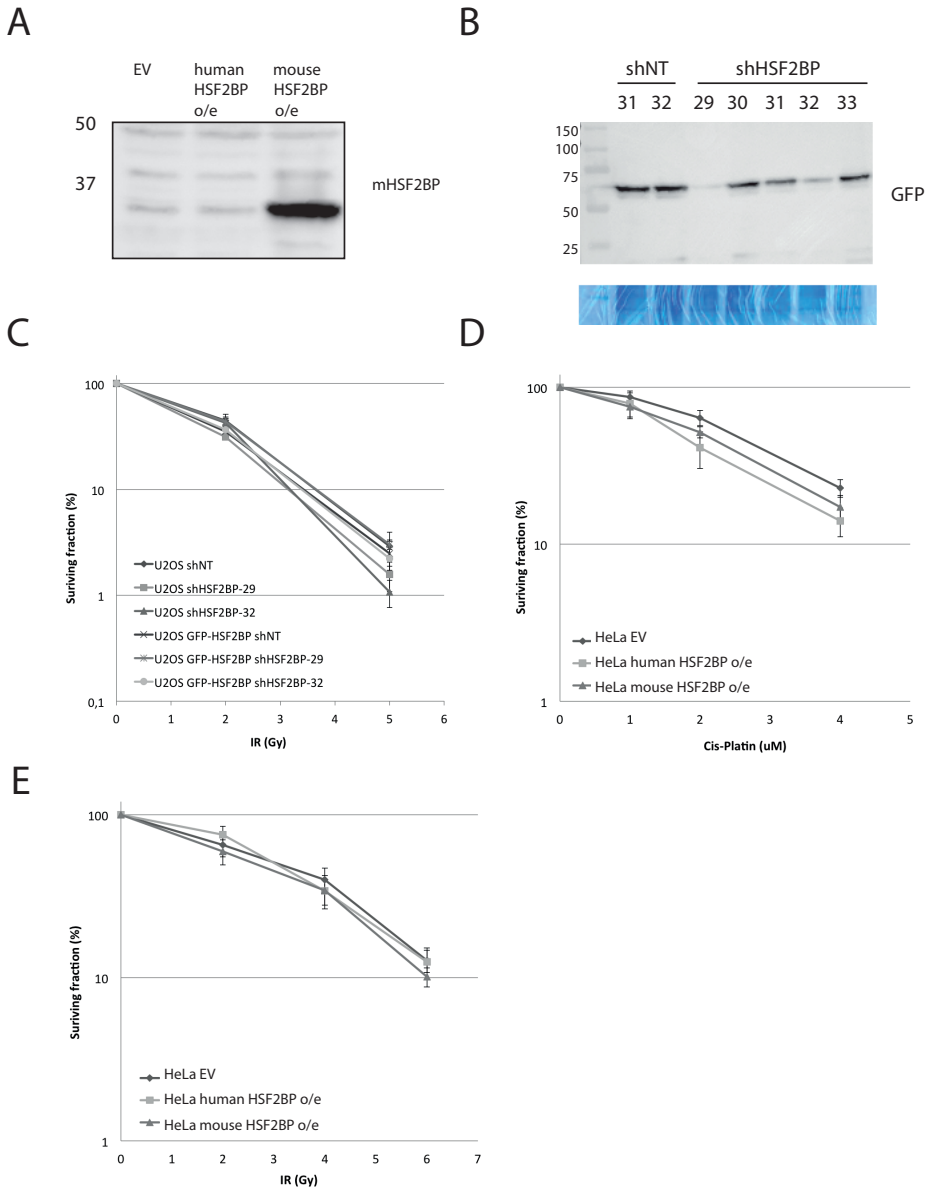


Figure S2 HSF2BP survivals

(A) Immunoblot showing the overexpression of mouse HSF2BP. Overexpression of human HSF2BP is not detectable with this antibody. (B) Immunoblot showing GFP-HSF2BP expression after stable induction with lentivirally delivered shRNAs targeting HSF2BP in U2OS cells. Coomassie stained gel as loading control. (C) Clonogenic survival using ionizing radiation as damaging agent using U2OS cells or U2OS cells stably overexpressing GFP-HSF2BP and stably transduced with a control non-targeting shRNA or shRNA targeting HSF2BP. Data represents mean \pm SD (D) Clonogenic survival on HeLa cells expressing an empty vector or overexpressing mouse or human HSF2BP. Cells were damaged using increasing doses of cisplatin. Data represents mean \pm SD. (E) Clonogenic survival on HeLa cells expressing an empty vector or overexpressing mouse or human HSF2BP. Cells were damaged using ionizing radiation. Data represents mean \pm SD.

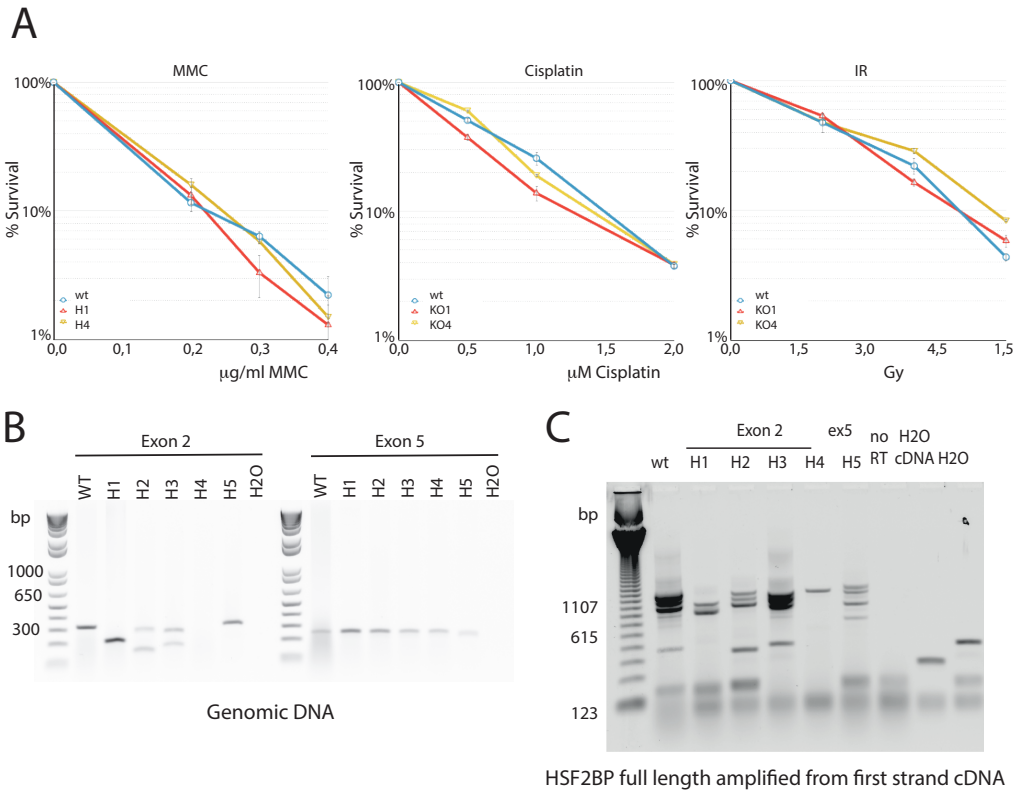


Figure S3 HSF2BP knock-out using CRISPR/Cas9

(A) Clonogenic survival using MMC, cisplatin and ionizing radiation as damaging agents using wild-type HeLa cells or clones (clone H1 and H4) in which HSF2BP is inactivated using the CRISPR/Cas9 system (targeting exon 2). Data represents mean \pm SD (B) PCR on genomic DNA from indicated cell lines. Primers designed to span the gRNA target site in exon 2. PCR conditions were set up such that with integration of the donor, the primers were too far apart to allow amplification across the donor. Smaller bands indicate loss of part of the sequence. (C) Amplification of full length HSF2BP from cDNA from indicated clones. cDNA synthesis reactions without reverse transcriptase enzyme were used as negative controls

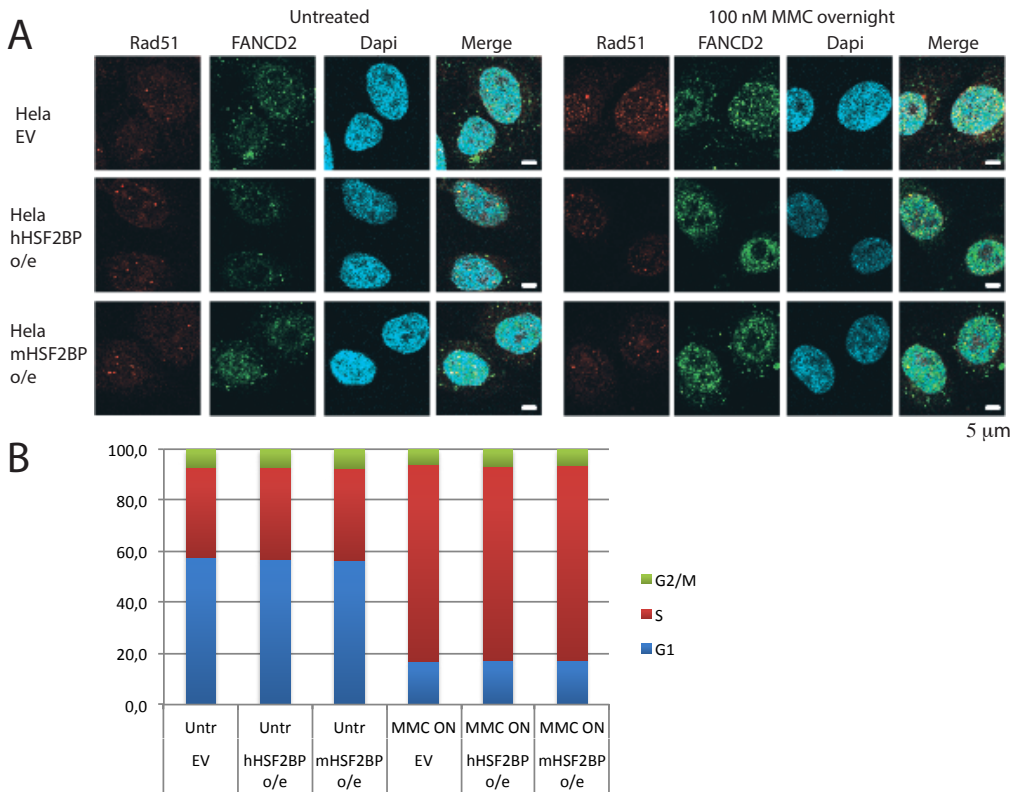


Figure S4 Effects of MMC treatment on Rad51 and FANCD2 foci and cell cycle distribution.

(A) Examples of HeLa cells with an empty vector or overexpressing mouse or human HSF2BP showing Rad51 (Red) and FANCD2 (green) foci after treatment with MMC. Dapi in Blue. Scale bar represents 5 μm. (B) Cell cycle distribution of undamaged HeLa cells expressing an empty vector or overexpressing mouse or human HSF2BP with and without MMC treatment overnight. Cell cycles distribution was analysed by incubating the cells with BrdU. Cells were stained with an anti-BrdU-FITC antibody and PI and analysed by FACS.

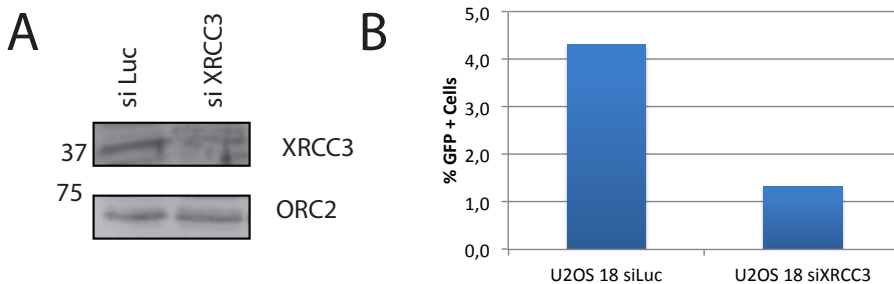
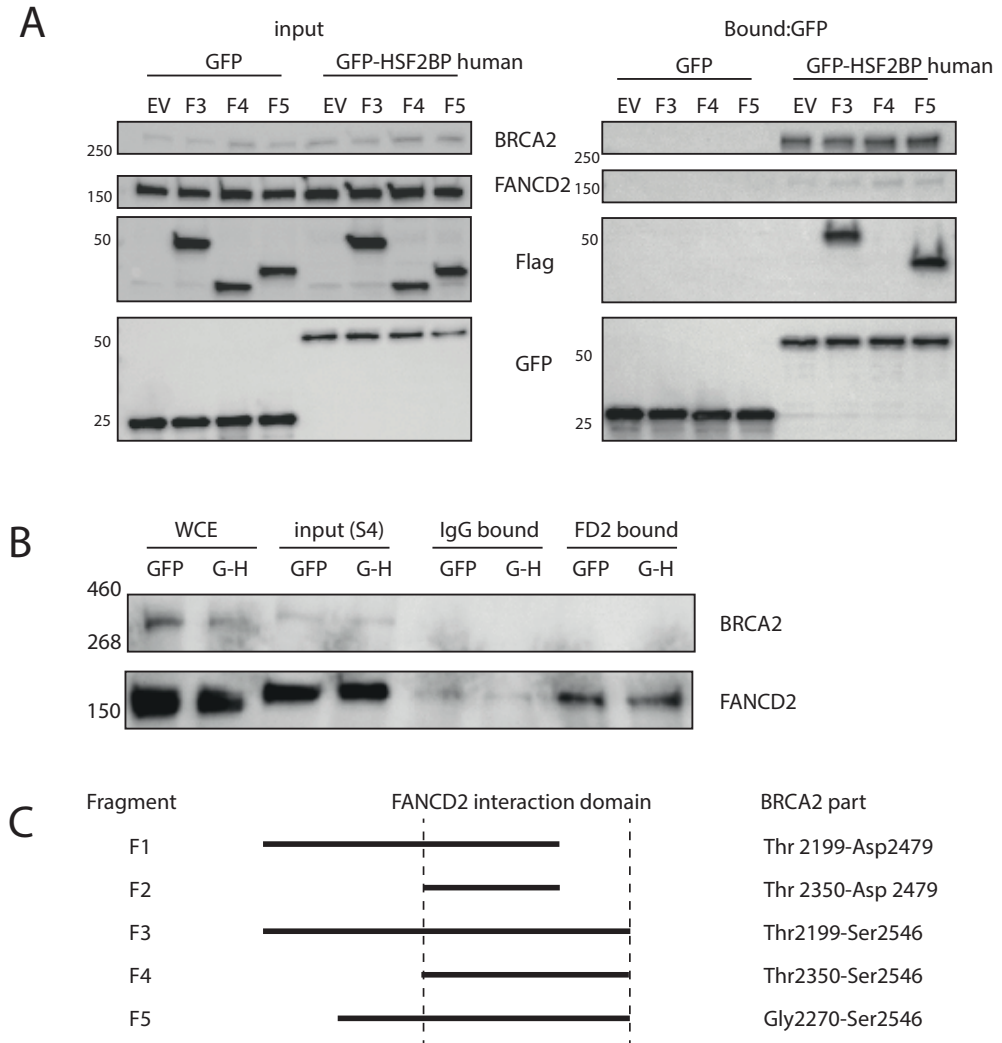


Figure S5 Recombination assay

(A) Immunoblot showing the knock-down of XRCC3. ORC2 was used as a loading control. (B) Recombination experiment in U2OS #18 cells treated with siRNA targeting XRCC3 or luciferase. Data was corrected for transfection efficiency and the number of GFP-positive cells in untransfected cells.

**Figure S6 Mapping the BRCA2-HSF2BP interaction**

(A) HeLa cells stably expressing GFP or GFP-HSF2BP were transiently transfected with a Flag empty vector (EV) or the flag-tagged BRCA2 fragments. Pull-downs were performed using anti-Flag beads. Bound fractions were analysed by immunoblot using indicated antibodies. (B) Fractionation and pull-down of endogenous FANCD2 using a FANCD2 antibody or mouse IgG as a control from HeLa cells stably expressing GFP or GFP-HSF2BP (G-H). Immunoblot using indicated antibodies. (C) Schematic overview of Flag-tagged BRCA2 fragments in table 1.

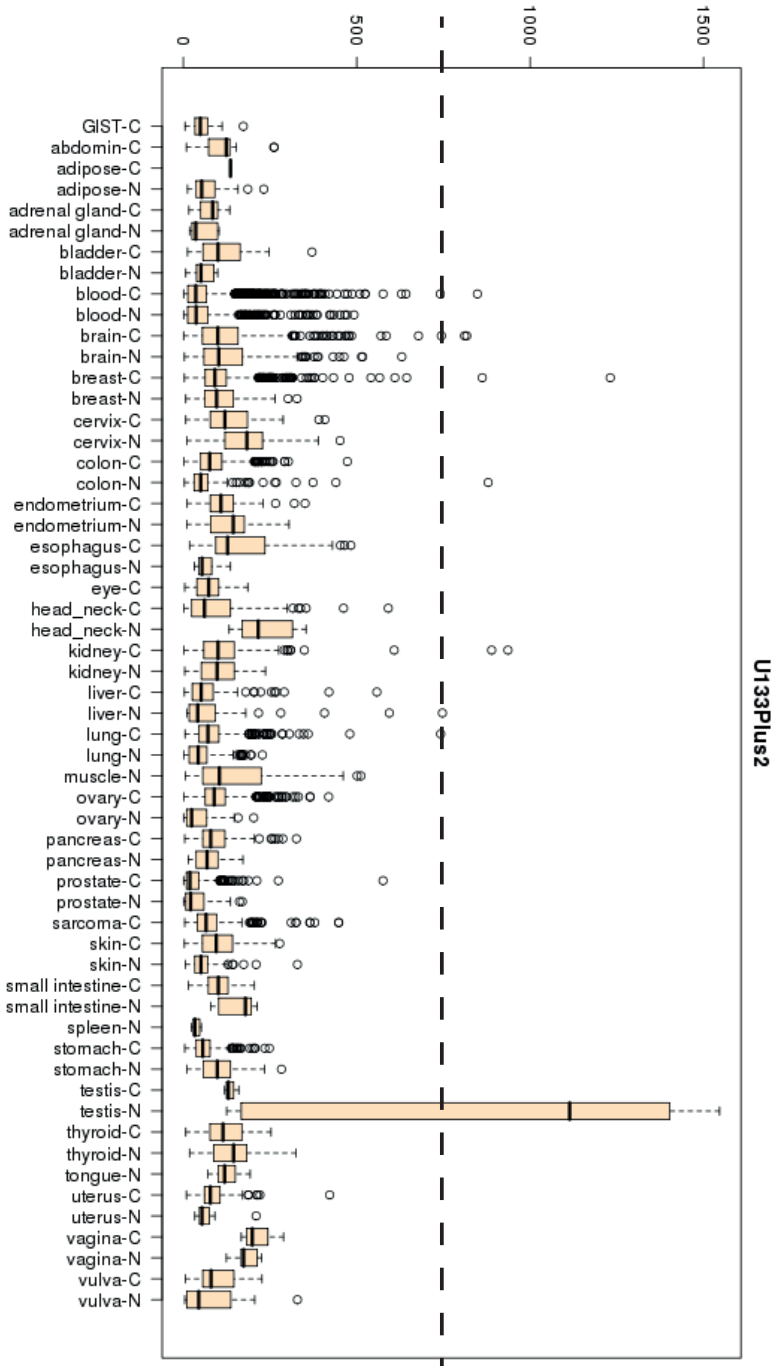


Figure S7 HSF2BP is overexpressed in some human tumours compared to normal tissue

HSF2BP expression levels on microarray in normal and tumour tissue from the GENT (Gene Expression across Normal and Tumour tissue) database. The GENT database contains more than 34000 samples, profiled by Affymetrix U133A or U133plus2 platforms, allowing identification of outliers (value higher than ± 750 , black dashed line) in a subset of patients⁴⁴.

Table S1 Oligonucleotide sequences

HSF2BP-CG-F	gcccaggagctcctggaagacctccgcgcctggactgtaatggtGTGAGCAAGGGCGAGGAGCT
HSF2BP-CG-R	tggaccactggcattttcaccgggctcctggtgtagagcacatctaTGGTCGACCTGCAGGCGGC
HSF2BP-CG-scrF	ggtggtggtgattgtgtca
HSF2BP-CG-scrR	ttcatgcattcaaagggtga
HSF2BP-CG-rtrL	caaagtgagttccaggacagccaaggctacacagagaaacctatctcaACGCGTgcggaaccttattgttat
HSF2BP-CG-rtrR	taaggaatgtgggcaccaagaacaaccagcaagtgttgacttacctctcACGCGTtccagtcgggaacctgtc
HSF2BP-pr5-F	CCAGTGGCCTTTTGCATATT
HSF2BP-pr5-R	TGGGAATGCTAAATGTGTTCA
gRNA-hHe2u-F	TTCTTGGCTTTATATATCTTGTGAAAGGACGAAACACCGCGCCGACGCTCAGGCGAA
gRNA-hHe2u-R	GACTAGCCTTATTTAACTGCTATTCTAGCTCTAAAACCTCGCCTGAGCGTCGGCGCG
gRNA-hHe2d-F	TTCTTGGCTTTATATATCTTGTGAAAGGACGAAACACCGCTGAGGGGAGCGAATGGCGA
gRNA-hHe2d-R	GACTAGCCTTATTTAACTGCTATTCTAGCTCTAAAACCTCGCCATTGCTCCCTCAG
gRNA-hHe5-F	TTCTTGGCTTTATATATCTTGTGAAAGGACGAAACACCGCAGCAGTGAGGAAGTCGTCA
gRNA-hHe5-R	GACTAGCCTTATTTAACTGCTATTCTAGCTCTAAAACCTGACGACTTCCTCACTGCTG
hHe5-surv-F	CAGTTGAATGAAGCGAAGCA
hHe5-surv-R	TGAGTGAACAAAAGAAAATGGAAA
hHe2-surv-F	GAATACTGCGCAAATTCTGG
hHe2-surv-R	ACGCCGTTAGGGGAGGAA
hHSFko-e5-recF1	GCAGAGTATTGTACAGAAATGGGAGCAGCAGCGTGACCCTCTTGTGtggctgacctgcaggcggc
hHSFko-e5-recR1	ACAAGCAGTAATCAACAATATCTGGAGAGCCCACTGACCATACTTAacgtcgcatgctcccgcc
hHSFko-e5-recR2	GCAGTATTGCTTTACTGCAGTGGTCTGGAAGCAAACAGGCAACATacgtcgcatgctcccgcc
hHSFko-e5-rtrR	ACCAGTTTTCTGTATCCTAAGCTAAAGCTGGAATCAGAAATTTATTtccagtcgggaacctgtc

hHSFko-e5-rtlL	CATATTGCAAACAAATTGCAACATATACATACCATGGAATATGAGGCAACGCGTgcggaacccta ttgtttat
hHSFko-e2-recF1	CGACCCCCGGCGTGGATTCTGTTCCCGCGCTTTCTGGCGTGAGGGGTggtcgcactgcaggcgcc
hHSFko-e2-recR1	CCCCAAGCACGCGACAGCGAGCCGTCTCCGAGCGCACGGGGCAGGCacgtcgcactgctcccgcc
hHSFko-e2-recR2	GTTTACAATTATTACCTAGGGTAAATCTGCTAGAACAAATTACTGacgtcgcactgctcccgcc
hHSFko-e2-rtlL	GGCCCAAAGTCAGTTGACAGTTTTCTGATACTGGGCCCTGTCAGCACGCGTgcggaaccctattgtttat
hHSFko-e2-rtlR	GAAGGTAGGAATGAATACAGGCAGGGAAGGAGTAGACCTGATTTGAttccagtcgggaaacctgct
hHSF2BP-rt-F1	CGCAAATTCTGGGAGGTTT
hHSF2BP-rt-R1	GATCTGGGGAGAAGGGACAC
hHSF2BP-rt-F2	TGGCTTTTGAGTGATCCAGA
mHSF2BP-rt-F1	AGCTGAGGCAGCGGCTAT
mHSF2BP-rt-R1	GATGGACCACTGGCATTTC
mHSF2BP-rt-F2	CCAAACTCAAAGTTCTAATGCTGA
hHSF2BP-pETM-F	atctttatcttcaggcgccATGGGCGAAGCGGGCGCC
hHSF2BP-pETM-R	cttgtcgcaggagctcgaattcCTACACATTATGCTCCAGAG
hHSF2BP-EGFP-F	cagatctcgagctcaagcttcgGCCATGGGCGAAGCGGGCGC
hHSF2BP-EGFPN-R	ggtggcgaccggtggatccCACATTATGCTCCAGAGTGC
hHSF2BP-EGFPC-R	ttatctagatccggtggatcc TACACATTATGCTCCAGAGT
mHSF2BP-GFPN-F	cagatctcgagctcaagcttcgGCTATGGCCGAACCGTGG
mHSF2BP-GFPN-R	ggtggcgaccggtggatccAACATTACAGTCCAGGGCGC

mHSF2BP-GFPC-R	ttatctagatccggtggatccCTAAACATTACAGTCCAGGGCGC
mHSF2BP-pETM-F	atctttatttcaggcgccATGGCCGCAACCGTGG
mHSF2BP-pETM-R	cttgtcgacggagctcgaattcCTAAACATTACAGTCCAGGGCGC
GFP-HSFdcc-F	ctcagatctcgagctcaagcttccatttgggaggagataaagcttgaag
GFP-HSFdcc-R	tcagttatctagatccggtggatccctacacattatgctccagagtgcg
GFP-HSFdArm-F	ctcagatctcgagctcaagcttggggaagcgggcg
GFP-HSFdArm-R	tcagttatctagatccggtggatccCTAaggccttgacgacttctcac

Table S2 Constructs

Code	Name	Vector	Comment
pAZ013	pCR4+mHSF2BP	pCR4	mHSF2BP full-length CDS
pAZ014	pCR4+mHSF2BPde7	pCR4	mHSF2BP splice variant missing exon 7
pAZ015	pCR4+hHSF2BP	pCR4	hHSF2BP CDS full-length
pAZ016	pCR4+hHSF2BPde7,8	pCR4	hHSF2BP CDS splice variant skipping exons 7,8
pAZ017	pETM30+hHSF2BP	pETM30	his-GST-hHSF2BP
pAZ018	pETM11+hHSF2BP	pETM11	his-hHSF2BP
pAZ019	pEGFPC1+hHSF2BP	pEGFP-C1	GFP-hHSF2BP
pAZ020	pETM30+mHSF2BP	pETM30	his-GST-mHSF2BP
pAZ021	pETM11+mHSF2BP	pETM11	his-mHSF2BP
pAZ022	pEGFPN1+mHSF2BP	pEGFP-N1	mHSF2BP-GFP
pAZ023	pEGFPC1+mHSF2BP	pEGFP-C1	GFP-mHSF2BP
pAZ075	hHSF2BPe2u_gRNA	pCR-BluntII	CRISPR gRNA human HSF2BP exon 2 upstream
pAZ076	hHSF2BPe2d_gRNA	pCR-BluntII	CRISPR gRNA human HSF2BP exon 2 downstream

pAZ077	hHSF2BPe5_gRNA	pCR-BluntII	CRISPR gRNA human HSF2BP exon 5
pAZ086	GFP-hHSF2BP Δ Arm	pEGFP-C1	hHSF2BP coiled coil domain (residues 1-)
pAZ088	GFP-hHSF2BP Δ cc	pEGFP-C1	GFP+hHSF2BP C-terminal armadillo domain
pAZ089	hHSF2BP-GFP	pEGFP-N1	
pAZ099	pGb-LPL-CMV->hHSF2BP	pGb-LPL	over-expression of human hHSF2BP
pAZ100	pGb-LPL-CAG->mHsf2bp-GFP	pGb-LPL	
pAZ102	pGb-LPL-CAG->mHsf2bp	pGb-LPL	over-expression of mouse HSF2BP
pAZ103	pGb-LPL-CAG->GFP-mHsf2BP	pGb-LPL	
pAZ117	pBS+hHSF2BP-e5ins-hygro	pBS	CRISPR-assisted GT donor for hHSF2BP exon 5 (cassette insertion)
pAZ118	pBS+hHSF2BP-e5 Δ -hygro	pBS	CRISPR-assisted GT donor for hHSF2BP exon 5 (deletion)
pAZ119	pBS+hHSF2BP-e2 Δ -hygro	pBS	CRISPR-assisted GT donor for hHSF2BP exon 2 (deletion)
pAZ148	pGb-LPL-CAG Flag~BRCA2	pGB-LPL	
pAZ147	pGb-LNL-CAG mHSF2BP		
pAZ149	pGb-LPL-CAG Flag~BRCA2 Δ HSF		Δ T2198-D2478
pAZ159	pGb-LNL-CAG BRCA2-HSF-bigger	pAZ125	fragment of BRCA2 that binds HSF2BP (bigger variant T2198-D2478)
pAZ160	pGb-LNL-CAG BRCA2-HSF-smaller	pAZ125	fragment of BRCA2 that binds HSF2BP (smaller variant T2349-D2478)
pAZ167	pGb-LNL-CAG BRCA2-F3	pAZ125	HSF-bigger + full FANCD2 interaction domain

pAZ168	pGb-LNL-CAG RCA2-F4	pAZ125	FANCD2 interaction domain alone
pAZ169	pGb-LNL-CAG BRCA2-F5	pAZ125	C-terminal part of the HSF-bigger + full FANCD2 domain

Table S3 siRNA and shRNA

siRNA

siLuc	sense sequence	CGUACGCGGAAUACUUCGAdTdT
siXRCC3	sense sequence	GGACCUGAAUCCCAGAAUUUU

shRNA targeting HSF2BP

shNT32		no insert	
shNT 33		CCGGCAACAAGATGAAGAGCACCAACTCGAGTTGGT GCTCTTCATCTTGTGTTTTT	
8029	human	CCGGGCTGGAATTGTCACGAATGTTCTCGAGAACATT CTGACAATCCAGCTTTTT	TRCN0000017473
8030	human	CCGGCGGGACTTCTTACCCAGAATACTCGAGTATTCT GGGTAAGAAGTCCGTTTTT	TRCN0000017474
8031	human	CCGGCGGATGAAAGTCAGTTTGTCTCGAGAAACAA ACTGACTTTCATCCGTTTTT	TRCN0000017475
8032	human	CCGGGCTAATGCTGATGTCCTATACTCGAGTATAGGG ACATCAGCATTAGCTTTTT	TRCN0000017476
8033	human	CCGGCGACAACATAAGAGAGAAGAAGTCTCGAGTTCTTC TCTTATGTTGTCGTTTTT	TRCN0000017477
8034	mouse	CCGGTGCCGGAACATGGAATCTAAACTCGAGTTTAGA TTCCATGTTCCGGCATTTTTTG	TRCN0000239566
8035	mouse	CCGGGCGGCAGGAGATGTCATTTACTCGAGTAAATG GACATCTCCTGCCGTTTTTG	TRCN0000239567
8036	mouse	CCGGGTATAATGTGAGCATCAATCCTCGAGGAATTG ATGCTCACATTACTTTTTTG	TRCN0000239568
8037	mouse	CCGGGGATGTCAAGGAGTTGATTCTCGAGGAATCA ACCTCTTGACATCCTTTTTG	TRCN0000239569
8038	mouse	CCGGGACGACGGAAGTATGCAAATCTCGAGATTTGC ATCACTCCGTCGCTTTTTTG	TRCN0000239570

6

Chapter 6

**New findings and the future of
cancer treatment**

General discussion

Part I – Results from this thesis

Over the last few decades the field of the DNA Damage Response (DDR) has been evolving rapidly. By now we have a general idea how most types of DNA damage are repaired, from bacteria to mammalian cells. However, there are many open questions regarding the finer details of these repair pathways and still new factors involved in DNA repair are discovered regularly. With the introduction of genome-wide screening methods using siRNA and shRNA, it became easier to identify drug sensitivities and resistance mechanisms, linking new proteins to DNA repair. Expression of GFP-tagged versions of proteins, efficient pull-downs and sensitive analysis by mass spectrometry allowed easy identification of new interaction partners. Since the advent of CRISPR/Cas9 technology generating knockouts has become easier in any transfectable cell line and making knock-out mice is less time-consuming¹. While most main players in the DNA damage response have been known for several decades, new proteins are still being connected to the DDR. Recent examples are PAXX in non-homologous end-joining (NHEJ)^{2,3} and UVSSA in transcription coupled nucleotide excision repair⁴⁻⁶. Lately the focus is shifting more to chromatin remodelling and post-translational modifications such as phosphorylation, ubiquitylation and sumoylation. Additionally, new roles for proteins already known to be involved in DNA repair are identified. An example of that is REV7, which has been shown to affect DNA double strand break repair (Chapter 3 and 4).

DNA double strand breaks are among the most detrimental types of DNA damage. The main pathways to repair these breaks are NHEJ and homologous recombination (HR). A proper balance between these pathways is important for the maintenance of an uncompromised genome. Several proteins such as BRCA1 and 53BP1, are known to affect the balance between HR and NHEJ (Chapter 2). Mutations in BRCA1 lead to defects in HR

and repair via end-joining is likely to increase to compensate this deficiency. This defect in HR can be partially rescued by the loss of 53BP1^{7,8}. Due to the defect in HR, BRCA1-deficient cells are extremely sensitive to PARP inhibitors, but upon loss of 53BP1, the cells become resistant. In Chapter 3 we found that the same holds true for REV7.

REV7 function in PARP inhibitor resistance

REV7 was originally identified as a gene involved in UV mutagenesis in yeast⁹ and was later shown to form a complex with REV3¹⁰. It has now become clear that REV7 is a multi-functional protein that plays a role in cell cycle progression, translesion synthesis and transcriptional activation. As described in chapter 3, we found that loss of REV7 leads to PARP inhibitor resistance in BRCA1-deficient cells by restoring HR. Currently, it is still unclear why REV7 loss restores HR. The restoration of HR is specific to BRCA1-deficient cells; loss of REV7 does not cause PARP inhibitor resistance in BRCA2-deficient cells.

We considered the possibility that the role of REV7 in inhibition of the anaphase promoting complex/cyclosome (APC/C) is important. REV7 inhibits the activity of the APC/C-CDH1 complex to prevent premature activation of this complex before mitosis¹¹. In the absence of REV7, mitosis is accelerated and mitotic aberrations occur more frequently. It does not seem very likely that misregulation of mitosis would lead to restoration of HR, as this repair pathway functions mainly in the S and G2 phases of the cell cycle. Additionally, if changes in mitosis would rescue a HR defect, it is unlikely that this is specific for BRCA1-deficiency. However, to test this hypothesis, we inhibited the APC/C to see whether this had an effect on RAD51 foci formation after ionizing radiation in BRCA1-deficient cells (chapter 4). Although the inhibitor was active, there was no effect on RAD51 foci formation in BRCA1-deficient cells with REV7 depletion.

An alternative explanation is that REV7 plays a role at the level of pathways choice

between HR and NHEJ. BRCA1 and BRCA2 are both involved in HR, but BRCA1 has been shown to affect resection^{12,13}, while the main function of BRCA2 in HR is to load RAD51 onto these resected DNA ends¹⁴.

REV7 could directly stimulate end-joining. Boersma et al. showed that REV7 affects fusion of deprotected telomeres by inhibiting end resection¹⁵. Telomeres are protected by the Shelterin complex containing TRF2. Boersma et al. used MEFs expressing a temperature-sensitive TRF2 variant. When these cells were exposed to elevated temperatures (39°C), the telomeres became uncapped and fused, a process that depends on end-joining. In the absence of REV7, the telomeres did not fuse and 3' telomeric overhangs were elongated. Additionally, Flag-tagged REV7 co-localized with 53BP1 after telomere uncapping. This suggests that REV7 promotes NHEJ. The effect is dependent on 53BP1 and RIF1, but not PTIP. So far, no catalytic activity for REV7 has been linked to NHEJ. REV7 does not seem to interact with either RIF1 or 53BP1 and why the phenotype is dependent on these proteins remains unclear.

REV7 has also been linked to HR. Sharma et al. showed that HeLa cells transfected with siRNA targeting REV1, REV3 or REV7 showed more RAD51 foci 24 hours after damage than HeLa cells transfected with control siRNA¹⁶. REV1, REV3 and REV7 depleted cells also showed decreased recombination in the assay, an assay to measure intra chromatid gene conversion. The authors argue that this is because REV1 and Polymerase ζ are required to bypass damaged bases and aberrant structures in resected DNA (after strand invasion). Failure to bypass these lesions might result in stalled or delayed HR repair. On the other hand, there are several translesion polymerases, so it is not so likely that the bypass of the aberrant structures would exclusively depend on REV1 and Polymerase ζ .

Whether the interaction between REV3 and REV7 is important for stimulating end joining and restoring HR in BRCA1-deficient cells is still under debate. In the screen

performed by Boersma and colleagues, REV1 and REV3 depletion did not result in the same phenotype as REV7 depletion, but the C70R and the L186A mutants (defective in REV3 and REV1 interaction respectively), showed an intermediate phenotype in the telomere deprotection assay. Also in our experiments, the REV7 point mutants show an intermediate phenotype when comparing the results obtained in the alpha-track experiment or when comparing the efficiency of the formation of RAD51 foci in BRCA1-deficient cells (Chapter 4). This indicates that the interaction with REV3 could play a role, but other processes or interaction partners might be important as well. The intermediate phenotype could also be due to incomplete loss of the interaction or loss of other binding partners (see below).

There are several possible models for how REV7 could favour end joining (Figure 1). One possibility is that it blocks resection by sitting on the DNA and preventing access of nucleases. Similar models have been proposed for 53BP1 and in fractionations REV7 is found in the chromatin fraction as well as the nucleus and the cytoplasm. REV7 recruitment to sites of damage also depends on 53BP1. However, no direct interaction between REV7 and 53BP1 has been detected in our mass spectrometry experiments or immunoprecipitations. Also no interaction between REV7 and any of the nucleases known to be involved in resection was found.

Another possibility is that REV3 and REV7 together fill in resected DNA, thereby reversing resection. DNA is resected from 5' to 3'. All polymerases synthesize DNA from 5' to 3', in the same direction as resection is taking place. A polymerase can therefore not directly fill in the resected DNA, assuming that resection starts at the end of the broken DNA. Recently it was shown in yeast that resection can start some distance away from the break. Cannavo and Cejka showed that in vitro, MRX (Mre11, Rad50, Xrs2) and Sae2 (yeast homolog of CtIP), can make a nick in double stranded DNA 15-20 base pairs from a break¹⁷. At this site, resection then takes place

in both directions. If the same would be the case in mammalian cells and a small piece of double strand DNA would stay on the end of the DNA, Polymerase ζ might be able to fill the gap and reverse resection. The DNA synthesis could also start from a small DNA or RNA primer or a microhomology at the end could fold back on itself to form a hairpin, which could serve as a primer.

Currently it is unknown whether REV3 loss also causes PARP inhibitor resistance in *BRCA1*-deficient cells. REV3 depletion is poorly tolerated and attempts to knock down REV3 using shRNA were not efficient. In chicken DT40 cells deletion of REV3 is tolerated¹⁸ and also *BRCA1* knock-out DT40 cells are viable¹⁹. To find out whether REV3 deletion restores HR in *BRCA1* knock out cells, we set out to make *BRCA1*^{-/-}*REV7*^{-/-} and *BRCA1*^{-/-}*REV3*^{-/-} double knock out cells. *BRCA1*^{-/-}*REV7*^{-/-} cells were viable and REV7 loss restored RAD51 foci formation in *BRCA1* knock-out cells (data not shown). *BRCA1*^{-/-}*REV3*^{-/-} cells could not be obtained. This might indicate that the combination is lethal. We are currently making cells with a conditional *BRCA1* deletion allele combined with REV3 deletion. It is, however, possible that REV3 function is essential and that REV3 loss would never lead to PARP inhibitor resistance because REV3 loss results in cell death, even if the REV3 polymerase activity is needed for this phenotype.

As an alternative approach and to circumvent the problem of the lethality of REV3 loss, we made point mutations in REV7 to disrupt the interaction with REV1 or REV3 (Chapter 4). When looking at PARP inhibitor resistance and RAD51 foci formation, the mutants show an intermediate phenotype compared to wild-type REV7. The explanation for this intermediate phenotype could either be that the interaction between REV7 and REV3 or REV7 and REV1 is not completely lost or that other factors play a role in this interaction as well. Binding partners of wild-type REV7 and two point mutants were analysed by mass spectrometry to see whether any interaction partners other than

REV1 and REV3 change as well.

The point mutations in REV7 also affect the interaction with CHAMP1 and POGZ. A complex with REV7, POGZ and CHAMP1 was identified in a screen for readers of histone marks²⁰. POGZ, CHAMP1 and REV7 interacted with HP1 isoforms CBX1, CBX3 and CBX5, which bind to the repressive histone modification H3K9me3. CHAMP1 (C13orf8, Znf828) has been reported to regulate kinetochore microtubule attachment during mitosis upstream of CENP-E and CENP-F²¹. CHAMP1 localizes to chromosomes and CHAMP1-depleted cells show chromosome misalignment. POGZ, a domesticated transposase, contains a DDE domain that can be used for DNA cleavage, strand nicking and ligation²². Nozawa et al. showed that POGZ is important for the dissociation of heterochromatin protein 1 alpha (HP1 α) and Aurora B kinase from chromosome arms during mitosis²³.

REV7, POGZ and CHAMP1 have all been linked to mitosis, so the complex might play a role there. For CHAMP1 and POGZ there is no link to DNA repair yet. However, these two proteins have not been studied as thoroughly as REV7. POGZ contains a DDE domain that might be used to connect two DNA ends in a manner that is similar to the joining reaction in transposition²⁴. It is possible that this activity could be used in alternative end-joining and that REV7 facilitates end-joining via this complex. However, it is not known whether the DDE domain in POGZ has maintained any transposase-like activity. In our experiments, depletion of POGZ and CHAMP1 with siRNA (and shRNA for POGZ) was inefficient and there was no effect on the formation of RAD51 foci. One *BRCA1*-deficient G3 clone with stable depletion of POGZ was Olaparib resistant comparable to G3 cells with shRNA targeting 53BP1 or REV7. However, since none of the other clones showed resistance and there was no formation of RAD51 foci after irradiation, it could well be off target effect. The currently available data on the role of POGZ and CHAMP1 in HR is inconclusive and these proteins cannot be linked yet to

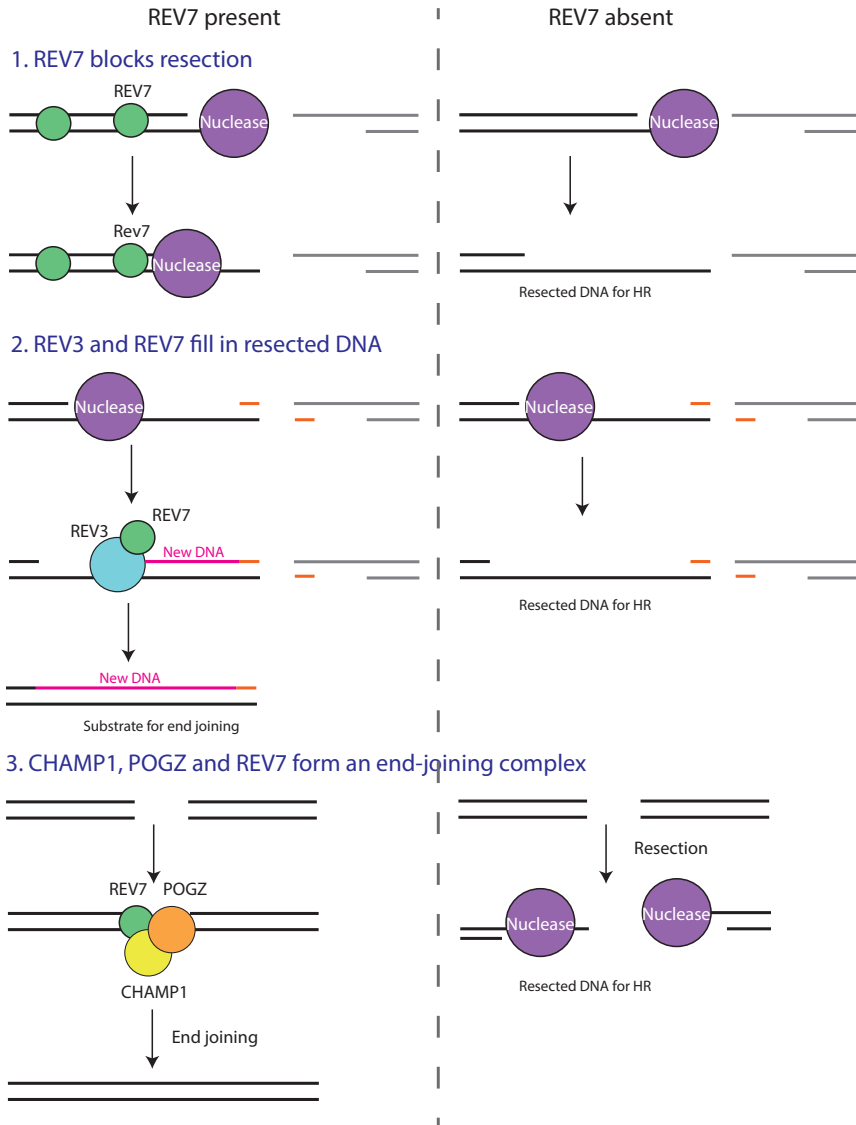


Figure 1 Models for the role of REV7 in DNA repair

1. REV7 blocks resection. REV7 could be DNA bound and block access of nucleases to prevent resection. In the absence of REV7, nucleases are no longer blocked and resection can proceed, generating a substrate suitable for HR. 2. REV3 and REV7 fill in resected DNA. If resection does not start from the end of broken DNA, but some distance from it and a small piece of double stranded DNA remains at the end (orange), Polymerase ζ might be able to fill in the resected DNA (pink). This would reverse resection and create a DNA end that is suitable for repair via NHEJ. After loss of REV7, the resected DNA is no longer filled in by Polymerase ζ and is suitable for repair via HR. 3. CHAMP1, POGZ and REV7 form an end-joining complex. In the absence of REV7, end-joining of deprotected telomeres decreases. REV7 therefore might stimulate end joining and the DDE domain of POGZ might be able to perform a transposition/integration like reaction. It is possible that this complex is involved in an alternative form of end-joining. This complex could prevent resection by joining the broken DNA ends before resection takes place. In the absence of REV7 this end-joining reaction does not take place and the DNA ends are processed for HR.

restoration of HR. More experiments with complete deletion of CHAMP1 and POGZ, for example using CRISPR/Cas9 technology, would be required to determine whether these proteins affect HR in BRCA1-deficient cells.

How to treat PARP inhibitor resistant tumours

Finding out how REV7 loss leads to restoration of HR is important for the treatment of patients whose tumours have become resistant to PARP inhibitors due to REV7 loss. Once the mechanism is known, other drugs can be used to target resistant cells or to prevent resistance by using a combination of drugs. For example, PARP inhibitor resistance due to overexpression of a multi-drug resistance transporter could be prevented by using a PARP inhibitor that is a poor substrate for this protein²⁵ or by inhibiting this multi-drug transporter using Tariquidar²⁶. In cell culture experiments, the formation of RAD51 foci and increased Olaparib resistance of BRCA1-deficient cells with depletion of REV7 could be abrogated by the addition of an ATM inhibitor. Whether this also works on tumour bearing mice has not been tested yet.

For the treatment of (resistant) tumours, especially the possibilities and drawbacks of drug combinations are important. Ovarian cancers with BRCA2 mutations are very sensitive to cisplatin treatment. This patient group could also benefit from PARP inhibitor treatment, but it has been shown that cisplatin resistance due to genetic reversion correlates with PARP inhibitor resistance in a BRCA2-mutated breast-cancer cell line, HCC1428²⁷. Also in patients with hereditary ovarian carcinoma, cisplatin and PARP inhibitor resistance were correlated²⁸, although the number of patients in this study was small.

Tumours that have become resistant to treatment with PARP inhibitors through genetic reversion might still be sensitive to other chemotherapeutics that inflict a different type of DNA damage. Issaeva and

colleagues showed such cells and tumours are still sensitive to treatments with the chemotherapeutic 6TG (6-thioguanine)²⁹. HR is required for the repair of 6TG-induced damage and one explanation for the sensitivity to 6TG is that the restoration of HR in PARP inhibitor resistant cells is insufficient to cope with this type of damage.

HSF2BP and crosslinker sensitivity

Certain repair deficiencies make cells very sensitive to specific types of DNA damage. As described above, HR-deficient cells are very sensitive to the treatments with PARP inhibitors. These repair deficiencies are usually caused by mutations. In Chapter 5 we describe a novel mechanism for repair deficiency: overexpression of a wild-type protein. Overexpression of HSF2BP sensitizes HeLa and U2OS cells to Mitomycin C. HSF2BP was identified as a protein interacting with BRCA2. BRCA2 is essential for HR and the formation of RAD51 foci³⁰. Overexpression of HSF2BP does not lead to a HR defect but the formation of RAD51 and FANCD2 foci after MMC exposure is decreased. Also, the number of chromosomal aberrations after MMC exposure is dramatically increased in HeLa cells overexpressing HSF2BP compared to HeLa cells expressing an empty vector. These phenotypes are very similar to the phenotype observed for Fanconi Anemia patient cells³¹.

HSF2BP interacts with the C-terminus of BRCA2. In this region FANCD2 has also been reported to interact with BRCA2. We hypothesized that the interaction between HSF2BP and BRCA2 prevents or weakens the interaction between BRCA2 and FANCD2. However, in immunoprecipitations we could not show an interaction between FANCD2 and BRCA2 and therefore we could not test this hypothesis.

Another possibility is that another interaction between BRCA2 and an interaction partner required for the repair of interstrand crosslinks is disrupted by the overexpression of HSF2BP. To investigate this, we used quantitative mass spectrometry to identify

proteins that specifically interact with the flag-tagged BRCA2 domain that interacts with HSF2BP and a larger BRCA2 domain that also contains the reported FANCD2 interaction domain. In these experiments we could not identify an interaction with FANCD2 either. Among the proteins that interacted with the BRCA2 domains and not with the Flag peptide itself and whose interaction changed upon overexpression of HSF2BP was GAPDH. Other proteins the BRCA2 domains strongly interacted with were histones and histone variants. No other proteins that could directly be linked to the repair of DNA interstrand crosslinks were found. Therefore, at the moment, the disturbance of the interaction between BRCA2 and FANCD2 by HSF2BP overexpression seems to be the most logical explanation. However, we cannot exclude that the interaction between HSF2BP and BRCA2 results in an overall change in BRCA2 structure, affecting interactions in other parts of BRCA2.

Fanconi Anemia due to overexpression

As described above, the phenotype of cells overexpressing HSF2BP is reminiscent of Fanconi Anemia (FA) patient cells. Historically, these patient cell lines have been analysed by screening metaphase spreads for chromosomal aberrations after MMC exposure³¹. To identify the specific genetic defect and for a definitive diagnosis, a genetic complementation analysis was performed. So far at least 16 genes have been identified in which mutations cause Fanconi Anemia. Some of these genes had already been identified in other DNA repair pathways, such as PALB2/FANCD2³² and FANCD1/ERCC1³³. The most recently identified Fanconi Anemia subtypes are FA-S (mutations in BRCA1)³⁴ and FA-T (mutations in de E2 ubiquitin ligase UBE2T that is required for the ubiquitination of FANCD2 and FANCD1)^{35,36}. Both of these subtypes were discovered by searching for bi-allelic mutations in patients with typical FA features that had no mutations in other known FA genes.

All FA subtypes described to date are

caused by mutations. HSF2BP is the first example where overexpression of a wild-type protein gives a Fanconi Anemia-like phenotype. Currently it is still unknown whether there are any cases of HSF2BP overexpression among patients with an unclassified FA subtype. Standard methods such as sequencing of genomic DNA are not suitable to find overexpression of HSF2BP. RNA sequencing or microarray analysis would be more suitable. In the future these methods should be used on all patients with an unclassified type of Fanconi Anemia.

Part II – How can we apply our findings in the clinic?

Genome-wide screens for drug sensitivities as well as bioinformatics analysis on sequenced tumours and their therapy response regularly reveal new prognostic markers for all types of tumours. In this thesis a resistance mechanism and a sensitization mechanism are described. This type of information is very valuable for mechanistic insight and knowledge on how cells repair DNA damage, but it is not very easy to apply this knowledge to the treatment of patients. Main questions when trying to apply 'fundamental' findings to the clinic are the following: How relevant is the finding for patients? Does it only happen in cultured cells or also in (human) tumours? In which types of tumours does it occur? In how many patients does this happen? How big is the effect?

To find quantitative and statistically significant answers to these questions, material from many patients needs to be tested on a large scale. This material could be acquired from clinical trials or by collecting material from surgery. Sequencing of large numbers of tumours, as was done for the Cancer Genome Atlas (TCGA) provides the data to answer these questions. Currently the TCGA project has collected approximately 11000 samples for 33 tumour types and in the future more cancer types will be analysed (www.cancergenome.nih.gov). For breast cancer, DNA methylation, exome sequencing,

messenger RNA arrays and several other techniques were used to analyse the tumours³⁷. Genomic analysis of these tumours is just the first step. To be able to predict treatment outcome based on sequencing information, the data from all these tumours should be related to parameters such as treatment response and overall survival.

Once such data on a large cohort of tumours is available, the next step is to characterize patient material for diagnosis. To characterize tumours based on morphology or expression of a single receptor, standard immuno-histological methods suffice. For example, breast cancers can easily be stained for the HER2-receptor or Estrogen-receptor to determine whether any targeted treatments (Herceptin or Tamoxifen respectively) will be suitable. Also sequencing of the *BRCA1* and *BRCA2* genes is very useful to test whether the tumour is likely to be HR-deficient. However, for a thorough analysis for many markers, other methods are more suitable.

Sequencing of patients' tumours (whole genome sequencing) is already feasible. With this data, one can look for possible disease causing mutations or mutational signatures. However, there are often very many mutations detected in tumour material compared to normal tissue and it is difficult to determine which mutations are the driver mutations.

Driver mutations are genetic changes that give selective advantages to cancer cells and thereby drive cancer development. Mutational signatures can be indicative of specific types of DNA damage and/or repair mechanisms that have been taking place in the genome³⁸. A disadvantage of looking at those signatures is that they reflect the history of the tumour and not necessarily the current status. For example, a *BRCA1*-deficient tumour can show specific genomic scars, but if the tumour has restored *BRCA1* expression by genetic reversion or restored HR via the loss of 53BP1, the scars will remain but the tumour is no longer HR-deficient and will respond accordingly to therapy.

Methods that would better reflect the

tumours' current status are microarray analysis and RNA sequencing. A disadvantage of microarray analysis is that the number of probes per gene is limited and that the probes need to be specifically designed. You will only detect what you are looking for. This method has been used to classify molecular subtypes to identify *BRCA1* and *BRCA2* mutation carriers³⁹. RNA sequencing is unbiased and mutations, different splice forms and other variations can be detected. For RNA sequencing, one can focus on the exome to look at expressed genes or also sequence small and non-coding RNAs. The latter provide a wealth of data, but are not easy to interpret and relatively little is known about their role in cancer. One of the current challenges for RNA seq is the quantification of expression levels and accurate identification and quantification of different splice forms⁴⁰.

A completely different strategy to test how a tumour will respond to therapy is to treat tumours *ex vivo*. This can either be done by culturing slices of tumours collected after surgery⁴¹, dissociating tumour samples into single cells⁴² or by growing organoids from patient material. So far, only an organoid biobank for material from colorectal cancer patients has been established⁴³, but this might be achievable for other tumour types as well. An advantage of organoid cultures over tissue slices is that organoids can be expanded and more treatments can be tested. However, in tissue slices the tumour morphology remains intact and the analysis does not require time-consuming expansion of the material.

Although there are many techniques available to characterize a patient's tumour, tumour heterogeneity remains a challenge for all techniques. Tumours often consist of different clones, which might harbour different mutations and respond differently to treatment. In *ex vivo* assays using tissue slices, tumour heterogeneity can be observed after treatment, but for subsequent genetic analysis the material is analysed as a mix of the total tumour. Single cells sequencing methods might help to

overcome this problem, but these tools are still being developed⁴⁴. Another challenge for all techniques mentioned above is the contamination of tumour tissue with normal tissue. This problem could also be resolved by using single cell sequencing methods, but this technology needs further development before it can be used for routine analysis. Lastly, these sequencing techniques generate large amounts of data and the storage, but most of all the analysis and interpretation of data remains challenging. The sequencing data should be related to the current literature for accurate analysis. One question that remains is how can we integrate all data that has been acquired so far?

Data integration and interpretation

The sensitivity of a tumour to a drug is determined by the total composition, not only the expression or mutation of a single protein. Therefore new models and methods are required to integrate all data. An example of such an approach is the Cancer Cell Map Initiative⁴⁵. The goal of this project is to chart the interaction networks and pathways that operate in cancer and healthy cells. Tumours often have a variety of mutations but these mutations might hijack the same pathways. For the interpretation of sequencing data it is therefore important to take these pathways into account.

In 2011, Roychowdhury and colleagues used whole-genome sequencing of the tumour, targeted whole-exome sequencing of tumour and normal DNA, and transcriptome sequencing (RNA-Seq) of the tumour to find clinically relevant genetic defects in two patients⁴⁶. For the interpretation of the results they made use of a multidisciplinary team with experts on clinical oncology, pathology, cancer biology, bioethics, bioinformatics, and clinical genetics. In the future, computer models that interpret all data might perform this task. However, a team of experts should still verify the results or outcome of the model. If a bioinformatics model is developed to take over this task, it will need continuous updates to integrate new findings and clinical data to

obtain the best results.

Ideally, the model for data interpretation should be understandable and usable for oncologists in the clinic. This will enable them to make the optimal therapeutic choice for their patients. Johnson et al. described an example of a decision support platform for oncologists using next generation sequencing data⁴⁷. In this approach, the first step is to determine whether a DNA variant found in tumour material is actionable (i.e. could a treatment based on this aberration benefit the patient?). If this is the case, the team tries to find a clinically available drug that targets this aberration. Also here the decision is made by a team of experts and based on the literature and a functional genomics platform.

Deciding whether a mutation has functional consequences for a protein is, even for a team of experts, often not straightforward. For mutations in the known catalytic site of a protein it is likely that they will inactivate the protein and mutations that change an amino acid to a proline will probably change the folding of the protein. However, most missense mutations or small insertions and deletions, it is difficult to predict what the effect will be. Therefore laborious functional experiments with these mutants, preferably in cells, are required to determine the effect of a mutation on protein function. Another factor complicating the interpretation of tumour data is the effect epigenetic modifications have on protein expression. Although a gene might show no mutations, promotor hypermethylation or other histone modifications could still affect the expression. For example, tumours showing hypermethylation of the *BRCA1* promotor are HR-deficient, although there are no mutations in the *BRCA1* gene⁴¹. For the optimal analysis of tumours, these factors should be taken into account as well.

The availability of a computer program or platform that helps oncologist to interpret the sequencing data from patients will allow them to make the best therapeutic choice for their patients. This should increase treatment

efficiency and overall survival of cancer patients. If more is known about resistance mechanisms, unnecessary treatment can be prevented as well and patients would not have to suffer from the side effects without benefit. However, there are also other steps that can be taken to improve cancer treatment in the future.

The future of cancer treatment

To be able to treat cancer better, there are several aspects that can be improved. One of them is early detection of tumours. The earlier a tumour is detected, the smaller the chances that the tumour has already metastasized and the better the chances of curing the patient. Ideally one would detect tumours while they are still on the scale of just a few thousand cells using for example tumour-specific antibodies or other markers. However, it is unlikely that a tumour of this size will cause symptoms in the patient. Still, investing in strategies for early detection of tumours will be beneficial, also to detect residual cancer cells. On the other hand, not all lesions that will be detected are malignant and some might never grow out. To avoid over-treating patients, and potentially causing secondary cancers due to treatments with DNA-damaging agents, methods are required to determine how likely a lesion is to grow out. Unfortunately, such methods are currently not available yet.

The second aspect is to make cancer treatment more personalized. Several strategies to characterize a patient's tumour and to determine which treatment will be best are described above. Personalized treatments generally aim at giving the patient the best treatment by looking for sensitivities. However, detection of resistance may prevent unnecessary treatment and patient suffering from treatment side effects needlessly.

Another part of personalized medicine is the development of drugs that target specific genetic defects. Examples of this type of drugs are the BRAF kinase inhibitor Vemurafenib, which is used to treat melanomas with a V600

mutation in BRAF⁴⁸ and the PARP inhibitor Olaparib^{49,50}. Both of these drugs have been approved for clinical use for certain types of tumours. For example Olaparib has only been approved for the treatment of advanced ovarian cancer associated with BRCA-defective genes. Olaparib might also be a very effective treatment for other HR-deficient tumours such as gastric cancers with low ATM expression⁵¹ and that is currently being tested in clinical trials⁵². Once it has been demonstrated that for those HR-deficient tumours PARP inhibitor treatment is better than the current standard treatment, effort should be made to approve the drug for those tumour locations as fast as possible to make sure that patients can benefit. Extensive clinical trials to verify the safety of the drug might not be necessary, since this has already been done for the initial approval of the treatment of ovarian cancer.

Strategies contrasting personalized medicine aim for a drug to treat all types of cancer. One example of a general cancer drug is the MTH1 inhibitor. MTH1 is required to hydrolyse oxidized nucleotides to prevent the incorporation of these damaged bases. For many cancers, this process is essential for survival, while normal cells are less dependent on it. MTH1 inhibition leads to DNA damage and eventually cell death^{53,54}. Normal cells also depend on MTH1 and inhibition of this enzyme will lead to DNA damage⁵⁴. Furthermore, *MTH1* knock-out mice have an increased long-term tumour burden⁵⁵. Whether the benefit of the drug outweighs the toxic effect of the DNA damage in healthy cells is not yet clear. MTH1 inhibitors are currently being developed and tested in mice, but not yet on patients.

Lastly, the treatment should be focussed on completely eradicating the tumour. The remaining (treatment resistant) cells are likely to grow out again eventually and can metastasize, turning cancer into a sort of chronic disease. At the moment the treatments also aim at complete eradication of the tumour, but the treatment choice is mostly based on the type or location of the

tumour and a few biomarkers (for example hormone status for breast cancer). With the use of personalized treatments based on sequencing of individual tumours, the treatment could be optimized to eliminate all individual sub-clones of a tumour. To be able to do that, detailed characterization of a patient's tumour is required and the treatments will differ between patients. Maybe a combination of treatments would be required to completely eliminate a heterogeneous tumour. Once sequencing on biopsies is possible, samples could be taken from treated tumours to see which treatment should be used next.

The price to pay

Personalized medicine is very promising for the treatment of cancer, but is this new technology affordable? Can these techniques be used on a large scale in hospitals? *Ex vivo* treatment of organoids grown from a patient's tumour is very exciting, but also time-consuming and labour intensive. Specific growth conditions are required to keep the organoids alive and the results should be obtainable in a clinically relevant time span to make a decision on the best treatment for the patient.

Drugs targeting a specific genetic defect are very effective, but only useful for a relatively small group of patients. Patients clearly benefit from these treatments, not only because of the efficacy but also because the side effects are less severe than for conventional chemotherapy. However, the development of these drugs is very costly and the resulting drugs are very expensive. Additionally, resistance occurs and in many cases, the treatment results in an increase of life span of several months, not a cure⁵⁶.

The tests to characterize tumours such as whole genome sequencing and exome sequencing are very expensive as well. In the future, sequencing will become cheaper, as the technology progresses. Also the integration of data and the accessibility of the knowledge should improve over time, although the interpretation of tumour data

will remain complex. Sequencing and data analysis should also become faster to allow oncologists to design treatment plans based on the results.

As described above, a program or model for clinicians that helps to guide their treatment plan and that takes current literature and new drugs into account would be very valuable. Another aspect that such a program could address is the cost of the treatment and the net health benefit. The price of cancer care is increasing rapidly and to address this problem the American Society of Clinical Oncology (ASCO) has set up "a framework to assess the value of cancer treatment options"⁵⁷. This tool should help patients and oncologist to decide which treatment to take.

Conclusion

The field of cancer treatment is rapidly developing, both on the fundamental and the clinical side. To transfer all new knowledge from bench to bedside, models should be developed to integrate all data and to make it accessible for clinicians. With the introduction of more targeted treatments and precision oncology, more cancers will become treatable and more patients will survive. Combinations of treatments will hopefully lead to complete eradication of tumours, killing the whole heterogeneous tumour. In the future cancer should not become a chronic disease, but one that can be cured.

References

1. Wang, H. et al. One-step generation of mice carrying mutations in multiple genes by CRISPR/cas-mediated genome engineering. *Cell* 153, 910–918 (2013).
2. Ochi, T. et al. DNA repair. PAXX, a paralog of XRCC4 and XLF, interacts with Ku to promote DNA double-strand break repair. *Science* 347, 185–188 (2015).
3. Xing, M. et al. Interactome analysis identifies a new paralogue of XRCC4 in non-homologous end joining DNA repair pathway. *Nat. Commun.* 6, 1–12 (2015).
4. Schwertman, P. et al. UV-sensitive syndrome protein UVSSA recruits USP7 to regulate transcription-cou-

- pled repair. *Nature Genetics* 44, 598–602 (2012).
5. Nakazawa, Y. et al. Mutations in UVSSA cause UV-sensitive syndrome and impair RNA polymerase I processing in transcription-coupled nucleotide-excision repair. *Nat Genet* 44, 586–592 (2012).
 6. Zhang, X. et al. Mutations in UVSSA cause UV-sensitive syndrome and destabilize ERCC6 in transcription-coupled DNA repair. *Nature Genetics* 44, 593–597 (2012).
 7. Bunting, S. F. et al. 53BP1 inhibits homologous recombination in *brca1*-deficient cells by blocking resection of DNA breaks. *Cell* 141, 243–254 (2010).
 8. Bouwman, P. et al. 53BP1 loss rescues BRCA1-deficiency and is associated with triple-negative and BRCA-mutated breast cancers. *Nat. Struct. Mol. Biol.* 17, 688–695 (2010).
 9. Lawrence, C. W., Das, G. & Christensen, R. B. REV7, a new gene concerned with UV mutagenesis in yeast. *Mol. Gen. Genet.* 200, 80–85 (1985).
 10. Murakumo, Y. et al. A human REV7 homolog that interacts with the polymerase ζ catalytic subunit hREV3 and the spindle assembly checkpoint protein hMAD2. *J. Biol. Chem.* 275, 4391–4397 (2000).
 11. Listovsky, T. & Sale, J. E. Sequestration of CDH1 by MAD2L2 prevents premature *apc/c* activation prior to anaphase onset. *J. Cell Biol.* 203, 87–100 (2013).
 12. Cruz-García, A., López-Saavedra, A. & Huertas, P. BRCA1 Accelerates CtIP-Mediated DNA-End Resection. *Cell Rep.* 9, 451–459 (2014).
 13. Ciccía, A. & Elledge, S. J. The DNA Damage Response: Making It Safe to Play with Knives. *Molecular Cell* 40, 179–204 (2010).
 14. Thorslund, T. & West, S. C. BRCA2: a universal recombinase regulator. *Oncogene* 26, 7720–7730 (2007).
 15. Boersma, V. et al. MAD2L2 controls DNA repair at telomeres and DNA breaks by inhibiting 5' end resection. *Nature* (2015). doi:10.1038/nature14216
 16. Sharma, S. et al. REV1 and polymerase ζ facilitate homologous recombination repair. *Nucleic Acids Res.* 40, 682–691 (2012).
 17. Cannavo, E. & Cejka, P. Sae2 promotes dsDNA endonuclease activity within Mre11–Rad50–Xrs2 to resect DNA breaks. *Nature* 514, 122–125 (2014).
 18. Sonoda, E. et al. Multiple roles of REV3, the catalytic subunit of polzeta in maintaining genome stability in vertebrates. *EMBO J.* 22, 3188–3197 (2003).
 19. Martin, R. W. et al. RAD51 up-regulation bypasses BRCA1 function and is a common feature of BRCA1-deficient breast tumors. *Cancer Res.* 67, 9658–9665 (2007).
 20. Vermeulen, M. et al. Quantitative Interaction Proteomics and Genome-wide Profiling of Epigenetic Histone Marks and Their Readers. *Cell* 142, 967–980 (2010).
 21. Itoh, G. et al. CAMP (C13orf8, ZNF828) is a novel regulator of kinetochore-microtubule attachment. *EMBO J.* 30, 130–144 (2011).
 22. Bartholomeeusen, K. et al. Lens epithelium-derived growth factor/p75 interacts with the transposase-derived DDE domain of *pogZ*. *J. Biol. Chem.* 284, 11467–11477 (2009).
 23. Nozawa, R.-S. et al. Human POGZ modulates dissociation of HP1alpha from mitotic chromosome arms through Aurora B activation. *Nat. Cell Biol.* 12, 719–727 (2010).
 24. Montano, S. P. & Rice, P. A. Moving DNA around: DNA transposition and retroviral integration. *Curr. Opin. Struct. Biol.* 21, 370–378 (2011).
 25. Jaspers, J. E. et al. Loss of 53BP1 causes PARP inhibitor resistance in BRCA1-mutated mouse mammary tumors. *Cancer Discov.* 3, 68–81 (2013).
 26. Rottenberg, S. et al. High sensitivity of BRCA1-deficient mammary tumors to the PARP inhibitor AZD2281 alone and in combination with platinum drugs. *Proc. Natl. Acad. Sci. U. S. A.* 105, 17079–17084 (2008).
 27. Sakai, W. et al. Secondary mutations as a mechanism of cisplatin resistance in BRCA2-mutated cancers. *Nature* 451, 1116–1120 (2008).
 28. Norquist, B. et al. Secondary somatic mutations restoring BRCA1/2 predict chemotherapy resistance in hereditary ovarian carcinomas. *J. Clin. Oncol.* 29, 3008–3015 (2011).
 29. Issaeva, N. et al. 6-thioguanine selectively kills BRCA2-defective tumors and overcomes PARP inhibitor resistance. *Cancer Res.* 70, 6268–6276 (2010).
 30. Tutt, A. et al. Mutation in *Brca2* stimulates error-prone homology-directed repair of DNA double-strand breaks occurring between repeated sequences. *EMBO J.* 20, 4704–4716 (2001).
 31. Kee, Y. & D'Andrea, A. D. Molecular pathogenesis and clinical management of Fanconi anemia. *J. Clin. Invest.* 122, 3799–806 (2012).
 32. Xia, B. et al. Fanconi anemia is associated with a defect in the BRCA2 partner PALB2. *Nat. Genet.* 39, 159–161 (2007).
 33. Bogliolo, M. et al. Mutations in ERCC4, encoding the DNA-repair endonuclease XPF, cause Fanconi anemia. *Am. J. Hum. Genet.* 92, 800–806 (2013).
 34. Sawyer, S. L. et al. Biallelic Mutations in BRCA1 Cause a New Fanconi Anemia Subtype. *Cancer Discov.* 5, 135–142 (2015).
 35. Hira, A. et al. Mutations in the Gene Encoding the E2 Conjugating Enzyme UBE2T Cause Fanconi Anemia. *Am. J. Hum. Genet.* 96, 1001–1007 (2015).
 36. Rickman, K. A. et al. Deficiency of UBE2T, the E2 Ubiquitin Ligase Necessary for FANCD2 and FANCI Ubiquitination, Causes FA-T Subtype of Fanconi Anemia. *Cell Rep.* 12, 35–41 (2015).
 37. Koboldt, D. C. et al. Comprehensive molecular portraits of human breast tumours. *Nature* 490, 61–70 (2012).
 38. Helleday, T., Eshtad, S. & Nik-Zainal, S. Mechanisms underlying mutational signatures in human cancers. *Nat. Rev. Genet.* 15, 585–598 (2014).
 39. Larsen, M. J. et al. Classifications within Molecular Subtypes Enables Identification of BRCA1/BRCA2 Mutation Carriers by RNA Tumor Profiling. *PLoS One* 8, (2013).
 40. Xuan, J., Yu, Y., Qing, T., Guo, L. & Shi, L. Next-generation sequencing in the clinic: Promises and challenges. *Cancer Lett.* 340, 284–295 (2013).

41. Naipal, K. A. T. et al. Functional ex vivo assay to select Homologous Recombination deficient breast tumors for PARP inhibitor treatment. *Clin. Cancer Res.* 20, 4816–4827 (2014).
42. Naipal, K. A. T. et al. Attenuated XPC Expression Is Not Associated with Impaired DNA Repair in Bladder Cancer. *PLoS One* 10, e0126029 (2015).
43. van de Wetering, M. et al. Prospective Derivation of a Living Organoid Biobank of Colorectal Cancer Patients. *Cell* 161, 933–945 (2015).
44. Wang, Y. & Navin, N. E. Advances and Applications of Single-Cell Sequencing Technologies. *Mol. Cell* 58, 598–609 (2015).
45. Krogan, N. J., Lippman, S., Agard, D. A., Ashworth, A. & Ideker, T. The Cancer Cell Map Initiative: Defining the Hallmark Networks of Cancer. *Mol. Cell* 58, 690–698 (2015).
46. Roychowdhury, S. et al. Personalized Oncology Through Integrative High-Throughput Sequencing: A Pilot Study. *Sci. Transl. Med.* 3, 111ra121–111ra121 (2011).
47. Johnson, A. et al. The right drugs at the right time for the right patient: the MD Anderson precision oncology decision support platform. *Drug Discov. Today* 00, 1–6 (2015).
48. Chapman, P. B. et al. Improved survival with vemurafenib in melanoma with BRAF V600E mutation. *The New England journal of medicine* 364, (2011).
49. Farmer, H. et al. Targeting the DNA repair defect in BRCA mutant cells as a therapeutic strategy. *Nature* 434, 917–921 (2005).
50. Bryant, H. E. et al. Specific killing of BRCA2-deficient tumours with inhibitors of poly(ADP-ribose) polymerase. *Nature* 434, 913–917 (2005).
51. Kubota, E. et al. Low ATM protein expression and depletion of p53 correlates with olaparib sensitivity in gastric cancer cell lines. *Cell Cycle* 13, 2129–2137 (2014).
52. Naipal, K. A. T. & van Gent, D. C. PARP inhibitors : the journey from research hypothesis to clinical approval. *Per. Med.* 12, 139–154 (2015).
53. Gad, H. et al. MTH1 inhibition eradicates cancer by preventing sanitation of the dNTP pool. *Nature* 508, 215–21 (2014).
54. Huber, K. V. M. et al. Stereospecific targeting of MTH1 by (S)-crizotinib as an anticancer strategy. *Nature* 508, 222–7 (2014).
55. Tsuzuki, T. et al. Spontaneous tumorigenesis in mice defective in the MTH1 gene encoding 8-oxo-dGTPase. *Proc. Natl. Acad. Sci. U. S. A.* 98, 11456–11461 (2001).
56. Gelmon, K. A. et al. Olaparib in patients with recurrent high-grade serous or poorly differentiated ovarian carcinoma or triple-negative breast cancer: A phase 2, multicentre, open-label, non-randomised study. *Lancet Oncol.* 12, 852–861 (2011).
57. Schnipper, L. E. et al. American Society of Clinical Oncology Statement : A Conceptual Framework to Assess the Value of Cancer Treatment Options. (2015). doi:10.1200/JCO.2015.61.6706



Appendix

**Summary
Samenvatting**

**Curriculum Vitae
List of publications
PhD Portfolio**

Acknowledgements

Summary

All information a cell needs to live and survive is stored in the DNA. Most DNA molecules consist of two complementary chains of linked nucleic acids that twist into a helix. During replication the helix is unwound and new complementary bases are placed opposite the 'old' bases, resulting in two identical daughter helices. The place where the DNA is unwound and replicated is called the replication fork.

Maintenance of an intact and uncompromised genome is of vital importance for cell survival. Damaged DNA can block transcription and replication, processes essential for cell viability. Additionally, once a permanent change such as a point mutation or translocation has been made in the DNA, it will be inherited by the daughter cells. Persistent DNA damage can result in cell death or the accumulation of mutations, which may lead to accelerated ageing or malignant transformation (i.e. cancer).

The DNA is constantly attacked by endogenous as well as exogenous agents that cause DNA damage. For example, UV light from the sun can damage the DNA by crosslinking two adjacent bases and ionizing radiation can either break one or both strands of the DNA. Chemotherapeutics such as Mitomycin C and cisplatin make crosslinks in the DNA and between DNA and nearby proteins. To counteract the deleterious effects of DNA damage, cells evolved an intricate network of pathways to detect and repair DNA damage, the DNA Damage Response (DDR). These pathways can recognize specific types of damage and also halt cell cycle progression to gain time to repair the damage before the next cells division. **Chapter 1** gives a general introduction into the topic of DNA repair.

The nucleotide excision repair pathway repairs damaged bases that distort the DNA helix, such as bases damaged by UV light. Mismatches between two opposing bases can arise during replication, because the

polymerases that replicate the DNA sometimes incorporate the wrong nucleotide. Mismatch repair deals with these mistakes by removing the wrong base. Another polymerase then replaces the missing base. For the repair of DNA double strand breaks there are two pathways, homologous recombination and non-homologous end joining. Assays to measure the repair via these pathways and the importance of a proper balance between the two are reviewed in **chapter 2**.

DNA interstrand crosslinks connect two opposing strand of DNA, preventing the transcription and replication machinery from opening the helix. This type of damage is recognized and repaired via the Fanconi Anemia (FA) pathway, homologous recombination, translesion synthesis and nucleotide excision repair. Unlike most other DNA repair pathways, the translesion synthesis (TLS) pathway is a DNA damage tolerance pathway. When a replication fork stalls at a damaged base, translesion polymerases can take over to bypass the damage. The damaged base is then removed at a later stage, for example by the nucleotide excision repair pathway.

Mutations in proteins involved in DNA repair can predispose to specific types of cancer. For example, women with a heterozygous mutation in the homologous recombination proteins BRCA1 and BRCA2 are more prone to develop breast and ovarian cancer. Usually the wild-type copy of BRCA1 or BRCA2 is inactivated in the tumour and only the mutated variant is expressed. These cells are then no longer able to repair DNA breaks via homologous recombination. This defect makes the cells exquisitely sensitive to PARP inhibitors, such as Olaparib. PARP1 is required for the efficient repair of single-strand breaks in the DNA. When these breaks are repaired inefficiently due to inhibition of PARP1, replication forks collapse at these sites of damage, resulting in DNA double strand breaks. To repair these breaks, BRCA1 and BRCA2 are required. In tumours where these proteins are not functioning properly, DNA damage accumulates, eventually leading to

cell death.

The treatment of homologous recombination deficient tumours with PARP inhibitors is very promising, but a fraction of the tumours eventually becomes resistant to the treatment. Resistance can be due to overexpression of a drug-efflux pump, reversion of the mutation in BRCA1 or BRCA2 or restoration of homologous recombination due to the loss of 53BP1 expression. However, these mechanisms do not explain all cases of resistance. In **chapter 3** we therefore set out to identify novel mechanism of resistance in BRCA1 deficient mouse mammary tumour cells.

To identify mechanism of PARP inhibitor resistance in BRCA1 deficient cells, a loss-of-function shRNA screen was performed on mouse mammary tumour cells. Resistant clones were selected with a high dose of the PARP inhibitor Olaparib. One of the hits from the screen was 53BP1. For 53BP1 it had already been demonstrated that its loss in BRCA1 deficient cells results in restoration of homologous recombination and PARP inhibitor resistance. A new hit from the screen was Rev7 and Rev7 loss also resulted in Olaparib resistance. In the absence of Rev7, Rad51 foci formation was restored and CtIP dependent-resection was increased in BRCA1 deficient cells.

From the initial study it was still unclear why loss of Rev7 led to restoration of HR in BRCA1 deficient cells. Rev7 plays a role in translesion synthesis together with Rev3 and Rev1, but Rev7 has also been implicated in regulation of cell cycle progression via the anaphase-promoting complex and in several other processes. In **chapter 4** we investigate the importance of the different roles of Rev7 in the restoration of homologous recombination and mediating PARP inhibitor resistance. The role of Rev7 in cell cycle progression does not seem to be important for restoration of homologous recombination in BRCA1 deficient cells, but the interaction between Rev3 and Rev7 is.

In **chapter 5** we studied BRCA2 and its interactions partners. BRCA2 is, like BRCA1,

essential for homologous recombination and BRCA2 deficient cells are also extremely sensitive to PARP inhibition. In a mass spectrometry screen, a new BRCA2 interacting protein, HSF2BP (Heat Shock Factor 2 Binding Protein), was identified. Although HSF2BP expression was reported to be testis specific, we showed that it is expressed in mouse embryonic stem cells, mouse tissue and several human cancer cell lines. HSF2BP overexpression resulted in hypersensitivity to the interstrand-crosslinking agent mitomycin C (MMC). Additionally, exposure to MMC resulted in increased numbers of chromosomal aberrations in cells overexpressing HSF2BP. Both of these phenotypes are also characteristic for Fanconi Anemia patient cells, which have a defect in the pathway that repairs DNA interstrand crosslinks.

HSF2BP interacts with the C-terminal part of BRCA2, in the same region as FANCD2. Our current model is that the MMC hypersensitivity upon overexpression of HSF2BP is caused by disturbing the interaction between FANCD2 and BRCA2.

Chapter 6, the general discussion, examines the results and implications of this thesis for the treatment of cancer and also how new findings can be implemented in the clinic or which steps should be taken before this can be done. Finally, the future of cancer treatment and the implications for the costs are considered.

Samenvatting

Alle informatie die een cel nodig heeft om te kunnen (over)leven is opgeslagen in het DNA. De gangbare conformatie van DNA is een dubbele helix bestaande uit nucleotiden die om elkaar heen gewonden zijn. Tijdens de replicatie, het kopiëren, van DNA worden nieuwe basen, de bouwstenen van het DNA, tegenover een vaste partner in het 'oude' DNA geplaatst. Zo wordt een exacte kopie van de originele streng gemaakt. De plek waar de oude strengen gescheiden worden en het DNA gekopieerd wordt, heet de replicatie vork.

Het in stand houden van intact en onbeschadigd DNA is voor een cel van levensbelang. Beschadigd DNA kan de transcriptie en replicatie blokkeren en deze processen zijn van essentieel belang voor cellen. Daarnaast zullen mutaties en translocaties, wanneer deze eenmaal ontstaan zijn, overgeërfd worden in het nageslacht. Bovendien kan de permanente aanwezigheid van beschadigd DNA leiden tot het ophopen van mutaties, versnelde veroudering en kanker.

Het DNA is constant blootgesteld aan interne en externe factoren die DNA schade kunnen veroorzaken. UV licht van de zon kan er voor zorgen dat twee naast elkaar liggende bases aan elkaar vast komen te zitten terwijl ioniserende straling enkelstrengs- en dubbelstrengsbreuken in het DNA kan veroorzaken. Chemotherapeutische medicijnen, zoals Mitomycine C en cisplatine, maken dwarsverbindingen (crosslinks) tussen DNA strengen onderling en naburige eiwitten, waardoor het DNA niet geopend kan worden voor transcriptie en replicatie. Om DNA schade efficiënt te kunnen detecteren en repareren beschikken cellen over een arsenaal aan DNA reparatiemechanismen: de DNA schade respons (DNA damage response, DDR). Deze reparatiemechanismen herkennen specifieke soorten DNA schade en kunnen de celcyclus stil leggen zodat er voldoende tijd is om de schade te repareren voor de volgende mitose (celdeling).

Hoofdstuk 1 is een algemene introductie over DNA reparatie.

Basen die de DNA helix verstoren, zoals basen beschadigd door UV licht, worden gerepareerd via het nucleotide excisie reparatiemechanisme (NER). Soms plaatst een polymerase tijdens het kopiëren van DNA per ongeluk een verkeerde base. Wanneer twee verkeerde basen tegenover elkaar zitten, worden deze verwijderd door een mechanisme dat verkeerde combinaties (mismatches) herkent. De verkeerde base wordt verwijderd en een polymerase plaatst de juiste base terug. Voor de reparatie van DNA dubbelstrengsbreuken zijn er twee verschillende mechanismen: homologous recombination (HR) en non homologous end-joining (NHEJ). Testen om de activiteit van deze twee reparatiemechanismen te meten en het belang van een gezonde balans tussen de twee mechanismen worden besproken in **hoofdstuk 2**.

DNA crosslinks verbinden twee tegenoverliggende strengen van DNA, waardoor de DNA helix niet geopend kan worden tijdens de replicatie. Dit type DNA schade wordt herkend door het Fanconi Anemie mechanisme (FA), door HR, door trans-laesie synthese (TLS) en door NER. TLS is een bijzonder mechanisme, omdat het niet zo zeer voor reparatie van de schade zorgt, maar voorkomt dat replicatie vastloopt. Het zorgt ervoor dat schade getolereerd wordt door een base tegenover een beschadigde base te zetten met een flexibele polymerase, zodat de cel kan overleven en de schade later gerepareerd kan worden.

Mutaties in eiwitten die betrokken zijn bij DNA reparatie verhogen de kans op specifieke soorten kanker. Vrouwen met een mutatie in de eiwitten BRCA1 en BRCA2, betrokken bij HR, hebben een verhoogde kans op borst- en eierstok kanker. In de meeste gevallen is in de tumor het gezonde allel uitgeschakeld en komt alleen de gemuteerde versie van het eiwit tot expressie. De cellen zijn dan niet langer in staat om DNA dubbelstrengsbreuken te repareren via HR. Dit defect maakt de cellen extreem

gevoelig voor PARP inhibitors zoals Olaparib. Het enzym PARP1 is noodzakelijk voor de efficiënte reparatie van enkelstrengs breuken. Wanneer deze breuken niet gerepareerd worden voor de replicatie, dan ontspooit de replicatievork wanneer deze bij een breuk komt. De ontspoorde vork vormt een dubbelstrengs breuk met een enkel uiteinde en voor de reparatie hiervan is HR nodig. Wanneer HR geïnactiveerd is door mutaties in bijvoorbeeld BRCA1 of BRCA2, hoopt de DNA schade zich op in de aanwezigheid van de PARP inhibitor. Dit leidt uiteindelijk tot de dood van de kankercel.

PARP inhibitors zoals Olaparib zijn veelbelovend voor de behandeling van tumoren met defecten in HR, maar een deel van de tumoren wordt uiteindelijk resistent. De resistentie kan veroorzaakt worden door overexpressie van een membraanpomp die de PARP inhibitor uit de cel pompt, door het terug muteren van de mutatie in BRCA1 of BRCA2 waardoor er geen HR defect meer is, of door het verlies van de expressie van het eiwit 53BP1. Echter, niet alle gevallen van resistentie kunnen via deze mechanismen verklaard worden. **Hoofdstuk 3** beschrijft dan ook een zoektocht naar andere resistentiemechanismen in BRCA1 deficiënte borstkankercellen van de muis.

Om nieuwe resistentie mechanismen te identificeren, voerden we een 'loss-of-function'- shRNA screen uit in de muizencellen. Resistente kolonies werden geselecteerd door middel van een hoge concentratie PARP inhibitor. Een van de 'hits' uit de screen was 53BP1. Van dit eiwit was al bekend dat verlies van expressie leidt tot PARP inhibitor resistente in BRCA1 deficiënte cellen. Een nieuwe hit uit de screen was REV7 en het verlies van REV7 expressie, leidde ook tot PARP inhibitor resistentie. In afwezigheid van REV7 konden RAD51 foci weer gevormd worden en was resectie hersteld in BRCA1 deficiënte cellen.

Aan de hand van de eerste studie was nog niet duidelijk waarom het verlies van REV7 leidt tot herstel van HR in BRCA1 deficiënte cellen. REV7 is van belang voor TLS,

samen met REV3, maar REV7 is vooral van belang voor de celcyclus en diverse andere processen. In **hoofdstuk 4** wordt beschreven op welke wijze REV7 van belang is voor de PARP inhibitor resistentie. De rol van REV7 in de celcyclus lijkt niet van belang te zijn, maar de interactie met REV3 is wel belangrijk voor het herstel van HR.

Hoofdstuk 5 gaat over BRCA2 en haar interactie partners. BRCA2 is, net als BRCA1, essentieel voor HR en BRCA2 deficiënte cellen zijn ook heel gevoelig voor PARP inhibitors. In een massaspectrometrie experiment ontdekten we een nieuwe interactie partner van BRCA2: HSF2BP. Volgens de literatuur komt HSF2BP alleen tot expressie in de testis, maar wij zagen ook expressie in embryonale stamcellen van de muis en in verschillende humane kankercellijnen. Overexpressie, maar niet depletie, van HSF2BP zorgde ervoor dat cellen extreem gevoelig werden voor de crosslinker MMC. Ook leidde overexpressie van HSF2BP tot meer chromosomale afwijkingen na blootstelling aan MMC. Deze eigenschappen zijn ook karakteristiek voor cellen van Fanconi Anemie patiënten. Deze patientencellen hebben een defect in de reparatie van DNA crosslinks.

HSF2BP bindt aan BRCA2 in dezelfde regio als FANCD2 aan BRCA2 bindt. Ook leidt overexpressie van HSF2BP tot een afname in FANCD2 en RAD51 foci, nadat cellen blootgesteld zijn aan MMC. We hebben de regio van BRCA2 waar HSF2BP aan bindt exact bepaald.

Hoofdstuk 6 is de algemene discussie, waarin zowel de resultaten van deze thesis als de implicaties voor de behandeling van kanker in de toekomst besproken worden. Er wordt bovendien aandacht besteed aan de vraag hoe de nieuwe bevindingen optimaal geïmplementeerd zouden kunnen worden in de kliniek en welke stappen genomen zouden moeten worden voordat de implementatie mogelijk is. Ook worden ontwikkelingen op het gebied van nieuwe medicatie voor de behandeling van kanker en de daarmee gemoeide kosten en bijkomende consequenties besproken.

Curriculum Vitae

Personal details

Full name: Inger Brandsma
Date of birth: 11 December 1987
Place of birth: Nieuwegein, the Netherlands
Nationality: Dutch

Education

October 2015-present

Postdoctoral training fellow at the Breast Cancer Now Research Centre, the Institute of Cancer Research, London, United Kingdom.

September 2011-September 2015

PhD project 'DNA repair and Breast Cancer' as part of the EU Framework7 project 'DDRresponse' under supervision of Dik van Gent and Roland Kanaar at the department of Genetics, Erasmus Medical Center Rotterdam, the Netherlands.

September 2009-August 2011

Master 'Molecular and Cellular Life Sciences' at the Utrecht Univeristy (UU), the Netherlands.

September 2006-August 2009

Bachelor's degree in Chemistry at Utrecht University.

September 2000- July 2006

VWO at O.R.S. Lek en Linge (secondary school) in Culemborg, the Netherlands.

Scientific publications

I. Brandsma and D.C. van Gent *Pathway choice in DNA double strand break repair: observations of a balancing act* Genome Integrity 2012 Nov 27;3(1) p. 9

G Xu, J. R. Chapman*, **I Brandsma***, J Yuan, M. Mistrik, P. Bouwman, J. Bartkova, E. Gogola, D. Warmerdam, M. Barazas, J.E. Jaspers, K. Watanabe, M. Pieterse, A. Kersbergen, W. Sol, P.H. Chelie, P.C. Scouten, B. van den Broek, A. Salman, M. Nieuwland, I. de Rink, J. de Ronde, K. Jalink, S.J. Boulton, J. Chen, D.C. van Gent, J. Bartek, J. Jonkers, P. Borst, S. Rottenberg *REV7 counteracts DNA double-strand break resection and its loss causes PARP inhibitor resistance of BRCA1-deficient mammary tumors* Nature 2015 521(7553) pp. 541-544

* these authors contributed equally

K.A.T Naipal, J. Raams, S.T. Bruens, **I. Brandsma**, N.S. Verkaik, N.G.J Jaspers, J.H.J Hoeijmakers, G.J.L.H van Leenders, J. Pothof, R. Kanaar, J. Boormans, D.C. van Gent. *Attenuated XPC Expression Is Not Associated with Impaired DNA Repair in Bladder Cancer* Plos One 2015 10 (4) pp. e0126029

I. Brandsma, G. Xu, M. Siragusa, B. Geverts, D. Dekkers, K. Bezstarosti, N.S. Verkaik, J. Demmers, A. Houtsmuller, S. Rottenberg, D.C. van Gent *Mechanistic insight into PARP inhibitor resistance due to REV7 loss in BRCA1-deficient cells* (Manuscript in preparation)

I. Brandsma, J. Odijk, A. Oostra, D. Dekkers, K. Bezstarosti, N. van den Tempel, J. Demmers, J. Dorsman, D.C. van Gent, R. Kanaar, A. Zelensky *Overexpression of HSF2BP, a new BRCA2 interactor, results in a Fanconi anemia-like phenotype* (Manuscript in preparation)



PhD Portfolio
Summary of PhD training and teaching

Name PhD student: Inger Brandsma Erasmus MC Department: Genetics Research School: MGC	PhD period: Sept. 2011-Sept. 2015 Promotor(s): Jan Hoeijmakers Supervisor: Dik van Gent	
1. PhD training		
	Year	Workload (ECTS)
General courses -Biomedical English Writing and Communication -Research Integrity -Laboratory animal science -Statistics -Methodology -Basiscursus Regelgeving Klinisch Onderzoek -Didactic skills -Stralingshygiene 5B	2015 2012 2012	3 ECTS 2 ECTS 30 hours
Specific courses (e.g. Research school, Medical Training) -"Safely Working in the Laboratory" Boerhaave LUMC 8.12.2011 -Biochemistry and Biophysics PhD course Erasmus MC Oct-Nov 2011 -Cell and Developmental Biology PhD course Erasmus MC -Genetics PhD course Erasmus MC April-May 2012 -Genome Maintenance and Cancer MGC -Literature course Reproduction and Development	2011 2011 2012 2012 2012 2013	8 hours 3 ECTS 3ECTS 3ECTS 16 hours 2 ECTS

<p>Seminars and workshops</p> <ul style="list-style-type: none"> -Ex vivo imaging workshop DDRresponse Erasmus MC Rotterdam -MGC PhD workshop 2012 Dusseldorf (poster) 	<p>2012</p> <p>2012</p>	<p>4 hours</p> <p>24 hours</p>
<p>Presentations</p> <ul style="list-style-type: none"> -MGC PhD Workshop 2013 Luxemburg -KWF meeting, Lunteren, The Netherlands -Annual DDRresponse meeting, Leuven, Belgium -MGC PhD Workshop 2014 Munster -DDR Response Meeting Madrid 2014 -DDR Response Meeting Amsterdam 2015 	<p>2013</p> <p>2013</p> <p>2013</p> <p>2014</p> <p>2014</p> <p>2015</p>	<p>8 hours</p> <p>24 hours</p> <p>24 hours</p> <p>30 hours</p> <p>24 hours</p> <p>30 hours</p>
<p>(Inter)national conferences</p> <ul style="list-style-type: none"> -MGC day September 2011-2012-2013-2014 -CGC day January 2012 -DDRresponse meeting 2012 Manchester (poster) -NVRB symposium Noordwijkerhout -CGC Day January 2013 -Gordon Research Conference: Mammalian DNA Repair (poster) 	<p>2011-14</p> <p>2012</p> <p>2012</p> <p>2012</p> <p>2013</p> <p>2015</p>	<p>32 hours</p> <p>8 hours</p> <p>30 hours</p> <p>16 hours</p> <p>8 hours</p> <p>40 hours</p>
<p>2. Teaching</p>		
<p>Supervising practicals and excursions, Tutoring</p> <ul style="list-style-type: none"> -Supervised two secondary school pupils Junior Science project -HBO student -Visting Japanese Student from Takeda's lab -HBO student -Genetics course for Nanobiology students 	<p>2011</p> <p>2012</p> <p>2012</p> <p>2013</p> <p>2012-15</p>	<p>1.5 ECTS</p> <p>3 months</p> <p>50 hours</p> <p>9 months</p> <p>20 hours</p>
<p>Supervising Master's theses</p> <ul style="list-style-type: none"> -Master student -Master student from Takeda's lab 	<p>2014</p> <p>2015</p>	<p>4 months</p> <p>3 months</p>

Acknowledgements

Beste lezer,

Allereerst bedankt dat je mijn thesis leest. Ik hoop dat je, naast het dankwoord, ook andere stukken zult lezen. Voor leken raad ik de samenvatting hier in de appendix aan en voor mensen die nieuw zijn in het veld van de DNA damage response geeft de introductie een overzicht om mee te beginnen.

Dik, bedankt voor je hulp en begeleiding de afgelopen jaren en voor de plaats in je groep die je mij aanbood. Ik heb met veel plezier aan de projecten gewerkt en veel geleerd. Je gaf me veel vrijheid om zelf experimenten op te zetten en ik kon altijd bij je binnen lopen voor vragen en advies. Wat wetenschappelijk schrijven betreft heb ik ook veel van je geleerd en je keek mijn teksten en figuren altijd vlot maar zorgvuldig na. Qua kennis, maar ook qua algemene ontwikkeling als wetenschapper kon ik veel van je opsteken. Ik hoop dat we ook in de toekomst nog vaker samen zullen werken.

Roland, ook jou wil ik graag bedanken voor je hulp en begeleiding de afgelopen jaren en vooral nu in de laatste fase. Je kritische blik en opbouwende kritiek hielpen me goed naar mijn eigen data en de bijbehorende controles te kijken. Van je kennis van en connecties binnen het DDR-veld heb ik ook mogen profiteren. Ik hoop dat we over het HSF2BP-project binnenkort kunnen publiceren.

Jan, bedankt voor je input tijdens de presentaties en vooral bij het afronden van mijn thesis. Ook van jou heb ik veel kunnen leren de afgelopen jaren en ik bewonder je tomeloze enthousiasme voor onderzoek. Ook denk ik met veel plezier terug aan de meeting in Ventura.

Alex, without your project, help and guidance, I don't think I would have been able to finish this thesis. You helped me out a lot with practical things, but also shared your views on science with me and challenged me to think more (and better). I really enjoyed working with you and I hope I can keep bothering you in the future, because I will certainly miss you, your skills, knowledge and constructs.

Sven and **Guotai**, thank you for allowing me to help you with your project. It was a great experience to collaborate and work with you. I am very proud of the work we published and I hope to publish more Rev7-related work in the years to come. I wish you both the best for the future and hope that we may work together again.

Yusuke and **Professor Takeda**, thank you for your help with the Rev7-project. The DT40 part of the project is very challenging, but hopefully you will be successful. Supervising Yusuke in our lab was also a rewarding experience and I learned a lot from that.

Josephine Dorsman en **Anneke Oostra**, bedankt voor jullie hulp bij het HSF2BP-project. Het maken van goede metafase spreads en het scoren hiervan is een vak apart en ik ben erg blij dat jullie dit voor mij konden doen.

De projecten in deze thesis waren niet mogelijk geweest zonder hulp van de massaspectrometrie, FACS en de microscopie-afdeling. **Karel, Dick, Jeroen, Reinier, Gert-Jan** en **Gert**, bedankt voor jullie hulp en ondersteuning hierbij! Ik kon altijd bij jullie terecht met al mijn vragen. Ook wil ik graag **Maarten**

en **Bert-Jaap** bedanken voor hun hulp bij het opzetten van FRAP en andere microscopie-experimenten. De FRAP-experimenten en de analyse daarvan waren niet mogelijk geweest zonder **Adriaan** en **Bart**. Ook jullie hartelijk bedankt voor jullie hulp en advies!

During my PhD, I supervised several bachelor and master students. **Guus, Yu, Mattia** and **Yusuke**, thank you for your contributions to my projects. Supervising you has taught me a lot and I hope you have learned from working with me. I hope you will all have successful careers in science or other fields.

Nathalie en **Hanny**, bedankt dat jullie mijn paranimfen willen zijn! Jullie hebben me ontzettend veel geholpen met het regelen van alle praktische dingen, het nakijken van drukproeven en afhandelen van andere klusjes. Ik weet niet hoe ik het zonder jullie had kunnen doen. Daarvoor stonden jullie ook altijd voor me klaar als ik hulp nodig had met experimenten en ik heb met veel plezier met jullie samengewerkt!

Kishan, Nicole en **Anja**, over ieder van jullie afzonderlijk zou ik een pagina vol kunnen schrijven, maar ik zal het kort houden. Bedankt voor al jullie hulp en gezelligheid! Het was altijd plezierig op het lab en ik voelde me er helemaal thuis. Ik denk niet dat ik snel weer zulke collega's zal treffen en ik mis jullie (en iedereen in lab 663 en de naastgelegen labs) en de vissen en de krabben!

I would also like to thank all other (former) colleagues from the sixth floor: **Nicole van Vliet, Bibi, Marcel, Mascha, Ingrid, Julie, Berina, Elza, João, Joyce B, Paula, Cecile, Yanto, Humberto, Arnold, Gosia, Sari, Dejan, Claire, Jeroen, Joyce L, Koos, Wenhao, Titia, Stefan, Klaas, KC** and **Natasja**. I had a great time in the lab and that was certainly because of you! Whenever I needed help or was looking for something, someone would always help me out and I really enjoyed the borrels, cocktail parties and other activities. I wish you all the best for the future and hope to see you again soon.

Over the past years, I paid regular visits to the genetics department on the 7th floor for advice, materials and small talk. I would like to thank all (former) colleagues there for their help and gezelligheid: **Wim, Jan, Hannes, Jurgen, Arjan, Imke, Karen, Franzi, Loes, Petra, Maikel, Serena, Mariangela, Yasemin, Christina, Barbara, Joris, Maria T, Maria V, Peter, Marjolein, Diana** and **Kasper**.

De afgelopen jaren heb ik ook vaak hulp gehad met praktische zaken van **Jasperina, Bep, Riet, Rini, Sonja, Marieke, Enno, Koos, Annet** en **Leo**. Ook jullie wil ik graag bedanken voor jullie behulpzaamheid.

Als laatste wil ik graag mijn ouders en Lennart bedanken voor de hulp bij het nakijken van vooral de Nederlandse stukken van deze thesis. En als laatste wil ik graag de rest van mijn familie en vrienden bedanken voor alle steun en hulp de afgelopen vier jaar!